

Co-Tutorship PhD Thesis

**UNIVERSITÀ DEGLI STUDI DI
MILANO**

PhD Course in Experimental Medicine and
Medical Biotechnologies (XXXIII cycle)
Curriculum: Neuroscience and
Neuropathology

Department of Medical Biotechnology and
Translational Medicine (BIOMETRA)

AIX-MARSEILLE UNIVERSITÉ

Ecole Doctorale des Sciences de la Vie et de
la Santé
Faculté des Sciences de Luminy



Oxytocin receptors in neurodevelopmental disorders: innovative approaches for the quantification of supramolecular receptor complexes

PhD thesis of: Francesca SANTINI

R12120

Tutor: Prof. Massimo LOCATI

Supervisors: Dr. Bice CHINI and Dr. Françoise MUSCATELLI

PhD Coordinator: Prof. Massimo LOCATI

a.a. 2019-2020

INDEX

1. <u>ABBREVIATIONS</u>	5
2. <u>AIMS</u>	7
3. <u>GENERAL INTRODUCTION</u>	8
3.1. G PROTEIN COUPLED RECEPTORS in brain disorders.....	8
3.2. THE OXYTOCINERGIC SYSTEM.....	9
3.2.1.Oxytocin.....	9
3.2.2.The oxytocin receptor (OTR).....	11
3.3 THE OXYTOCINERGIC SYSTEM IN NEURODEVELOPMENTAL DISORDERS	18
3.3.1 Neurodevelopmental disorders: pathogenesis and animal models.....	18
3.3.2 Animal models to study autistic-like correlates	20
3.3.3 The oxytocinergic system in mouse models of neurodevelopmental disorders.....	23
3.4 GPCR DIMERS IN BRAIN PATHOLOGY.....	26
3.4.1 GPCR dimerization: an overview.....	26
3.4.2 GPCR dimers in brain pathology.....	27
4. <u>PHARMACOLOGICAL INVESTIGATION OF OXYTOCIN RECEPTOR DIMERS BY BIVALENT LIGANDS</u>	29
4.3 INTRODUCTION.....	29
4.4 CONTRIBUTIONS.....	29
4.5 Manuscript: “Oxytocin receptor homobivalent ligands untangle homodimeric receptor specific signaling”.....	30
5. <u>DEVELOPMENT OF A “NANORULER” SYSTEM TO MAP OTR HOMODIMERS IN THE RODENT BRAIN</u>	46
5.1. METHODS CURRENTLY EMPLOYED TO STUDY OTR DIMERIZATION.....	46
5.2. GENERAL STRATEGY AND EXPERIMENTAL PLAN	49
5.3. MATERIALS AND METHODS.....	52
5.4. RESULTS.....	56
5.4.1.Design and optimization of the oligonucleotides.....	56
5.4.2.Design and characterization of the “clickable” OT analogues.....	60
5.4.3.Work in progress: cellular and brain tissue staining protocol optimization.....	78

6. <u>OXYTOCIN RECEPTOR MAPPING IN A MOUSE MODEL OF SCHAAF-YANG SYNDROME</u>	81
6.1 METHODS CURRENTLY EMPLOYED TO STUDY OTR DISTRIBUTION.....	81
6.2 OXYTOCINERGIC SYSTEM ALTERATIONS IN MAGEL2-KO, A MOUSE MODEL OF SCHAAF-YANG SYNDROME	84
6.3 MATERIALS AND METHODS.....	85
6.4 RESULTS.....	86
6.4.1 OTR levels are differently modified in males and females Magel2-KO mice.....	88
6.4.2 An OT treatment in the first week of life has rescuing effects in male, but not female mice....	89
6.5 DISCUSSION.....	93
6.6 CONCLUSIONS AND FUTURE DIRECTIONS	95
7. <u>EVALUATION OF NEONATAL OXYTOCIN ADMINISTRATION ON HIPPOCAMPAL DEVELOPMENT IN THE MAGEL2 MOUSE MODEL OF AUTISM</u>	97
7.1. CONTRIBUTIONS.....	97
7.2. Article: “Acute neonatal oxytocin impacts hippocampal network development and restores adult social memory deficits in a mouse model of autism”.....	97
8. <u>GENERAL DISCUSSION AND CONCLUSIONS</u>	126
9. <u>BIBLIOGRAPHY (GENERAL)</u>	130
10. <u>RESUME</u>	155
10.1. Resume (French).....	155
10.2. Resume (English)	157

1. ABBREVIATIONS

ADHD: attention-deficit hyperactivity disorder

AONm: anterior olfactory nucleus, medial part

AP2: adaptor protein 2

ASD: autism spectrum disorder

AVP: arginine vasopressin

AVPR: arginine vasopressin receptor

AVPV: anteroventral periventricular nucleus

AT1: angiotensin receptor, type 1

BiFC: Bimolecular Fluorescence Complementation

BLA: basolateral amygdala

BNST: bed nucleus of the stria terminalis

BRET: Bioluminescence Resonance Energy Transfer

CA1/CA2/CA3: hippocampal regions CA1, CA2, CA3

cAMP: cyclic adenosine monophosphate

CeA: central amygdala

CNS: central nervous system

CNTNAP2: contactin associated protein-like 2

CREB: cAMP-responsive element binding

DAG: diacyl glycerol

DG: dentate gyrus

D1R: dopamine receptor 1

D2R: dopamine receptor 2

dOTK: 1-deamino [Lys⁸] - vasotocin

DMEM: Dulbecco Modified Eagle's medium

ECL: extracellular domain

EGFP: enhanced green fluorescent protein

ER: estrogen receptor

ERK: Extracellular signal-regulated kinases

FBS: Fetal Bovine Serum

FCS: Fluorescence Correlation Spectroscopy

FMR1: fragile X mental retardation 1 gene

FMRP: fragile X mental retardation protein

FRET: Fluorescence Resonance Energy Transfer

GABA: gamma (γ) aminobutyric acid

GABAAR: gamma (γ) aminobutyric acid receptor, type A

GFP: green fluorescent protein

GPCR: G protein coupled receptor

GRK: G protein coupled receptor kinase

GTP: guanosine triphosphate

HCR: hybridization chain reaction

HEK293: Human Embryonic Kidney 293

HPLC: high-performance liquid chromatography

IP3: inositol 1,4,5-trisphosphate

JNK: c-Jun N-terminal kinases

KCC2: K-Cl co-transporter type 2

LS: lateral septum

MAGE: melanoma antigen

MAPK: mitogen-activated protein kinase

MeA: medial amygdala

MECP2: methyl CpG binding protein 2

mGluR: metabotropic glutamate receptor

MIA: maternal immune activation

MPOA: medial preoptic area

NDD: neurodevelopmental disorder

NLGN3: neuroligin 3

NO: nitric oxide

NKCC1: Na-K-Cl cotransporter, type 1

OT: oxytocin

OTR: oxytocin receptor

PBS: phosphate buffered saline

PEI: polyethylenimine

PIP2: phosphatidylinositol 4,5-bisphosphate

PKC: protein kinase C

PLA: Proximity Ligation Assay

P-LAP: placental leucine aminopeptidase

PLC: phospholipase C

PVN: paraventricular nucleus

PWS: Prader-Willi Syndrome
RAR: retinoic acid receptor
RCA: rolling circle amplification
RLuc: *Renilla* luciferase
SHANK3: SH3 and multiple ankyrin repeat domains 3
SON: supraoptic nucleus
SYS: Schaaf-Yang Syndrome
TM: transmembrane domain
TMH: transmembrane helix
TR: thyroid hormone receptor
Tr-FRET: time resolved FRET
V1aR: vasopressin receptor, type V1a
V1bR: vasopressin receptor, type V1b
V2R: vasopressin receptor, type V2
VPA: valproic acid
YFP: yellow fluorescent protein

2. AIMS

There is growing evidence that in a number of animal models of neurodevelopmental disorder, GPCRs alterations in the central nervous system can affect neurobiological, neurochemical and behavioural phenotypes. Oxytocin and its receptor are two actors strongly involved in these pathogenetic processes: neurobiological alterations of the oxytocinergic system are indeed often detected in a wide variety of neurodevelopmental and neuropsychiatric disorders characterized by alteration in social behaviour. Interestingly, oxytocin-based treatments have proved to be effective in rescuing behavioural alterations typical of these conditions, in patients as well as in animal models. Oxytocin is thus a promising therapeutic molecule in the field; however, as detailed information about the functioning of the oxytocinergic system in the CNS is still missing, its true translational potential has still to be defined. In particular, it is critical to clarify the brain areas involved in the pharmacological activity of exogenous oxytocin administration, as well as the precise pharmacology of oxytocin receptor in these areas.

The oxytocin receptor (OTR) is a GPCR, and, as many other members of this family, it can dimerize or exist as monomeric units. Depending on its dimerization state, the OTR can have different signaling properties, a different cellular localization, or different desensitization mechanisms; therefore, knowing exactly where the different receptor populations can be found is a crucial step to understand how the oxytocinergic system acts in the CNS, in physiological and pathological conditions.

However, the lack of suitable methodologies to study OTR homo and heterodimers in native tissues makes this task an unsolved experimental problem. No reliable antibodies for this receptor are available, and the low levels at which these receptors are expressed make it problematic to efficiently detect them in endogenous tissues.

For these reasons, the aims of my project were:

- 1) To complete the pharmacologic characterization of a series of bivalent ligands targeting OTR dimers that were designed in our laboratory;
- 2) To develop a new, sensitive and specific approach to map the presence and the distribution of OTR homodimeric receptors in the mouse brain;
- 3) To flank this new technique with more common and universally accepted methodologies in order to investigate possible region-specific changes of OTR distributions (in their monomeric or dimeric/oligomeric forms) in a mouse model of neurodevelopmental disorder, the *Magel2*-KO mouse;
- 4) To evaluate differences in OTR distribution in males and females, in order to highlight any possible sexual dimorphism in receptor fluctuations in wild type and *Magel2*-KO mice.

3. GENERAL INTRODUCTION

3.1 G PROTEIN COUPLED RECEPTORS IN BRAIN DISORDERS

G protein coupled receptors are the largest family of transmembrane signaling proteins in mammals. In humans, more than 800 different GPCRs have been reported, and the number of ligands that can act on these receptors is even greater (Gurevich and Gurevich, 2017). GPCR endogenous ligands include molecules of extremely different chemical nature, like proteins, peptides and aminoacids, nucleotides, lipids, ions, and even photons (Lagerstrom et Schiöth, 2008). Once bound to its ligand, a GPCR can transduce a wide variety of signals through the interaction with several classes of molecules: heterotrimeric G proteins, β -arrestins and a variety of scaffolding interactors (Gurevich and Gurevich, 2017). GPCRs regulate the vast majority of physiological and pathological processes in the organism, and are currently targeted by more than 50% of the drugs used in clinical practice; moreover, many receptors belonging to this family do not have an identified endogenous ligand yet, and for this reason they're also called "orphan" receptors. Therefore, the study of GPCRs continues to be one of the most promising research fields for the development of new therapeutic strategies. In the central nervous system (CNS), GPCRs regulate the most diverse functions, including, among others, neuronal survival and differentiation, neurotransmitter and neuropeptides release, synaptic transmission and plasticity (Katritch et al, 2012; Lagerstrom et Schiöth, 2008). Because of their extensive effects in the CNS, it is not a surprise that GPCRs can often be involved in the pathogenesis of many psychiatric, neurodegenerative and neurodevelopmental disorders. Here, we will focus the attention on the role of GPCRs in neurodevelopmental disorders and in particular on the role of the oxytocin receptor.

3.2 THE OXYTOCINERGIC SYSTEM

3.2.1 Oxytocin

Oxytocin (OT) is a neuropeptide constituted by 9 aminoacids (Cys-Tyr-Ile-Gln-Asn-Cys-Pro-Leu-GlyNH₂). A disulfide bridge between cysteines in positions 1 and 6 gives to the peptide a circular structure (figure 1); the last three aminoacids form a “tail” that sticks out of the binding pocket when the molecule is inserted in its receptor. Its structure is almost identical to those of another closely related neuropeptide, vasopressin (AVP). AVP and OT genes are evolutionarily very close: their locus is on the same chromosome (20p13 in human; Mohr et al, 1988), and the two proteins only differ for aminoacids in position 3 and 8. The different polarity of the aminoacids in these positions (basic for AVP and neutral for OT) is able to determine the right interaction between each peptide and its receptor (Chini et al, 1995).

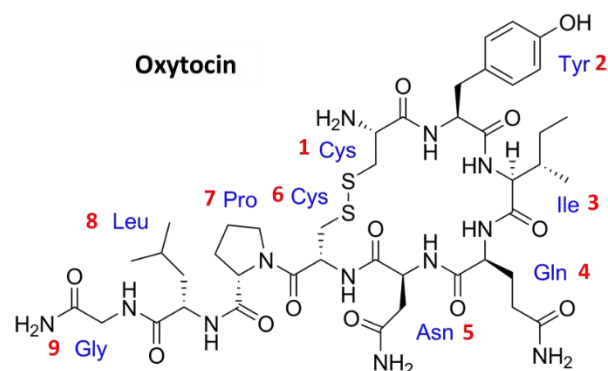


Figure 1: Oxytocin molecule. Aminoacids are reported in blue, their position in red.

Synthesis and release. Oxytocin is mainly synthesized in the hypothalamus, by the magnocellular neurons of the supraoptic (SON) and the paraventricular (PVN) nuclei, and by parvocellular neurons of the PVN (Buijs, 1978; Buijs and Swaab, 1979; Sofroniew, 1980, 1983). Its gene is composed by three different exons, that together encode the peptide itself but also a translocator signal, a tripeptide processing signal (GKR) and a neurophysin, a carrier protein responsible of the correct storage and release of oxytocin (Brownstein et al, 1980; Ivell & Richter, 1984). The whole peptide is initially translated as a preprohormone, and then it is cleaved and furtherly modified while travelling down the axons to the neuronal terminals in the posterior pituitary. Once in the neurohypophysis, it is stored in large dense-core vesicles and released in the bloodstream, generally following an intracellular increase in calcium levels (Jin et al, 2007) (Figure 2). Vesicles can be found in the dendrites as well as in the neuron soma.

One of the molecules mostly involved in the release of intracellular calcium stores is a transmembrane glycoprotein with ADP-ribosyl cyclase activity, CD 38. CD38 has been proved to be fundamental for oxytocin release and differentiation (Jin et al, 2007; Higashida et al, 2010, 2011).

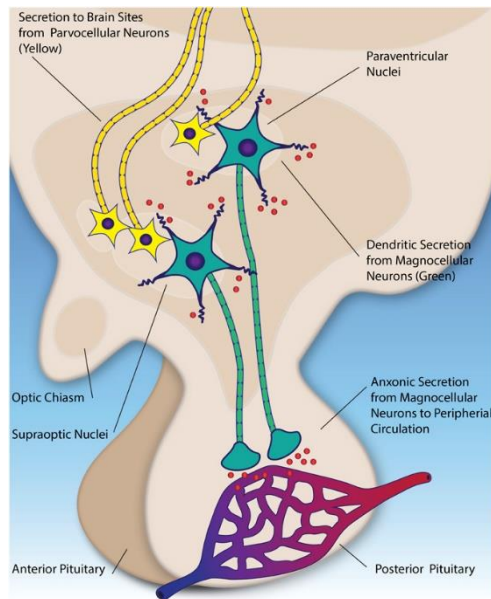


Figure 2: main sites of OT synthesis and periferic release. *Oxytocin is initially synthesized in the hypothalamus and then reaches the posterior pituitary packed into secretory vescicles through hypothalamic magnocellular neurons axons. Parvocellular neurons (in yellow) are responsible of oxytocin distribution to various CNS sites. From Frontiers in Neuroscience.*

In the brain, oxytocin is mainly released by dendrites of hypothalamic neurons in the surrounding areas. However, it can also be released by axonal projections that reach brain regions far from the hypothalamus, like central amygdala (CeA), the septum and the olfactory bulb, the brainstem and the spinal cord (Knobloch et al, 2012; Nicholas et al, 1989).

In mice, precursors of OT cells start to migrate already at embryonic day 9, align laterally to the third ventricle, and by E12 begin to migrate lateroventrally to reach their final position at day E14.5. Intermediate forms of oxytocin are not detected in these precursors until E16. The synthesis and release of the mature form of the peptide will only occur around birth (Grinevich et al, 2014, 2016).

Functions. While in periphery oxytocin is mainly involved in the regulation of parturition and lactation, in the CNS it modulates a range of social and non social behaviours. In particular, there is growing evidence of its involvement in social bonding, aggression, anxiety and fear, but also in social cognition in general (Albers, 2014; Ebert et al, 2018), memory and learning.

In pups, it is important in regulating ultrasonic distress calls that pups emit when separated from their mothers, a phenotype associated with a lower quality of maternal bonding.

In adults, oxytocin contributes to reduce maternal aggression right after delivery, regulates sexual behaviours in males and females, and permits the formation of stable and preferential bonds in rodents (Neumann, 2008; Bosch e Young, 2017). Male mice with a deletion of the first exon of the oxytocin gene suffer from social amnesia (Ferguson et al, 2000) and have an altered acoustic startle response (Winslow et al, 2000).

Regulation mechanisms. The lack of an appropriate cellular system to study oxytocin synthesis regulation is the reason why most of the knowledge comes from heterologous systems and non-physiologic environments. The strongest regulators of human and rat OT promoters could be the ligand-activated estrogen receptors ER α and ER β , the thyroid hormone receptor TR α , and the retinoic acid receptors RAR α and RAR β (Richard and Zingg, 1990, 1991; Adan et al, 1993). A region between 2172 and 2148 bp on its gene seems to be the one responsible for responsiveness to these receptors (Adan et al, 1992). The presence in this region of an ERE responsive element is supportive of the thesis of ERs. However, estrogen receptors are not expressed in oxytocinergic cells of the rat hypothalamus (Axelson, 1990), and therefore their influence on OT expression and/or release by magnocellular neurons is not direct. Instead, in parvocellular OT-expressing neurons an estrogen responsiveness ER β was reported to be expressed (Chung et al, 1991). TRs have been detected both in rat SON and PVN; however, their regulation of OT expression seems to be weaker (Adan et al, 1992). Another important regulation mechanism is guaranteed by oxytocin degradation rate, that is controlled by an enzyme with aminopeptidase activity, called oxytocinase or P-LAP. Other than oxytocin, P-LAP is also known to be able to inactivate other peptides, like vasopressin (Mizutani et al, 1995) and angiotensin III (Tsujiimoto et al, 1992). P-LAP regulates fetal development and maintenance of homeostasis during pregnancy (Yamahara et al, 2000). In human umbilical vascular endothelial cells (HUVEC), it is OT itself that, through OTR signaling, triggers P-LAP translocation from the cytosolic compartment to the cell surface via a PKC-dependent pathway (Nakamura et al, 2000).

3.2.2. The oxytocin receptor

The oxytocin receptor (OTR) is a Class A G-protein-coupled receptor (GPCR). Together with vasopressin receptors V1aR, V1bR and V2R, it forms a receptor family on its own. Due to their high homology degree, both OT and AVP can bind all the receptors belonging to this family, even if with different affinities (Grinevich et al, 2017).

Structure. The OTR protein (388 aminoacids in mouse, 389 in humans) is encoded by a single gene located in chromosome 3 in humans, and 6 in mice. Many variants of the gene have been reported in the non coding region of the gene. It is believed that some of these variants could impact the transcription regulation of the OTR gene, modulating the OTR expression level, a key factor to determine the cellular response to OT, and, by consequence, affecting social behavior responses (King et al, 2016; Rilling e Young, 2014; Skuse et al, 2014). Genetic variants in the coding region have also been described; they could have an effect on the binding affinity of OT, or on the intracellular trafficking of the receptor, and therefore these variants could lead to different phenotypes and responses to therapies (Kim et al, 2013; Liu et al, 2015; Ma et al, 2013).

As all GPCRs, the OTR is inserted in the cellular membrane through 7 transmembrane domains.

The N-terminal part sticks out on the extracellular environment, while the C-terminal tail goes into the cytoplasm (Fig. 3).

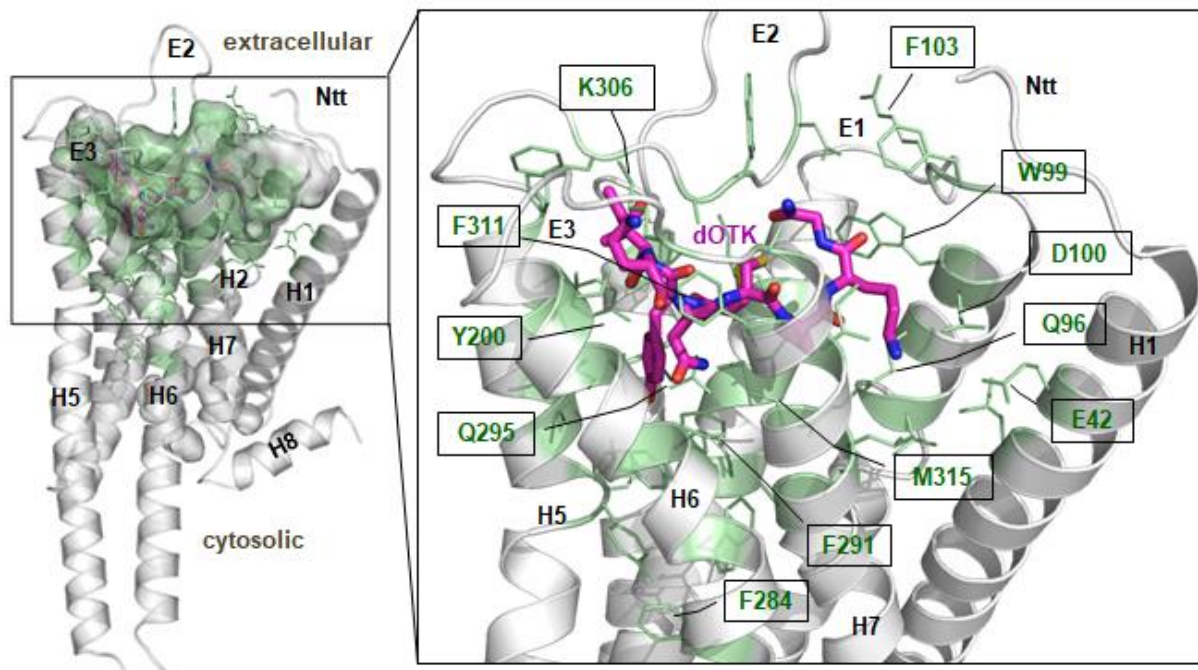


Figure 3: Oxytocin receptor structure (Busnelli et al, 2016). The receptor (gray) is bound to an oxytocin analog (magenta). The indicated aminoacids are those that take part in ligand binding (from Busnelli et al, 2016).

The actual structure of the OTR has remained obscure for a long time. Recently, Waltenspuhl et al. provided a crystallographic structure for the human version of this receptor, bound by the antagonist Retosiban. Their model allowed the identification of many interesting structural features of the antagonist-bound OTR, such as the localization and the shape of the cholesterol binding site (found to be between transmembrane helices IV and V), which is an essential allosteric modulator of OTR activity. (Waltenspuhl et al, 2020). Other OTR proposed structures are based on homology models, built starting from similar receptors (Busnelli et al, 2016; Busnelli et al, 2013; Chini et al, 1995). Through these same homology modeling studies, as well as through site-specific mutagenesis experiments, it has been established how the oxytocin molecule binds to the OTR: the circular part is deeply inserted into the binding pocket, where it interacts with TM5 and TM6 domains, while the tripeptide tail sticks outwards and binds to more extracellular portions of the receptor (Fanelli et al, 1999; Busnelli et al, 2016, 2013; Chini et al, 1995). Single aminoacidic changes can be crucial in the regulation of the receptor-agonist interaction, and this is true for OTRs but also for AVPRs. For example, substitution of Tyr209 in the TM5 and of Phe284 in the TM6 with aminoacids normally present in the V1aR drastically increases AVP's activity, that becomes a full agonist for the resulting mutant OTR (Chini et al, 1996).

Signaling. Just as many other GPCRs, the OTR is a “promiscuous” receptor, because it can couple to different subtypes of G protein. Depending on the different G α subunit isoform which is involved in the coupling, a different signaling pathway will be activated, leading to different, sometimes even opposite, functional effects. For example, it has been demonstrated that in HEK293 cells OTR coupling with G q stimulates cellular growth, while coupling with G i inhibits it (Rimoldi et al, 2003; Busnelli et al, 2012).

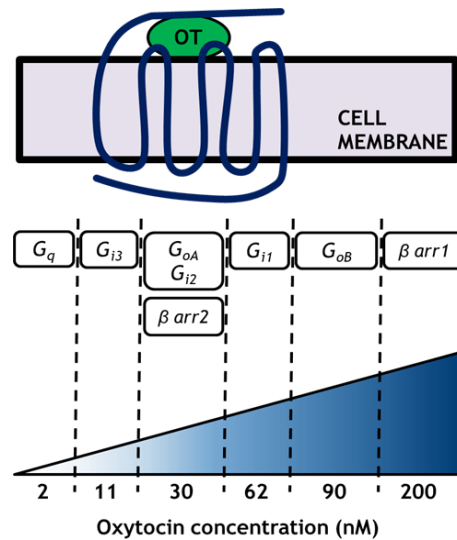


Figure 4: oxytocin promotes the activation of different G-protein subtypes depending on its extracellular concentration (reported in nM).

Following OT stimulation, the OTR is able to activate G q , G i (1, 2, 3 isoforms), and G o (G oA and G oB) G proteins. The discriminating factor that drives differential activation of one subtype over the other is OT concentration: a lower concentration leads to G q activation, while other G proteins are activated at values at least 10 times higher (Busnelli et al, 2012) (Fig. 4).

For this reason, the main pathway activated by the OTR is considered to be the G q -dependent one, that brings to the activation of the beta isoform of phospholipase C (PLC β). PLC β splits the membrane phospholipid phosphatidylinositol-4,5-bisphosphate (PIP $_2$) generating two second messengers: inositol-triphosphate (IP $_3$), that triggers the release of intracellular calcium deposits by binding to its receptors on the endoplasmic reticulum, and 1,2-diacilglycerol (DAG), that activates a protein-kinase C (PKC) and MAP kinases (MAPK) cascade (Fig. 5). MAPK cascade is the most important cellular effector activated by the OTR: out of the four known MAP kinase families (ERK1/2, p38 MAPK, c-Jun and ERK5; Sun e Nan, 2016), those that mediate OTR effects on social behaviour are of the ERK1/2 kind (Satoh et al, 2011). It is also known that OTR activation brings to cAMP-responsive element binding (CREB) phosphorylation, a signaling cascade that stimulates long-term potentiation (LTP) (Tomizawa et al, 2003). Moreover, the OTR/MEK/ERK signaling is also what mediates anxiolytic effects of OT (Blume et al, 2008; Jurek et al, 2012).

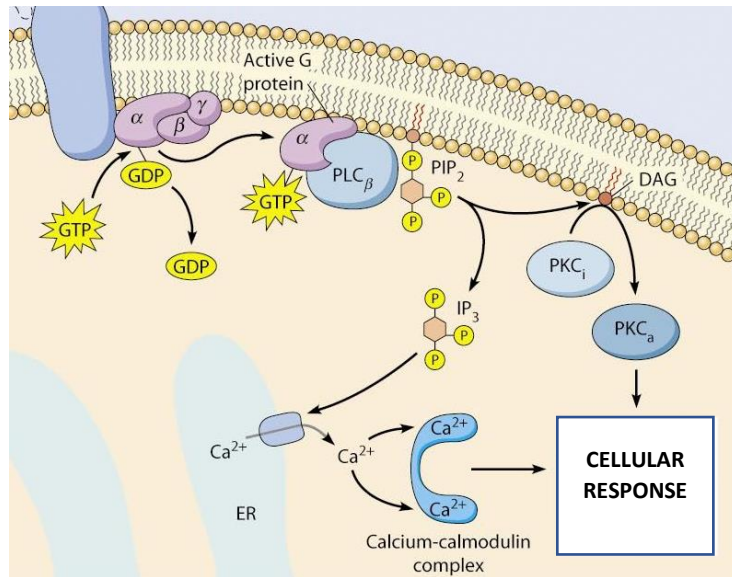


Figure 5: Gq-mediated signaling pathway. Gαq-activated PLC β catalyzes the hydrolysis of the phospholipid phosphatidylinositol 4,5-bisphosphate (PIP2) into diacyl glycerol (DAG) and inositol 1,4,5-trisphosphate (IP3). Both are second messengers that mediate different cellular responses. Copyright © Pearson Education, 2009 (adapted).

OTR activation also leads to nitric oxide (NO) production. In male rats, OT increases NO production in the PVN (Melis e Succu, 1997), and it can also have an antinociceptive effect by activating a neuronal NO synthase (nNOS) in dorsal ganglia roots, even if the activation mechanism of the synthase has not been elucidated yet (Gong et al, 2015).

Another crucial downstream effect of OTR activation is the regulation of the “GABA switch”. GABA switch is a process that occurs early during development. At this stage, GABA has a depolarizing effect, because intracellular chloride levels are much higher than the extracellular one, and therefore when chloride channels open chloride goes exits the cell, depolarizing it. Chloride concentration is normally regulated by two co-transporters, NKCC1 and KCC2; it is the down-regulation of NKCC1 (Cl⁻ importer) and the up-regulation of

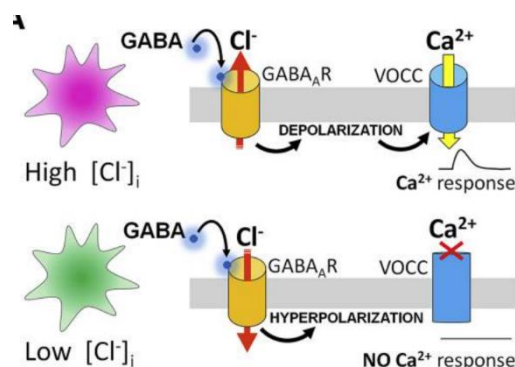


Figure 6: GABA switch. Intracellular Cl⁻ concentration determines the depolarizing or hyperpolarizing action of GABA during neurodevelopment. VOCC = Voltage-Opened Calcium Channels. (From Leonzino et al., 2016).

KCC2 (Cl⁻ exporter) that triggers this “switch”, and gives to GABA an hyperpolarizing action (Rivera et al, 1999) (Fig. 6).

In mice, the GABA switch occurs in the first postnatal week (Valeeva et al, 2013). OT is highly involved in the regulation of this process: in two animal models of autism, where the GABA switch had not occurred correctly, OT administration was able to correct the pathologic GABA phenotype (Eftekhari et al, 2014; Tyzio et al, 2014). In our laboratory we also observed a delay in the onset of GABA switch in neuronal cultures coming from OTR-KO mice, compared to WT cultures; in particular, our data indicate that OTR signaling is contribute to KCC2 upregulation (Leonzino et al, 2016).

Desensitization, internalization and other regulation mechanisms. Two of the most powerful regulators of OTR activity are the cholesterol content of the cellular membrane and the presence of divalent cations such as magnesium, zinc, nickel or manganese. Ions act modifying the binding pocket shape (Antoni and Chadio, 1989; Pearlmutter and Soloff, 1979) and inducing a conformational modification in the OT molecule itself, in order to make receptor binding easier (Liu et al, 2005). Cholesterol content regulates the fluidity of the cellular membrane, and participates in the formation of microdomains and lipid rafts that regulate the functionality of many membrane proteins (Zocher et al, 2012; Villar et al, 2016; Gimpl, 2016). Not only cholesterol can stabilize OTR’s affinity for OT, but it can even modify OTR’s signaling (Gimpl and Fahrenholz, 2002; Gimpl et al, 1995).

Another important regulation mechanism that modulates OTR activity is receptor internalization. To switch off the signal and prevent overstimulation, the OTR needs to be desensitized. In our laboratory we used HEK 293 cells expressing an EGFP-tagged OTR (OTR-EGFP) to follow the receptor after OT stimulation: we found that already after 15 minutes of OT administration the OTR is rapidly internalized, and is recycled on the plasma membrane after 4 hours (Conti et al, 2009).

OTR internalization is a fast process, that occurs in multiple steps. At first, the C-terminal tail of the activated receptor is phosphorylated by specific kinases called GRK (G-protein coupled kinases), or by the PKC itself (Grotegut et al, 2016; Hasbi et al, 2004; Smith et al, 2006). Such phosphorylation interrupts the coupling with the G protein and recruits the non-visual arrestins β -arrestin 1 and 2 to the plasma membrane. Arrestins are cytoplasmatic proteins that mediate receptor internalization throughout endocytosis; differently from the visual arrestins 1 and 4, that are only expressed in the retina, β -arrestin 1 and 2 are ubiquitous (Lohse & Hoffmann, 2014). Once a β -arrestin molecule is bound to the receptor, it promotes its internalization in clathrin-coated vesicles (Oakley et al, 2001) (Fig. 7). β -arrestins can also mediate signaling pathways on their own, the most important being the MAPK one (Shenoy e Lefkowitz, 2005).

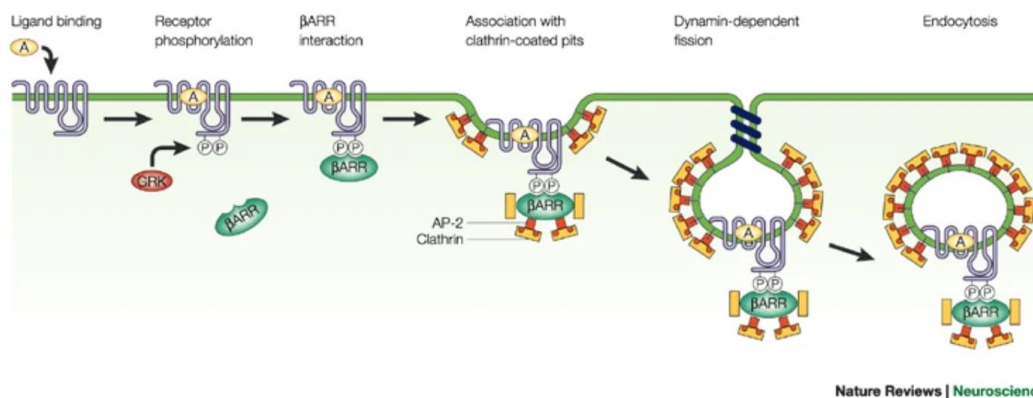


Figure 7: β -arrestin-mediated receptor internalization through clathrin-coated pits. Activated receptor is phosphorylated by a GRK, bound by a β -arrestin molecule and internalized in clathrin-coated vesicles. The interaction between β -arrestin and clathrin is mediated by the adaptor protein AP2. From Pierce and Lefkowitz, 2001.

In HEK293, the OTR recruits both β -arrestin 1 and 2, but has a higher affinity for the latter. Their interaction starts rapidly and continues until reaching a *plateau* (Busnelli et al, 2012). Despite having more than 70% of sequence homology, each one has its specific function in the regulation of GPCRs internalization and in intracellular signaling (Srivastava et al, 2015).

β -arrestin independent receptor internalization have also been described: for example, carbetocin, a Gq-selective agonist for the OTR, is able to induce receptor internalization with no detectable β -arrestin involvement. Receptors endocytosed through this mechanism are then degraded (Passoni et al, 2016).

Functional selectivity. Receptor activity can be modulated by the ligand itself. This phenomenon is quite common in GPCRs, and it's called "functional selectivity" or "biased signaling"; consequently, ligands that can promote the preferential activation of a certain signaling pathway over others are called "functional selective".

A few functional selective ligands have been identified for the OTR too; however, the mechanisms that regulate their mechanisms of action have not been elucidated yet. What we do know is that all the four intracellular loops take part to Gq/11 coupling and PLC interaction (Qian et al, 1998; Sanborn et al, 1998). Removal of the last 51 residues makes the receptor unable to couple to Gq, but it retains its ability to activate Gi (Hoare et al. 1999). It has been hypothesized that OT cyclic part (which is deeply inserted into the transmembrane portions) might be the one mostly involved in differential G protein activation, while the tripeptide tail that "sticks" out of the receptor would have a more marginal role (Postina et al, 1998; Favre et al, 2005).

In our laboratory we've identified three functionally selective ligands for the OTR: carbetocin, Atosiban and D-Nal-OVT (Busnelli et al, 2012; Passoni et al, 2016; Reversi et al, 2005) (Fig.8). Carbetocin is a Gq-biased OTR agonist with ansiolytic and antidepressants effects (Chaviaras et al, 2010; Mak et al, 2012). As it only activates Gq signaling, it can be considered a powerful tool to dissect Gq-mediated effects in the brain (Passoni et al. 2016). Atosiban is an agonist that selectively promotes only Gi3 coupling. Its main effects are the

inhibition of cellular proliferation (Busnelli et al. 2012; Reversi et al. 2005) and the induction of inflammation (Kim et al. 2016). D-Nal-OVT is a Gi1-biased agonist; its main effect is the inhibition of proliferation. A better understanding of how these molecules interact with the receptor to activate a specific G protein isoform would be useful not only in the research field, but also for the development of new therapeutic molecules.

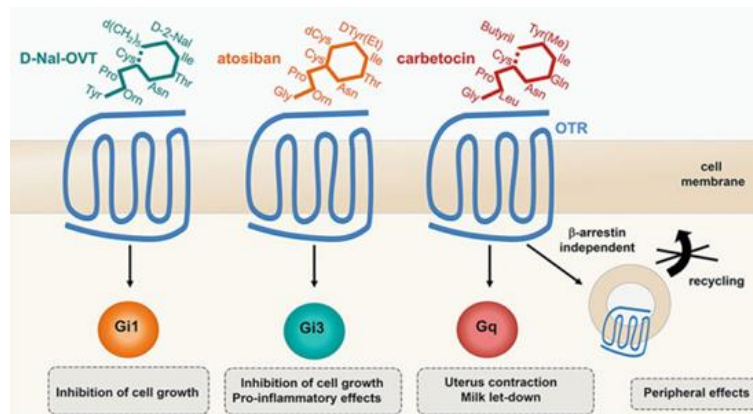


Figure 8: three functional selective ligands for the OTR (Busnelli and Chini, 2017).

Localization and developmental regulation. The OTRs is distributed both centrally and peripherally. In the periphery, it can be found in a variety of different organs, such as the uterus, ovaries, testicles, blood vessels, gut and adipose tissue (Freeman et al, 2014; Jurek & Neumann, 2018). In the central nervous system of rodents it is mainly localized in the olfactory network, in the amygdala, hippocampus, lateral septum and other areas of the limbic system. OTR localization in areas involved in the processing of olfactory stimuli is especially important in rodents (Freeman e Young, 2016), because olfaction is the main route through which they build the so-called “social memory”, the ability to recognize conspecifics inside a social group (Lee et al, 2009). OTR expression begins early during development; in the cortical brain regions, its peak coincides with critical postnatal developmental windows for social learning (Hammock et al, 2013, 2016; Grinevich et al, 2015). In rodents, postnatal receptor distribution has been mapped by means of autoradiographic studies (Hammock and Levitt, 2013) and immunohistochemistry (Mitre et al, 2016). Newmaster et al showed that in postnatal mouse brains OTR distribution pattern changes rapidly in time and localization (Newmaster et al, 2020). Such rapid and temporized expression patterns suggest that oxytocin signaling is important for initial network organization and/or refinement (Vaidyanathan and Hammock, 2016).

3.3 THE OXYTOCINERGIC SYSTEM IN NEURODEVELOPMENTAL DISORDERS

3.3.1 Neurodevelopmental disorders: pathogenesis and animal models

Neurodevelopmental disorders (NDDs) are a class of genetic diseases and syndromic conditions all associated with the disruption of brain development. Affecting 3% of children worldwide (Glissen et al, 2014), NDDs constitute a serious health problem (Parenti et al, 2020). Most NDDs have a childhood onset, and cause delays in developmental domains such as social and adaptive behaviour, cognition, learning and memory (May et al, 2019).

NDDs include autism spectrum disorder (ASD), intellectual disability (ID), attention deficit hyperactivity disorder (ADHD), and epilepsy; schizophrenia is increasingly considered to have neurodevelopmental origins, even though symptoms typically appear in late adolescence or early adulthood (Rapoport et al, 2012). These conditions can exist as diseases on their own, co-exist in the same patient (Ronald et al, 2008; Matson et al, 2013) or they can be associated to more complex genetic syndromes (Bennet et al, 2015; Dykens et al, 2011; Percy, 2011).

In recent years it has become increasingly clear that NDDs have a multifactorial origin. In their pathogenesis are often involved genetic alterations, but also hormones and environmental risk factors (stress, contaminants/drug exposure...) (May et al, 2019). One interesting point is the involvement of gender in NDDs: males have a two to four times higher probability than females to develop NDDs (Christensen et al, 2018; May et al, 2017). Although several possible explanations for this phenomenon have been proposed, the underlying molecular mechanisms that are responsible for this gender bias are not known yet (May et al, 2019).

Different types of mutation have been associated with NDDs, including chromosomal rearrangements, copy number variations (CNVs), small insertions and deletions, and point mutations (Parenti et al, 2020; Wilfert et al, 2017; Alonso-Gonzalez et al, 2018). Despite some NDD-causative genes have actually been identified (as for example in Mac Pherlan Syndrome), many individuals with NDDs still do not receive a molecular diagnosis. In imprinting-caused NDDs, such as Prader-Willi and Angelman syndromes, or in large deletions/insertions, the genomic region that is involved comprehends different genes, and therefore the individuation of a single candidate is often difficult. Genes identified as responsible for ASD are involved in synaptic transmission, chromatin remodeling, cell proliferation and differentiation (Cardoso et al, 2019).

Environmental factors have an important role in NDDs pathogenesis too. The strongest correlation between environment and the development of NDDs is with *in utero* damage and poor quality of maternal care. During pregnancy there is a wide array of insults that can impair brain development in the fetus (Marco et al, 2011), such as maternal immune activation (Solek et al, 2018), maternal obesity (Edlow et al, 2017) or drug assumption (Black et al, 1993; Kwok et al, 2020).

It is important to notice that the timing of the environmental stimulus influences differently the phenotypic outcome, and that also other perinatal risk factors, as obstetrical complications, preterm birth or caesarean birth, may increase the vulnerability to neurodevelopmental disorders (Boog et al, 2004; Curatolo et al, 1995). Recently, autoimmunity has been pointed at as another potential risk factor for NDDs, and in particular for

autism. Many independent studies highlighted abnormal cytokines responses, immune cells unbalances, neuroinflammation and the presence of autoantibodies in individuals with autism spectrum disorders (Hughes et al, 2018).

Autism. Out of all NDDs, autism spectrum disorder is the most frequent and heterogeneous condition. Under the umbrella term of Autism Spectrum Disorder indeed falls a number of behavioural and cognitive phenotypes characterized by different clinical manifestations and gravity. The autistic condition was originally described by Kanner and Asperger in the 1930s. However, the diagnostic criteria were not codified until the 1994 Diagnostic and Statistical Manual of Mental Disorders (DSM). An ASD diagnosis can be formulated evaluating a patient on two core domains of symptoms: i) impairments in social interaction and social communication, and ii) restricted repetitive patterns of behaviors, interests, and activities. (American Psychiatric Association, 2013). In these two categories falls an extremely wide range of pathological traits such as impairments in social interactions, hyper or hyporesponsivity to environmental stimuli, obsessive-compulsive and repetitive behaviours. Together with these more behavioural phenotypes, other frequently associated symptoms include intellectual disability, seizures, anxiety, attention-deficit hyperactivity syndrome, sleep disruption and gastrointestinal distress (Bauman et al, 2019). During the last 40 years, autism prevalence has increased from estimates of roughly 0.5–1.0:10 000 in the eighties to more than 1:100 in 2018 (Biao et al, 2018; Fombonne, 2009, 2018).

Autism can be considered as a condition on its own, but it is also often associated with other neurodevelopmental syndromes, such as Prader Willi (Dykens et al, 2011;), Phelan McDermid Syndrome (Soorya et al, 2013) and Fragile X Syndrome (Niu et al, 2017; McDuffie et al, 2015). A recently discovered Prader-Willi-like syndrome, called Schaaf-Yang Syndrome (SYS), despite sharing many phenotypic traits with PWS is characterized by a higher prevalence of autism spectrum disorders (Negishi et al, 2019).

There are multiple evidences that ASD has a genetic, heritable component. Monozygotic twins have 60–90% concordance rate, and the prevalence among siblings with autistic disorder ranges from 2-6% to 14% (Charman et al, 2017; Huguet et al, 2016; Messinger et al, 2015; Robin and Shprintzen, 2005; Rosenberg et al, 2009; Tick et al, 2016). However, the pathogenesis of ASD often involves multiple genes belonging to different molecular categories (De Rubeis and Buxbaum, 2015; Ramaswami and Geschwind, 2018; Talkowski et al, 2014; Wilfert et al, 2017; Woodbury-Smith and Scherer, 2018).

The environment also plays a fundamental role in the pathogenesis of autism. Environmental factors can alter gene expression through epigenetic modifications, and exposure to harmful environmental factors can change the expression of developmental key genes in critical periods of embryo formation, increasing the risk of developing neurodevelopmental disorders later in life. Parental age, maternal health condition, exposure to certain drugs and medications, complications during delivery and poor maternal care are all associated with a higher risk for the offspring to develop ASD (Karimi et al, 2017).

Despite the wide variety of possible causes, some basic neurobiological processes involved in the pathogenesis of ASD are believed to be, at least in part, common (Voineagu et al, 2011; Gilman et al, 2011). The

individuation of such common, overlapping pathogenic pathways that lead to NDDs, as well as reliable and specific biomarkers for these diseases, are two key points for the development of specific and effective therapies (McPartland, 2016).

3.3.2 Animal models to study autistic-like correlates

The complex phenotypes observed in autism are impossible to be reproduced in animal models. Nonetheless, animal models showing relevant endophenotypes are useful research tools to test hypotheses about their pathogenesis, and to discover effective and targeted therapies. An ideal animal model for ASD should provide: (1) *face validity*, that should mimic the highest possible number of phenotypes that are typical of the human disease; (2) *construct validity*, that is, it should contain the hypothesized pathogenetic element (i.e., genetic mutation, environmental stimulus etc.); (3) *predictive validity*, meaning that the specific pharmacological treatments that are usually effective in human should be equally effective in the model (Crawley, 2012). Mice, rats and non-human primates are the species currently employed to study ASD.

Mouse models of neurodevelopmental disorders obtained through genetic manipulations include KO and knock-in humanized animals. They can be grouped on the basis of the function of the gene involved:

- 1) Synaptic genes such as neuroligins, *Shank3*, *Cntnap2*. This class of proteins regulates the connections and transfer of information between pre- and postsynaptic terminals in neurons.
- 2) Signaling and regulatory proteins such as *Fmr1*, *Mecp2*, *Foxp2*, *Pten*, *Magel2*
- 3) Genes that encode for neurotransmitters and receptors, such as AVP and AVPR, OT and OTR, 5HT1B, GluN3A (Crawley, 2012).

Neuroligins are a family of adhesion molecules. In humans, NLGN3 deletion is associated with non-syndromic ASD (Jamain et al, 2003; Ylisaukko-oja et al, 2005; Levy et al, 2011; Sanders et al, 2011; C. Yuen et al, 2017). Neuroligin2-deficient KO mice displayed normal social behaviours but higher levels of anxiety-like behaviours than WT controls (Blundell et al., 2009). Male mice lacking Nlgn3 are socially submissive to their WT littermates, and show increased anxiety; Neuroligin2-overexpressing transgenic mice also displayed higher anxiety-like behaviours, along with stereotyped jumping, enlarged synaptic contact sizes in the frontal cortex and reduced GABA receptor clustering in retinal circuitry (Hines et al, 2008; Hoon et al, 2009).

The *Shank3* gene encodes a key postsynaptic density (PSD) protein, present in glutamatergic synapses. It is involved in the pathogenesis of a number of neurodevelopmental disorders such as autism spectrum disorders (ASDs), Phelan-McDermid syndrome (PMS) and different kinds of intellectual disabilities. Both rats and mice have been successfully used to develop reliable models of these diseases; Shank3-KO mice display high levels of repetitive self-grooming and social deficits in some mutant lines (Chang et al, 2016; Dhamne et al, 2017; Jaramillo et al, 2017; Peca et al, 2011; Wang et al, 2011; Yang et al, 2012). Shank3-KO rats display impairments in synaptic function and plasticity; at the behavioural level, they show an impaired social memory,

but not impaired social interaction. Learning and memory alterations, anxiety, increased mechanical pain threshold and decreased thermal sensation were also observed in this model (Song et al, 2019).

Cntnap2 encodes a neuronal member of the neurexin superfamily; it is responsible of K⁺ channels clustering in myelinated axons, and it is also involved in neuron-glia interactions (Poliak et al, 1999; 2003). It has been found to be linked to autism spectrum disorder and cortical dysplasia–focal epilepsy (CFDE) syndrome (Feliciano, 2011). The *Cntnap2*^{-/-} mouse is a robust model of ASD: *Cntnap2*^{-/-} mice show deficits in the core ASD behavioral domains, as well as hyperactivity, stereotypic motor movements, reduced isolation-induced ultrasonic vocalizations, and epileptic seizures. Moreover, neuropathological and physiological analyses revealed neuronal migration abnormalities, a reduced number of interneurons and an abnormal neuronal network activity (Penagarikano et al, 2011).

Fmr1 encodes the Fragile X mental retardation protein (FMRP), which is important for early neural development. As in FXS the expression of this protein is completely silenced, the observed phenotypes include intellectual disability, autism and autism-related behaviours (Hagerman et al, 2009; Hernandez et al, 2009). In particular, because of the high incidence of ASD in FXS, the mouse model that recapitulates FXS is highly relevant to research on autism. *Fmr1*-KO mouse displays impaired learning and memory, poor motor performance, hyperactivity and altered social interactions (Mineur et al, 2006; Spencer et al, 2008). Interestingly, it has been demonstrated that FXS is potentially reversible, because inserting a FMR1 human transgene in these mouse model rescues the pathologic phenotype (Spencer et al, 2008).

The *MECP2* gene codes for methyl-CpG binding protein 2 (MECP2), a transcriptional repressor (Chahrour et al, 2008). Mutations in this gene cause an X-linked dominant neurodevelopmental disorder called Rett Syndrome (RTT). *Mecp2* mutations are rare in ASD, but single nucleotide polymorphisms (SNPs) around MECP2 may increase the risk to develop autism (Loat et al, 2008). In addition, reduced MECP2 expression is observed in 79% of autism cortex samples and correlated with increased MECP2 promoter methylation in autistic males (Nagarajan et al, 2006; Samaco et al, 2004). Little information is available concerning social behaviours in RTT model mice, except for *Mecp2*^{308^y}, which has been reported to show low social motivation, reduced social interaction (Moretti et al, 2005) and deficits in spatial memory (Stearns et al, 2007). RTT mouse models in this case have been extremely useful to test experimental genetic and pharmacological therapies to bypass or reverse the effects of *MECP2* mutations.

Despite most studies have been focused on male mice only to avoid the genetic variability caused by the X chromosome inactivation in females, some studies conducted on heterozygous *Mecp2* females (*Mecp2*^{+/-}) demonstrated that even these mice recapitulate many behavioural deficits observed in RTT (such as breathing defects, alterations in social approach behaviour and in contextual fear memory, etc.; Samaco et al, 2013) as well as molecular alterations typical of the syndrome (Krishnan et al, 2017).

Mage12 is a maternally imprinted gene located in the PWS locus (15q11–15q13) (Fountain and Schaaf, 2016), that encodes for a protein which is part of a large ubiquitination complex, involved in the most diverse cellular processes: in mouse models, it regulates the cell cycle, neuronal signal transduction, neurite growth, and

muscle function (Mejlachowicz et al, 2015). Mutations in the paternal copy of this gene have been found in patients with a Prader-Willi-like disorder, called Schaaf-Yang Syndrome (SYS). Despite sharing many phenotypical traits with PWS, SYS patients also present some unique pathological traits, the most important of those is a high prevalence of ASD (Schaaf and Yang, 2013). For this reason, the Magel2-KO mouse is a valuable model to study autism in neurodevelopmental disorders.

Other frequently altered genes in ASD and neurodevelopmental disorders encode for neurotransmitters, neuropeptides and their receptors. Many neurotransmitters/neuropeptides are critically involved in neurodevelopment, contributing to shape neuronal networks that will regulate behaviour in the mature brain (Marder, 2012; Nusbaum and Blitz, 2012).

A crucial process in neurodevelopment is the excitation/inhibition imbalance, mediated by GABA transporters and glutamate receptors. Autistic patients show significant variations of GABAAR in different brain areas involved in behaviour (Fatemi et al, 2009, 2014); in two mouse models of autism, Heise et al found deregulations of different subtypes of glutamate receptors in the striatum and in the thalamus, as well as a downregulation of GABA receptors in several brain regions. Interestingly, the mutation of different genes (*Shank2*^{-/-}, *Shank3αβ*^{-/-} and *Cttn4*^{-/-} in this specific study) leads to different (in some cases even opposite) receptor rearrangements throughout the brain; this means that, at least for what concerns GABA and glutamate receptors, it is not possible to define a common molecular phenotype that would be typical of autism (Heise et al, 2018).

Other neurotransmitter systems that have been found to be deregulated in autism include the dopaminergic (Scott et al, 2004; Ditcher et al, 2012), the serotonergic (Tanaka et al, 2018) and the histaminergic one (Wright et al, 2017). As many of these molecules often collaborate to regulate the same downstream pathways, it is very likely that alterations affecting one of them might have repercussions on the others too.

Non genetic models. As it is becoming increasingly clear that autism pathogenesis is complex and obscure, and not exclusively based on genetic alterations, animal models that develop an autistic-like phenotype have been obtained also through exposure to environmental or chemical stimuli.

An example of non-genetic cause of ASD is Maternal Immune Activation (MIA). The connection between an activation of the maternal immune system during pregnancy and neurodevelopmental disorders in the offspring has been convalidated by several studies (Knuesel et al, 2014). MIA can be triggered by a number of possible factors, and it doesn't necessarily involve a specific pathogen; it can be caused by any external damage capable of disrupting normal brain development.

Since the placenta is a source of hematopoietic stem cells for the fetus (Gekas et al, 2005), it has been suggested that maternal infection may permanently modify the immune system of the offspring and consequently alter the immune status of the fetal brain (Patterson, 2009).

MIA can be elicited through different approaches, such as the injection of immune stimulating agents (influenza virus, RNA, LPS). The offspring of pregnant mice experiencing respiratory infection show deficits in social interaction, reluctance to interact with a novel object and increased anxiety (Shi et al, 2003). In the

offspring cerebellum, MIA causes a localized loss of Purkinje cells, which is a neuroanatomical trait typical of autism (Shi et al, 2009). Moreover, MIA was shown to cause a delay in a process which is fundamental for neurodevelopment, the GABA “switch” from an excitatory to an inhibitory neurotransmitter (Corradini et al, 2018).

Another widely used non genetic model is the valproic acid (VPA)-exposed mouse, a well-known teratogen agent. In humans, exposure to VPA during the first trimester of life can cause defects in neural tube formation and development, a generalized delay in neurodevelopment, verbal impairments and also autism (Nicolini et al, 2018). The pathological mechanism of action is not entirely known; however, it has been observed that, in mice exposed to VPA during the first trimester of gestation, postnatal autistic behaviours are often associated with an increase in H3 and H4 histones hyperacetylation that appear during a window of time which is critical for mouse brain development (Kataoka et al, 2013; Moldrich et al, 2013). Behavioural phenotypes of this model recapitulates different behavioural patterns typical of autism. For this reason, the valproic acid mouse model is one of the most reliable to study the molecular mechanisms underlying autism pathogenesis, because it provides both construct and face validity (Nicolini et al, 2018).

There are also growing evidences of how autoimmunity, intended as any kind of immune response directed towards self antigens, can cause autism. In particular, patients with autism often produce autoantibodies against central nervous system self-proteins (Wills et al, 2007) and some mothers who have autistic children produce autoantibodies against fetal brain proteins (Braunschweig et al, 2008). Therefore, several animal models have been developed to evaluate pre and postnatal exposure to potentially pathogenic antibodies. Seven antigen proteins have been identified (Edmiston et al, 2018).

3.3.3 The oxytocinergic system in mouse models of neurodevelopmental disorders

Being a pro-social peptide, oxytocin has been extensively studied as a potential therapeutic molecule to correct behavioural deficits. (Guastella and Hickie, 2016; Wagner and Harony-Nicolas, 2017). Indeed, many alterations of the oxytocinergic system have also been reported in many models of neurodevelopmental disorders (Table 1), indicating that other than being a cure oxytocin could also be implicated in their pathogenesis.

RODENT MODEL	OT PHENOTYPE	REF.	RESCUE AFTER OXT ADMINISTRATION
OT-KO	↓ OT production and/or release	Ferguson et al, 2000	Rescue of deficits in social memory
OTR-KO (mouse, prairie vole)	No OTR expression	Takayanagi et al 2005; Sala et al, 2011, 2013; Horie et al, 2018	Rescue by OT and AVP by activation of vasopressin V1a receptors
CD38-KO	↓ OT production and/or release	Higashida et al, 2011 Jin et al, 2007	Rescue of social memory and maternal care
CD157-KO	↓ OT in cerebrospinal fluid	Gerasimenko et al, 2020	-

Magel2-KO	↓ OT production and/or release	Meziane et al, 2015; Schaller et al, 2010	Prevention of social behaviour deficits in adult age; rescue of lethal feeding behaviour
Maged1-KO	↓ Mature OT production and/or release in hypothalamus	Dombret et al, 2012	Rescue of deficits in social memory
Cntnap2-KO	↓ OT production and/or release	Penagarikano et al, 2015	Rescue of social deficits
Necdin-deficient	↓ OT-producing neurons in hypothalamus	Muscatelli et al, 2020	-
Shank3-KO (rat, mouse)	Not examined (rat), ↓ OT neurons in the PVN (mouse)	Harony-Nicolas et al, 2017; Song et al, 2019; Sgritta et al, 2019	Rescue of attention, social recognition memory, synaptic plasticity (rat); rescue of social deficits; rescue of LTP impairment in VTA dopaminergic neurons (mouse)
Oprm1-KO	↑ OTR expression in AONm, CeA, MeA, NAcc	Gigliucci et al, 2013	Rescue of social impairments
Neurologin-3-KO	Impaired oxytocin signaling in dopaminergic neurons	Hörnberg et al, 2020	-
Reelin^{+/-}	↓ OTR expression	Liu et al, 2005	-
Peg3-KO	↓ OTR expression in MPOA and LS	Champagne et al, 2009	-
GluN3A-KO	↓ OTR expression in PFC;	Lee et al, 2018	Rescue of social activity deficits
5-HT1B-KO	-	Lawson et al, 2016	Rescue of social novelty preference in mice treated with a 5-HT1B agonist; Attenuation of 5-HT1B agonist-induced sociability and rearing deficits
Tet1-KO	↓ OTR mRNA in hippocampus	Aaron et al, 2018	-
Grin1-KO	Not examined	Teng et al, 2016	Reversal of hyperactivity but not of impaired sensorimotor gating; subchronic treatment rescues the impaired social preference
Stx1a-KO	↓ OT expression in CSF; ↓ OT release in amygdala	Fujiwara et al, 2016	Restoration of social memory
BTBR T+ tf/J	↑ OT production and/or release	Silverman et al, 2010	-
C58/J	Not examined	Teng et al, 2016	Increase of sociability and rescue of repetitive stereotypy in adolescent mice
BALB/cByJ	Not examined	Moy et al, 2019	Rescue of sociability deficits, social preference (OT metabolite)

			4-9; no rescue by sintetic OTR agonists)
5-MT treatment	↓ OT production and/or release in the PVN	Whitaker-Azmitia, 2005	-
Valproate treatment (mouse, rat)	↑ OT and OTR expression (Stefanik); ↓ OT production and/or release (Dai)	Stefanik et al, 2015; Dai et al, 2018; Wang et al, 2018; Sgritta et al, 2019	Rescue of social interaction and social preference deficits (Wang, Sgritta); restoration of social preference (Dai)
MIA (Maternal Immune Activation)	↑ OTR expression	Minakova et al, 2019	Rescue of sociability
mHFD (Maternal High Fat Diet – induced obesity)	↑ OTR mRNA in the hippocampus of male, but not female, GD 17.5 offspring	Glendining et al, 2019	-
HFD (High Fat Diet) induced obesity	↓ OTR in hypothalamus and hippocampus	Hayashi et al, 2020	Rescue of impaired object recognition memory and impaired object location memory

Table 1: animal models of neurodevelopmental disorders showing oxytocinergic system involvement. Where not stated otherwise, the animal is a mouse.

OT-KO and OTR-KO mice display a strong autistic-like phenotype: OT-KO mice display social amnesia (Ferguson et al, 2000) and high aggressivity levels (Takayanagi et al, 2005), while OTR-KO mice display a deficit in social discrimination (Takayanagi et al, 2005). In addition, OTR-KO mice adult males are highly aggressive and display impaired cognitive flexibility and a higher susceptibility to seizures (Sala et al, 2011). Interestingly, heterozygous OTR mice show only some of the impairments observed in the KO mice. An autoradiographic analysis revealed that these mice have 50% less OTR in their brain; therefore, this model demonstrates that OTR acts as an haploinsufficient gene, because a partial reduction in its expression is sufficient to compromise the phenotype. While a partial reduction in receptor levels is enough to impair social behaviour, defects in aggressivity and cognitive flexibility require its complete inactivation (Sala et al, 2013). Importantly, in both models OT administration is able to rescue the observed alterations, at least at the behavioural level.

OT alterations. Alterations of circulating oxytocin or in oxytocin mRNA levels have been reported in a number of different animal models. In the CD38 KO mice, that recapitulates many behavioural defects of OTR KO and OT KO models, lower plasmatic OT was detected (Jin et al, 2007). The same decrease is found in the previously mentioned *Cntnap2*-KO mouse (Penagarikano et al, 2015), while in other models like in the Shank3 KO mouse and the Necdin-deficient mouse are OT-producing neurons that decrease (Muscatelli et al, 2000; Sgritta et al, 2019). In the *Maged1*-KO as well as in the *Maged2*-KO mice, by using antibodies that could

discriminate between mature and immature OT, it has been possible to observe a severe impairment in the maturation of the peptide, and consequently an accumulation of immature oxytocin in some brain areas (Meziane et al, 2015; Schaller et al, 2010; Dombret et al, 2012). Importantly, restoring normal OT levels was effective in rescuing the pathologic behavioural phenotypes observed in these animals.

OTR alterations. Consistent variations in oxytocin receptor quantities have also been detected. While in *Oprm1*^{-/-} and in various environmentally-induced autism mouse models protein and/or mRNA levels were found to be increased (Gigliucci et al, 2014; Minakova et al, 2019; Glendining et al, 2019), in others, like in *GluN3A* and *Tet1*-KO mice, the opposite trend was observed (Lee et al, 2018; Aaron et al, 2018). In most of these cases, variations were present in areas linked to social behavior (Gigliucci et al, 2014; Glendining et al, 2019; Hayashi et al, 2020; Aaron et al, 2018). Behavioural phenotypes of all these models include traits typical of ASD, and most importantly, different therapeutic approaches, all based on OT somministration, proved to be effective in restoring a normal social behaviour.

3.4 GPCR DIMERS IN BRAIN PATHOLOGY

3.4.1 GPCR dimerization: an overview

The quaternary structure of GPCRs is a topic of very active research and accumulating evidences indicate that receptors that belong to different GPCR classes have different quaternary structures.

Receptors that belong to Class A (Rhodopsin like), the most numerous GPCRs subfamily after the odorant receptors, were generally thought to exist mostly in monomeric form. However, growing evidence from different experimental approaches is strongly indicating that these receptor can form dimers or even higher-order oligomers (Lohse, 2009). On the contrary, receptors that belong to Class C receptors (metabotropic-like) have been shown to exist as dimeric entities.

GPCR dimers are a receptor population that is quite difficult to study, as dimerization is often a transient and fast process; moreover, many of the studies are performed using non adequate techniques, or strongly manipulated cells and/or molecules (i.e., transfected cellular cultures; Calebiro et al, 2013; Kasai et al, 2018). Determination of the proportion between dimeric and monomeric populations is therefore a difficult task to achieve (Milligan et al, 2019).

Dimerization has crucial implications for GPCRs functionality. Evidences suggest that both homo and heterodimeric complexes acquire peculiar pharmacological properties that the monomeric forms of the receptor do not have: for example, association of two or more protomers can modify the affinity of one of them for its ligand, enhancing or reducing it through positive or negative cooperativity mechanisms (Rivero-Müller et al, 2013), or it could even create new binding sites for other molecules (Heineke et al, 2009). Some GPCRs, as the GABAB receptor, function as “obligate dimers”, as they can function properly only if they are in the dimeric state (White et al, 1998; Robbins et al, 2001). Dimerization has also been shown to modify other crucial features of GPCRs, such as their cellular trafficking, their signaling properties and internalization rates (Lohse, 2009; Binder et al, 1990). For example, while the monomeric D1 dopamine receptor signals through

Gs activation and the monomeric D2 through Gi activation, D1/D2 heterodimers signal mainly through Gq (Lee et al, 2004). Studies on dopamine D2 receptor homodimers also revealed that in this complex the minimal functional unit is composed by two receptors and one G protein.

3.4.2 GPCR dimers in brain pathology

Alterations of GPCR dimerization might be linked to neurodevelopmental, neurodegenerative and psychiatric conditions.

In schizophrenic patients, an abnormal dimerization between 5-HT_{2A} and mGluR2 receptors seems to be involved in the generation of cortical dysfunction (González-Maeso et al, 2008). Another receptor family whose dimerization mediates pathologic effects in schizophrenia is the one of dopamine receptors: an alteration in the sensibility of a D1-D2 heterodimer in the globus pallidus of schizophrenic patients and in the striatum of a rat model of schizophrenia seems to cause a pathologic increase in the calcium signaling in these regions (Perreault et al, 2010). Another receptor often involved in different cerebral pathological processes in the CNS is the 5-HT₇ receptor: in fact, some of the contradictory data obtained in studies conducted on 5-HT₇ KO mice (that develops depressive-like and anxiogenic behaviors during adulthood) could be explained through receptor dimerization (Matthys et al, 2011). In brains of Alzheimer patients, Abdalla et al reported abnormal aggregation of angiotensin AT₂ receptors, thus extending the pathologic relevance of GPCR aggregation to neurodegenerative diseases (Abdalla et al, 2009). Abnormal GPCR dimerization has also been reported in a rat model of neuropathic pain: in these animals, an increased dissociation of GABAB1 heterodimers by 14-3-3 ζ leads to impairment of GABAergic inhibitory signaling. This study in particular is a good example of how the study of GPCR dimers can have a positive outcome on pathologic phenotypes, because disrupting the interaction between 14-3-3 ζ and the GABAB1 receptor restored a functional inhibitory signaling (Laffray et al, 2012).

A better understanding of GPCR homo and heterodimers localization, as well as of their structural and functional properties, would certainly represent a great step towards the design of new therapeutic approaches. However, the lack of proper methodologies to investigate GPCR dimerization in native environments leaves important gaps in this research field.

OTR dimerization. The OTR, just like many others Class A GPCRs, can form oligomeric complexes with peculiar structural and functional properties (Cottet et al, 2010). It can both homodimerize with other OTRs or form heterodimers with other GPCRs, such as the vasopressin V1aR and V2R receptors (Devost and Zingg, 2003; Terrillon et al, 2003).

Dimerization seems to occur already during receptor synthesis (Terrillon et al, 2003) leading to the formation of a stable fraction of dimeric complex at the cell surface, as confirmed in our laboratory (Busnelli et al, 2016). OTR homodimers have been detected *in vivo*, in mammary glands of lactating rats, thus confirming their existence in physiologic endogenous environments (Albizu et al, 2010). The existence of endogenous dimeric

form of OTR has also been shown by the use of bivalent ligands, as we will discuss in the following section (Bunelli et al, 2016).

OTR's association with other GPCRs generates heterodimers that often activate a broader range of signaling pathways. For example, it has been demonstrated that in myometrial cells OTR- β 2-AR heterodimers formations can act as a regulation mechanism to modulate ERK1/2 activation (Wrzal et al, 2012). When in complex with D2 *in vitro* it is able to preferentially promote CREB, MAPK and PLC signaling pathways. *In vivo*, D2/D3 antagonists blocked the anxiolytic effects of OT injections in mice. Alterations of the dimerization state of these structures might lead to the development of anxiety (Romero-Fernandez et al, 2013; De la Mora et al, 2016). OTR and the serotonin receptor 5-HT_{2A} have been detected *ex vivo* in brain regions normally associated with cognition and social behaviour using Proximity Ligation Assay (PLA); at the functional level, association in heterodimers reduces the potency and the efficacy of both carbetocin and WAY267464 on OTR-mediated Gq signaling, and has an attenuating effect also on 5-HT_{2A} activation by its endogenous agonist, 5-HT. Heterodimerization is also able to modify cellular trafficking of the two receptors (Chruścicka et al, 2019).

Although not extensively studied yet, oxytocin receptor dimers seem to play an important role in this field too. In our laboratory we gave an important contribution to this topic: we developed two bivalent ligands able to target OTR homodimers specifically, and through them we could demonstrate that selective stimulation of this receptor population has a rescuing effect on pathological behaviours in two animal models of autism. This is a strong proof not only of the existence of OTR homodimers in endogenous tissues, but also of their involvement in the regulation of behaviour (Busnelli et al, 2016).

4. PHARMACOLOGICAL INVESTIGATION OF OXYTOCIN RECEPTOR DIMERS BY BIVALENT LIGANDS

4.1 INTRODUCTION

In our laboratory, we previously designed a series of bivalent ligands to specifically target OTR homodimers. These ligands are formed by two OT analogues (dOTK) linked by carboxylic spacers of different lengths, to allow their specific binding to dimeric receptors.

Previous work in Dr. Chini's laboratory indicates that two molecules, dOTK₂-C8 and dOTK₂-C10, were able to induce Gq coupling at a concentration 1000 times lower than the monomeric dOTK, thus acting as "superagonists". Moreover, it was demonstrated that this phenomenon also occurs *in vivo*, because in mice and zebrafish models presenting social behaviours deficits these two ligands were able to rescue the pathologic phenotypes at a concentration respectively 100 and 40 times lower than their monomeric counterpart. By molecular modelling and site directed mutagenesis, it was also showed that the particular shape of these ligands allows them to exploit a channel passage in the homodimer upper part to insert their carboxylic spacer. (Busnelli et al, 2016).

During the first part of my PhD project, I completed the pharmacological characterization of this series of analogues, in particular to identify their possible functional selectivity or other peculiar signaling properties.

4.2 CONTRIBUTIONS

In this study, I performed all the BRET assays and fluorescence microscopy experiments, and contributed to the statistical analysis of the obtained data.

4.3

Oxytocin receptor homobivalent ligands untangle homodimeric receptor specific signaling

Francesca Santini^{1,2}, Alessandro Gori³, Bice Chini² and Marta Busnelli²

¹ Department of Medical Biotechnology and Translational Medicine, Università degli Studi di Milano, Milan, Italy 20129; ² CNR, Institute of Neuroscience, Milan, Italy 20129; ³ CNR, Istituto di Chimica del Riconoscimento Molecolare, Milan, Italy 20131

ABSTRACT G protein-coupled receptors (GPCRs) are the largest and most diverse group of membrane receptors that function to regulate a wide range of physiological functions. Increasing evidence has shown that GPCRs may form functional dimers and even higher-order oligomers. Despite it has been extensively demonstrated that the interaction of two receptors of different families, to form heterodimers, can influence various aspects of GPCR function, including ligand binding, G protein coupling, signaling and receptor trafficking, the functional effects of homodimerization are largely unknown.

We used the oxytocin receptor (OXTR), known to form homodimers *in vitro* and *in vivo*, to study the pharmacological properties of GPCR homodimers and we applied homobivalent ligands (dOTK₂-Cn), as chemical probes.

Using BRET biosensors, designed to measure the activation of specific G α protein subtypes and the recruitment of β arrestins, we found that, differently from the endogenous ligand oxytocin that activate Gq, Gi1, Gi2, Gi3, GoA and GoB, the bivalent ligands activated only a subset of G protein complexes, i.e. Gq, Gi2 and Gi3. In addition, they potentiate β arrestins recruitment, possibly inducing or stabilizing OTR conformations with an increased affinity for β arrestins.

These bivalent compounds, by activating specific OTR down-stream signaling pathways, thus represent molecules with very peculiar selective profiles that could be exploited to treat specific neurodevelopmental and psychiatric conditions.

INTRODUCTION

Oxytocin (OT) is a small nonapeptide produced in the hypothalamus, which in mammals controls

many functions in reproduction and in all the aspects of social behavior, facilitating the processing of social information, improving cognitive empathic abilities and increasing interpersonal trust (Grinevich, Knobloch-Bollmann et al. 2016). To exert its functions, OT binds to its receptors (OTRs) that are expressed in many different organs and tissues, with particularly high concentrations in the limbic regions of the brain, spinal column, heart, intestines, immune tissue, uterus and breast (Zingg and Laporte 2003). OTRs are seven-helix transmembrane receptors and belong to the rhodopsin-type I (Class A) G protein-coupled receptor (GPCR) superfamily (Busnelli and Chini 2018).

As many other GPCRs, OTR can couple to and activate different G protein subtypes and β -arrestins, initiating different intracellular signalling pathways (Busnelli, Sauliere et al. 2012). OTR-Gq/11 and OTR-Gi/Go coupling were investigated in various cell systems and it was demonstrated that, depending on the cellular context and the cellular function considered, the different signal transduction systems can act in a synergic or contrasting manner. For example, in myometrial cells, the activation of the OTR/Gq calcium-dependent pathway and the OTR/Gi-mediated cAMP level decrease contributed together to the uterus contraction during labor (Sanborn 2001, Zhou, Lutz et al. 2007). In human embryonic kidney cells expressing OTRs (HEK293-OTR), the activation of the OTR/Gi pathway inhibited cell growth whereas the activation of the OTR/Gq pathway reduced it (Rimoldi, Reversi et al. 2003, Busnelli, Sauliere et al. 2012). In GN11 cells, OTR activation differently affected neuronal excitability, as its coupling to Gq/G11 inhibited the inward rectifier K⁺ currents whereas its coupling to Gi/o promoted them (Gravati, Busnelli et al. 2010).

During the last years, OT administration has been proposed and tested as a treatment in a number of neuropsychiatric disorders such as autism spectrum disorders, depression, anxiety and addiction, but also for various types of cancers. In these studies, the responses to treatment were in many cases highly variable (Dadds, MacDonald et al. 2014, Yatawara, Einfeld et al. 2016) not only for the clinical condition under consideration but also for the type of cellular/biological response induced, indicating that a further development of OT for clinical applications is necessary (Yamasue, Okada et al. 2020).

Biased agonists, promoting a selective receptor-G protein coupling, offer the possibility to specifically modulate one specific cellular/tissue response activated by a given receptor, and open a new avenue for a better control and a precise modulation of cell and tissue functions (Michel and Charlton 2018). Atosiban, an OT peptidic analogue, was the first functional selective agonist identified for the OTR, and one of the first developed for GPCRs (Reversi, Rimoldi et al. 2005). Atosiban was used for a long time as an OTR antagonist, being known for its anti-OT uterotonic effects *in vivo* and its dose-dependent inhibitory effects on OT-stimulated inositol triphosphate (IP₃) production *in vitro* (Phaneuf, Asboth et al. 1994, Manning, Miteva et al. 1995). Surprisingly, cellular studies using pertussis toxin as Gi/o inhibitor and the use of BRET biosensors, designed to investigate the activation of a single G-protein subtype, showed that atosiban is an agonist on OTR/Gi3 signaling (Reversi, Rimoldi et al. 2005, Busnelli, Sauliere et al. 2012), has pro-inflammatory effects (Kim, MacIntyre et al. 2016) and inhibitory actions on cell growth (Cassoni, Sapino et al. 1996, Reversi, Rimoldi et al. 2005). Atosiban inhibitory effects were demonstrated on the firing properties of “sensory wide dynamic range” neurons responsible for the pain in the deep laminae of the spinal cord (Eliava, Melchior et al. 2016). After Atosiban other two OT peptidic-derived analogues were identified as “OTR-biased agonists”: carbetocin, specifically acting on OTR/Gq and DNalOVT, specifically acting on OTR/Gi1, respectively (Busnelli, Sauliere et al. 2012, Passoni, Leonzino et al. 2016).

OTRs can form dimers and higher-order oligomers with partners of the same subfamily (AVP receptors) (Terrillon, Durroux et al. 2003) or with GPCRs which respond to different ligands

(hetero-dimers/oligomers) (Wrzal, Goupil et al. 2012, Romero-Fernandez, Borroto-Escuela et al. 2013, Chruscicka, Wallace Fitzsimons et al. 2019). In addition, OTR protomers can dimerize with themselves to form homo-dimers/oligomers (Devost and Zingg 2004, Busnelli, Mauri et al. 2013, Busnelli, Kleinau et al. 2016).

OTR homodimerization in transfected cell lines has been confirmed by different sets of experiments: co-expression of c-terminally c-myc and FLAG-tagged OTR receptors in COS7 cells, followed by immunoprecipitation of the cell lysates with anti-FLAG antibodies and immunoblotting with anti-c-myc antibodies (Devost and Zingg 2004) and the measurement of the efficiency of bioluminescent resonance energy transfer (BRET) between OTR tagged at the C-terminal with the *Renilla* luciferase (RLuc) and a variant of the green fluorescent protein (YFP or GFP²) co-expressed in HEK293 cells (Terrillon, Durroux et al. 2003, Busnelli, Mauri et al. 2013). Most importantly, the existence of OTR dimers *in vivo* and in native tissues has been demonstrated thanks to the application of a time-resolved fluorescence resonance energy transfer (TR-FRET)-based approach performed with labelled OTR selective ligands (Albizu, Cottet et al. 2010). Thus, OTR homodimers represent a novel druggable target.

While it has been extensively reported that heterodimerization of GPCRs can activate intracellular signaling pathways, that can be different from those triggered by the individual receptors, very little is known about the effects of homodimerization on the receptor properties (Parmentier 2015).

Bivalent ligands, constituted by two molecules that are joined by a spacer and that are specifically designed to simultaneously bind both dimers, are a valid tool to study and to pharmacologically target GPCR homodimers. Homobivalent ligands for the OTR, made up of two identical modified OT molecules joined by a flexible spacer, used in an previous study (Busnelli, Kleinau et al. 2016) revealed to specifically target OTR homodimers and to act at very low concentrations to potentiate OTR/Gq signaling and promote social behavior in mice and zebrafish at concentrations that were much lower than those of the monovalent corresponding molecule and of the endogenous neuropeptide (Busnelli, Kleinau et al. 2016).

To better understand the molecular mechanisms that underlie the behavioral responses determined by the use of these OT-derived homobivalent molecules and to try to predict the therapeutic potential applications of these ligands, we continued the analysis of the activated signaling pathways. Using BRET biosensors transfected in HEK293 cells, we analyzed the ability of each bivalent ligand to activate the OTR, in terms of G protein activation and β -arrestin recruitment, and we compared them with endogenous OT and monovalent dOTK. We found that all the bivalent ligands tested, as well as their monovalent relative dOTK, are “functionally selective”, as they activate Gq, Gi2 and Gi3 but not Gi1 and Go and promote OTR internalization. We also found that, differently from the monovalent dOTK and bivalent ligands with shorter and longer spacers (that promote the interaction between the OTR and the β -arrestin 2 only) the dOTK₂-C8 and dOTK₂-C10 induce the OTR recruitment of both β -arrestin 1 and β -arrestin 2. These data suggest that dOTK₂-C8 and dOTK₂-C10 ligands stabilize or induce an OTR conformation with an increased affinity for β -arrestins.

RESULTS

Monovalent dOTK and bivalent dOTK ligands activate a specific subset of OTR/G proteins complexes

We used homobivalent ligands, composed by two oxytocin-derived analogues deaminated in position 1 and bearing a lysine in position 8 (dOTK) (**Figure 1A**) joined by a linear spacer with an increasing number of carbon atoms (namely C6, C8, C10, C12, C14) (**Figure 1B**), and already described in Busnelli et al. 2016 (Busnelli, Kleinau et al. 2016).

Using BRET-based biosensors specifically developed to measure the ligand induced G protein activation (Busnelli, Sauliere et al. 2012, Sauliere, Bellot et al. 2012) (**Figure 2A**) we tested their capability to activate the different OTR/G protein complexes. A significant reduction of the BRET signal was observed in the presence of OT (10 μ M) for all the G α protein analyzed, confirming our previous observations that the endogenous OT ligand can activate the OTR-Gq, -Gi1, -Gi2, -Gi3, -GoA and -GoB (Busnelli, Sauliere et al. 2012). For the monovalent dOTK (10 μ M) and all the derived

bivalent ligands (10 μ M), we observed the activation only of Gq, Gi2 and Gi3 and not of the Gi1, GoA and GoB subunits.

This data indicate that the modifications introduced into the chemical structure of the OT molecule to generate dOTK and dOTK₂-Cn bivalent ligands (**Figure 1**) determine the activation of specific OTR-downstream signaling pathways; we can therefore consider our bivalents (and the monovalent dOTK) as “functional selective” or “biased” agonists.

Bivalent ligands activate OTR/Gi2 and OTR/Gi3 with monotonic curves

We have previously reported that, for OTR/Gq activation, dOTK, dOTK₂-C6, dOTK₂-C12 and dOTK₂-C14 generated monophasic dose-response curves, while dOTK₂-C8 and dOTK₂-C10 ones were biphasic. In particular, these biphasic curves were characterized by a first phase (in the pM range) presumably corresponding to the activation of OTR homodimers, and by a second phase (in the nM range) corresponding to the activations of monomers and/or a single protomers into a dimer (Busnelli, Kleinau et al. 2016).

Here we tested the effects of the bivalent analogues on all OT/Gi and Go-coupled receptors. Our results indicate that all the bivalent ligands tested, including dOTK₂-C8 and dOTK₂-C10, only activate OTR/Gi2 and OTR/Gi3 but not OTR/Gi1, GoA and GoB. In addition, we obtained monotonic curves in the presence of dOTK and all the bivalent ligands tested, including dOTK₂-C8 and dOTK₂-C10. The EC₅₀s are all in the nanomolar range, suggesting that the bivalent ligands bind and activate only one receptor population, as the monovalent dOTK.

Bivalent ligands recruit β -arrestins differently from OT and dOTK

The binding of OT to OTR leads to receptor activation, phosphorylation, and the translocation of – β -arrestin 1 and β -arrestin 2 to the receptor complex, an event that turns off the G protein-dependent signaling pathway (Conti, Sertic et al. 2009, Busnelli, Sauliere et al. 2012). In addition to its desensitizing function, β -arrestins have recently been shown to simultaneously activate downstream signaling regulating a wide array of cell functions (Smith and Rajagopal 2016). It has been reported

that OTR/ β -arrestin mediated signaling regulates many cell functions i.e uterine contractility and cell migration (Grotegut, Feng et al. 2011).

To determine to which degree dOTK and bivalent ligands promote OTR/ β -arrestin activation we used a specifically designed BRET¹ biosensor to evaluate β -arrestin1 and β -arrestin2 recruitment in HEK293 cells (**Figure 5A**). In this case, the energy acceptor molecule is a YFP fused to the β -arrestin of interest, while the RLuc is attached to the cytoplasmatic side of the OTR receptor. Following receptor activation, if the β -arrestin is recruited to the plasma membrane, the YFP comes in close proximity to the RLuc, and the energy transfer measured increases.

We stimulated the cells with a maximal concentration (10 μ M) of dOTK and the bivalent ligands and we measured the energy transfer in continuous for 8 minutes. All the ligand tested were effective in promoting β -arrestin 2 recruitment by OTR, although with differences in the maximal efficacy (E_{max}). The bivalent ligands dOTK₂-C8 and dOTK₂-C10 were the most efficient and their E_{max} was also statistically different from the monovalent dOTK. We calculated the half time ($t_{1/2}$) to be 103 s for dOTK, 116 s for dOTK₂-C6, 88 s for dOTK₂-C8, 57 s for dOTK₂-C10, 79 s for dOTK₂-C12 and 90 s for dOTK₂-C14, respectively.

The bivalent ligands dOTK₂-C8 and dOTK₂-C10 were also the only two ligands able to promote the recruitment of β -arrestin 1.

OT, dOTK and bivalent analogues all induce OTR internalization

Once activated by OT, the OTR is desensitized and internalized. However, some OT-derived ligands, and in particular those that activate only OTR/Gi complexes, do not induce OTR internalization (Busnelli et al., 2012). We thus tested if dOTK and dOTK₂-Cn bivalent ligands that activate only a subset of OTR/G protein complexes are also capable to promote OTR internalization. To this aim, we stimulated OTR stably expressing HEK 293 cells with 100 nM OT, dOTK and all the bivalent ligands.

Our results indicate that all the bivalent ligands tested are able to promote receptor internalization, that could be visualized as intracellular fluorescent spots (**Figure 6**) that in a previous work we

identified as endosomal vesicles (Conti, Sertic et al. 2009)

DISCUSSION

The extent and functional relevance of the interactions between GPCRs is still a matter of controversy (Milligan, Ward et al. 2019). Dimerization and oligomerization of GPCRs seems not to be generally necessary for receptor mediated G-protein activation; indeed, several analysis have confirmed that monomeric signaling of GPCRs is possible: single μ -opioid receptors as well β 2-adrenergic and rhodopsin inserted in small lipid vesicles have been shown to couple to their G-proteins (Whorton, Bokoch et al. 2007, Whorton, Jastrzebska et al. 2008, Kuszak, Pitchiaya et al. 2009) and monomeric rhodopsin in solution has been shown to activate its G-protein transducin (Ernst, Gramse et al. 2007). However, an increasing number of examples suggests that GPCR receptor interactions in living cells are required for proper tissue function. For example, it has been reported that mutations that are present in the transmembrane domain 1 (TM1H) of the thromboxane A2 receptor, involved in receptor dimerization, not only cause the reduction of receptor dimerization *in vitro* but cause bleeding disorders associated with reduced platelet function in patients (Capra, Mauri et al. 2017).

There is growing evidence that GPCR receptor interactions occur initially during biosynthesis and are an integral aspect of GPCR maturation. At least for the family C GABA-B receptor (White, Wise et al. 1998), protein-protein interactions provided by dimerization are necessary for the export from the Golgi apparatus and the insertion into the plasma membrane. It is also noteworthy that both artificially produced and naturally occurring GPCR truncation and splice variants can act to limit cell surface delivery of GPCRs, likely preventing the final maturation of the dimer (Coge, Guenin et al. 1999, Karpa, Lin et al. 2000). In studies of OT and vasopressin (AVP) receptors, Terrillon and coworkers demonstrated that immature forms of OTR and AVPRs were present as dimers already in the endoplasmic reticulum (Terrillon, Durroux et al. 2003).

In our earlier studies, from the analysis of the amplitude of the OTR/Gq concentration/response curve, we were able to determine that at least 30%

of OTR, activable and present at the plasma membrane, are expressed in a dimeric form and that stimulation with dOTK does not perturb dimeric complexes (Busnelli, Mauri et al. 2013, Busnelli, Kleinau et al. 2016).

The dOTK₂-C8 and dOTK₂-C10 bivalent ligands demonstrated to be super-active agonists on the OTR/Gq pathway, generating a particular biphasic curve. These analogues have a great translational value, displaying a significant gain (40- and 100-fold) over the endogenous ligand OT and isotocin, in promoting social behavior in OTR heterozygous mice (which is a model of social impairments; Sala, Braida et al. 2013) and in zebrafish (Busnelli, Kleinau et al. 2016). These effects observed *in vivo* are consistent with the existence of OTR homodimers not only in the mammary gland as reported by Albizu et al. in 2010 (Albizu, Cottet et al. 2010), but also in the CNS. Remarkably, these analogues could be an important tool for translational studies in neurodevelopmental and psychiatric disorders but could also pave the way for novel therapeutic molecules.

To obtain safer, targeted and personalized therapies, it is important to understand and dissect the peculiar features of OTR homobivalent ligands and OTR homodimers functions. From the BRET studies done to test OTR/G protein activation, we found that dOTK and its derived bivalent ligands are different from OT, and activate selectively OTR/Gq, OTR/Gi2 and OTR/Gi3 complexes; thus, they can be considered “functional selective” ligands. These different responses are consistent with the hypothesis that OTRs exist as a collections of conformations in equilibrium, and that OT, dOTK and bivalent ligands have different affinity for the various conformations adopted by the receptor (Vaidehi and Kenakin 2010). Moreover, we found that dOTK and all the bivalent ligands have similar efficacy in activating OTR/Gi2 and OTR/Gi3 and generated monophasic curves. Although more verification experiments will be necessary, we can put forward several hypotheses to explain the disappearance of the first phase of the G protein activation concentration-curve, observed for dOTK₂-C8 and dOTK₂-C10. First, only the monomeric OTRs could interact with the Gi2 and Gi3 proteins, and therefore the monovalent dOTK and the bivalent ligands dOTK₂-Cn would induce the same response. Second, it could be that dimeric OTRs could also interact with Gi2 and Gi3 proteins,

but the bivalent ligands used in this study are not able to bind simultaneously the two protomers forming the dimer. Concerning our first hypothesis, it has been well established that heterodimerization generates conformations that increase the affinity for a specific subset of G-proteins and that can be different from those of the single receptors; however, to our best knowledge no studies have demonstrated that GPCR monomers have a coupling different from their respective homodimers. Probably these studies are limited by the difficulties in the isolation of GPCR receptors in their monomeric and homodimeric form. Our second hypothesis can find confirmation in the crystal structures obtained for several rhodopsin-like GPCRs homodimers (β 2AR; β 1AR; H1R; μ OR), that used multiple side surfaces of their helical bundle for dimerization (Cherezov, Rosenbaum et al. 2007, Shimamura, Shiroishi et al. 2011, Manglik, Kruse et al. 2012, Huang, Chen et al. 2013). OTR homodimers can assume at least two dimeric conformations, one involving a TMH1/TMH2/helix8 interface and the other TMH5/TMH5 interface (Busnelli, Kleinau et al. 2016). Molecular docking analysis of the bivalent ligands used in this study, with spacer lengths of C8 and C10, showed to perfectly fit into the TMH1/TMH2 dimers, but also proved to be too short to bridge the two binding pockets predicted into the TMH5/TMH5 dimeric complexes. The spacer length C6 is too short, leading to an extraction of the ligand-moieties from the orthosteric binding sites, whereas the C12 and C14 spacers are too long to be fitted into the channel formed by the TM1H/TMH2 interaction, would be kinked and their binding disfavored (Busnelli, Kleinau et al. 2016). Interpreting our data, it can thus be possible TMH1/TMH2/helix 8 OTR dimers can interact with the Gq protein complexes, whereas TMH5/TMH5 dimeric complexes can interact with the Gi2 and Gi3 proteins. Bivalent ligands with much long spacers, as the estimated straight linear distance between the two binding sites is ~ 50 Å in TMH5/TMH5 OTR, would be able to target these alternative dimeric complexes, but their use could be counterproductive as a very long alkane chain, with high probability, will negatively impact the docking and binding for its higher hydrophobicity and will bind also distant receptors that are not complexed in a dimer.

From the analysis of the OTR/ β -arrestins recruitment, we observed that in general the bivalent ligands were more efficient than dOTK in promoting β -arrestin 2 recruitment, and only dOTK₂-C8 and dOTK₂-C10 were able to promote the recruitment of β -arrestin 1. More experiments will be necessary to demonstrate that OTR homodimers likely have a conformation that predisposes the OTRs to a more efficient interaction with β -arrestins. However it is very likely, as it has been already demonstrated for another GPCR, the sphingosine 1-phosphate receptor 1 (S1PR1), that receptor oligomerization/dimerization is necessary to stabilize the ligand-induced β -arrestin association and modulate β -arrestin activity (Patrone, Cammarota et al. 2020). It is also possible that dOTK₂-C8 and dOTK₂-C10, by simultaneously binding to the two receptors forming the TMH1/TMH2/helix 8 dimer, not only boost Gq protein activation but also potentiate β -arrestins recruitment. Accordingly with our hypothesis, it has been reported that the paired activation of the two components of the muscarinic M3 receptor dimer is required for the recruitment of β -arrestin 1 and the induction of ERK1/2 phosphorylation (Novi, Scarselli et al. 2004).

In conclusion, this study provides novel information about the “functional selective agonism” of the dOTK₂-Cn homobivalent compounds, and opens the way to the development of novel OT compounds with better therapeutic profiles.

More in general, the use of homobivalent compounds revealed to be a unique tool to investigate the signaling properties of the different homodimer conformations and to determine the functional aspects of GPCRs homodimers.

MATERIALS AND METHODS

Reagents, Constructs, and Peptides

Oxytocin was purchased from Bachem. All the monovalent and bivalent ligands used in this work have been originally synthesized through the Merrifield protocol in solid phase (as previously described in (Busnelli, Kleinau et al. 2016). Luciferase substrates, coelenterazines 400A and H were purchased from Cayman.

Cell Cultures

Human embryonic kidney 293 (HEK293) cells were cultured at 37°C and 5% CO₂, in Dulbecco's modified Eagle's medium (DMEM) (Sigma-Aldrich, St. Louis, MO, USA) supplemented with 10% (v/v) Fetal Bovine Serum (FBS) (Euroclone, Pero, Italy), 100 units of penicillin (Euroclone), 100 g/mL streptomycin (Euroclone), and 2 mM L-glutamine (Euroclone).

Cell Transfection

The day before transfection for BRET experiments, cells were seeded in 100 mm plates to let them reach a 50% confluence. Transient transfections with the BRET biosensors components were performed using linear polyethyleneimine 25 kDa (PEI MW 25,000, Polysciences, Inc., Warrington, PA, USA) maintaining a PEI / plasmid DNA ratio of 2:1. The DNA/PEI mix was incubated for 15 minutes in non-supplemented DMEM before administration to cells; 24 hours after transfection, the DMEM was renewed, and the cells were cultured for a further 24 hours before the experiments.

BRET assays

For BRET² assays measuring the different G α subtypes activation, HEK293 cells were transfected with DNA encoding for OTR-pRK5 (7 μ g), *Renilla Luciferase* (RLuc8)-tagged G α_q , G α_{i1} , G α_{i2} , G α_{i3} , G α_{oA} , G α_{oB} (BRET energy donor) (4 μ g), GFP¹⁰-G γ_2 (BRET energy acceptor) (5 μ g), and G β_1 (5 μ g). 48 hours after transfection, cells were washed twice with PBS, detached and resuspended in PBS, 0.1% (w/v) glucose, MgCl₂ 0.5 mM and CaCl₂ 0.7 mM. Protein concentration was determined using a colorimetric protein assay (DC protein assay, Biorad, Milan, Italy). Cells were then distributed in a 96-well microplate (Optiplate, PerkinElmer, Milan, Italy) at a concentration of 80 μ g cells/well, and incubated with different ligand concentrations or vehicle (PBS) for 2 min prior to the addition of 5 μ M of the BRET² substrate, coelenterazine 400A. Immediately after this step, RLuc8 and GFP¹⁰ emissions were recorded using an Infinite F500 multidetector plate reader (Tecan, Milan, Italy) that allows the sequential integration of light signals detected with two filter settings (RLuc8 filter, 370–450 nm; GFP¹⁰ filter, 510–540 nm). Data were recorded for 2 minutes after substrate addition, and

used to determine the resulting BRET² signal, calculated as the ratio between the light emitted by the GFP¹⁰ acceptor and that emitted from the RLuc8 donor. The “ligand promoted BRET” value was eventually calculated as the difference between the BRET² signal measured in the presence of the ligand and the BRET² signal obtained in vehicle condition.

For BRET¹ assays measuring β -arrestin recruitment, HEK293 cells were transfected with DNA encoding for OTR-RLuc (BRET energy donor) (1.5 μ g), YFP-tagged β -arrestin 1 or β -arrestin 2 (BRET energy acceptor) (5 μ g), and pcDNA 3.1 (13.5 μ g). 48 hours after transfection, cells were washed twice with PBS, detached and resuspended in PBS, 0.1% (w/v) glucose, MgCl₂ 0.5 mM and CaCl₂ 0.7 mM. Protein concentration was determined using a colorimetric protein assay (DC protein assay, Biorad, Milan, Italy). Cells were then distributed in a 96-well microplate (Optiplate, PerkinElmer, Milan, Italy) at a concentration of 80 μ g cells/well, and incubated with RLuc substrate coelenterazine H (Biotium, Hayward, CA) 8 min prior to the addition of the ligand or vehicle (PBS). After ligand addition, RLuc and YFP emissions were recorded using the previously mentioned Infinite F500 plate reader (RLuc filter, 370-480 nm; YFP filter, 520-570 nm). Data were recorded for 8 minutes after stimulation, and used to determine the resulting BRET¹ signal, calculated as the ratio of the light emitted by the YFP acceptor and that emitted from the RLuc donor. The “ligand promoted BRET” value was eventually calculated as the difference between the BRET¹ kinetic measured in the presence of the ligand and the BRET¹ kinetic obtained in vehicle condition.

Receptor internalization imaging using confocal microscopy

To induce and visualize receptor internalization, HEK293-OTR EGFP cells were seeded on 24 mm glass coverslips at a starting concentration of 250,000 cells/mL, and used 24 hours later at a 50%-70% confluence. On the day of the experiment, cells were washed twice with PBS and stimulated for 30 min with the different ligands at 37°C. If required, YM-254890 was added 5 minutes prior ligand stimulation, diluted in the last PBS wash. After stimulation, cells were quickly washed three times with ice-cold PBS and fixated in 4%

paraformaldehyde for 20 minutes. After further rinsing for two times with PBS and lastly with ddH₂O, coverslips were mounted on glass slides using MOWIOL, and EGFP signal was visualized through a Zeiss LSM800 confocal microscope.

Statistic analysis

All the statistic analysis and curve fitting were performed through GraphPad Prism 5 (GraphPad Software Inc., San Diego, CA). BRET data of G protein activation were analyzed with a non-linear regression curve fitting procedure and to determine the best model fitting, monophasic vs biphasic were compared for each data set. Data points are reported as mean \pm SEM.

Monophasic curves were analyzed using the four-parameter logistic model:

$$Y = \text{Bottom} + (\text{Top} - \text{Bottom}) / (1 + 10^{((\text{LogEC}_{50} - X) * \text{Hill Slope}))}$$

where Top and Bottom represent the lower and upper *plateaus*.

Biphasic curves were analyzed using a seven parameters model for non-monotonic curves (Rovati and Nicosia 1994) as modified in (Ambrosio, Fanelli et al. 2010)

$$\delta = \text{bottom} + \frac{\text{Plateau}_1 - \text{Bottom}}{1 + 10^{(\text{LogEC}_{50,1} - X) * b_1}} + \frac{E_{\text{max}} - \text{Plateau}_1}{1 + 10^{(\text{LogEC}_{50,2} - X) * b_2}}$$

Where: δ = response; X = Log concentration of the agonist; Bottom = response when X = 0; EC_{50,1} and EC_{50,2} = concentrations of the agonist that produce half of the response of the first and second component, respectively; b₁ and b₂ = slopes of the first and second component, respectively; Plateau₁ = maximal response of the first component; E_{max} = response for an infinite concentration of X, with constrained b₁ and b₂ equal to -1.

For the analysis of E_{max} and β arrestin recruitment *plateau* values, significances were determined through a one-way ANOVA test, followed by a Tukey's multiple comparison post-hoc test to highlight any possible difference between the effects of each compound.

A statistical level of significance of $P < 0.05$ was accepted.

AUTHOR CONTRIBUTIONS

F.S. performed BRET experiments and fluorescence microscopy studies, performed data analysis, and contributed to write the manuscript. A.G. synthesized dOTK, and bivalent ligands. B.C. contributed to write the manuscript and to interpret data. M.B. conceived and supervised the project, performed data analysis and wrote the manuscript.

COMPETING FINANCIAL INTERESTS

The authors declare that this study was conducted in the absence of any commercial or financial relationships that could represent a potential conflict of interest.

ACKNOWLEDGEMENTS

This work was supported by the NARSAD Young Investigator Grant 24917 from Brain and Behavior Foundation to M.B.; the Fritz Thyssen Foundation grant 10.16.2.018, Telethon Foundation grant GGP12207, CNR Research Project on Aging and Regione Lombardia (Project MbMM-convenzione n°18099/RCC) to B.C., EBRI-CNR research agreement to M.B. and B.C..

We thank Dr. C. Galés, INSERM, France who provided the BRET biosensor cDNAs.

BIBLIOGRAPHY

Albizu, L., M. Cottet, M. Kralikova, S. Stoev, R. Seyer, I. Brabet, T. Roux, H. Bazin, E. Bourrier, L. Lamarque, C. Breton, M. L. Rives, A. Newman, J. Javitch, E. Trinquet, M. Manning, J. P. Pin, B. Mouillac and T. Durroux (2010). "Time-resolved FRET between GPCR ligands reveals oligomers in native tissues." *Nat Chem Biol* **6**(8): 587-594.

Ambrosio, M., F. Fanelli, S. Brocchetti, F. Raimondi, M. Mauri, G. E. Rovati and V. Capra (2010). "Superactive mutants of thromboxane prostanoid receptor: functional and computational analysis of an active form alternative to constitutively active mutants." *Cell Mol Life Sci* **67**(17): 2979-2989.

Busnelli, M. and B. Chini (2018). "Molecular Basis of Oxytocin Receptor Signalling in the Brain: What We Know and What We Need to Know." *Curr Top Behav Neurosci* **35**: 3-29.

Busnelli, M., G. Kleinau, M. Muttenthaler, S. Stoev, M. Manning, L. Bibic, L. A. Howell, P. J. McCormick, S. Di Lascio, D. Braida, M. Sala, G. E. Rovati, T. Bellini and B. Chini (2016). "Design and Characterization of Superpotent Bivalent Ligands Targeting Oxytocin Receptor Dimers via a Channel-Like Structure." *J Med Chem* **59**(15): 7152-7166.

Busnelli, M., M. Mauri, M. Parenti and B. Chini (2013). "Analysis of GPCR dimerization using acceptor photobleaching resonance energy transfer techniques." *Methods Enzymol* **521**: 311-327.

Busnelli, M., A. Sauliere, M. Manning, M. Bouvier, C. Gales and B. Chini (2012). "Functional selective oxytocin-derived agonists discriminate between individual G protein family subtypes." *J Biol Chem* **287**(6): 3617-3629.

Capra, V., M. Mauri, F. Guzzi, M. Busnelli, M. R. Accomazzo, P. Gaussem, S. P. Nisar, S. J. Mundell, M. Parenti and G. E. Rovati (2017). "Impaired thromboxane receptor dimerization reduces signaling efficiency: A potential mechanism for reduced platelet function in vivo." *Biochem Pharmacol* **124**: 43-56.

Cassoni, P., A. Sapino, M. Papotti and G. Bussolati (1996). "Oxytocin and oxytocin-analogue F314 inhibit cell proliferation and tumor growth of rat and mouse mammary carcinomas." *Int J Cancer* **66**(6): 817-820.

Cherezov, V., D. M. Rosenbaum, M. A. Hanson, S. G. Rasmussen, F. S. Thian, T. S. Kobilka, H. J. Choi, P. Kuhn, W. I. Weis, B. K. Kobilka and R. C. Stevens (2007). "High-resolution crystal structure of an engineered human beta2-adrenergic G protein-coupled receptor." *Science* **318**(5854): 1258-1265.

Chruscicka, B., S. E. Wallace Fitzsimons, D. O. Borroto-Escuela, C. Druelle, P. Stamou, K. Nally, T. G. Dinan, J. F. Cryan, K. Fuxe and H. Schellekens (2019). "Attenuation of Oxytocin and Serotonin 2A Receptor Signaling through Novel Heteroreceptor Formation." *ACS Chem Neurosci* **10**(7): 3225-3240.

Coge, F., S. P. Guenin, A. Renouard-Try, H. Rique, C. Ouvry, N. Fabry, P. Beauverger, J. P. Nicolas, J. P. Galizzi, J. A. Boutin and E. Canet (1999). "Truncated isoforms inhibit [3H]prazosin binding and cellular trafficking of native human

alpha1A-adrenoceptors." Biochem J **343 Pt 1**: 231-239.

Conti, F., S. Sertic, A. Reversi and B. Chini (2009). "Intracellular trafficking of the human oxytocin receptor: evidence of receptor recycling via a Rab4/Rab5 "short cycle"." Am J Physiol Endocrinol Metab **296**(3): E532-542.

Dadds, M. R., E. MacDonald, A. Cauchi, K. Williams, F. Levy and J. Brennan (2014). "Nasal oxytocin for social deficits in childhood autism: a randomized controlled trial." J Autism Dev Disord **44**(3): 521-531.

Devost, D. and H. H. Zingg (2004). "Homo- and hetero-dimeric complex formations of the human oxytocin receptor." J Neuroendocrinol **16**(4): 372-377.

Eliava, M., M. Melchior, H. S. Knobloch-Bollmann, J. Wahis, M. da Silva Gouveia, Y. Tang, A. C. Ciobanu, R. Triana Del Rio, L. C. Roth, F. Althammer, V. Chavant, Y. Goumon, T. Gruber, N. Petit-Demouliere, M. Busnelli, B. Chini, L. L. Tan, M. Mitre, R. C. Froemke, M. V. Chao, G. Giese, R. Sprengel, R. Kuner, P. Poisbeau, P. H. Seeburg, R. Stoop, A. Charlet and V. Grinevich (2016). "A New Population of Parvocellular Oxytocin Neurons Controlling Magnocellular Neuron Activity and Inflammatory Pain Processing." Neuron **89**(6): 1291-1304.

Ernst, O. P., V. Gramse, M. Kolbe, K. P. Hofmann and M. Heck (2007). "Monomeric G protein-coupled receptor rhodopsin in solution activates its G protein transducin at the diffusion limit." Proc Natl Acad Sci U S A **104**(26): 10859-10864.

Gravati, M., M. Busnelli, E. Bulgheroni, A. Reversi, P. Spaiardi, M. Parenti, M. Toselli and B. Chini (2010). "Dual modulation of inward rectifier potassium currents in olfactory neuronal cells by promiscuous G protein coupling of the oxytocin receptor." J Neurochem **114**(5): 1424-1435.

Grinevich, V., H. S. Knobloch-Bollmann, M. Eliava, M. Busnelli and B. Chini (2016). "Assembling the Puzzle: Pathways of Oxytocin Signaling in the Brain." Biol Psychiatry **79**(3): 155-164.

Grotegut, C. A., L. Feng, L. Mao, R. P. Heine, A. P. Murtha and H. A. Rockman (2011). "beta-Arrestin mediates oxytocin receptor signaling, which regulates uterine contractility and cellular migration." Am J Physiol Endocrinol Metab **300**(3): E468-477.

Huang, J., S. Chen, J. J. Zhang and X. Y. Huang (2013). "Crystal structure of oligomeric beta1-adrenergic G protein-coupled receptors in ligand-free basal state." Nat Struct Mol Biol **20**(4): 419-425.

Karpa, K. D., R. Lin, N. Kabbani and R. Levenson (2000). "The dopamine D3 receptor interacts with itself and the truncated D3 splice variant d3nf: D3-D3nf interaction causes mislocalization of D3 receptors." Mol Pharmacol **58**(4): 677-683.

Kim, S. H., D. A. MacIntyre, A. C. Hanyaloglu, A. M. Blanks, S. Thornton, P. R. Bennett and V. Terzidou (2016). "The oxytocin receptor antagonist, Atosiban, activates pro-inflammatory pathways in human amnion via G(alphai) signalling." Mol Cell Endocrinol **420**: 11-23.

Kuszak, A. J., S. Pitchiaya, J. P. Anand, H. I. Mosberg, N. G. Walter and R. K. Sunahara (2009). "Purification and functional reconstitution of monomeric mu-opioid receptors: allosteric modulation of agonist binding by Gi2." J Biol Chem **284**(39): 26732-26741.

Manglik, A., A. C. Kruse, T. S. Kobilka, F. S. Thian, J. M. Mathiesen, R. K. Sunahara, L. Pardo, W. I. Weis, B. K. Kobilka and S. Granier (2012). "Crystal structure of the micro-opioid receptor bound to a morphinan antagonist." Nature **485**(7398): 321-326.

Manning, M., K. Miteva, S. Pancheva, S. Stoev, N. C. Wo and W. Y. Chan (1995). "Design and synthesis of highly selective in vitro and in vivo uterine receptor antagonists of oxytocin: comparisons with Atosiban." Int J Pept Protein Res **46**(3-4): 244-252.

Michel, M. C. and S. J. Charlton (2018). "Biased Agonism in Drug Discovery-Is It Too Soon to Choose a Path?" Mol Pharmacol **93**(4): 259-265.

Milligan, G., R. J. Ward and S. Marsango (2019). "GPCR homo-oligomerization." Curr Opin Cell Biol **57**: 40-47.

Novi, F., M. Scarselli, G. U. Corsini and R. Maggio (2004). "The paired activation of the two components of the muscarinic M3 receptor dimer is required for induction of ERK1/2 phosphorylation." J Biol Chem **279**(9): 7476-7486.

Parmentier, M. (2015). "GPCRs: Heterodimer-specific signaling." Nat Chem Biol **11**(4): 244-245.

Passoni, I., M. Leonzino, V. Gigliucci, B. Chini and M. Busnelli (2016). "Carbetocin is a Functional Selective Gq Agonist That Does Not Promote

Oxytocin Receptor Recycling After Inducing beta-Arrestin-Independent Internalisation." J Neuroendocrinol **28**(4).

Patrone, M., E. Cammarota, V. Berno, P. Tornaghi, D. Mazza and M. Degano (2020). "Combinatorial allosteric modulation of agonist response in a self-interacting G-protein coupled receptor." Commun Biol **3**(1): 27.

Phaneuf, S., G. Asboth, I. Z. MacKenzie, P. Melin and A. Lopez Bernal (1994). "Effect of oxytocin antagonists on the activation of human myometrium in vitro: atosiban prevents oxytocin-induced desensitization." Am J Obstet Gynecol **171**(6): 1627-1634.

Reversi, A., V. Rimoldi, T. Marrocco, P. Cassoni, G. Bussolati, M. Parenti and B. Chini (2005). "The oxytocin receptor antagonist atosiban inhibits cell growth via a "biased agonist" mechanism." J Biol Chem **280**(16): 16311-16318.

Rimoldi, V., A. Reversi, E. Taverna, P. Rosa, M. Francolini, P. Cassoni, M. Parenti and B. Chini (2003). "Oxytocin receptor elicits different EGFR/MAPK activation patterns depending on its localization in caveolin-1 enriched domains." Oncogene **22**(38): 6054-6060.

Romero-Fernandez, W., D. O. Borroto-Escuela, L. F. Agnati and K. Fuxe (2013). "Evidence for the existence of dopamine D2-oxytocin receptor heteromers in the ventral and dorsal striatum with facilitatory receptor-receptor interactions." Mol Psychiatry **18**(8): 849-850.

Rovati, G. E. and S. Nicosia (1994). "Lower efficacy: interaction with an inhibitory receptor or partial agonism?" Trends Pharmacol Sci **15**(5): 140-144.

Sala, M., D. Braidà, A. Donzelli, R. Martucci, M. Busnelli, E. Bulgheroni, T. Rubino, D. Parolaro, K. Nishimori and B. Chini (2013). "Mice heterozygous for the oxytocin receptor gene (Oxtr(+/-)) show impaired social behaviour but not increased aggression or cognitive inflexibility: evidence of a selective haploinsufficiency gene effect." J Neuroendocrinol **25**(2): 107-118.

Sanborn, B. M. (2001). "Hormones and calcium: mechanisms controlling uterine smooth muscle contractile activity. The Litchfield Lecture." Exp Physiol **86**(2): 223-237.

Sauliere, A., M. Bellot, H. Paris, C. Denis, F. Finana, J. T. Hansen, M. F. Altie, M. H. Seguelas, A. Pathak, J. L. Hansen, J. M. Senard and C. Gales (2012). "Deciphering biased-agonism complexity

reveals a new active AT1 receptor entity." Nat Chem Biol **8**(7): 622-630.

Shimamura, T., M. Shiroishi, S. Weyand, H. Tsujimoto, G. Winter, V. Katritch, R. Abagyan, V. Cherezov, W. Liu, G. W. Han, T. Kobayashi, R. C. Stevens and S. Iwata (2011). "Structure of the human histamine H1 receptor complex with doxepin." Nature **475**(7354): 65-70.

Smith, J. S. and S. Rajagopal (2016). "The beta-Arrestins: Multifunctional Regulators of G Protein-coupled Receptors." J Biol Chem **291**(17): 8969-8977.

Terrillon, S., T. Durroux, B. Mouillac, A. Breit, M. A. Ayoub, M. Taulan, R. Jockers, C. Barberis and M. Bouvier (2003). "Oxytocin and vasopressin V1a and V2 receptors form constitutive homo- and heterodimers during biosynthesis." Mol Endocrinol **17**(4): 677-691.

Vaidehi, N. and T. Kenakin (2010). "The role of conformational ensembles of seven transmembrane receptors in functional selectivity." Curr Opin Pharmacol **10**(6): 775-781.

White, J. H., A. Wise, M. J. Main, A. Green, N. J. Fraser, G. H. Disney, A. A. Barnes, P. Emson, S. M. Foord and F. H. Marshall (1998). "Heterodimerization is required for the formation of a functional GABA(B) receptor." Nature **396**(6712): 679-682.

Whorton, M. R., M. P. Bokoch, S. G. Rasmussen, B. Huang, R. N. Zare, B. Kobilka and R. K. Sunahara (2007). "A monomeric G protein-coupled receptor isolated in a high-density lipoprotein particle efficiently activates its G protein." Proc Natl Acad Sci U S A **104**(18): 7682-7687.

Whorton, M. R., B. Jastrzebska, P. S. Park, D. Fotiadis, A. Engel, K. Palczewski and R. K. Sunahara (2008). "Efficient coupling of transducin to monomeric rhodopsin in a phospholipid bilayer." J Biol Chem **283**(7): 4387-4394.

Wrzal, P. K., E. Goupil, S. A. Laporte, T. E. Hebert and H. H. Zingg (2012). "Functional interactions between the oxytocin receptor and the beta2-adrenergic receptor: implications for ERK1/2 activation in human myometrial cells." Cell Signal **24**(1): 333-341.

Yamasue, H., T. Okada, T. Munesue, M. Kuroda, T. Fujioka, Y. Uno, K. Matsumoto, H. Kuwabara, D. Mori, Y. Okamoto, Y. Yoshimura, Y. Kawakubo, Y. Arioka, M. Kojima, T. Yuhi, K. Owada, W. Yassin, I. Kushima, S. Benner, N.

Ogawa, Y. Eriguchi, N. Kawano, Y. Uemura, M. Yamamoto, Y. Kano, K. Kasai, H. Higashida, N. Ozaki and H. Kosaka (2020). "Effect of intranasal oxytocin on the core social symptoms of autism spectrum disorder: a randomized clinical trial." Mol Psychiatry **25**(8): 1849-1858.

Yatawara, C. J., S. L. Einfeld, I. B. Hickie, T. A. Davenport and A. J. Guastella (2016). "The effect of oxytocin nasal spray on social interaction deficits observed in young children with autism: a randomized clinical crossover trial." Mol Psychiatry **21**(9): 1225-1231.

Zhou, X. B., S. Lutz, F. Steffens, M. Korth and T. Wieland (2007). "Oxytocin receptors differentially signal via Gq and Gi proteins in pregnant and nonpregnant rat uterine myocytes: implications for myometrial contractility." Mol Endocrinol **21**(3): 740-752.

Zingg, H. H. and S. A. Laporte (2003). "The oxytocin receptor." Trends Endocrinol Metab **14**(5): 222-227.

FIGURE 1

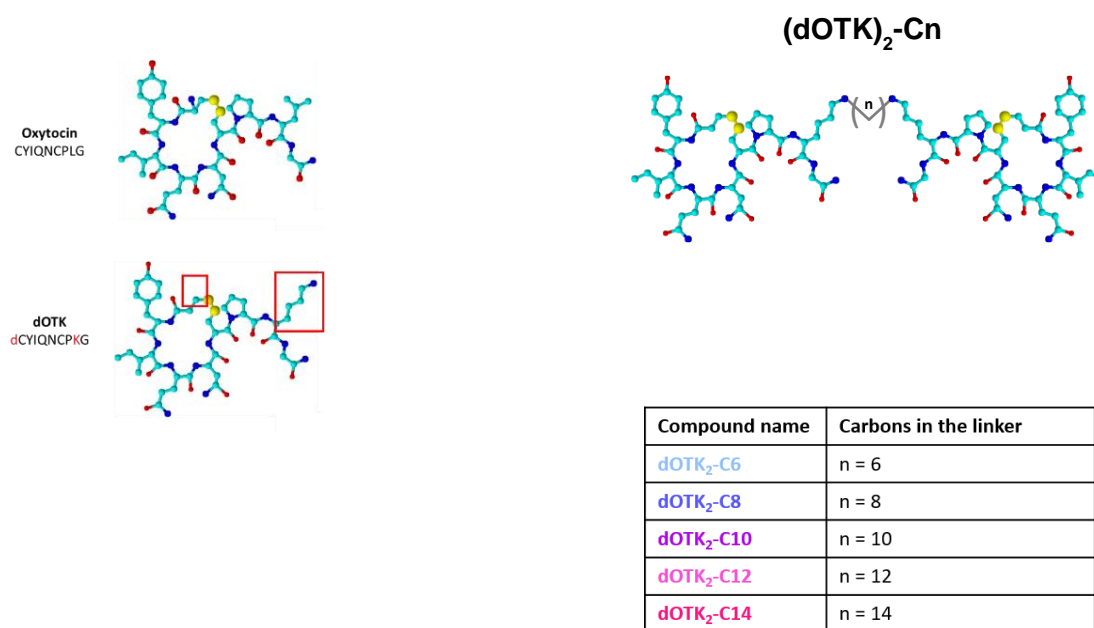


Figure 1 - Chemical structure of the OT analogs used in the experiments. Carbons are represented in light blue, aminic groups in blue, oxygen atoms in red, and sulfur atoms in yellow. Left: oxytocin and monomeric dOTK molecule. The red squares highlight the chemical structures that differ from endogenous OT. Right: structure of the average bivalent ligand designed by Busnelli et al. in 2016. Two dOTK molecules have been linked by a carbonylic spacer of different lengths ($n =$ from 6 to 14 carbon atoms).

FIGURE 2

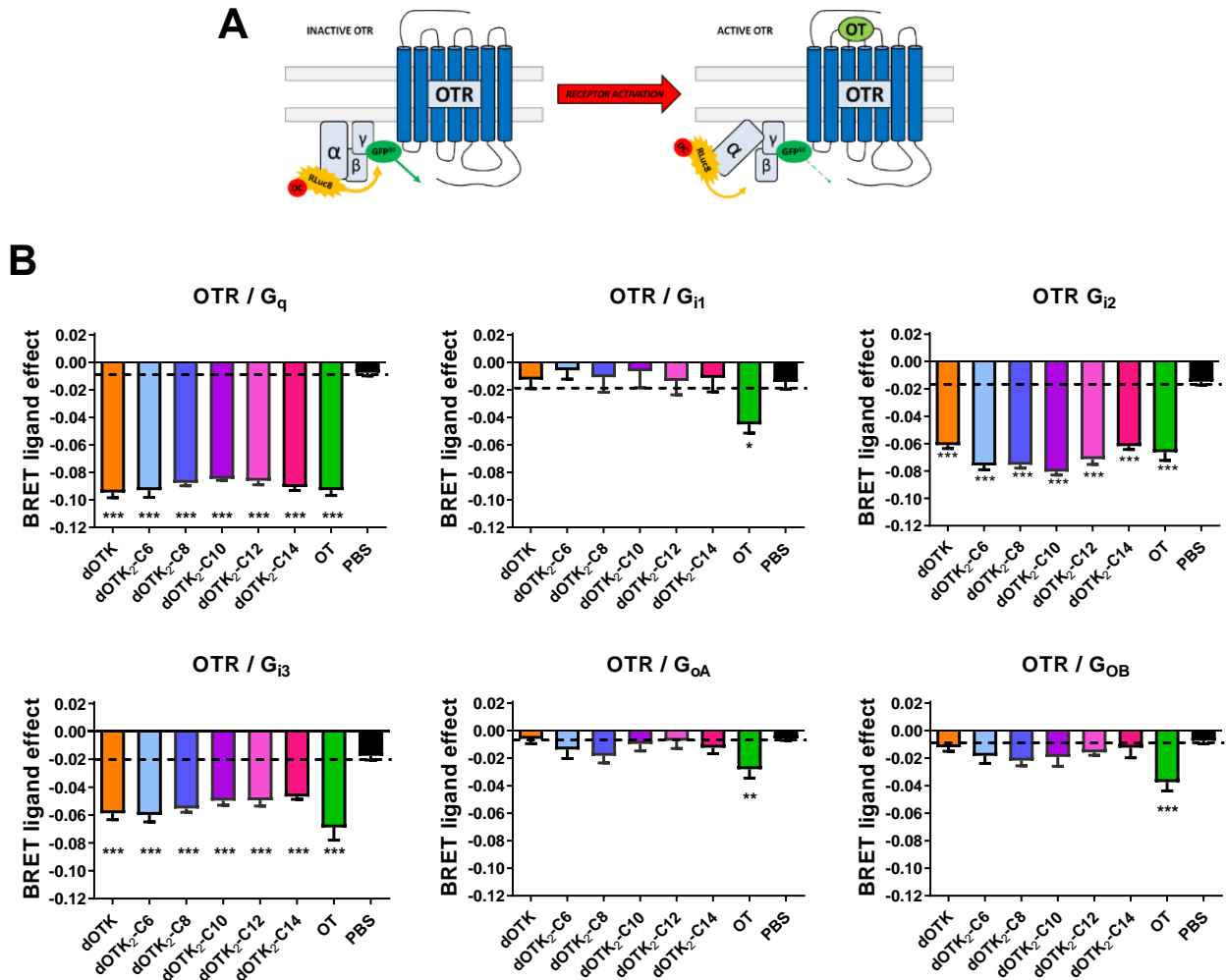


Figure 2 – BRET² measurements of maximal OTR activation by monovalent and bivalent analogues. **2A**, scheme of the BRET biosensor used for the test. The energy donor RLuc8 is fused to the α subunit of the heterotrimeric G protein, while the energy acceptor GFP¹⁰ is fused to the γ subunit. Upon receptor activation, the conformational change that occurs in the G protein increases the distance between the α and $\beta\gamma$ subunits, consequently decreasing the BRET energy transfer. **2B**, maximal activation (E_{max}) screening panel. Transfected HEK293 cells were stimulated for 2 minutes with the different molecules, at a maximal concentration of 10 μ M. In the graphs, the maximal activation for each ligand is represented as the difference between the BRET ratio induced by the ligand itself and the values obtained in the negative controls (PBS). Data are expressed as mean \pm SEM and come from at least 3 independent experiments for each ligand. Statistical differences between maximal activation values were obtained by one-way ANOVA followed by Tukey's Multiple Comparison test (* $p < 0.05$, ** $p < 0.01$, *** $p < 0.001$ vs PBS).

FIGURE 3

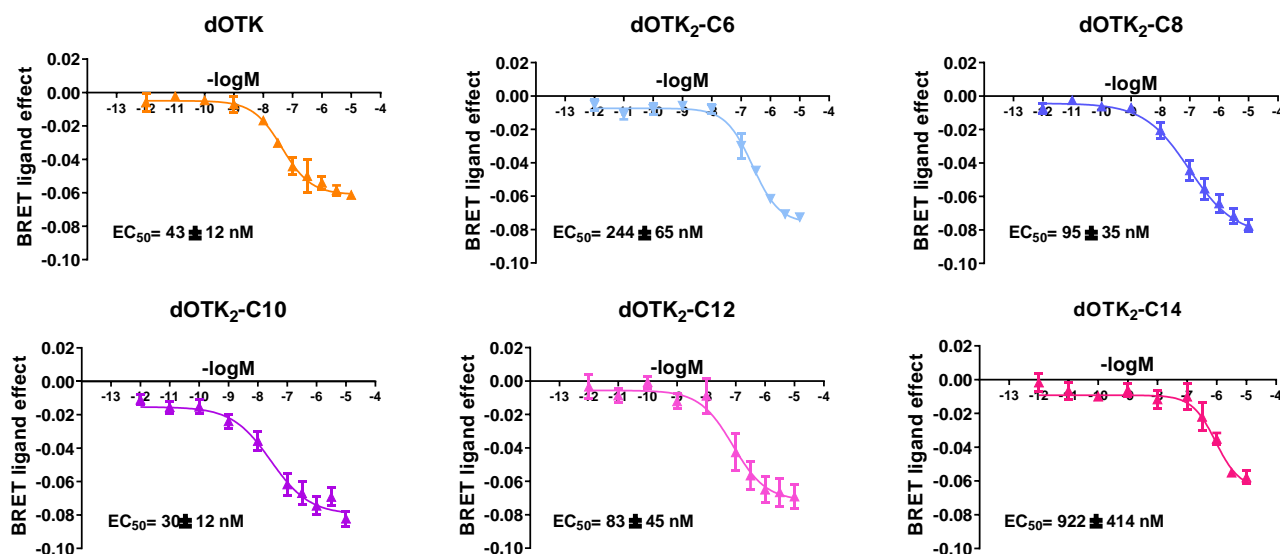


Figure 3 – BRET² dose-response curves in Gai2-coupled OTR receptors. Transfected HEK293 cells were stimulated for 2 minutes with the different molecules at different ligand concentrations. In the graphs, the BRET ligand effect is represented as the difference between the BRET ratio induced by the ligand itself and the values obtained in the negative controls (PBS). Data are expressed as mean ± SEM and come from at least 3 independent experiments for each ligand, performed at least in duplicate.

FIGURE 4

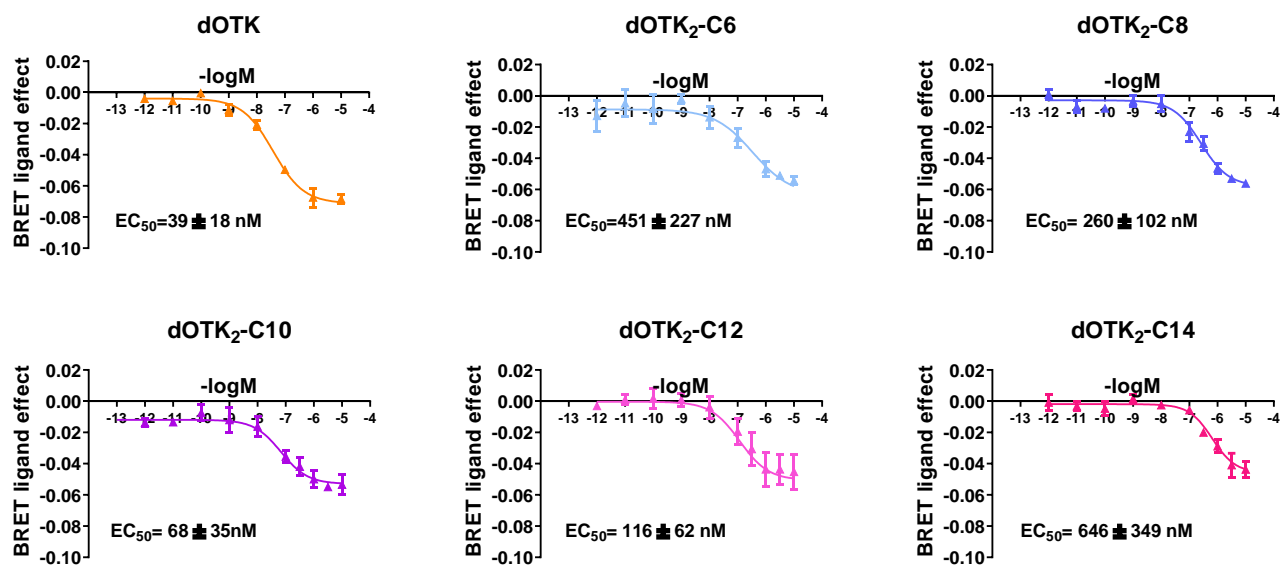


Figure 4 – BRET² dose-response curves in Gai3-coupled OTR receptors. Transfected HEK293 cells were stimulated for 2 minutes with the different molecules at different ligand concentrations. In the graphs, the activation level is represented as the difference between the BRET ratio induced by the ligand itself and the values obtained in the negative controls (PBS). Data are expressed as mean ± SEM and come from at least 3 independent experiments for each ligand, performed at least in duplicate.

FIGURE 5

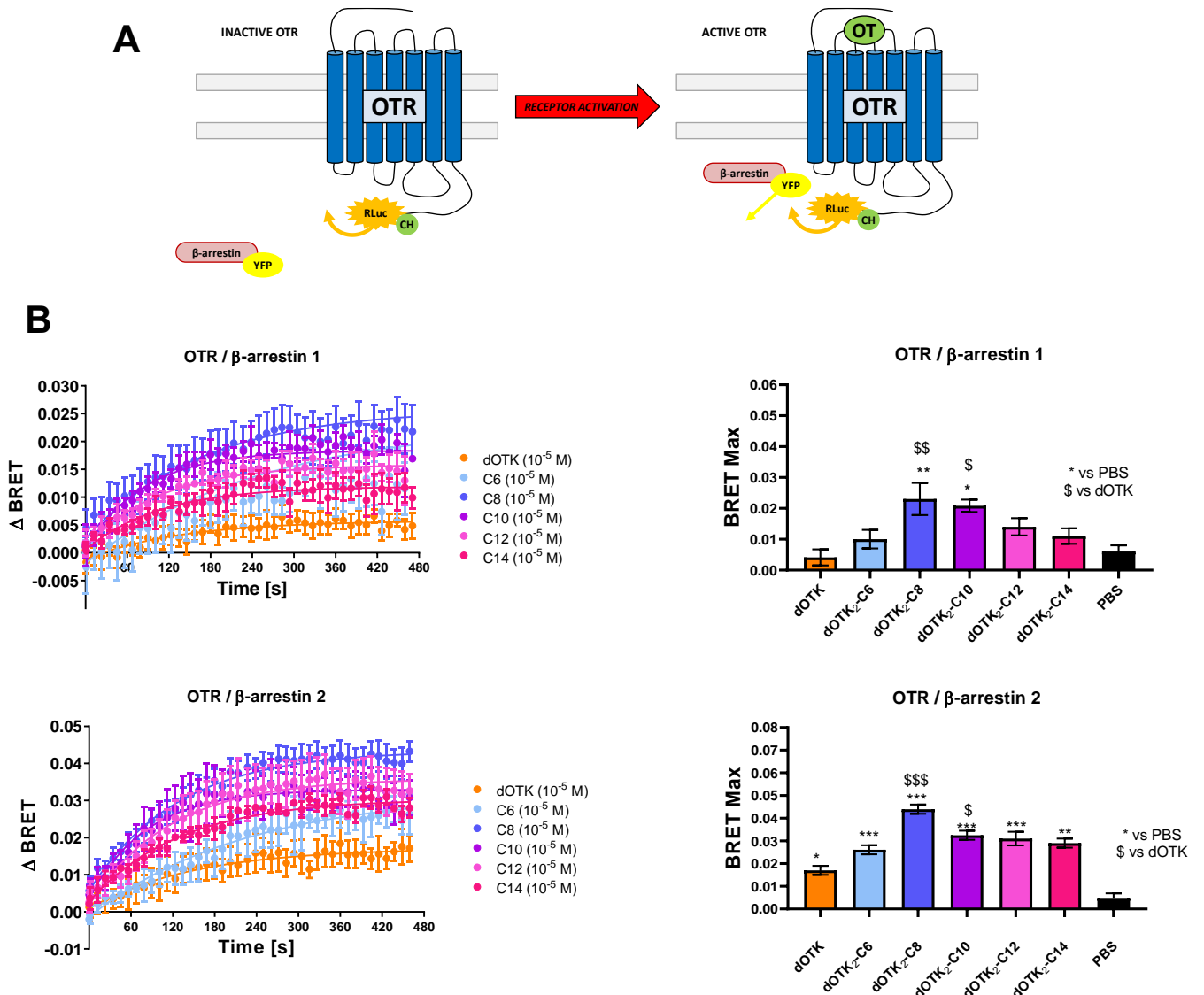


Figure 5 – BRET¹ kinetics showing the β-arrestin recruitment profiles of mono- and bivalent OT analogues. 5A, scheme of the BRET biosensor used for the test. In this case, the energy donor RLuc is fused directly to the OTR, while the energy acceptor YFP is positioned on the β-arrestin molecule. When the receptor is activated by the ligand, the β-arrestin is recruited to the plasma membrane to promote the internalization process, and therefore donor and acceptor are brought in close contact. The result is an increase of the BRET energy transfer. 5B, β-arrestin recruitment kinetics of dOTK and of the bivalent analogues. One-way ANOVA test followed by Tukey’s Multiple Comparison post-hoc were used to compare plateau values (on the right). Data come from at least three independent experiments, performed in duplicate. * $p < 0.05$, ** $p < 0.01$, *** $p < 0.001$ vs PBS; * \$ < 0.05, **\$ < 0.01, ***\$ < 0.001 vs dOTK .

FIGURE 6

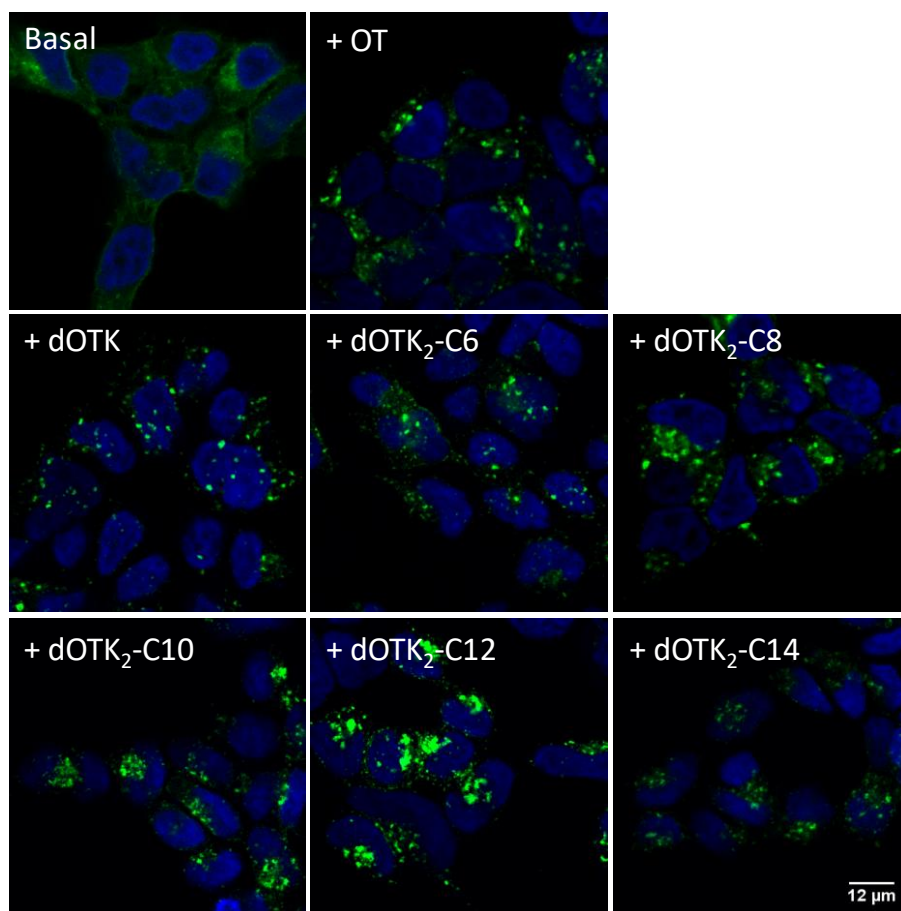


Figure 6 - Internalization of OTR following OT, dOTK or bivalent ligands stimulation. The ability of the series to induce receptor internalization was assessed in HEK293 cells stably expressing OTR-EGFP. After a 30 min stimulation (final ligand concentration: 10 μ M), internalization green spots could be seen in all the stimulated cells. Nuclei (shown in blue) were stained with DAPI. Data are representative of two independent experiments.

5. DEVELOPMENT OF A “NANORULER” SYSTEM TO MAP OTR HOMODIMERS IN THE RODENT BRAIN

During my PhD, I worked to develop a new technique that would allow the visualization and the quantification of dimeric OTR receptors in the rodent brain. Although OTR identification is already possible through receptor autoradiography, with this technique the obtained resolution is always quite low, and most importantly, it is not possible to discriminate between monomeric and dimeric receptors.

For the oxytocin receptor, dimers detection is especially difficult to achieve, because all the methodologies currently used to detect protein-protein interactions require a highly specific antibody for the proteins of interest. Moreover, the resolution guaranteed by these techniques is often not high enough to prove a direct contact between the two protomers; therefore, the risk of false positive results is always reasonably high.

5.1 METHODS CURRENTLY EMPLOYED TO STUDY OTR DIMERIZATION

Co-immunoprecipitation. Co-immunoprecipitation is one of the most common techniques to verify GPCR dimerization. It is based on the concept that in SDS-PAGE, receptors migrate differently depending on their mass, and therefore, ligand-bound receptors or oligomeric complexes will produce a slower band on the gel (Hiller et al, 2013). To avoid aspecific bands, each protomer is tagged with a different epitope: precipitation is done with an antibody against the first one, and then the immunoblotting is performed using an antibody against the second. Negative controls, made with cells expressing only one of the two epitopes, need to be included: as GPCRs are hydrophobic transmembrane proteins, removing them from their lipidic environment could induce the formation of aspecific aggregates (Milligan et al, 2005; Jordan et al, 1999).

One of the main disadvantages of Co-IP is actually that results always need to be confirmed with other techniques. Moreover, it does not really prove dimerization, but only interaction in a supramolecular complex (Hiller et al, 2013).

Biophysical techniques. One great advantage of biophysical techniques is that it allows to study homo and heterodimers in intact cells, without membrane disruptions. The most employed are those based on a “resonance energy transfer” (RET), as BRET (Bioluminescence Resonance Energy Transfer; Fig.1) and FRET (Fluorescence Resonance Energy Transfer) (Ferrè et al, 2014). Both evaluate the interaction between two proteins of interest by measuring the resonance energy transfer between a “donor” and an “acceptor” molecule (Cottet et al, 2012). The efficiency of this transfer is inversely proportional to the sixth potence of the distance between donor and acceptor (Förster,1948), allowing a high spatial resolution (10 nm). The main difference between BRET and FRET is the type of donor: in FRET it is a fluorophore (i.e. GFP), while in BRET it is a molecule able to emit light (i.e. the enzyme *Renilla* Luciferase). In both cases, it is fundamental for the donor-acceptor couple to have partially overlapping spectra (the excitation spectrum of the acceptor must overlap to the emission spectrum of the donor).

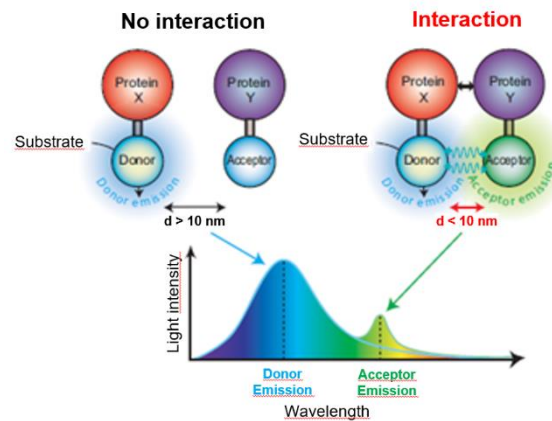


Figure 1: BRET mechanism. The energy transfer occurs only if donor and acceptor are closer than 10 nm, and only if the donor emission spectrum overlaps with the acceptor excitation spectrum.

Other variants of these techniques have been developed: one of them, the time-resolved FRET or tr-FRET, using a long-lasting emission lanthanide as donor, allows to significantly reduce signal to noise ratio (Cottet et al, 2012). Tr-FRET has been used by Albizu et al to prove for the first time the existence of OTR homodimers *in vivo* (Albizu et al, 2010).

Other biophysical techniques, such as Bimolecular Fluorescence Complementation, are based on the formation of a fluorescent molecule starting from two inactive, non-emitting fragments. The two fragments are linked to two receptor of interest: if they are brought close by dimerization, the fluorescent molecule is “recomposed” and it is now able to emit (if correctly excited) (Kerppola et al, 2008).

Despite being more informative about the actual dimerization state of a receptor compared to Co-IP, biophysical techniques have two main disadvantages: they don’t give information about the oligomer size, or about the dynamics that regulate its formation (Ferrè et al, 2014), and they require chimeric molecules, that might perturbate physiological conditions of the cellular environment. Moreover, the use of these techniques *in vivo* is problematic, in particular because the tagged fluorescent probes are quite bit (> 200 aa), and might influence the dimerization state of the receptors (Lohse et al, 2012).

Proximity Ligation Assay (PLA). Proximity Ligation Assay is one of the most recent techniques developed to study dimeric receptors in endogenous tissues. To achieve the best results, it is often used in combination with advanced imaging techniques, like super resolution microscopy.

PLA is an antibodies-based technique. In “direct” PLA, only a pair of primary antibodies is used, while in “indirect” PLA there is a double tagging step, with secondary antibodies directed against the primary ones. In both cases, antibodies must be specific for the receptors of interest (Gomes et al, 2015). Antibodies are tagged with a pair of DNA probes, and when they are close enough (20-40 nm), the two probes can interact, forming a primer for a DNA polymerase. DNA polymerase can use this structure to synthetize a long DNA filament,

through a process called Rolling Circle Amplification, or RCA. This DNA product can eventually be tagged with fluorescent probes and visualized in fluorescence microscopy as bright spots (Fig.2).

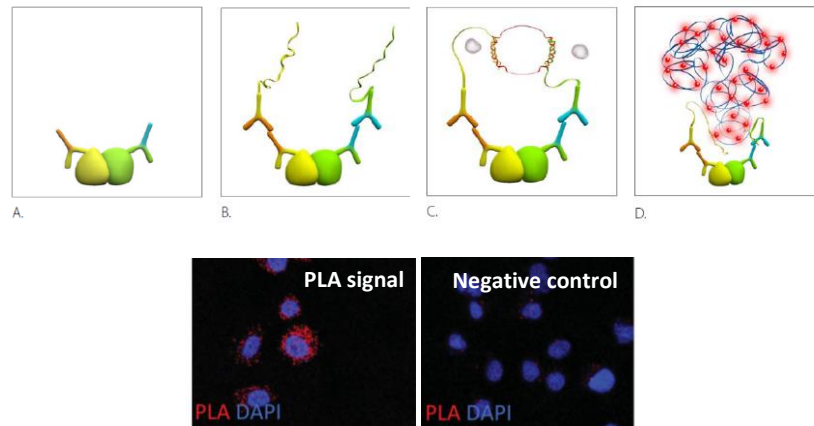


Figure 2: Proximity Ligation Assay. If two probe-tagged antibodies are close enough (i.e. because they're bound to two protomers of the same dimer) (B), the DNA probes can interact and function as a primer for a Rolling Circle Amplification step (C). The resulting DNA «tree» is detected using fluorescent probes (D), and appears as a red spot in confocal microscopy (bottom image).

The most relevant advantage of PLA is that it doesn't require any kind of protein engineering or chimeric receptor to work, and it can be easily employed even in tissues that don't express high levels of dimers (Boroto Escuela et al, 2013). However, as antibodies are bulky molecules, PLA can only prove molecular proximity between two receptors, but not their actual dimerization.

5.2 GENERAL STRATEGY AND EXPERIMENTAL PLAN

All the previously described techniques, which are the most commonly used to study receptor complexes in native tissues (and in particular in the brain) can only prove molecular proximity, but not actual dimerization. The precise localization and quantification of true dimeric complexes is still an unsolved experimental issue. For this reason, during my PhD I worked in collaboration with Prof. Bellini's group (Complex Fluids and Molecular biophysics Laboratory, University of Milan) to develop a new approach to map the presence and the distribution of OTR dimeric structures in the mouse brain. We aimed to develop a DNA "Nanoruler" technology based on *ad hoc* designed oligonucleotides conjugated with selective OT analogues to detect OTR homo and heterodimers. After binding to the receptors, these OT-DNA conjugates promote a single hybridization event between the two complementary oligonucleotides, followed by an Hybridization Chain Reaction (HCR) step capable to generate a detectable, fluorescently labelled DNA structure. In this way, the dimeric receptors will be detected with a spatial resolution much higher than that obtained with currently antibody-based techniques, such as Proximity Ligation Assay (PLA). The DNA hairpins have been designed and characterized *in vitro* by Prof. Bellini's research group, with my collaboration; in parallel, I worked to design and develop an OT analogue that would be suitable for DNA conjugation.

Our Nanoruler system is composed by 5 different DNA sequences: two different 50-nucleotides-long hairpins named Pan and Dis, a "triggering" 24-nucleotides-long sequence named Trigger, and two fluorescent reporter probes named H1 and H2. Pan, Dis and Trigger, that are the core components of the Nanoruler system, are represented in Fig.1.

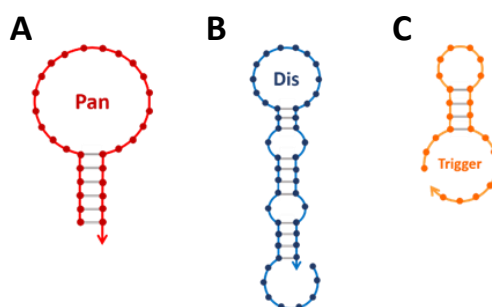


Figure 1: Sketch of the three DNA hairpins that compose the Nanoruler system.

Trigger is designed to be able to open Dis through a 6-nucleotides long toehold. Once opened, the Dis-Trigger complex becomes able to bind Pan through its complementary region, which is located in Pan's loop. This interaction forces Pan to open, generating a stable complex formed by Pan, Dis and Trigger (Fig. 2).

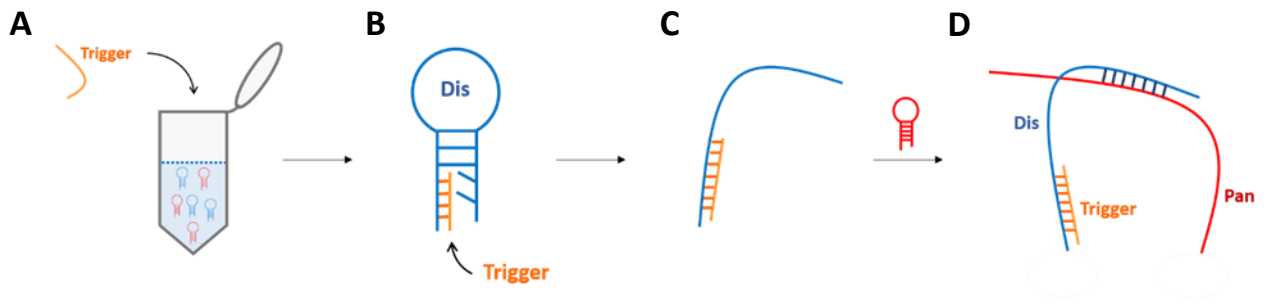


Figure 2: Nanoruler mechanism in vitro. When added in solution (A), Trigger opens Dis through hybridization with a short sequence on its stem (B), and if the opened Dis is close enough to Pan (C) it can form a complex with it (D).

To detect homodimers in our biological systems, the Nanoruler DNA hairpins need to be able to actually interact with OTRs. To do so, both Pan and Dis have been linked OT analogues, previously modified and characterized in order to retain the same pharmacological properties of endogenous OT (Figure 3).

In a biological environment, what is expected to happen is that a Pan-Dis complex will form only when two conditions are contemporarily achieved:

- 1) Trigger is present in solution
- 2) Pan and Dis are close enough to interact (i.e. because they are inserted in the two homomers of the same dimer).

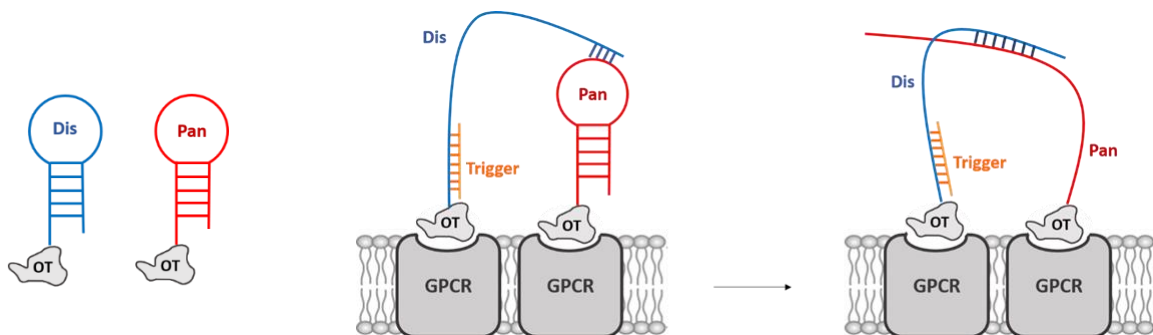


Figure 3: Nanoruler system application on biological environments. Left part: in order to use it on GPCRs, the Nanoruler components must be linked to a ligand selective for the GPCR of interest. Right part: once engineered with the ligand, the two hairpins can «interact» with the receptors; Pan and Dis will form a complex only if 1) Trigger is present, and 2) they are bound to the two protomers of the same GPCR dimer. In our specific case, the ligand will be a selective OT analogue.

It is important to notice that when used over homodimers, this system will let us detect approximately 50% of the total receptor population; all the dimeric receptors bound by two Pan or two Dis molecules will not be highlighted by the fluorescent “tree”, as Pan can only be opened by Dis.

To be able to detect a single OTR homodimer as a light spot without using high-resolution microscopy, we will need a strong amplification of the fluorescent signal. Because of that, we coupled our Nanoruler assay to a signal amplification technique called Hybridization Chain Reaction (HCR) by implementing two 36-nucleotides-long reporter sequences, H1 and H2, in the system (Fig.4). These two DNA strands have been designed to be cross-complementary, and just like for Pan and Dis, when in solution alone they are stable in their “closed” hairpin conformation.

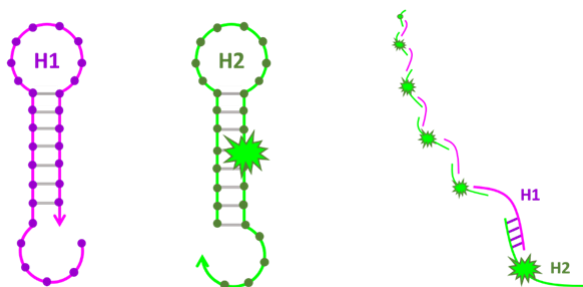


Figure 4: *H1 and H2, the two hairpins that reveal the Pan-Dis-Trigger complex.*

When Pan is in its “open” conformation, it can bind H1. In turn, the opened H1 can cross-hybridize with H2, and form a nicked double stranded chain. H2 sequence is tagged with a fluorophore; the more H2 strands are incorporated in the growing DNA “tree”, the brighter the fluorescent spot will be (Fig.5).

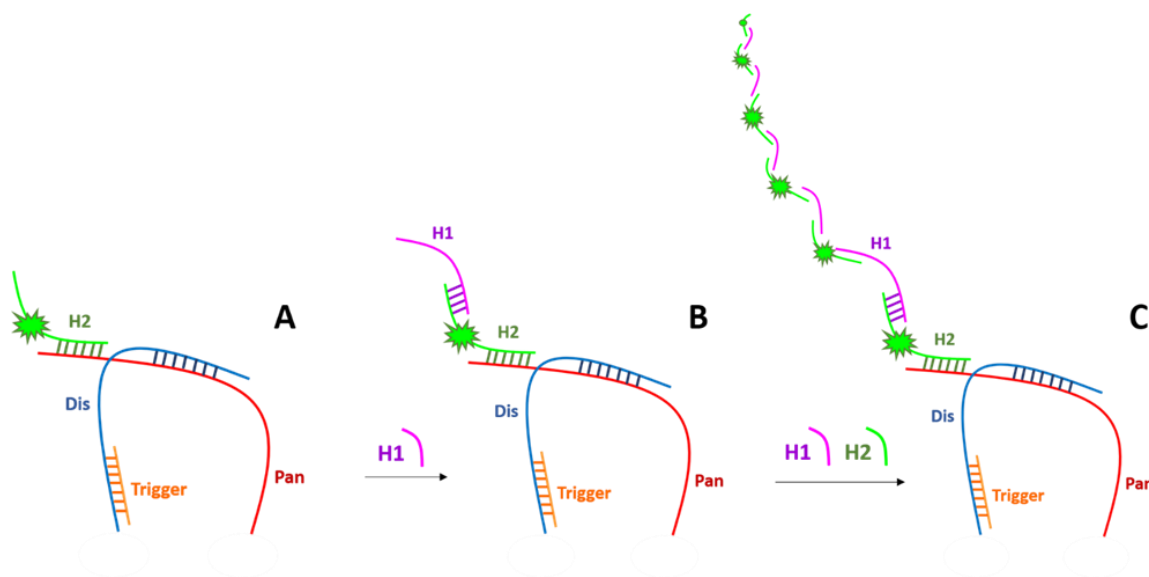


Figure 5: *Nanoruler detection system.* When Pan is in its «open» conformation, it can open Hairpin 1 (H1) (A). H1 has been designed to cross-hybridize with the fluorescent Hairpin 2 (H2) (B); the two hairpins can therefore start an amplification chain reaction that leads to the formation of a fluorescent «tree» (C).

5.3 MATERIALS AND METHODS

Ligands and reagents

Oxytocin was purchased from Sigma. Vasopressin was purchased from Bachem. Oxytocin analogues modified through the insertion of an azidic group (N_3) were synthesized in the laboratory of Dr. Alessandro Gori (Istituto di Chimica e del Riconoscimento Molecolare del CNR, Milan) through a peptidic, microwave-adiuvated solid phase synthesis (MW-SPPS) protocol, purified and analyzed through RP-HPLC (Reversed Phase – High Performance Liquid Chromatography). DBCO-Alexa594 used in the click-chemistry reactions was purchased by Click Chemistry Tools. [3H]-OT (specific activity 49.5 Ci/mmol) was purchased by Perkin Elmer. DNA hairpins Pan, Dis, Trigger, H1 and H2 were purchased from Integrated DNA Technology® (IDT®).

Click-chemistry conjugation

The day before each experiment, OTAha, OTLys N_3 , Thr⁴OTAha or Thr⁴OTLys N_3 were incubated O/N at RT in the dark with DBCO-tagged fluorophore Alexa594 or with the DBCO-tagged DNA hairpins Pan and Dis. Both the elements were diluted in PBS at a final concentration of 100 μ M in a 1:1 molar ratio.

HPLC analysis

Reversed Phase – High Performance Liquid Chromatography (RP-HPLC) was performed on a Shimadzu Prominence chromatograph, using a Shimadzu Shimpack GWS C18 column (5 micron, 4.6 mm i.d. x 150 mm). Analytes were eluted in a binary gradient of a mobile phase A (100% water, 0.1% trifluoroacetic acid) and a mobile phase B (30% water, 70% acetonitrile, 0.1% trifluoroacetic acid). The gradient used was the following: from 90% to 0% of A in 14 minutes; flow rate 1 mL/min.

Cell cultures

HEK293 (Human Embryonic Kidney) cells were maintained in DMEM (Dulbecco Eagle's Modified Medium, Sigma) complemented with FBS 10% (v/v) (Fetal Bovine Serum, Sigma), L-Glutamine 2 mM (Sigma), Penicillin 100 units/mL and Streptomycin 100 μ g/mL (Sigma), at 37°C and 5% CO₂.

HEK293 cells stably transfected with an OTR-EGFP plasmide were maintained in DMEM (Dulbecco Eagle's Modified Medium, Sigma) complemented with FBS 10% (v/v) (Fetal Bovine Serum, Sigma), L-Glutamine 2 mM (Sigma), Penicillin 100 units/mL and Streptomycin 100 μ g/mL (Sigma), at 37°C and 5% CO₂. Geneticin (G418, Sigma) was used as a selection antibiotic and added at a final concentration of 500 μ g/mL to the culture medium.

Transfection

For BRET studies and AVPR staining experiments HEK cells were transiently transfected using Polyethyleneimine (PEI, linear, (C₂H₅N)_n, P.M. 25000; Polysciences) as a transfecting agent.

Cells were seeded at a final concentration of 3.1×10^6 cells/mL in 100 mm Petri dishes, or 3.1×10^5 cells/mL in 35mm wells for cellular staining protocols.

The day after seeding, a 20 μ g total of DNA were transfected in each plate (or well), adding PEI (stock concentration: 1 mg/mL) in a 1:3 ratio and non-complemented DMEM in order to achieve a final transfection volume of 1/10 of the total medium contained in the plate/well. The transfection mix was briefly vortexed, incubated at RT for 15 minutes and slowly added to the cells. After 24h the culture medium was changed, and cells were maintained in culture for another day before being processed for the experiment.

BRET assays

In our work we used two different BRET biosensors and applied two different variations of BRET, BRET¹ and BRET².

BRET². To measure Gq activation, DNA plasmids encoding for the BRET donor *Renilla Luciferase* (RLuc8)-G α q (4 μ g), the BRET acceptor GFP¹⁰-G γ 2 (5 μ g), G β 1 (5 μ g) and OTR pRK5 construct (7 μ g) were used. 48h after transfection, HEK293 cells were washed twice with PBS, harvested and resuspended in PBS, 0.1% (w/v) glucose, 0.5 mM MgCl₂ and 0.7 mM CaCl₂. Protein concentration was determined using a colorimetric protein assay (DC protein assay, Biorad, Milan, Italy). For each BRET measurement, 80 μ g of proteins per well were distributed in a 96-well microplate (Optiplate, Perkin Elmer, Milan, Italy), stimulated with different ligands at different concentrations or with PBS for 2 min prior to the addition of RLuc8 substrate, coelenterazine 400A (Biotium, Hayward, CA), at a final concentration of (5 μ M). Immediately after the addition of coelenterazine 400A (5 μ M), RLuc8 and GFP¹⁰/GFP² emissions were recorded using a multidetector plate reader Infinite F500 (Tecan, Milan, Italy) that allows the sequential integration of light signals detected with two filter settings (RLuc filter, 370-450 nm; and GFP¹⁰/GFP² filter, 510-540 nm). Data were collected and the BRET² signal determined as the ratio of the light emitted by acceptors (GFP₁₀/GFP₂) over donors (RLuc8). The “ligand promoted BRET” value was calculated by subtracting the BRET signal measured ligand-stimulated cells from that obtained in PBS-stimulated negative controls, following this equation:

$$\text{BRET ligand effect} = \left(\frac{em_{GFP10}}{em_{RLuc8}} \right)_{\text{ligand}} - \left(\frac{em_{GFP10}}{em_{RLuc8}} \right)_{\text{PBS}}$$

BRET¹. To measure β -arrestin recruitment, DNA plasmids encoding for the BRET donor *Renilla Luciferase* (RLuc)-hOTR (1.5 μ g), the BRET acceptor β arr1-YFP (or β arr2-YFP depending on the experiment) (5 μ g), and pcDNA 3.1 (13.5 μ g) were used. For each BRET measurement, 80 μ g of proteins per well were distributed in a 96-well microplate (Optiplate, Perkin Elmer, Milan, Italy). Coelenterazine H substrate was added at a final concentration of 5 μ M, and cells were further incubated for 8 minutes prior the addition of the different ligands (final concentration 10 μ M) or PBS. For each well, BRET values to build the kinetic curve were read every 3 seconds using the multidetector plate reader Infinite F500 (Tecan, Milan, Italy). For BRET¹, two filters were

used: BLUE 370-480 nm (RLuc) and GREEN 520-570 nm (YFP). BRET measurements were calculated as the difference between ligand-stimulated cells and PBS-stimulated negative controls (Δ BRET).

Competition binding assay

Competition binding experiments were performed on HEK293 OTR-EGFP cellular membrane homogenates. 72h after transfection, cells were washed with PBS, and resuspended in phosphate buffer (NaCl 140 mM, KCl 2.7 mM, Na₂HPO₄ 8.3 mM; K₂HPO₄ 1.2 mM). After a centrifugation step at 670 g for 5 min at 4°C, cells were resuspended in ice-cold lysis buffer (Tris 15 mM, MgCl₂ 2 mM, EDTA 0.3 mM, pH 7.4 at 4°C) and homogenized in a glass potter. The homogenate was then centrifuged at 16.720 g for 20 min at 4°C; the membrane pellet was washed with ice-cold binding buffer (Tris 50 mM, MgCl₂ 5mM, 1 mg/mL BSA, pH 7.4), centrifuged again and resuspended in binding buffer. After determination of the proteic concentration through Lowry protein dosage protocol, the homogenate has been aliquoted and stored at -80°C until use.

For Post Nuclear Supernatant (PNS) membranes, after cell lysis and homogenization we added a mild centrifugation step to remove all the nuclear content.

Each competition binding experiment was performed in Pyrex tubes, analyzing the effects of each ligand concentration in triplicate. All the tubes were put in ice, and in each of them the following were added: 100 μ L of binding buffer 2X (Tris-HCl 100 mM pH = 7.4 , MgCl₂ 10 mM, 2 mg/mL BSA), 25 μ L of the ligand to be tested in increasing concentrations (from 10⁻¹⁴ to 10⁻⁵ M), 25 μ L of the radioligand [³H]-OT (Perkin Elmer) used at a final concentration of 2 nM, and a fixed concentration of cellular homogenates (from 20 μ g/tube to 40 μ g/tube, depending on the experiment). To determine all the unspecific binding of the radioligand, for each experiment a few tubes were included where the [³H]OT was incubated together with an excess (1000x) of “cold” (non-radioactive) OT. Once assembled, the tubes were briefly vortexed and left in incubation for 30 minutes at 30°C. The content of each tube was then transferred on a Whatman GF/C filter, previously equilibrated in a BSA solution (10 mg/mL). Tubes were washed three times using cold filtration buffer (Tris-HCl 1M pH 7.4, MgCl₂ 500 mM); filters were then left to dry, and their radioactivity content was determined using a β -counter (Packard). Data were used to draw displacement curves on GraphPad Prism 5, in order to calculate each ligand’s K_i through Cheng and Prusoff’s equation (Cheng & Prusoff, 1973).

Cellular staining protocols

For staining and colocalization studies, cells were seeded on glass coverslips coated with 0.1% poly-lysine as previously mentioned, and left to grow for 24 hours.

The day of the experiment, cells were washed three times with PBS and incubated for 30 min at 37°C in the dark, in a solution containing PBS, CaCl₂ 0.7 mM, MgCl₂ 5 mM, BSA 1% and either the fluorescent ligand or the clickable fluorophore alone, at a final concentration of 100 nM.

After incubation with the ligand, cells were rapidly washed three times in an ice-cold PBS solution containing MgCl₂ 5mM and CaCl₂ 0.7mM and fixed with paraformaldehyde 4% for 15 minutes. After the fixation step,

cells were washed again three times in PBS; their nuclei was stained with DAPI for 5 min at RT, and after three other washing steps each coverslip was mounted on a glass slide (Superfrost) using MOWIOL.

Slides were then observed at a confocal LSM 800 Meta (Zeiss) using the following filters: λ_{Ec} 353 nm and λ_{Em} 465 nm (DAPI), λ_{Ec} 493 nm and λ_{Em} 517 nm (EGFP), λ_{Ec} 508 nm and λ_{Em} 524 nm (YFP), λ_{Ec} 580 nm and λ_{Em} 618 nm (Alexa594). Images were then processed through ImageJ image analysis software.

PAGE experiments

To assess DNA hairpins stability, samples of Pan, Dis, Trigger, H2 and H1 were prepared at a final concentration of 500 nM, and incubated for different time intervals (10 min, 2h, 24h) and temperatures (4°C, 25°C and 37°C) before being loaded on a non-denaturing 6% polyacrylamide gel. The gel was then run in TAE 1X running buffer at 80V for 1 hour, and DNA bands containing Cy3 or stained with GelRed 1X were then visualized through a UVTEC transilluminator.

5.4 RESULTS

5.4.1 Design and *in vitro* characterization of the oligonucleotides.

Pan, Dis and Trigger have been designed using a structure prediction tool Nupack (Zadeh et al, 2011), while H1 and H2 sequences were taken from Ang and Yung work (Ang and Yung, 2016).

Evaluation of incubation conditions effects. We first evaluated the interactions between Pan and Dis in solution. To rule out the possible formation of non-specific complexes between each element and to determine which are the time and temperature effects on the sequences stability, we incubated Pan (P) and Dis (D) at different temperatures (4°C, 25°C and 37°C) and time intervals (10 min, 2h, 24h). Samples were then loaded on a non-denaturing 6% polyacrylamide gel (PAGE) and run in TAE 1X running buffer at 80V for 1 hour. As a positive control we used a combination of Pan and Dis previously annealed at 95 °C for 10 minutes; as the intense heat forces the two hairpins to open, in this sample we can actually observe the formation of a heavier DNA complex made by their pairing (Fig. 6).

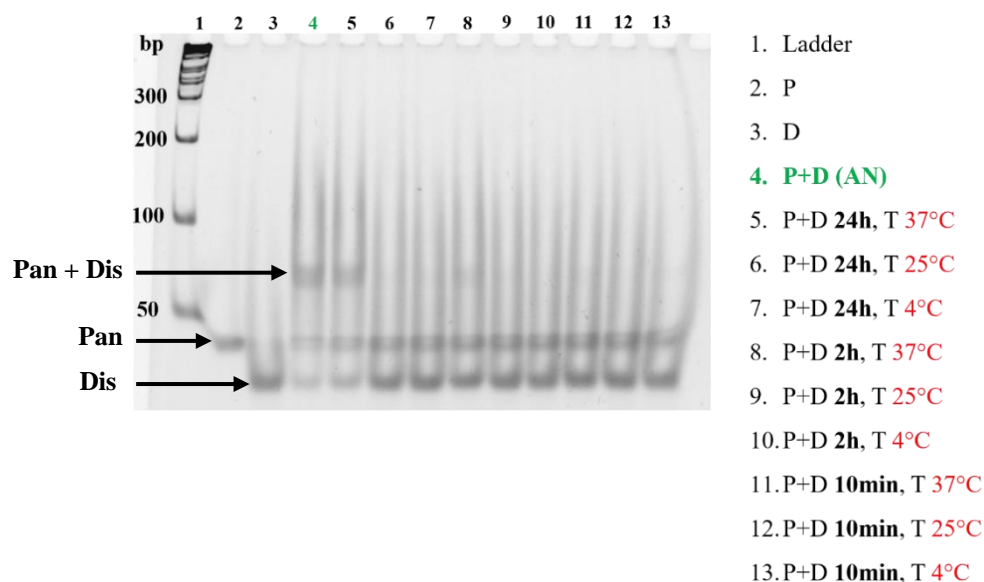


Figure 6: *In vitro* evaluation of Pan / Dis interaction. 6% PAGE gel loaded with Pan and Dis (final concentration: 500 nM) incubated alone (lanes 2, 3) or together (lanes from 4 to 13) for different times and at different temperatures. Lane 4 (highlighted in green) is a positive control: the sample has been annealed for 10 min at 95°C to assess the Pan+Dis complex formation (visible as a slower band on the gel). Bands corresponding to each molecular species are indicated by black arrows. P = Pan, D = Dis, AN = annealed.

From these first PAGE experiments it can be seen that both the DNA hairpins are stable at all the different temperatures. Lower incubation times do not affect stability either, while at 24 hours the sample that has been kept at 37°C develops a certain amount of non-specific Pan+Dis complexes. Quantification of the intensity of the heavier band confirmed these data

Analysis of the HCR cascade. Another important step in order to better characterize the DNA Nanoruler assay was to test Pan ability to bind an H2 reporter sequence and start an HCR amplification cascade, only when it finds itself in complex with Dis and Trigger.

To test the interaction between Pan and the two HCR fluorescent probes H1 and H2, different combinations of these sequences were mixed together, incubated for different time points and temperatures and loaded on a 6% polyacrylamide gel (Fig. 7). As a positive control we used a sample in which an annealing step at 95°C for 10 minutes causes the generation of aspecific HCR products formed by Pan, H1 and H2 (lane 4).

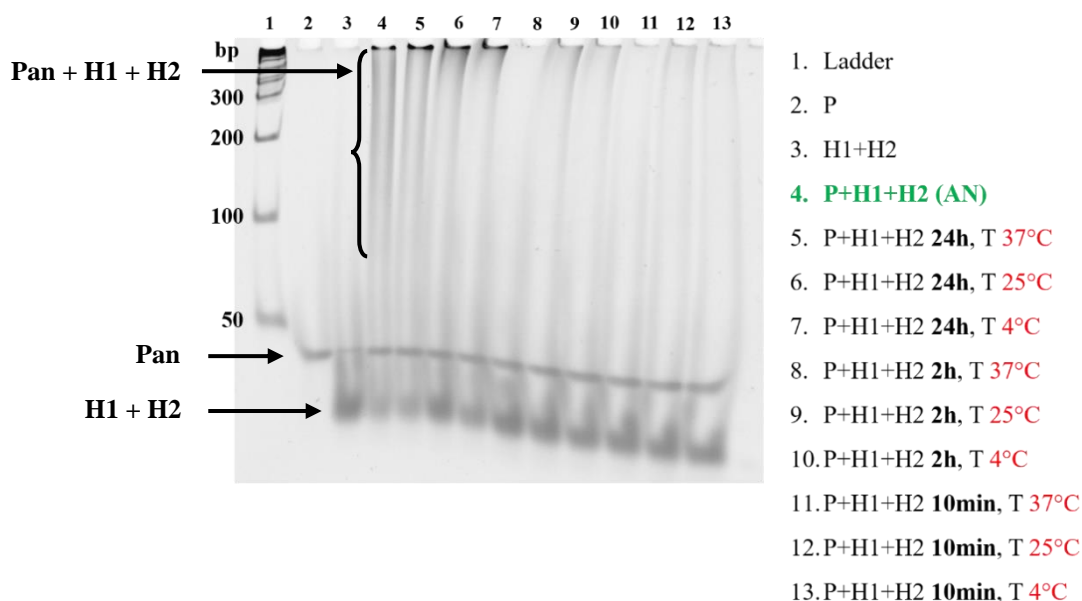


Figure 7: In vitro evaluation of Pan / H1 / H2 interactions. 6% PAGE gel loaded with Pan, H1 and H2 (final concentration: 500 nM) incubated alone (lanes 2, 3) or together (lanes from 4 to 13) for different times and at different temperatures. Lane 4 (highlighted in green) is the positive control, annealed at 95°C for 10 min. The Pan + H1 + H2 complexes are visible as a darker smear in the upper part of the lane. Each molecular species is indicated by black arrows. P = Pan, AN = annealed.

While the DNA sequences incubated for 2 hours remained stable at all temperatures (lanes from 8 to 13), after 24 hours we could observe the formation of unwanted HCR products in all the samples (lanes from 5 to 7), visible as high-molecular-weight products in the upper part of the gel.

To be able to quantify the Pan fraction in each band, we repeated the experiment using a fluorophore-tagged Pan sequence, PanCy3, and acquired its signal using a UVTEC transilluminator before GelRed staining (Fig. 8).

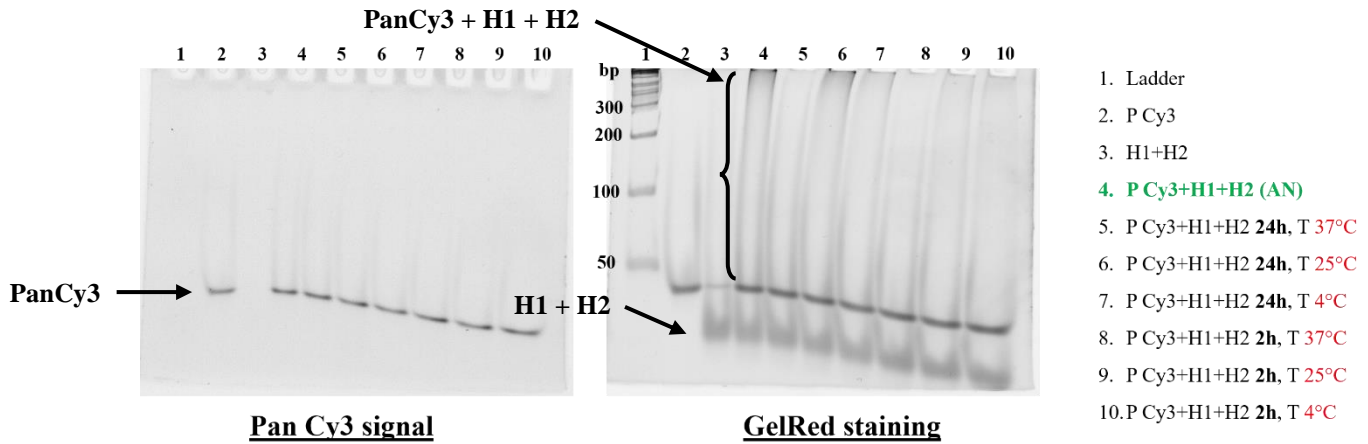
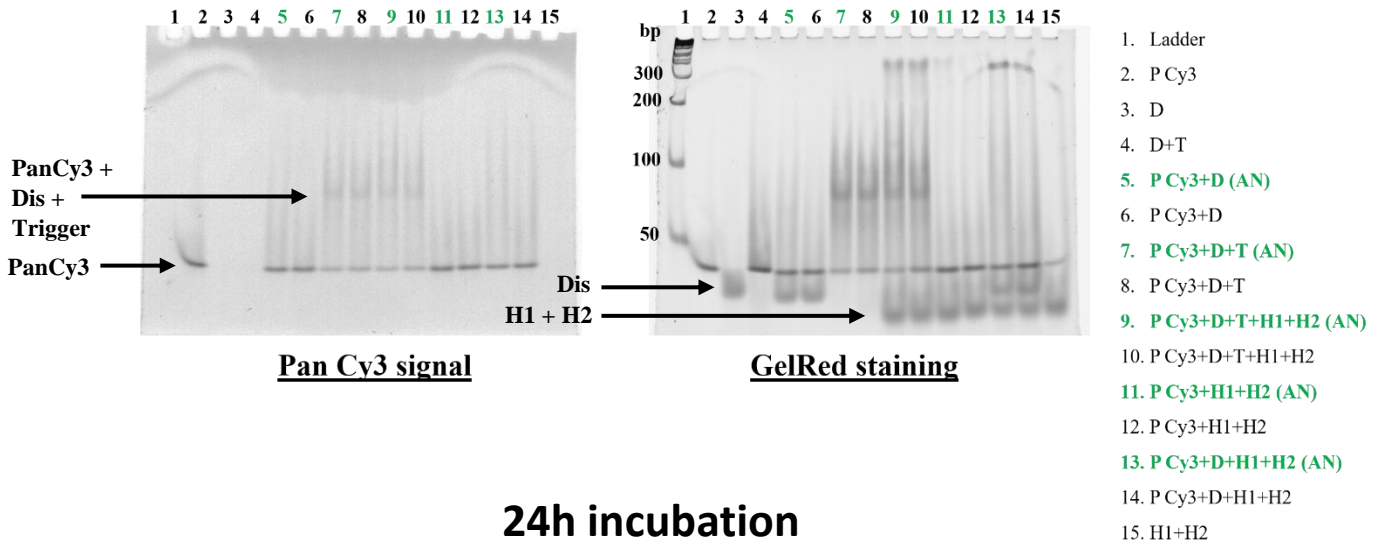


Figure 8: Quantification of Pan fraction inside putative aspecific Pan+H1+H2 complexes. 6% PAGE gel was loaded with PanCy3, H1 and H2, alone (lanes 2,3) or together (lanes from 4 to 10), for different times and at different temperatures. Left image shows only the Cy3 signal coming from Pan, while right image shows the same gel coloured with GelRed to reveal all the other DNA sequences present inside the bands. Lane 4 is the positive annealed control; Each molecular species is indicated by black arrows.

From this second experiment we can see that in the samples incubated for 24h, the amount of Pan is actually negligible, and therefore the products we see are mostly constituted by H1 and H2. Surprisingly enough, even when considering the annealed positive control in lane 4 it is evident that there is no PanCy3 signal in the upper band. This might mean that Pan is too stable in solution, and even after an annealing step it is not able to hybridize with H1 and H2.

Lastly, to try to quantify the efficiency of the hybridization reaction between Pan and H2, Cy3-tagged Pan sequence was used to establish the Pan fraction present in complex with H2 and in high-molecular weight HCR products. Samples were incubated for 2 hours or for 24h (Fig. 9).

2h incubation



24h incubation

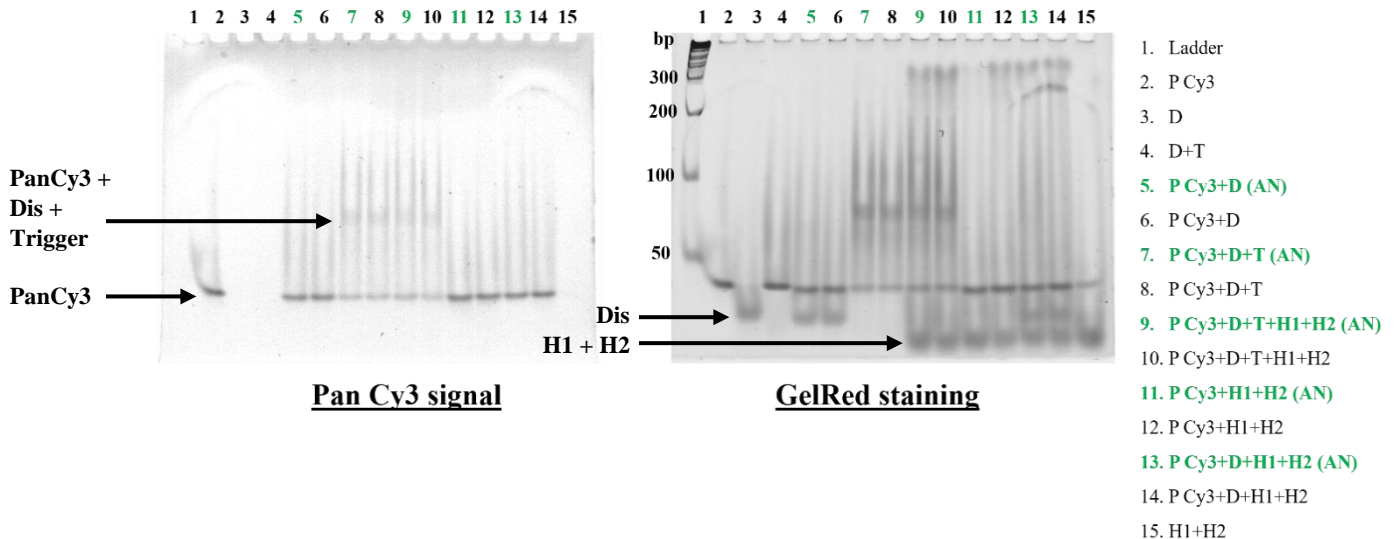


Figure 9: Evaluation of Pan+Dis+Trigger complex ability to start the HCR reaction. 6% PAGE gel loaded with Pan, Dis, Trigger, H1 and H2 in different combinations (final concentration 500 nM), incubated 2hours (upper gel) or 24 hours (bottom gel) at RT. Positive controls (highlighted in green) were annealed for 10 min at 95°C. Left images show only the Cy3 signal coming from Pan, while right images show the same gels coloured with GelRed to reveal all the other DNA sequences present inside the bands.

In both cases, we could not detect PanCy3 in the higher band containing the HCR product. However, we can be sure that at least a small fraction of PanCy3 reacts with H1 and H2, because in the samples where PanCy3 is not present there is no generation of high-molecular-weight products (lane 15) formed exclusively by the two reporters.

Assuming that when Dis and Trigger are present in solution the P+D+T complex forms with a high efficiency, there should be enough “opened” Pan able to start the HCR reaction. However, these results led us to hypothesize that Pan-H2 interaction is less stable/strong than expected. For this reason, Prof. Bellini’s group designed and tested three new H2 sequences, called H2+1, H2+2, H2+3, which respectively are able to interact with one, two or three more Pan nucleotides, to try to increase the stability of Pan-H2 interaction. Results showed that H2+3 bound Pan with the higher efficiency, making it more prone to start the HCR process. Therefore, we chose H2+3 as the election sequence for the following experiments.

5.4.2. Design and characterization of the “clickable” OT analogues

To generate the ligand that will be used in the complete system to detect OTR dimers, we then proceeded to link each hairpin to an oxytocin molecule.

Oxytocin is a small nonapeptide with two cysteines in position 1 and 6, linked by a disulfide bridge; its rough shape is that of a circle with a small 3-aminoacid-long tail. When it is bound in its receptor, the circular part is inserted in the binding pocket, while the tail protrudes in the extracellular space. In our laboratory we previously studied the molecular determinants of OT selectivity and specificity for its receptor (Busnelli and Chini, 2017; Busnelli et al, 2013). Through these studies we found that modifying the aminoacid in position 8 (a leucine) does not affect OT receptor binding properties, and therefore we chose this aminoacid to insert a chemical modification that would allow us to attach oxytocin to our DNA hairpins. In particular, for this conjugation step we used a “Click” chemistry reaction, in which an azide group spontaneously reacts with a diarylcyclooctyne (DBCO) moiety (Fig. 4). From literature we already know that the reaction is highly specific, because azide groups nor dibenzylcyclooctyne exist in biological systems, and it is also reasonably rapid (1-2h) and stable.

We worked with Alessandro Gori (affiliation) to synthesize two OT analogues suitable for click chemistry: OT-AhaN₃, bearing a N₃-L-azidohomoalanine (Aha) residue in position 8, and OTLysN₃, bearing a LysN₃ in the same position (Fig. 10).

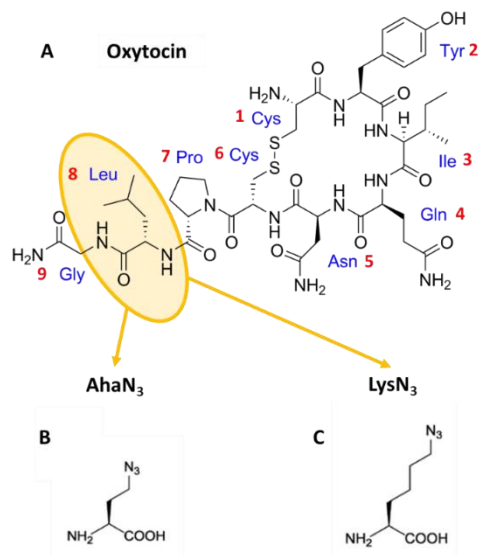
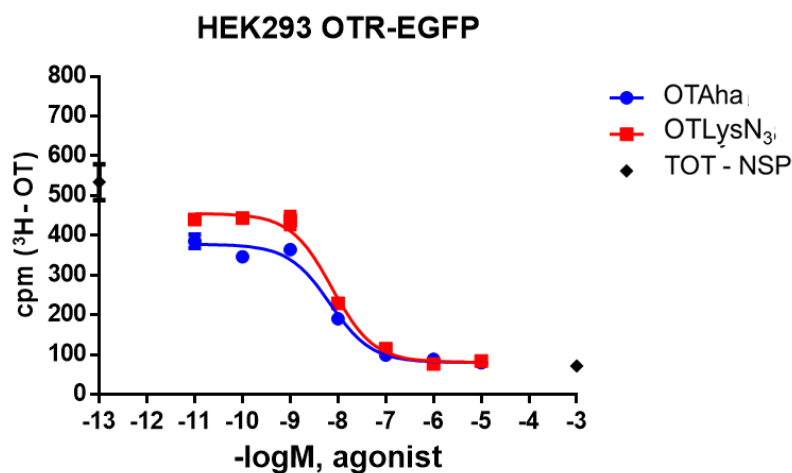


Figure 10: OT analogues structure design. To obtain «clickable» OTR ligands, the leucine in position 8 (highlighted in orange) was substituted either with an N_3 -L-azidohomoalanine (B) or with a $LysN_3$ (C). The azide group N_3 is the one required for the conjugation reaction.

We next tested the pharmacological properties of the two OT analogues through competition binding experiments, Bioluminescence Resonance Energy Transfer (BRET) assays and internalization studies.

Competition binding experiments. To determine OTAha and OTLysN₃ affinity for the OTR, we performed competition binding experiments on cellular homogenates of HEK293 cells stably transfected with an OTR-EGFP, using a radiolabeled [³H]-OT at a fixed concentration equal to his K_d (2nM) and testing different analogues concentrations (Fig. 11). The obtained K_i values for OTAha and OTLysN₃ were respectively of 1.9 ± 0.47 nM e 2.1 ± 0.40 nM, similar to that of the unmodified OT, which is 0.8 nM (Busnelli et al, 2012; Chini et al, 1995).



	OTAha	OTLysN ₃
Ki	1.934e-009	2.149e-009

Figure 11: evaluation of OTAha and OTLysN₃ affinity for the OTR. Competition binding on HEK293 OTR-EGFP cellular membranes. Black dots represent total and non-specific binding (obtained incubating membranes with an excess of «cold» oxytocin, final concentration 1 μ M); OTAha and OTLysN₃ dose-response curves are represented in blue and red, respectively. Each value is expressed as mean \pm SEM ($n=3$).

BRET² assays. Together with binding experiments we also performed BRET assays using different biosensors to evaluate the functional properties of the two analogues. In particular, we focused our attention on oxytocin (OTR) and vasopressin (V1aR and V1bR) receptors.

The first BRET biosensor we employed let us measure G protein coupling and receptor activation as a decrease in the resonance energy transfer between a “donor” molecule (in our case, a *Renilla Luciferase 8* or RLuc8) linked to the α subunit and an “acceptor” molecule (a GFP¹⁰) linked to the γ subunit. The BRET decrease is triggered by receptor activation, that induces a conformational change in the heterotrimeric G protein and brings apart the α and the γ subunits.

To evaluate the affinity of the two analogues towards the OTR and the two vasopressin receptors V1Ar and V1Br, we measured Gq activation, because Gq is the main signaling pathway activated by both receptor species. Results are summarized in Fig. 12.

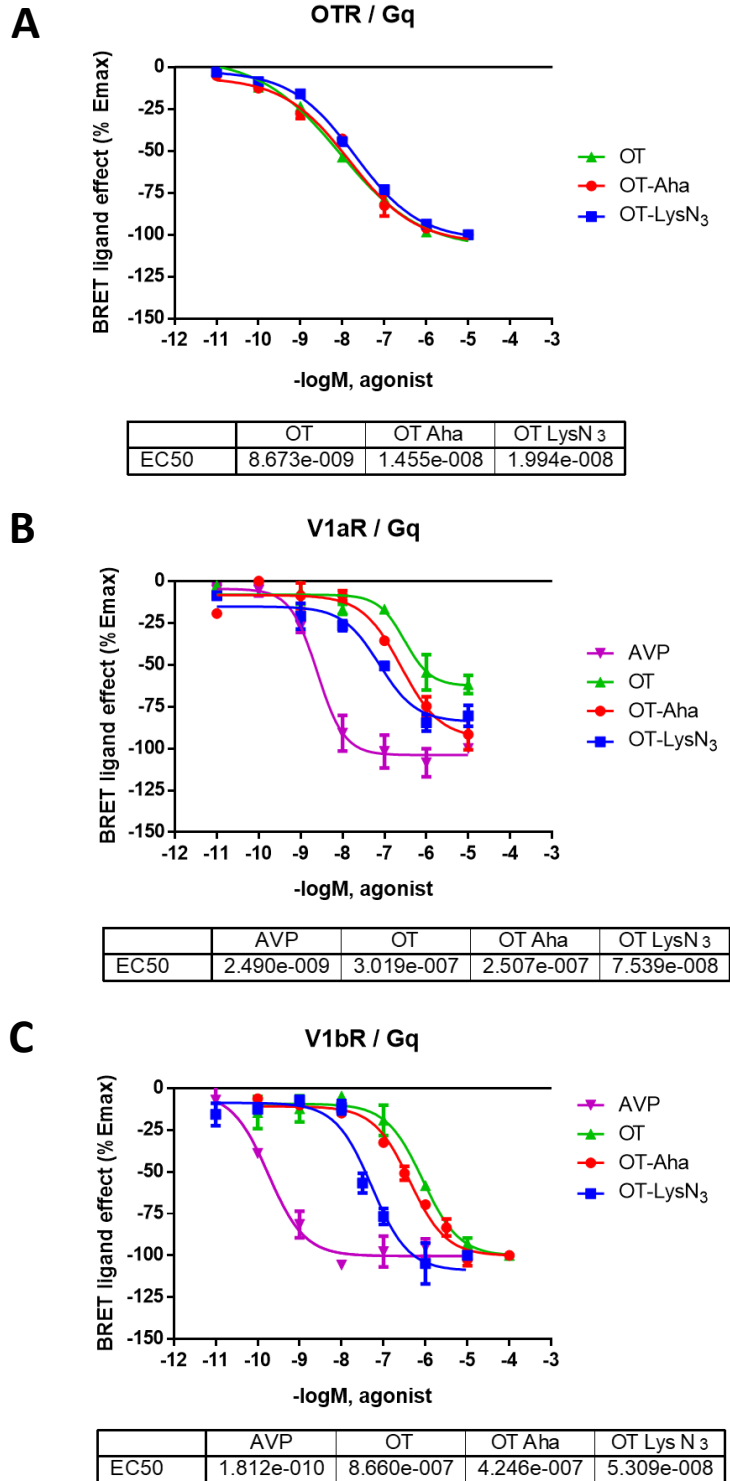


Figure 12: evaluation of OTR (A), V1aR (B) and V1bR (C) activation by OTAha and OTLysN₃. BRET dose-response curves were built stimulating cells for 2 min with increasing OT (green), AVP (violet), OTAha (red) or OTLysN₃ (blue) concentrations. Data are represented as the mean \pm SEM percentage of the BRET ligand effect compared to the agonist concentration logarithm, and were collected as the difference between the BRET value measured in presence of the agonist and the one measured in its absence.

All the ligands produced a monophasic dose-response curve. OTAha and OTLysN₃ EC₅₀ were calculated as 14.55 ± 12.4 nM and 19.94 ± 7.21 nM, respectively; both were not significantly different from OT (EC₅₀ = 8.67 ± 3.73 nM).

For what concerns vasopressin receptors, we determined that both the analogs are agonists for V1aR and V1bR. Again, the EC₅₀ values we obtained (V1aR = 250.7 ± 225 nM for OT Aha and 75.39 ± 68.7 nM for OTLysN₃; V1bR = 424.6 ± 108 nM for OTAha and 53.09 ± 27 nM for OTLysN₃) were not statistically different (p > 0.5) from OT (V1aR = 301.9 ± 549, V1bR = 866 ± 273 nM), and were all significantly higher than AVP EC₅₀ (V1aR = 2.49 ± 1.66 nM; V1bR = 0.18 ± 0.1 nM). However, OTLysN₃ proved to be 10 times more potent than OTAha and OT in activating the V1aR.

It is also interesting to note that while OT and OTLysN₃ behave like partial agonists for the V1aR, OTAha reaches the same E_{max} as AVP.

BRET¹ assays. Once activated by OT, the OTR recruits β-arrestins 1 and 2 to the plasma membrane, triggering its own internalization process (Busnelli et al, 2012; Conti et al, 2009). To understand if our analogs are also capable of inducing β arrestins recruitment we used a second BRET biosensor, where the energy donor RLuc is linked to the OTR, and the energy acceptor YFP is attached to β-arrestin 1 or 2. In this case, β arrestin recruitment can be observed as an increase in BRET signal. HEK293 were transiently transfected with the biosensor components and stimulated with all the different ligands at a concentration of 10⁻⁵M, which is already known to induce the maximal response in terms of β-arrestins recruitment (Busnelli et al, 2012). Results are shown in Fig. 13. 5 minutes kinetics show that the two analogs behave just like endogenous OT, recruiting β-arrestins with a comparable half time (t 1/2) (β-arrestin1: OT 120.5 s, OT Aha 119.5 s; β-arrestin 2: OT 72.28 s, OT Aha 71.40 s) and E_{max}.

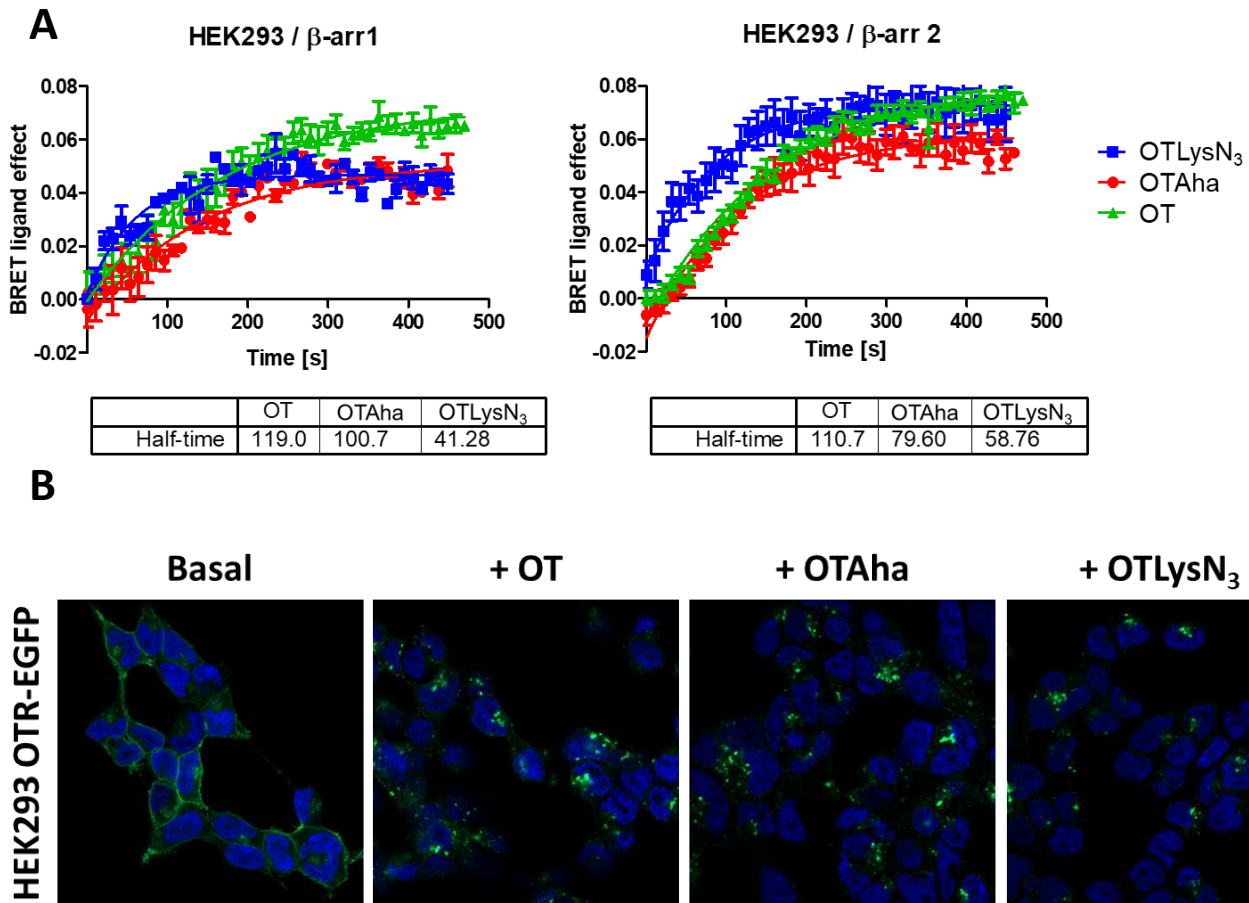


Figure 13: evaluation of β -arrestin 1 and 2 recruitment by OTAha and OTLysN₃ in HEK293 cells. **A**, BRET¹ kinetic curves show the β -arrestin recruitment over 8 minutes induced by OTLysN₃, OTAha or OT, all used at a saturating concentration of 10⁻⁵M; BRET signal was acquired every 3 seconds. Data were calculated as the difference between BRET ratio in stimulated cells vs. BRET ratio calculated in cells stimulated with PBS only. Each value is indicated as the mean \pm SEM of at least two independent measurements. **B**, ligand-induced internalization of the OTR in HEK293 OTR-EGFP cells. Cells were stimulated for 30 minutes with OT, OTAha or OTLysN₃ (final concentration 10 μ M), mounted on glass slides and observed in confocal microscopy. Nuclei are shown in blue, and the green signal comes from the OTR-EGFP. While in basal conditions the receptor is evenly distributed on the cell surface, in ligand-stimulated cells internalization vesicles appear as green spots inside the cytoplasm.

Visualization of OTR internalization by confocal microscopy. BRET¹ measurements let us visualize β -arrestin recruitment to the OTR, but β -arrestin recruitment does not necessarily correspond to receptor internalization. For this reason, we also set up a stimulation protocol to visualize OTAha and OTLysN₃-induced receptor internalization in HEK293 cells stably expressing OTR-EGFP. Cells were seeded on poly-l-lysine glass coverslips, and stimulated with the different ligands at a final concentration of 100 nM (which is able to induce the internalization of all the OTRs in a cell; Conti et al, 2009). Fig. 13 shows that while in PBS-stimulated cells the OTR is evenly distributed on the cellular surface, both analogs correctly induce the formation of internalization vesicles, that can be seen as fluorescent spots.

Oligonucleotide/OTLysN₃ conjugation by click chemistry.

The click conjugation reaction is illustrated in Fig. 14.

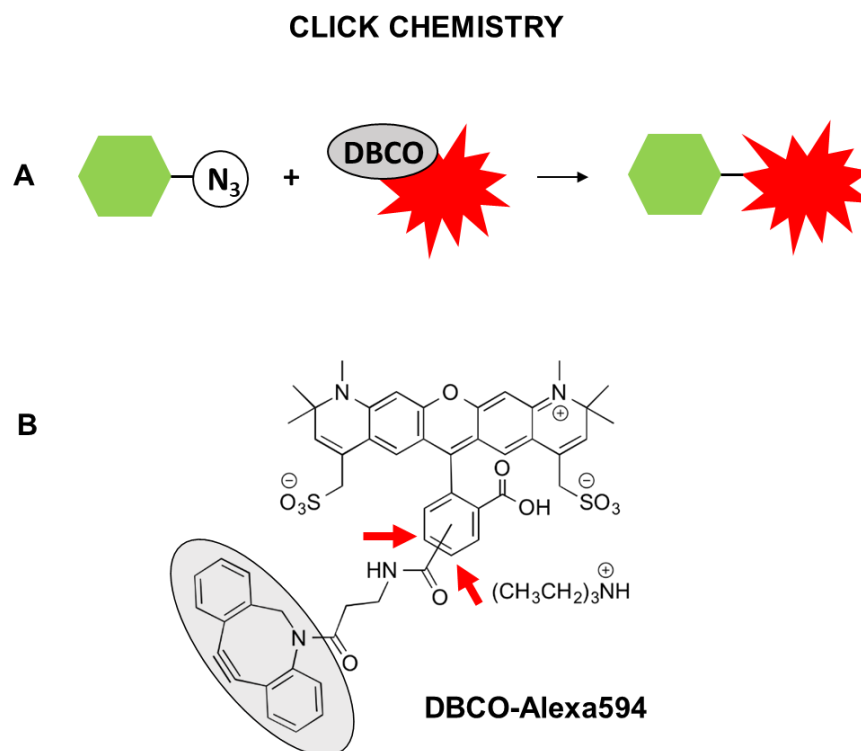


Figure 14: Conjugation of the OT analogues with DBCO-Alexa594 through click chemistry. A, reaction scheme. B, DBCO-Alexa594 structure. The DBCO group is highlighted in grey. Red arrows indicate the two positions on which the aromatic ring can link to the carboxylic chain; Alexa fluorophores can exist in two isomeric forms.

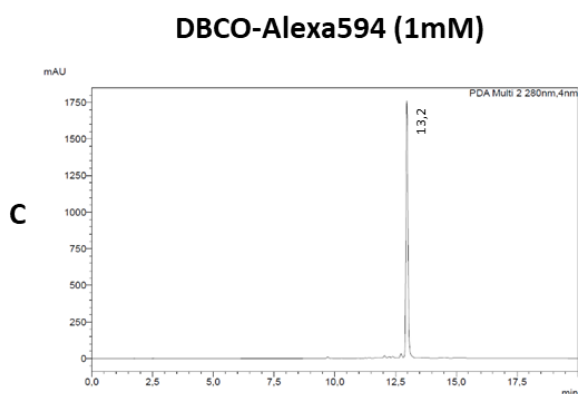
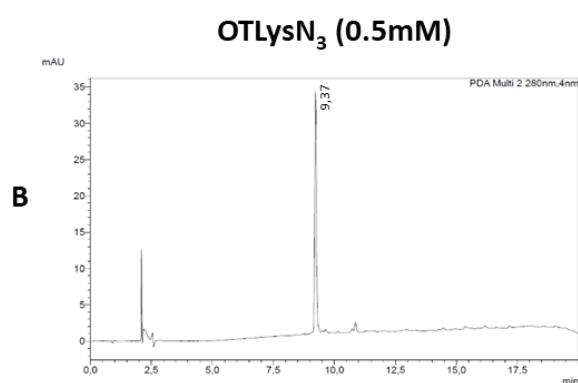
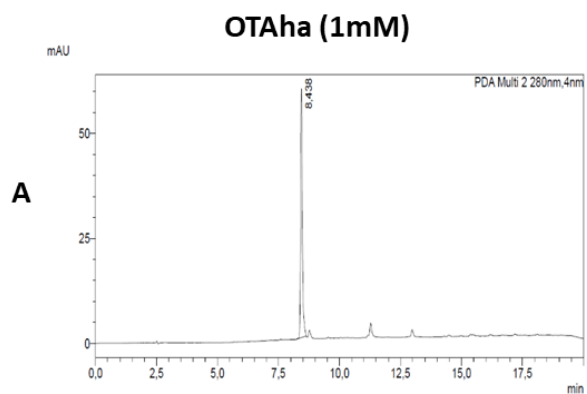
The OTLysN₃ analogue was incubated with a DBCO-tagged Alexa 594 fluorophore O/N at room temperature, and the percentage of free Alexa 594 remaining in the sample was determined by High Performance Liquid Chromatography (HPLC) analysis.

To determine our reaction yield we used a reversed-phase HPLC (RP-HPLC), that separates the different chemical species in a sample depending on their hydrophobicity. The stationary phase of the chromatographic column is apolar (C18), and therefore will interact in a stronger way with apolar molecules: the more hydrophobic they are, the more they will be retained into the column. Each chemical species can therefore be distinguished on the basis of its retention time inside the column. In our case, elution has been made through an incremental acetonitrile gradient in aqueous phase (10% to 100%), in a total analysis time of 20 minutes. Considering the chemical nature of our compounds, we expected a higher retention time for the fluorophores and a lower retention time for the hydrophilic unconjugated peptides. Fig.15 resumes the chromatograms

obtained for each conjugated or unconjugated sample, reporting variations in milliassorbance (mAU) read at 280 nm through time.

Chromatograms of the unconjugated species (Fig. 15) confirmed the purity of each molecule: only a peak is present in each sample, meaning that there are no degradation products in solution. The small peak that appears in OTLysN₃ is the DMSO in which the peptide has been dissolved.

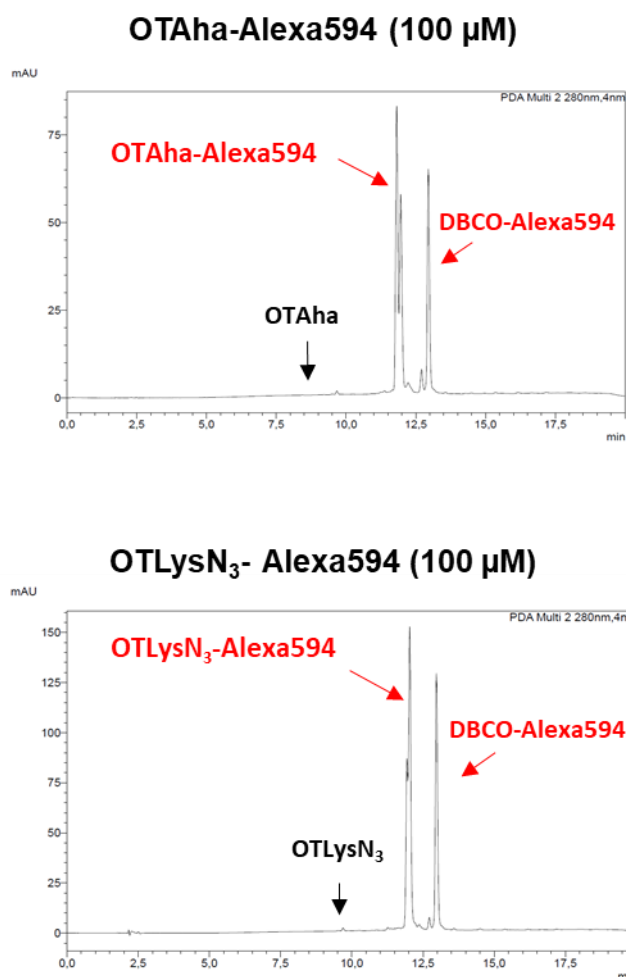
Calculated retention times, compatible with our previsions, are summarized in the table in Fig. 15.



Molecule	Retention time (min)
OTAha	≈ 8.5
OTLysN ₃	≈ 9.25
DBCO-Alexa594	≈ 13

Figure 15: HPLC analysis of OTAha (A), OTLysN₃ (B) and DBCO-Alexa594 (C) purity. Retention time is reported in minutes, while absorbance read at 280 nm is reported as milliabsorbance units (mAU). Each molecule was loaded on the column at a final concentration of 1 mM (0.5 mM for OT-LysN₃). In OTLysN₃, the first peak at 2 min has been produced by the DMSO in which the ligand had been previously resuspended.

We then proceeded to analyze the chromatographic properties of the two conjugated compounds (Fig. 16). As we expected, both OTLysN₃-DBCO594 and OTAha-DBCO594 showed retention times intermediate between those of the single unconjugated molecules, a result compatible with their chemical features. Morphologically speaking, we observed the appearance of a double peak in the OTAha-Alexa594 chromatogram: this is due to the structural isomery of the Alexa594 fluorophore, that brings to the formation of two different isomeric



Molecule	Retention time (min)
OTAha-Alexa594	≈ 11.75
OTLysN ₃ -Alexa594	≈ 12
DBCO-Alexa594	≈ 13

Figure 16: HPLC analysis of OTAha-Alexa594 and OTLysN₃-Alexa594 conjugation efficiency. DBCO-Alexa594 was incubated O/N at RT either with OTAha or OTLysN₃ at a final equimolar concentration of 100 μM, and then each compound was loaded onto the chromatographic column. The double peak in conjugation products is due to the structural isomery of Alexa fluorophores. Time is reported in minutes, while absorbance at 280 nm is reported in miliabsorbance units (mAU).

conjugated products. However, as the fluorescence is conserved in both isomers, and their retention time is also almost overlapping, this phenomenon won't interfere with our studies.

Moreover, from the chromatogram it is clearly visible that the click reaction is highly efficient: the peak corresponding to the unconjugated analogue disappears, meaning that all the OTLysN₃ present in the sample has been "clicked" with the fluorophore. The fluorophore peak is still visible because the two components were not in equimolar ratio: Alexa594 has been kept in excess, in order to facilitate the complete conjugation

of the ligand. This step will help us to be sure that in the next experiments we will not have unconjugated analogues in solution, that being “invisible” would very likely interfere with our evaluations.

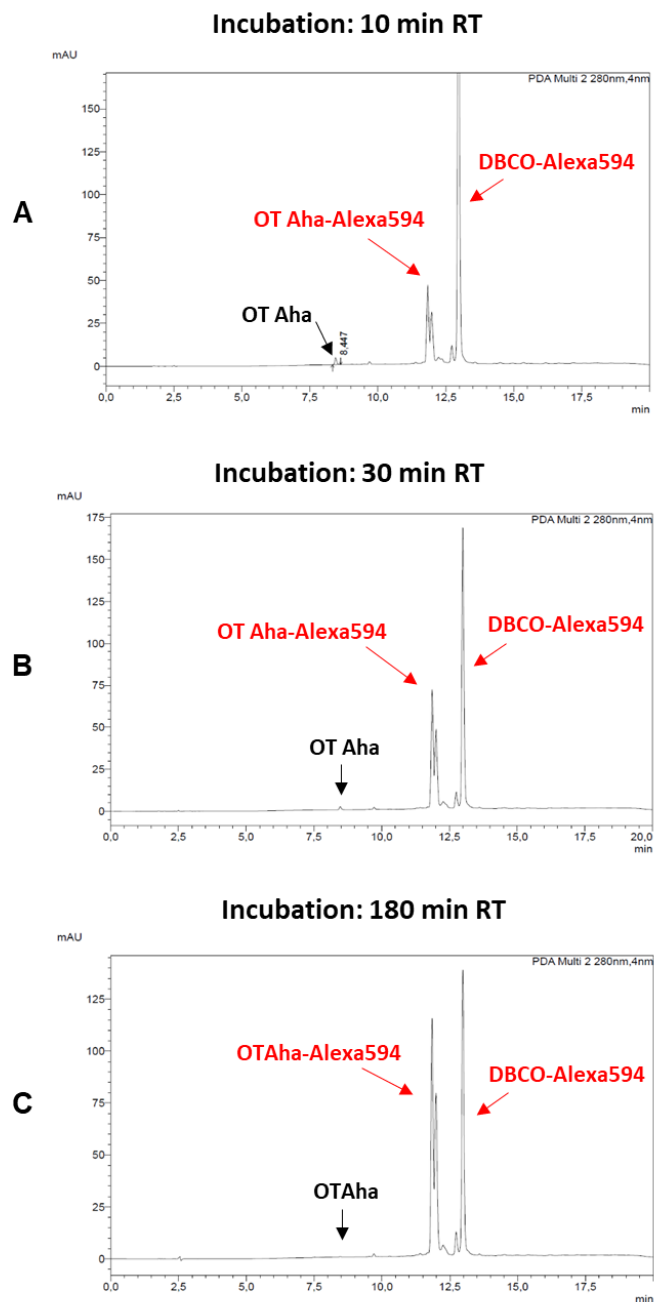


Figure 17: HPLC evaluation of OTAha-Alexa594 and OTLysN₃-Alexa594 conjugation efficiency after different incubation times. DBCO-Alexa594 was incubated for different time point either with OTAha or OTLysN₃ at a final equimolar concentration of 100 μ M, and then each compound was loaded onto the chromatographic column. The double peak in conjugation products is due to the structural isomery of Alexa fluorophores. Time is reported in minutes, while absorbance at 280 nm is reported in miliabsorbance units (mAU).

To determine the optimal conjugation time for our specific reaction, we used HPLC on samples incubated at different time points (10 minutes, 30 min, 180 min). Results in Fig. 17 show that the conjugated ligand peak can already be seen after 10 min of incubation. However, at this time point the unconjugated OTLysN₃ peak is still visible, and it only disappears after 3 hours.

Lastly, to evaluate the stability of our conjugated fluorescent analogue, we analyzed it 10 days after conjugation. The chromatogram in Fig. 18 shows no differences with the chromatogram of the O/N conjugation: therefore, we confirmed that our click reaction is irreversible and does not lead to the formation of degradation products.

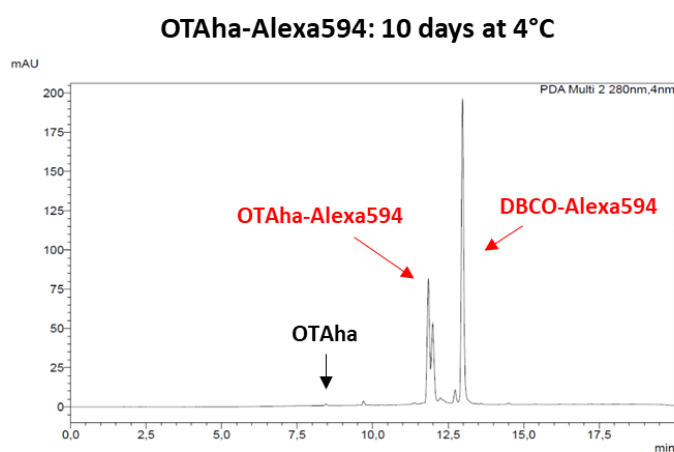
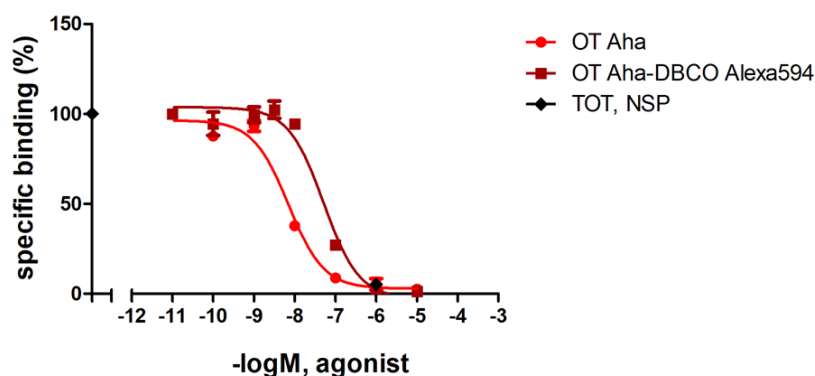


Figure 18: HPLC evaluation of OTAha-Alexa594 conjugation stability after 10 days. OTAha-Alexa594 (final concentration 100 μ M) was kept at 4°C for ten days and then loaded onto the chromatographic column. The double peak in conjugation products is due to the structural isomery of Alexa fluorophores. Time is reported in minutes, while absorbance at 280 nm is reported in milliabsorbance units (mAU).

HEK293 OTR-EGFP



	OT Aha	OT Aha-DBCO Alexa594
Ki	1.993e-009	1.460e-008

Figure 19: Evaluation of click conjugation effects on the OTAha analogue. Competition binding assay on HEK293 OTR-EGFP cellular membranes. Black dots represent total and non-specific binding (obtained incubating membranes with an excess of «cold» oxytocin, final concentration 1 μ M); OTAha-DBCO594 and OTAha dose-response curves are represented in dark and light red, respectively. Each point is represented as the percentage of specific binding. Each value is expressed as mean \pm SEM (n=3).

To verify that the click conjugation does not modify the binding properties of our analogues we determined previously, we also repeated a binding experiment comparing OTAha with its fluorescent counterparts. Results are shown in Fig. 19 and confirm that the affinity for the OTR of our analogues is not modified by the presence of the fluorophore.

To further confirm the correct functioning of the fluorescent version of the analogues, and to check if the DBCO group in the unconjugated fluorophore might produce some unspecific signal, we also conducted a colocalization study between our fluorescent ligands (red) and HEK293 cells stably expressing an OTR-EGFP (green). Cells were stimulated for 30 min at 37°C with either the fluorescent OTLysN₃-DBCO594 or with a DBCO594 fluorophore alone, at a final concentration of 100 nM (Fig.20).

While in the negative control the receptor remains evenly distributed on the cellular surface, and no red signal is detectable, in OTAha-DBCO594 OTLysN₃-DBCO594-stimulated cells we could observe the formation of the internalization vesicles, visible as green spots. Moreover, in these cells we could also see a red 594 signal, distributed in spots inside the cells and perfectly overlapping with the green EGFP signal. DAPI nuclear staining confirmed that our ligand stained selectively only the OTR-EGFP expressing cells.

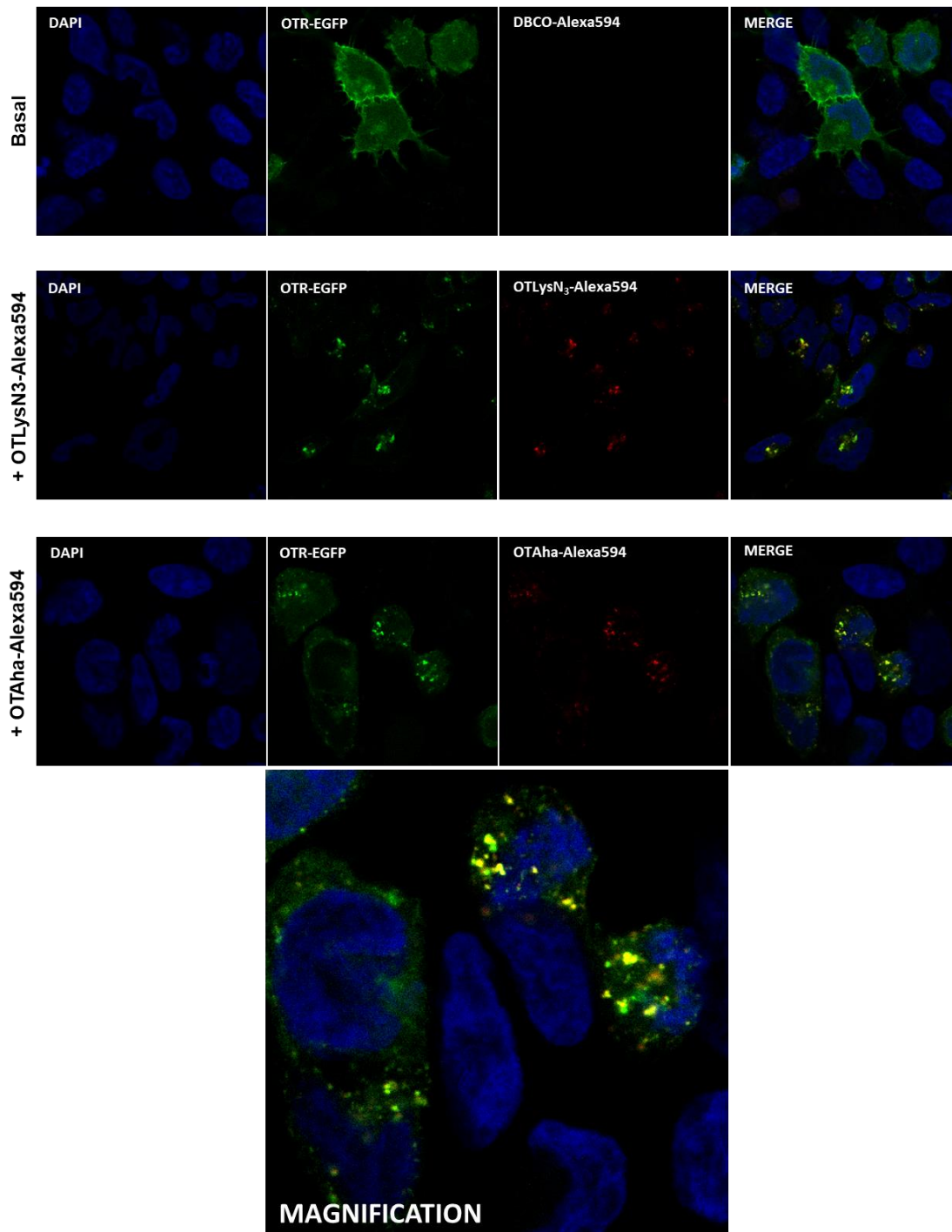


Figure 20: cellular culture staining with fluorescent OT analogs. HEK293 OTR-EGFP cells were incubated 30 min at 37°C with either the Alexa fluorophore alone or with one of the two fluorescent OT analogs, at a final concentration of 100 nM. While in the negative control (first row) the receptor remains evenly distributed on the cellular surface and no aspecific red signal is visible, in ligand-stimulated cells the formation of internalization vesicles can be seen as green and red spots inside the cytoplasm. In cells that don't express the OTR, no red signal is visible, indicating that the staining is specific. DAPI-stained cell nuclei are represented in blue; the OTR-EGFP signal is reported in green, while Alexa594 signal is reported in red. Overlapping signals between Alexa594 and OTR-EGFP are reported in yellow. Bottom image: Magnification of OTAha-Alexa594 staining merge that shows internalization vesicles containing the receptor and the fluorescent ligand. Images were obtained in confocal microscopy (LSM 800, Zeiss).

Lastly, as we previously determined that both the unconjugated ligands are able to bind and activate vasopressin receptors, we repeated the staining protocol on HEK293 cells transiently transfected with V1aR or V1bR to see if our working ligand concentration might also lead to a signal coming from these receptors. However, both V1aR and V1bR signal remained evenly distributed on the cellular surface, and no red OTLysN₃-Alexa594 signal could be detected. This means that our ligands used at a 100 nM concentration don't bind to vasopressin receptors, and therefore marks selectively and specifically OTR receptors only.

Staining with DNA hairpins-tagged ligands. The following step was to link OTAha and OTLysN₃ to a clickable fluorescent version of Pan (PanCy3), using the same conjugation protocol we set up for the Alexa594-linked analogues. We then used them to stimulate the same HEK293 OTR-EGFP cell line (Fig. 21) we had previously used for the colocalization and internalization experiments. However, while internalization vesicles kept appearing, in this case we could not observe any specific signal coming from the fluorescent PanCy3.

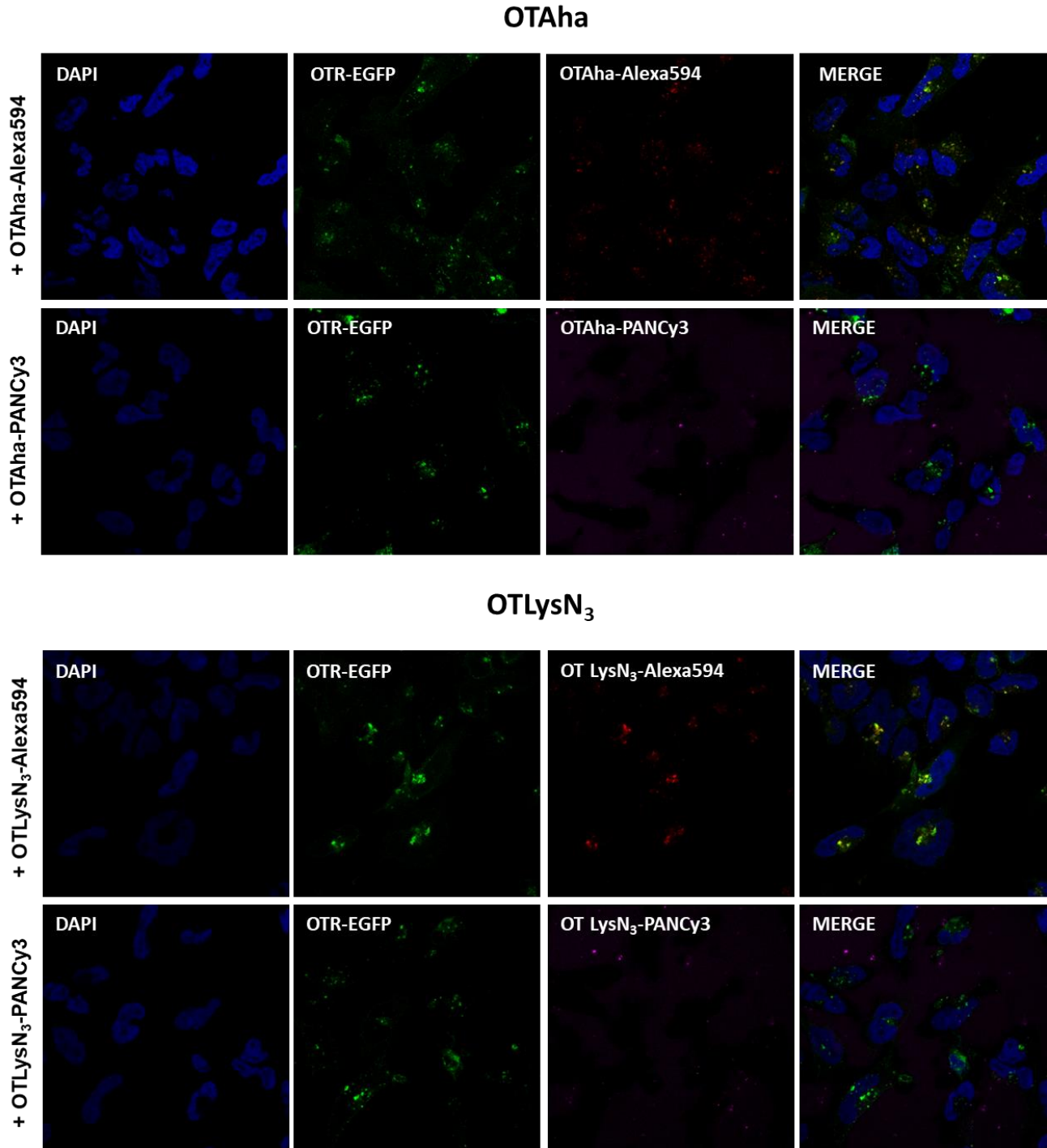


Figure 21: cellular culture staining with hairpin-tagged OT analogs. HEK293 OTR-EGFP cells were incubated 30 min at 37°C with one of the two PanCy3-tagged OT analogs, at a final concentration of 100 nM; fluorescent OT analogs were used as positive controls. In cells stimulated with the hairpin-tagged ligand, despite the appearance of internalization vesicles, no specific Cy3 signal was visible. DAPI-stained cell nuclei are represented in blue; the OTR-EGFP signal is reported in green, Alexa594 signal is reported in red, and Cy3 signal is reported in violet. Overlapping signals between Alexa594 and OTR-EGFP are reported in yellow. Images were obtained in confocal microscopy (LSM 800, Zeiss).

Hypothesizing that the steric hindrance of a 14-16 kB DNA hairpin might decrease the analogues' affinity for the OTR, we performed several competition binding experiments on HEK293 OTR-EGFP cells membranes, using curves produced by OTLysN₃-DBCO594 and OTLysN₃ as a reference. Results are shown in Fig. 22, and actually highlight a strong decrease in the total displacement ability of our DNA-conjugated analogues.

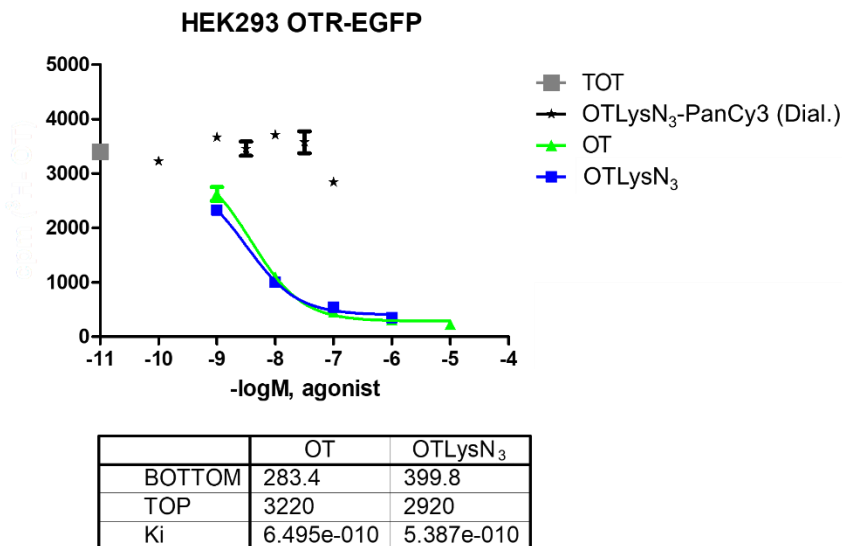


Figure 22: Evaluation of binding properties of OTLysN₃-PanCy3, compared with OT and OTLysN₃ alone. Competition binding assay on HEK293 OTR-EGFP cellular membranes. The grey square represents the total binding; OTLysN₃-PanCy3, OTLysN₃ and OT dose-response curves are represented in black, blue and green, respectively. Two days before the experiment, OTLysN₃-PanCy3 was dialyzed in order to remove any unconjugated OTLysN₃ molecule from the solution. Each point is represented as the percentage of specific binding. Each value is expressed as mean \pm SEM (n=3).

In an attempt to overcome this issue, we tried to add a threonine in position 4, a type of modification that we already know is able to increase affinity and specificity for the OTR, at least in its murine form. We generated two new modified OT analogues, Thr⁴OTAha and Thr⁴OTLysN₃, and repeated the BRET measurements and the competition binding experiments with both of them (Fig. 23).

As we could not observe any significant difference between the behaviour of the two analogues, for the next set of experiments we chose to focus mainly on Thr⁴OTLysN₃, because in this molecule the modified aminoacid LysN₃ “sticks out” of the receptor when the ligand is inserted in its binding pocket, helping the DNA hairpin linked to the analogue to create less steric hindrance.

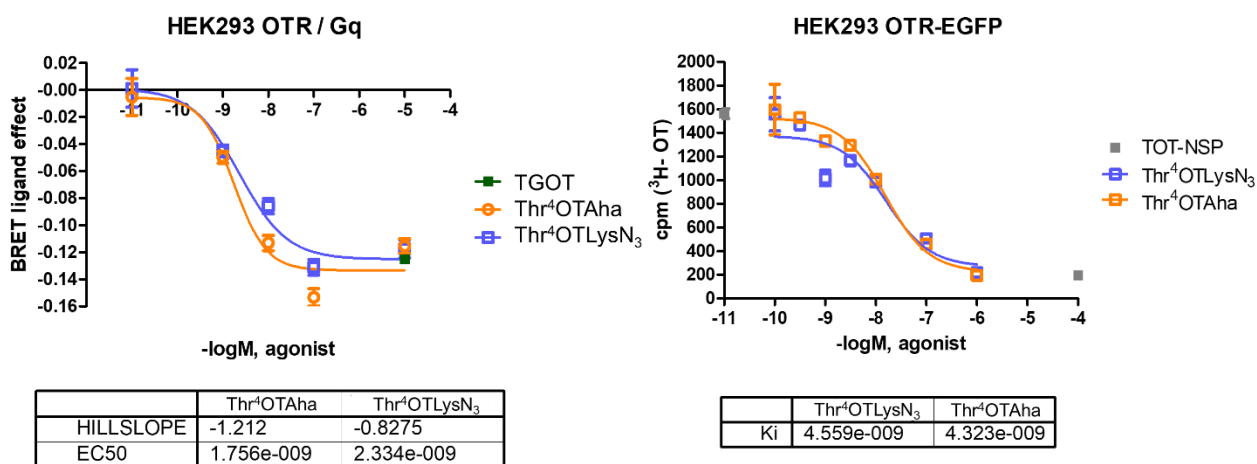
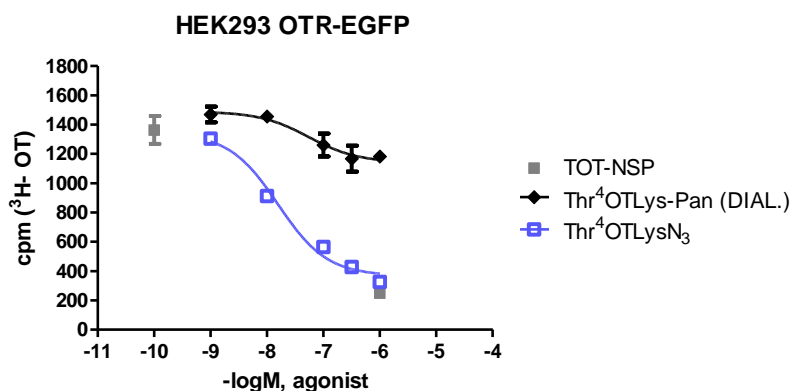


Figure 23: Evaluation of binding and OTR activation properties of the two new OT analogues Thr⁴OTLysN₃ and Thr⁴OTaha. **A**, BRET assay showing Gq activation properties of the two analogues in transfected HEK293 cells. BRET dose-response curves were built stimulating cells for 2 min with increasing Thr⁴OTLysN₃ (light blue) or Thr⁴OTaha (orange) concentrations. Data are represented as the mean \pm SEM of the BRET ligand effect compared to the agonist concentration negative logarithm, and were collected as the difference between the BRET value measured in presence of the agonist and the one measured in its absence. **B**, Competition binding assay on HEK293 OTR-EGFP cellular membranes. The grey square represents total and non-specific binding; Thr⁴OTLysN₃ and Thr⁴OTaha dose-response curves are represented in light blue and orange, respectively. Each point is represented as mean \pm SEM ($n=3$).

We then proceeded to link Thr⁴OTLysN₃ with Pan, and hypothesizing that results of the next set of experiments might be biased by the presence of unconjugated OTLysN₃, before running each test we dialyzed the sample after the reaction had taken place. Additionally, to remove any nuclear DNA that might interfere with the hairpin clicked with our ligand, for binding experiments we used Post Nuclear Supernatant (PNS) membranes. Results of the competition binding experiments on HEK293 OTR-EGFP membranes are shown in Fig. 24. The dialyzed compound curve has an E_{max} 60% lower than the unconjugated analogue one, but surprisingly, it retains the same K_i.

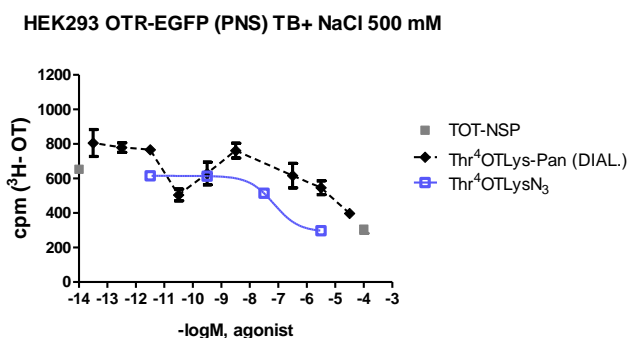
The fact that the ligand does not lose its affinity for the receptor but is not able to displace all the radioactive OT from it made us hypothesize that there was a steric hindrance problem with Pan. DNA is negatively charged, and our hypothesis was that when in proximity, the negative charges on two Pan hairpins might hamper their contemporary binding to two receptor protomers.



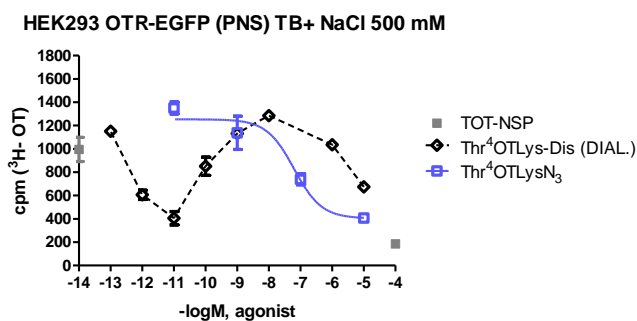
	Thr ⁴ OTLys-Pan (DIAL.)	Thr ⁴ OTLysN ₃
BOTTOM	1142	368.0
TOP	1489	1343
Ki	9.135e-009	2.620e-009

Figure 24: Evaluation of binding properties of Thr⁴OTLysN₃-PanCy3, compared with Thr⁴OTLysN₃ alone. Competition binding assay on HEK293 OTR-EGFP PNS cellular membranes. The grey squares represent the total and non-specific binding; Thr⁴OTLysN₃-PanCy3 and Thr⁴OTLysN₃ dose-response curves are represented in black and light blue, respectively. Two days before the experiment, Thr⁴OTLysN₃-PanCy3 was dialyzed in order to remove any unconjugated Thr⁴OTLysN₃ from the solution. Each point is represented as mean ± SEM (n=3).

In an attempt to overcome this issue and “mask” the negative charges on Pan, we repeated the binding experiments adding NaCl at a final concentration of 150 mM to the binding buffer. Results are shown in Fig. 25. Surprisingly, while NaCl had no effect on the binding curves of the OT analog alone, it completely modified the shape of the competition curve, that now behave as superagonists at low concentrations.



	Thr ⁴ OTLys-Pan (DIAL.)	Thr ⁴ OTLysN ₃
BOTTOM	374.0	290.5
TOP	699.5	615.1
Ki	5.063e-007	1.170e-008



	Thr ⁴ OTLys-Dis (DIAL.)	Thr ⁴ OTLysN ₃
BOTTOM	1032	403.7
TOP	729.4	1253
Ki	2.537e-011	1.051e-008

Figure 25: Evaluation of binding properties of Thr⁴OTLysN₃-PanCy3 and Thr⁴OTLysN₃-DisCy3 in «salted» binding buffer, compared with Thr⁴OTLysN₃ alone. Competition binding assay on HEK293 OTR-EGFP PNS cellular membranes. The grey squares represent the total and non-specific binding; Thr⁴OTLysN₃-PanCy3, Thr⁴OTLysN₃-DisCy3 and Thr⁴OTLysN₃ dose-response curves are represented in black, white and light blue, respectively. Two days before the experiment, the two hairpin-tagged OT analogues were dialyzed in order to remove any unconjugated ligand from the solution. Each point is represented as mean ± SEM (n=3).

5.4.3. Work in progress: cellular and brain tissue staining protocol optimization

The development of the Nanoruler technique still requires several steps to be finalized. However, through this first *in vitro* characterization phase we successfully demonstrated that the oligonucleotides-based system

designed by Prof. Bellini's group works as expected: Pan and Dis interact only if Trigger is present in solution. Polyacrylamide gels experiments let us determine which are the best environmental conditions for the hybridization and amplification reactions to occur; these parameters, such as pH and incubation times, will be crucial in the design of the different staining protocols on cellular cultures and brain slices. However, the lack of a suitable method to block Pan and Dis at a fixed distance prevented us to understand what happens when they are more than 6 nm apart, and Trigger is present. Therefore, the resolution of this system still needs to be confirmed.

The design of the two clickable OT analogs led us to obtain a powerful tool to target the OTR. Our two molecules retain the same pharmacological properties of endogenous OT, and can be easily tagged with DNA oligonucleotides as well as other kind of labels (i.e., Alexa fluorophores). Click chemistry has high efficiency and yield, and the conjugated product remains stable over time. The first staining experiments done in cellular cultures confirmed that all the analogs we synthesized are specific for our target: they cause receptor internalization in HEK293 cells transfected with a fluorescent OTR-EGFP receptor, but have no effect on the same cellular type transfected with the closely related vasopressin receptors V1aR-YFP and V1bR-EGFP. BRET experiments confirmed that these analogues are also able to functionally activate the receptor. As their calculated affinity for vasopressin receptors is considerably lower than that for the OTR, they have the potential to be successfully used to target the OTR also in native tissues without the risk of false positive and off-target binding.

Despite these promising results, we still need to understand why ligand conjugation with our DNA strands causes such a dramatic change in their pharmacological properties. In fact, while tagging our analogues with Alexa fluorophores had no effect on their ability to bind and activate the OTR, Pan- and Dis-tagged molecules revealed to have complex binding kinetics, that are proving to be quite difficult to interpret. Such behaviour could be due to some peculiar interaction between the DNA sequences, for example given by their steric hindrance, or by charge interference. To try to solve this issue we are currently modifying the composition of the binding buffer, to modulate pH and see which is the effect on the binding curves.

In parallel, we have started to develop a staining protocol to apply the Nanoruler technique on living cellular systems. We are currently using data coming from experiments performed in solution to set up the best labelling conditions on a simpler and more reproducible cellular environment, represented by HEK293 cells expressing a fluorescent version of the OTR (OTR-EGFP). Our plan is to label these cells using different concentrations of ligand tagged with a fluorescent Pan or a fluorescent Dis, previously dialyzed to remove any possible untagged analogue; once we find the optimal incubation conditions, we will give both ligands at the same time, adding Trigger in a second incubation step. HCR conditions will also need to be finely tuned, in order to avoid an insufficient or excessive amplification of the fluorescent "tree".

Next, we will have to optimize another fluorescent DNA probe that would allow us to target monomeric OTRs only. Here, choosing the right set of fluorophores at this stage will be crucial to label all the different receptor populations at the same time, without interfering with each excitation/emission spectrum. Being able to

identify monomeric receptors is, in our experimental procedure, as important as targeting dimers: these two populations have different functional properties, and very little is known about their localization, trafficking and regulation mechanisms inside the cell. Knowing which receptor species is the most diffused in each brain area and if their proportion changes in response to environmental or pathological stimuli will let us expand our knowledge about their role in the CNS.

Once the cellular culture staining protocol is fully optimized, we will switch to mouse brain slices, using receptor autoradiography as a reference technique to further optimize the Nanoruler. The most important test in this context will be the staining of *Oxtr* KO mouse brain slices: this experiment will actually let us prove that our DNA-tagged analogues can selectively target OTR even in native tissues. Heterozygous *Oxtr*^{+/-} mice will also be analyzed with this new technique: as they are known to express 50% less receptor than WT animals, their analysis will be useful to understand if the Nanoruler can distinguish effectively between different receptor quantities, and also to see how dimeric OTRs number and/or distribution changes in these mice.

6. OXYTOCIN RECEPTOR MAPPING IN A MOUSE MODEL OF SCHAAF-YANG SYNDROME

Alterations of the oxytocinergic system have been reported in different models of neurodevelopmental disorders, especially in those associated with an autistic phenotype. In the mouse brain, the OTR is a key regulator of behaviour and sociality. Moreover, during the first phases of neurodevelopment it contributes to neuronal circuits formation and shaping. An extensive knowledge of its distribution in the CNS is therefore a crucial step to design and test new therapeutic approaches for neurodevelopmental disorders. For this reason, during my PhD I collaborated with Dr. Françoise Muscatelli's research group to investigate OTR levels and distribution in a mouse model of PWS-like syndrome characterized by a high prevalence of ASD, the *Magel2*-KO mouse. *Magel2* (*melanoma-antigen-subfamily-like-2*) is part of a large deubiquitinase proteic complex, involved in the regulation of the most diverse cellular processes: the reason why mutations of this gene lead to the dramatic increase in ASD cases that is normally observed in SYS compared to PWS patients remains unknown. However, in this mouse model oxytocin has already been successfully employed to treat ASD-linked pathological behaviours; therefore, understanding which is the relationship between *Magel2* and the oxytocinergic system in mouse CNS could help to better define the pathogenetic mechanism of autism in SYS patients.

While the Nanoruler system will provide a new and unique tool to selectively detect OTR homodimers in the rodent brain (that also seem to have an important role in behaviour; Busnelli et al, 2016), in this work I gathered reliable data using a "reference" technique, in order to be able to compare them with results obtained through the Nanoruler once the technique will be ready.

6.1 METHODS CURRENTLY EMPLOYED TO STUDY OTR DISTRIBUTION

Autoradiography. Autoradiography is one of the oldest techniques that can be used to study the distribution of a molecule of interest, generally a receptor. It allows the detection of radioisotopes through the "impression" of ionizing radiations (usually β particles) on photographic sheets that contain silver halogenure granules. The image that results from the reaction between the granules and the emitted radiations is then "developed" using a developer (Bundy, 2001).

OTR mapping through autoradiography has been made in rodents, in non-human primates and also in humans. Frozen tissue sections (14-20 μm) are collected on chromallumated slides and usually marked with a iodinated OTR linear antagonist, $[^{125}\text{I}]\text{-d}(\text{CH}_2)^5[\text{Tyr}(\text{Me})_2\text{-Tyr-NH}_2]^9\text{-OVT}$. Non-specific binding is determined incubating sections in presence of a non-marked ("cold") oxytocin excess. After rinsing and drying, sections are exposed on a photographic sheet for one or more days, depending on the expected signal intensity (Fig.1).

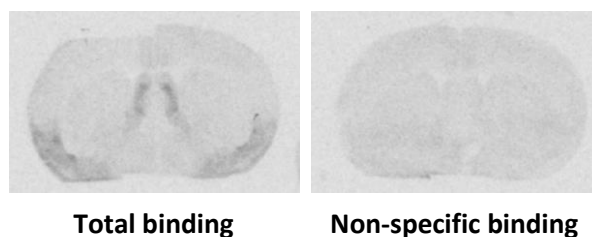


Figure 1: *autoradiographic image obtained from murine brain slices incubated with a radiolabelled receptor antagonist. Darker areas are those with a higher receptor density. Non-specific binding (right image) was determined incubating slices with an excess of «cold» (non labelled) ligand.*

Developed images are then analyzed through ImageJ to quantify the optical density of the obtained signal and to convert it to mole/mg tissue equivalents (Insel, 1990) or in cpm/mg tissue equivalents (Lukas et al., 2010), to normalize values depending on the chosen exposure time. Specific binding is calculated as the difference between total binding (incubation with the iodinated compound only) and non-specific binding (incubation with the iodinated compound and cold oxytocin in excess).

Despite being one of the most reliable, specific and sensitive techniques to map the OTR, it is indeed not free from risks and disadvantages. The employment of radioactive material requires adequate safety measures and a correct waste management; radioactive compounds and photographic sheets are often really expensive, and despite guaranteeing a high contrast, images have a low spatial resolution. For this reason, cellular and sub-cellular studies and co-localization studies could not be performed.

In situ hybridization. *In situ* hybridization is another commonly used technique to detect OTR expression at the mRNA level. It is a technique that allows the localization of specific DNA or RNA sequences in cells or tissues, through the employment of tagged complementary probes. Depending on the kind of tag (radioactive or fluorescent), the detection step occurs through autoradiography or through fluorescence microscopy (Jensen, 2014).

For the OTR, *in situ* hybridization has already been successfully used in rat brain, with radioactive probes (Ostrowski, 1998), but also in mouse (Yoshimura et al, 1996; Newmaster et al, 2020), rhesus macaque (Freeman et al, 2014) and human myometrium (Wathes et al, 1999).

The main disadvantage about this technique, other than the employment of radioactive material, is that often higher or lower mRNA levels don't necessarily correspond to a higher or lower protein expression; mRNA maturation and regulation processes must also be taken into account (Coulton & de Belleruche, 1992; Ostrowski, 1998).

Fluorescent ligands. The need to develop fluorescent ligands to map the OTR come from an effort to try to find new, safer and more versatile alternatives to radioligands (McGrath et al, 1996). For the OTR, fluorescent

ligands can function as powerful pharmacological tools to study not only its distribution, but also its trafficking at the subcellular level.

Both agonist and antagonist have been developed; most of them retain a cyclic peptidic structure, just like endogenous oxytocin, but also many linear compounds are available (Innamorati et al, 2001; Lutz et al, 1990; Mouillac et al, 2008). Fluorescent ligands are usually grouped into “first generation” and “second generation” depending on the kind of fluorophore linked to the ligand.

For the OTR, first generation ligands were obtained linking a fluorescein with the aminic group of deaminated OT analogs and putting a Lys in position 4 or 8, or instead linking it with the aminic group on the cysteine in position 1. However, between these, only the one with the modification in position 8 retained its affinity for the receptor, while the other two showed a lower activity (Buku et al, 1988; Eggena et al, 1990). Using these information, Dr. Durroux group worked on OT analogs to synthesize selective fluorescent compounds for the OTR, all deaminated in position 1 and bearing a Lys or an Orn in position 8 (d[Lys8]VT, d[Orn8]VT). Conjugation with the fluorophore (fluorescein or rhodamine) usually takes place on the eighth residue (Terrillon et al, 2002). The most selective of these ligands resulted to be d[Orn8(5/6C-Flu)]VT, that successfully marked human OTR overexpressed in CHO cells (Terrillon et al, 2002).

As fluorophores of first generation ligands were often not bright enough, new, Alexa fluorophore-linked ligands have been generated. Second generation analogs are all antagonists with the fluorophore linked in position 8. Other than Alexa488, Alexa546, Alexa647, also lanthanides have been used.

To maximize signal to noise ratio, “fluorescent turn-ons” systems have also been developed for the OTR: these ligands are bound to a fluorophore that emits a signal only in a hydrophobic environment (Karpenko et al, 2014), i.e. the hydrophobic binding pocket of the receptor (Rosenbaum et al, 2009; Sridharan et al, 2014).

So far, of all these different experimental approaches the most sensitive and reliable in terms of OTR detection is autoradiography. So, in parallel with Nanoruler development, I also conducted an extensive autoradiographic mapping of the OTR in the mouse brain. To identify any possible receptor variation in physiological or pathological conditions, I included in the analysis both WT mice and belonging to WT or mouse model of neurodevelopmental disorders, keeping males and females separated to evaluate sex-mediated changes in receptor levels too. Results obtained through this analysis will not only provide useful information about changes in OTR distribution and quantity in response to different factors, but it will also allow us to see if the results obtained with the new technique are coherent with the total amount of oxytocin receptors present in the brain.

6.2 OXYTOCINERGIC SYSTEM ALTERATIONS IN *MAGEL2*-KO, A MOUSE MODEL OF SCHAAF-YANG SYNDROME

Prader Willi syndrome (PWS, MIM176270) is an imprinting-related neurodevelopmental disorder caused in most cases by deletions in the paternal chromosomal region 15q11-q13. Among the genes contained in this region, the most affected by truncating mutations or deletions in PWS are several polypeptide coding genes located in the so-called “PWS paternal-only expressed region” (*MKRN3*, *MAGEL2*, *NECDIN*, *SNURF-SNRPN*) (Cassidy et al, 2012). However, there is no causative gene for PWS, and it has not been possible yet to correlate single candidate genes to specific phenotypic traits of the disease (Schaaf et al, 2013). PWS is characterized by infantile hypotonia with poor suckling activity and failure to thrive, childhood obesity (McAllister et al, 2011), intellectual disability and behavioural defects (Whittington and Holland, 2018). Many of these patients also manifest autism spectrum disorders (ASD) (Koenig et al, 2004).

One of the genes contained in the Prader-Willi locus is the *Melanoma antigen L2*, or *Magel2* gene. *Magel2* belongs to the *MAGE* family of ubiquitin ligase regulators, and encodes one of the largest *MAGE* proteins (1249 amino acids in human and 1284 in mouse). It is highly expressed in the CNS during neurodevelopment, and in the adult brain, high levels of *Magel2* mRNA can be found in the suprachiasmatic (SCN), the paraventricular (PVN) and supraoptic (SON) nuclei of the hypothalamus (Tacer et al, 2017).

The loss of this maternally imprinted, paternally inherited gene causes a Prader Willi-like disease called Schaaf Yang Syndrome (SYS; OMIM 615547). Despite sharing many pathological phenotypic traits with PWS, such as neonatal hypotonia, feeding difficulties and hypogonadism, this syndrome also presents peculiar characteristics, such as joint contractures, the absence of hyperphagia and a higher prevalence of autism spectrum disorders (up to 75% of affected individuals) (Negishi et al, 2019; Fountain and Schaaf, 2016).

The mouse bearing a truncating mutation of this gene (*Magel2*-KO) is proving to be a good model to study the autistic-like symptoms and other behavioural defects in SYS. Male mice with deletion of most of the *Magel2* gene and its promoter showed a 50% mortality rate at birth, suckling defects, and behavioural deficits in social novelty, novel object exploration, spatial learning and memory (Schaller et al, 2010; Fountain et al, 2017). At the molecular level, *Magel2*-KO mice show an hyperactivation of the mTOR pathway (Crutcher et al, 2019) and a general impairment of the melanocortin pathway (Oncul et al, 2018; Bischof et al, 2016; Mercer et al, 2013). Interestingly, both pathways are linked to the oxytocinergic system, which is strongly involved in the control of social behaviour. *Magel2*-KO mice show a reduction in hypothalamic oxytocin (Schaller et al, 2010), and a strong suppression of oxytocin neurons activity (Ates et al, 2019). Importantly, oxytocin-based therapies showed positive effects on specific symptoms of PWS and SYS patients (Tauber et al, 2017), and an early postnatal oxytocin injection could rescue neonatal lethality, social and learning deficits in adult *Magel2* KO mice (Schaller et al, 2010; Meziane et al, 2015).

Despite these evidences, little is known about the brain regions mostly affected by OT action in SYS patients, and detailed information about the distribution of its receptor (oxytocin receptor, OTR) are still missing. For this reason, in this work we run an extensive mapping of the oxytocin receptor in murine brains. We sampled brain areas known to be involved in social behaviour and/or social deficits, and compared receptor levels in *Magel2*-KO and WT brains to look for a genotype-induced effect on OTR levels and distributions.

There are also growing evidence of how CNS defects and deregulations in mouse models of neurodevelopmental disorders are sexually dimorphic. However, as most of the current studies on neurodevelopmental disorders are often conducted on male animals only, while male/female differences are seldom investigated, we also analyzed males and females separately, to check for possible sexual dimorphisms in OTR distribution and quantity.

Lastly, to investigate if OT administration at birth has an impact on OTR levels later in life, we included in the analysis a group of KO animals treated with OT subcutaneous injections (2 µg) at PN0, PN2, PN4 and PN6 (KO + OT), and compared them with KO mice treated only with NaCl (KO + Veh). Our findings demonstrate that male and female *Magel2*-KO mice have sex-specific deregulation of OTR levels, and that the effects to an OT early treatment are also sex-dependent.

6.3 MATERIALS AND METHODS

Animals

Magel2^{tm1.1Mus^{+/+}} (WT) and *Magel2*^{tm1.1Mus^{-/-}} (referred as *Magel2*-KO) mice were maintained on a C57BL/6J genetic background and stabulated in standard conditions, with ad-libitum access to food and water. Mice were handled and cared for in accordance with the Guide for the Care and Use of Laboratory Animals (N.R.C., 1996) and the European Communities Council Directive of September 22th 2010 (2010/63/EU, 74). Experimental protocols were approved by the institutional Ethical Committee guidelines for animal research with the accreditation no. B13-055-19 from the French Ministry of Agriculture.

Each of the three experimental groups (WT + Veh, KO + Veh, KO + OT) contained three males and three females, for a total of 6 mice/group. Male and female brains were processed together, but kept separated during data analysis. For this work, a total of 18 animals have been analyzed.

Treatments

Three to five hours after delivery, KO pups were injected with saline or with oxytocin (Phoenix Pharmaceuticals. Inc., Strasbourg, France; Catalog No.051-01) dissolved in isotonic saline at a final concentration of 0.1 µg/µL (20 µL/injection) at PN0, PN2, PN4 and PN6.

Brain collection and slices preparation

At three months of age, mice were sacrificed, the brains quickly extracted, fresh-frozen by dipping it in cold isopentane (-25°C; Sigma Aldrich) and stored at -80°C until processing. 14 µM coronal sections were collected using a Frigocut-2700 (Reichert-Jung) cryostat on cromallumated Superfrost slides. For each brain, 4 slides containing the regions of interest were chosen for receptor autoradiography.

Receptor autoradiography and ROI analysis

Quantification of OT binding sites was performed through receptor autoradiography using the iodinated antagonist [¹²⁵I]OVTA (Perkin Elmer). Briefly, slides were washed once with PFA diluted in PBS and once with PBS for 5 minutes, and then incubated for 2 hours in Binding Buffer 1X (50 mM Tris HCl, 0.025% bacitracin, 5 mM MgCl₂, 0.1% BSA) containing [¹²⁵I]OVTA 10 pM. Slides used as negative controls were incubated with Binding Buffer 1X additioned with an excess of OT (2 µM), to displace all the OVTA bound to OTRs and leave on the slice only the aspecific signal. After incubation, slides were rinsed twice in cold Wash Buffer (50 mM Tris HCl, 5 mM MgCl₂), once in ice-cold distilled water, and then evenly dried in a cold environment. Slides were exposed on photographic KODAK films in complete darkness, and after three or five days of exposure each film was developed and scanned for image analysis.

ROIs were chosen and analyzed with Imagej, using Paxinos' Mouse Brain Atlas as a reference and quantifying grey intensity in them. Grey intensity was then converted to nCi/mg tissue equivalent using a calibration curve. For each region, a at least 4 slices per brain were included in the analysis; results plotted on graphs are the mean of all the four measurements. Right and left hemispheres separately analyzed.

Statistical analysis

All the graphs have been created with GraphPad Prism 5. For male/female comparisons, data were analyzed using an unpaired, two-tailed Student t test. Genotype and treatment effects in each area were analyzed via a One-way ANOVA analysis of the variance, followed by a Bonferroni post-hoc test. In the results graphs, values are indicated as mean ± SEM. The level of significance was set at a p value of p <0.05.

6.4 RESULTS

The autoradiographic analysis was conducted on WT + Veh, KO + Veh and KO + OT mice; each group contained both males and females. All the mice were treated at birth with a subcutaneous injection of saline (Veh) or oxytocin (2 µg) each two days, until PN6. Brains were collected at 3 months of age, in order to evaluate long-term effects of the treatment on OTR distribution.

To choose the sampling for our mapping we took into consideration several brain areas highly involved in social behaviour and known to be enriched in OTR: in particular, we focused on the medial part of the anterior olfactory nucleus (AONm), the anterior, medial and posterior parts of the lateral septum (Ant, Med, Post LS),

the bed nucleus of the stria terminalis (BNST), the basolateral, medial and central amygdala (BLA, MeA, CeA), and the dorsal (CA2/CA3) and ventral (CA1/CA2/CA3) hippocampus, as well as the inner dentate gyrus (DG). OT binding sites in brain slices coming from these areas were quantified through receptor autoradiography employing the high affinity iodinated antagonist [¹²⁵I]OVTA. All the areas chosen for the analysis are reported in Figure 1. Results have been divided in such a way to be able to highlight any possible genotype, sex and/or treatment effect.

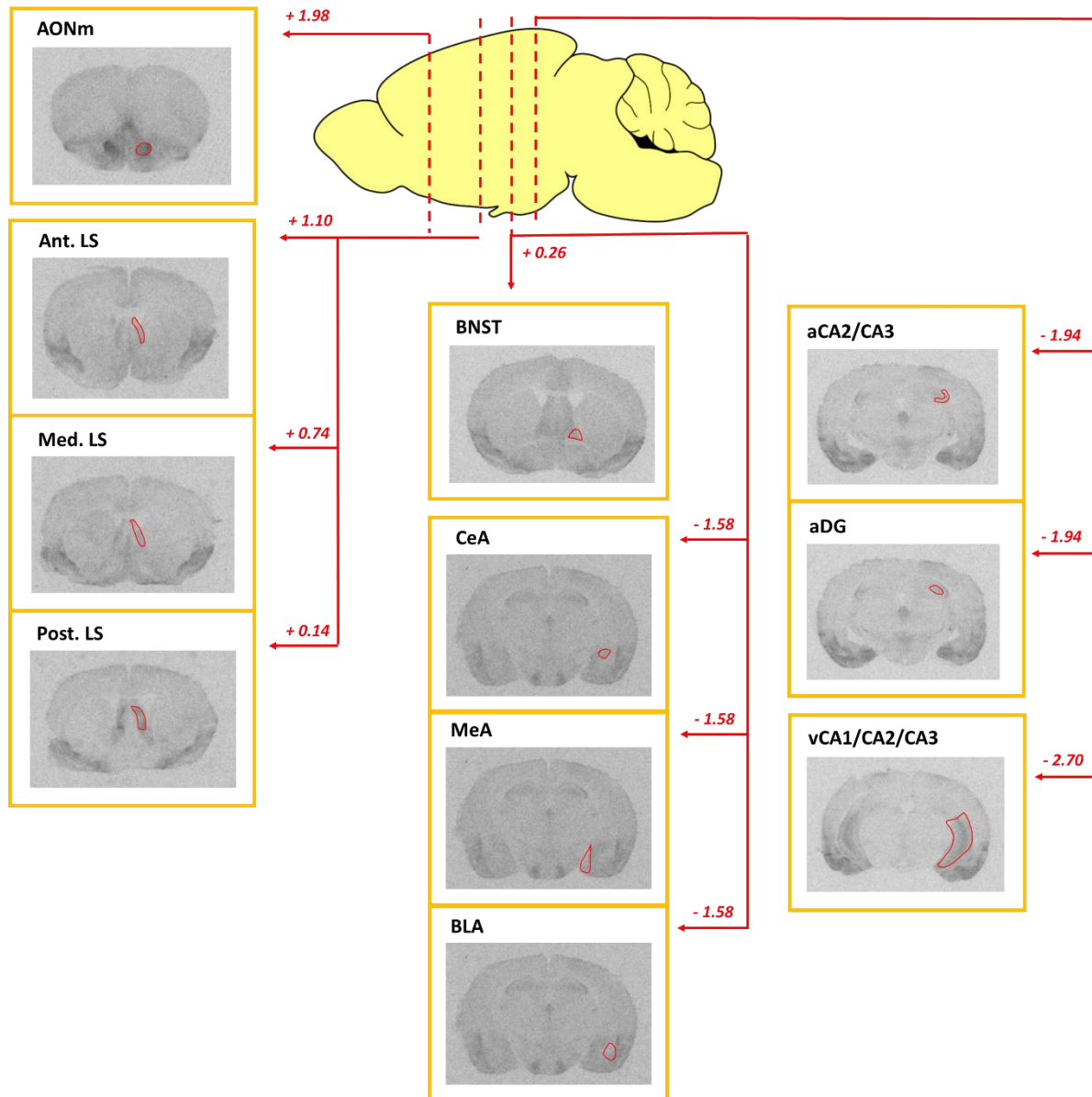


Figure 1: Scheme of all the analyzed brain areas. For each coronal plane, the distance from bregma is indicated over the arrow, and the ROI used for the analysis is traced in red over the brain slice.

6.4.1 OTR levels are differently modified in males and females *Magel2*-KO mice

To understand if and how OTR levels are modified in our pathological mouse model, we first considered only WT and KO mice treated with vehicle. Moreover, to see if there are any physiological differences between males and females, we analyzed the two groups divided by gender. Results for each area are displayed in Figure 2.

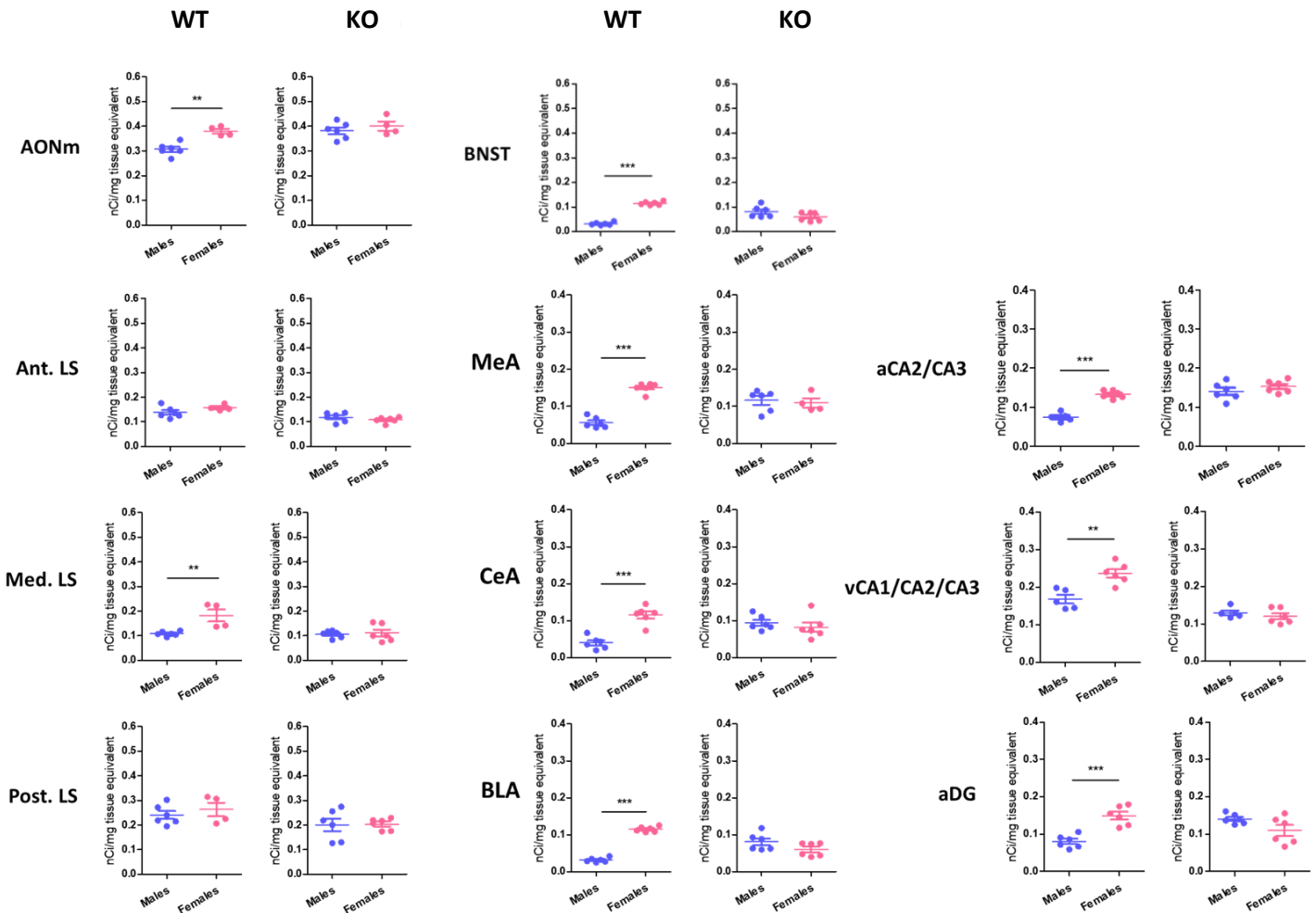


Figure 2: sex differences in OTR levels in WT and KO mice treated at birth with vehicle. Quantification of OT binding sites by receptor autoradiography in the AONm, LS, BNST, amygdala and hippocampus of WT and *Magel2*-KO male and female mice. OT binding sites levels are expressed as nCi/mg of tissue equivalent. Histograms report data as mean + SEM. Each plotted spot represents one hemisphere. In all the regions, WT females have higher receptor levels than males, the only exception being the LS. In KO animals, this difference is no longer present. Each graph was analyzed with a two-tailed unpaired t-test (* = $p < 0.05$, ** = $p < 0.01$, *** = $p < 0.001$).

AONm. In the medial part of the anterior olfactory nucleus, WT females have significantly more receptor than males (+ 22.8%, $p < 0.01$). However, given to OTR levels increase in KO males, this difference is completely lost in KO + Veh mice.

Lateral Septum. In the three portions of the lateral septum that we chose to analyze, OTR levels remain constant between WT and KO animals; we observe a significant difference only in the medial LS, where females have 63.6% more OTR than males ($p < 0.01$). In general, in the most posterior parts we also observe an increase in data variability: the interquartile range (IQR) of WT and KO females' posterior LS is almost four times higher than in the anterior portion (WT, from 0.02 to 0.10; KO, from 0.01 to 0.04;), and two and four times higher in males (WT, from 0.03 to 0.06; KO, from 0.03 to 0.13).

Amygdala. In all the three amygdala subregions we can observe the same strong differences: WT females have two or three times more OTR than males (MeA = + 167%, CeA = +200%, BLA = +300%; $p < 0.001$). In general, however, WT males have very low OTR levels in all the amygdala. Once more, because of the strong OTR increase in KO male mice, the differences in OTR quantities we observe in WT animals are completely lost in KO animals.

Hippocampus. In WT females' hippocampus, we find the same higher OTR levels we observed in the other regions (+73% in the dorsal part, $p < 0.001$; + 84,6% in the ventral part, $p < 0.01$; +87.5% in the dentate gyrus, $p < 0.001$) . Even in these regions, OTR increase in males eliminates the difference that was present in WT mice, the only exception being the vCA1/CA2/CA3 (where male levels remain stable and females' levels dramatically drop).

Overall, in the most ventral portions we can observe a high variability both in WT males and WT females (IQR; 0.05 and 0.04, respectively). Interestingly, this variability is sensibly reduced in KO males (0.02), but not females (0.04).

BNST. In the bed nucleus of the stria terminalis of WT mice, females have more than double OTR levels compared to males (+150%, $p < 0.001$). Once again, in KO + Veh animals, this difference is no longer present, because receptor levels increase in males and decrease in females.

6.4.2 An OT treatment in the first week of life has rescuing effects in male, but not female mice

To better understand how OTR levels are affected in SYS, we then directly compared WT and KO animals of the same sex. Moreover, knowing that a subchronic OT treatment is able to rescue many behavioural deficits in our mouse model, in this comparison we also included the mice groups treated at birth with OT, to see which is the long-term impact of this therapy on OTR levels in the brain.

Males.

All results regarding male mice are resumed in Figure 3.

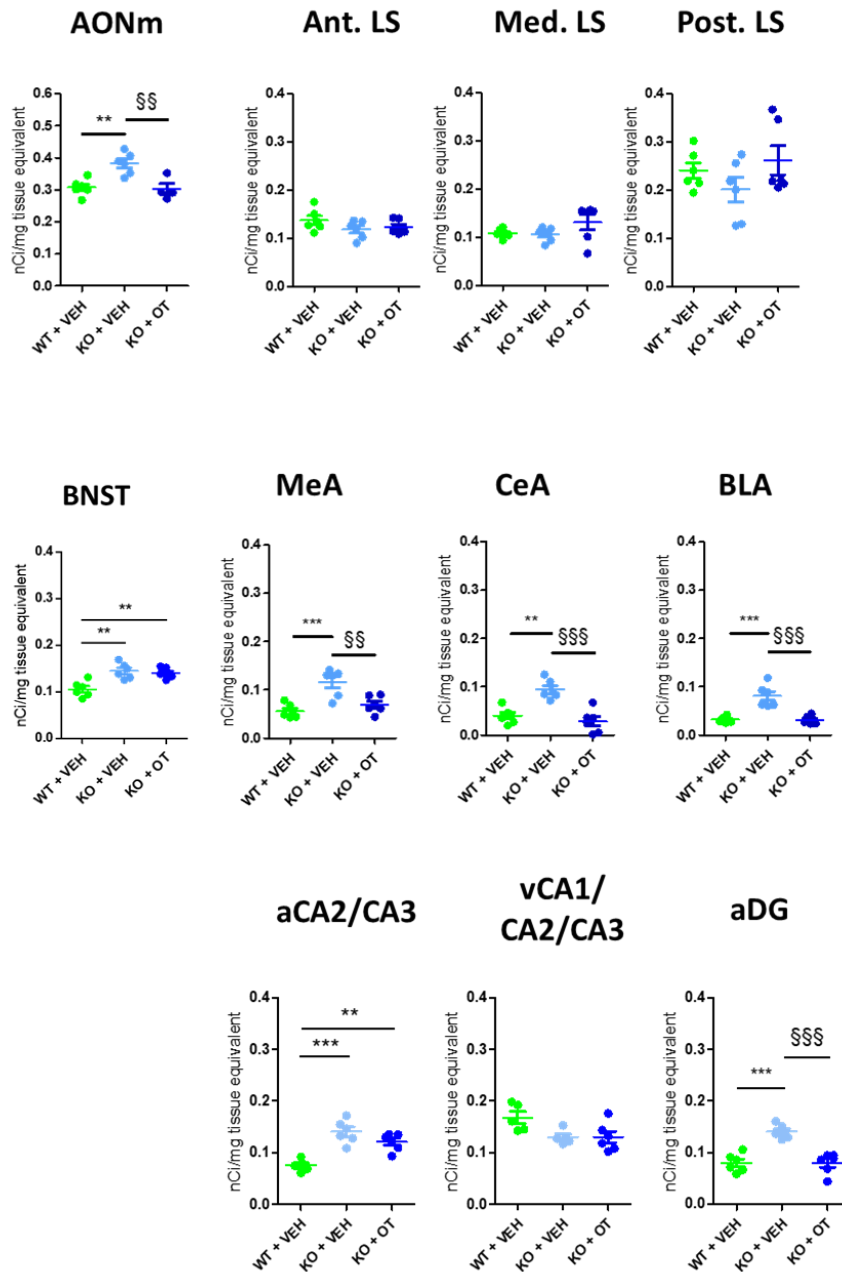


Figure 3: genotype and treatment effects in male KO + Veh and KO + OT mice. Quantification of OT binding sites by receptor autoradiography in the AONm, LS, BNST, amygdala and hippocampus of male *Magel2*-KO (treated at birth with vehicle or with oxytocin) and WT mice. OT binding sites levels are expressed as nCi/mg of tissue equivalent. Histograms report data as mean + SEM. Each plotted spot represents one hemisphere.

In the AONm, BNST, amygdala and hippocampus (aDG and aCA2/aCA3), there is a significant increase in OTR levels in KO males; subchronic OT treatment during the first week of life is able to normalize this increase only in the AONm, in the amygdala and in the aDG. Each graph was analyzed with a one-way ANOVA test, followed by a Bonferroni post-hoc test (* = $p < 0.05$, ** and \$\$ = $p < 0.01$, *** and \$\$\$ = $p < 0.001$).

AONm. In the medial part of the anterior olfactory nucleus we observe a significant OTR increase (+22.8%, $p < 0.01$) in KO mice. Interestingly, this increase is completely rescued by the treatment: in KO + OT mice, receptor levels return the same as those of WT animals.

Lateral Septum. In the three portions of the LS, OTR levels of KO males are never significantly different from WT. In the posterior part we can observe a slight decrease in Magel2-KO mice, but the high variability of plotted data (IQR of KO + OT males: 0.14) progressively makes this graph not easily interpretable.

Amygdala. In all the three subregions of the amygdala we observed the same, strong genotype and treatment effects. OTR levels are more than doubled in KO mice (+ 100% in MeA, $p < 0.001$; + 125% in CeA, $p < 0.01$; + 166,7% in BLA, $p < 0.001$), and decrease back to physiological levels in KO treated with oxytocin at birth.

Hippocampus. In male hippocampus, receptor levels behave differently depending on the subregion. While in the ventral part we see a non-significant decrease (- 23.5%) in KO mice, in the anterior CA2/CA3 regions and in the dentate gyrus we observe a marked increase (+100% in aCA2/CA3, +75% in aDG; $p < 0.001$). However, OT treatment has a significant rescuing effect only in the aDG, while in aCA2/CA2 OTR levels are still different from those of WT mice.

BNST. In the BNST of KO + Veh mice, OTR levels undergo a moderate but significant decrease (+27.7%, $p < 0.01$). Higher receptor levels are also present in OT-treated KO mice, meaning that such treatment has no visible effects on receptor expression in this area.

Females

All results regarding female mice are resumed in Figure 4.

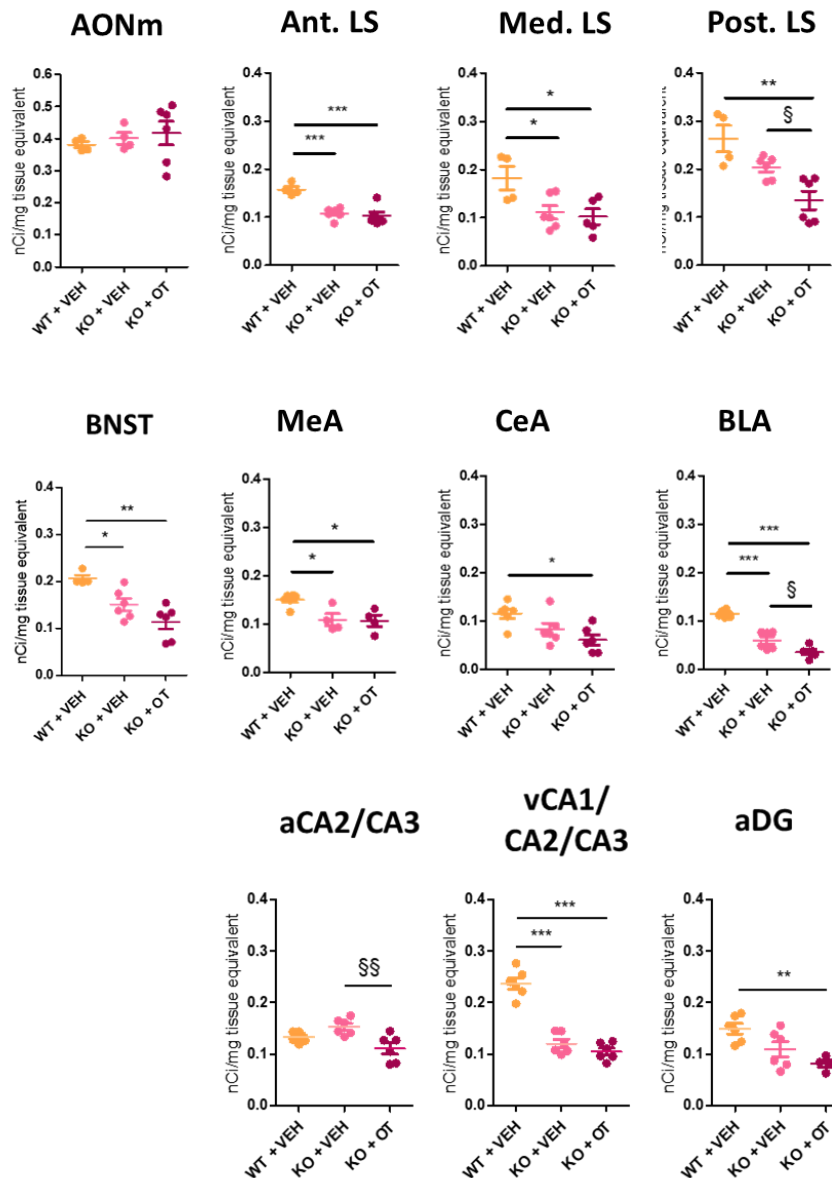


Figure 4: genotype and treatment effects in female KO + Veh and KO + OT mice. Quantification of OT binding sites by receptor autoradiography in the AONm, LS, BNST, amygdala and hippocampus of female Magel2-KO (treated at birth with vehicle or with oxytocin) and WT mice. OT binding sites levels are expressed as nCi/mg of tissue equivalent. Histograms report data as mean \pm SEM. Each plotted spot represents one hemisphere.

In all the analyzed areas but not in the AONm, there is a significant decrease in OTR levels in KO females; subchronic OT treatment during the first week of life has no rescuing effect on this decrease; in the posterior LS, BLA and in the anterior hippocampus it even “worsens” it. Each graph was analyzed with a one-way ANOVA test, followed by a Bonferroni post-hoc test (* = $p < 0.05$, ** and §§ = $p < 0.01$, *** and §§§ = $p < 0.001$).

AONm. Differently from males, in the AONm OTR levels remain stable throughout all the three groups. However, in KO females we can notice a slight increase in data variability, and this increase seem to be further

exasperated by OT treatment (the IQR progressively increases: from 0.03 in WT, to 0.06 in KO + Veh, to 0.17 in KO + OT animals).

Lateral Septum. In the lateral septum receptor levels are constant in the anterior parts, while in the medial and posterior LS variability becomes stronger (the IQR progressively increases: WT animals, from 0.01 of the anterior part to 0.04 of the posterior part; KO + Veh animals, from 0.01 to 0.04; KO + OT animals, from 0.02 to 0.09). In all the three portions of this area OTR decreases in KO mice (anterior LS, - 33% $p < 0.001$; medial LS, -38%, $p < 0.05$; posterior LS, -24%, non significant). OT treatment has no visible effects in the anterior and medial LS parts, but in the most posterior portion it causes a further decrease in receptor levels (-50% compared to WT mice; $p < 0.05$).

Amygdala. In the amygdala, receptor levels decrease in all the subregions, although in the CeA this decrease is not significant (-26.7% in the MeA, $p < 0.05$; -33.3% in the CeA, non significant, -50% in the BLA, $p < 0.001$). In the MeA of treated KO animals we do not observe any variation, while in the CeA and in the BLA OT treatment further reduced receptor levels (-50% in the CeA, -66.7% in the BLA compared to WT mice; $p < 0.05$).

Hippocampus. In the hippocampus, we observe three different trends depending on the portion: in the aCA2/CA3 dorsal part, the OTR drops only in treated KO animals, while in KO + Veh animals we can see a slight (but not significant) increase. In the ventral vCA1/CA2/CA3, OTR levels in KO + Veh mice dramatically drop (-47.8%, $p < 0.001$), and remain low after OT treatment. In the aDG there is a significant decrease of receptor in treated KO mice (-46.7% compared to WT; $p < 0.01$), but the high variability recorded in the KO + Veh group (IQR = 0.07) makes difficult to understand if this decrease was already present in this group too (as it happens in the ventral hippocampus).

BNST. In the BNST of female mice, we get a significant decrease (-28.57%, $p < 0.05$) in KO + Veh animals; this decrease, although not significantly, becomes more evident in KO + OT mice ($p < 0.01$). The high heterogeneity of values obtained in this area (IQR of 0.09 in both the KO + Veh and KO + OT groups) make difficult to understand if OT treatment actually lowers receptor levels or not.

6.5 DISCUSSION

Understanding the areas in which the oxytocin receptor modulates social behavior in neurodevelopmental disorders is one of the crucial points to develop new, safe and targeted oxytocin-based therapies. For this reason, in this work we performed an extensive mapping of the oxytocin receptor in the mouse brain, focusing our attention on a model of Schaaf-Yang Syndrome (*Magel2*-KO). We sampled a set of brain areas known to be involved in social behaviour, and used receptor autoradiography to compare OT binding sites between WT and KO animals.

In WT animals, the most prominent phenomenon we observed was a strong sexual dimorphism in OTR distribution. Males had lower OTR levels in almost every area, equal to those of KO females.

It is interesting to notice that sexual dimorphisms in the oxytocinergic system are not exclusive of the *Magel2*-KO model. In the offspring of C57BL/6 obese mothers, Glendining et al. observed a two-fold upregulation of oxytocin receptor (*Oxtr*) mRNA in the hippocampus of male, but not female pups (Glendining et al, 2019).

Using an OTR-*Venus* mouse, Sharma et al highlighted a strong difference in OTR-positive neurons in the medial preoptic area (MPOA) between females and males. In particular, in females OTR neurons were significantly denser in a specific subregion of the MPOA, the anteroventral periventricular nucleus (AVPV), and their number proved to be highly estrogen-sensitive (Sharma et al, 2019).

Murine models are not the only ones interested by sex differences: a study in WT rats showed a sexual dimorphism in the distribution of OT binding sites in different forebrain areas and in the spinal cord. Interestingly, the regions showing these differences are gonadal hormones- sensitive. (Uhl-Bronner et al, 2005). This could mean that sex steroids play a key role in this peculiar, sexually dimorphic regulation of the oxytocinergic system. However, other players could be taking part in this deregulation: for example, POMC hypothalamic neurons, that inhibit food intake, are strongly innervated by OT neurons, and express OTRs too. In *Magel2*-KO mice, these neurons have been reported to be insensitive to leptin stimulation (Mercer et al, 2013); moreover, this neuronal population is another example of sexual dimorphism between female and male brains, because females have a higher number of these neurons in the arcuate nucleus of the hypothalamus (Wang et al, 2018). Given the well-known interplay that exists between the systems that regulate food intake and oxytocin, it is very likely that the sexually dimorphic pattern of OTR distribution might have an impact on POMC functionality, and vice versa.

The oxytocinergic receptor is not the only case of sexual dimorphism reported in *Magel2*-KO mice. For example, even if corticosterone levels in this model are higher both in females and males, female animals, but not males, fail to respond to insulin-induced hypoglycemia, and are slower to restore a normal glycemia level; this suggests a sexually dimorphic impairment of the hypothalamic counterregulatory response. Moreover, females are not able to respond to GHRH, suggesting that their GH deficiency has a hypothalamic rather than pituitary origin (Tennese et al, 2011).

From other studies we already know that *Magel2*-KO mice have different phenotypes depending on their sex (Bertoni et al, 2020): in particular, female mice do not develop SYS dysfunctional behaviours. Notably, our receptor quantification shows that in almost all the chosen areas WT females have at least twice more receptor than males, and that in KO animals, this difference is completely abolished. Can this higher level of OTR in female have a “protective” effect on KO females’ phenotype? It is known that sex hormones can indirectly modulate sexual dimorphic phenotypes in social cognition by influencing OT, AVP and their spatially different expressed receptors; between the two neuropeptides, OT has a more prominent effect in enhancing relaxation, social cognition, trust and memory formation (Lu et al, 2019; Dumais et al, 2015). In our case, receptor downregulation in KO females could be due to an estrogen-dependent protective mechanism towards an abnormal quantity of oxytocin, a mechanism that could be triggered by the abnormal accumulation of an intermediate, non-mature form of OT that has been observed in this mouse model (Meziane et al, 2015).

To understand if the therapeutic effects of oxytocin previously observed in *Magel2*-KO mice (Meziane et al, 2015; Schaller et al, 2010) modify central OTR levels too, we also compared KO animals treated at birth with OT with KO mice treated only with NaCl. We highlighted an important OT effect on OTR levels in males only, where the treatment can revert the OTR increase we had observed in non-treated KO animals. In females, where we could not observe any pathologic phenotype, the reduction in OTR levels could not be rescued by OT treatment.

This is not the only example of how OT can modify OTR expression levels in the CNS. A chronic OT treatment in WT mice is known to alter selected social behaviours, and concomitantly cause a reduction of OTRs throughout the brain (Huang et al, 2013). Moreover, in a mouse model of autism (*Dysbindin*^{-/-}) Ferretti et al demonstrated that selectively enhancing the oxytocinergic signaling in the CeA through OTR levels increase rescued the emotion discrimination defect that is typical of this animals (Ferretti et al, 2015).

Other than in the *Magel2*-KO mouse, oxytocin therapeutic potential has already been demonstrated in different animal models of neurodevelopmental disorders. Treatments with oxytocin during early development often improve social deficits in adulthood. In pups prenatally exposed to valproic acid, oxytocin is able to rescue the decrease in USV (Tsuji et al, 2016); in a *Cntnap2* model of autism, a chronic early postnatal treatment with oxytocin is able to ameliorate social deficits during adulthood (Penagarikano et al, 2015). However, in these models no OTR mapping has been done yet. It will be interesting to see if the effect of an OT-based therapy on OTR levels is generalized, or if it occurs only in certain animal models of neurodevelopmental disorder. Moreover, it will also be crucial to understand if the long-term effects that our subchronic OT therapy has on OTR levels in the brain start at birth or happen later during postnatal development. To do so, we are now working to include in the autoradiographic analysis also PN7-PN8 WT and *Magel2*-KO pups. Some really interesting results have already started to emerge from a study recently performed by Newmaster and colleagues on 3D murine brain reconstructions coming from an OTR-*Venus* model: they imaged OTR expression in postnatally developing brains at five different time points (P7, P14, P21, P28, and P56), highlighting a temporally and spatially heterogeneous distribution in several cortical regions. Overall, cortical OTR neurons density seems to reach a peak around P21, and then progressively decreases; this temporization is also true for subcortical regions, with the exception of the hypothalamus, where OTR expression increases until adulthood. Most interestingly, in this reporter transgenic mice they also found two hypothalamic nuclei showing sexual dimorphisms; however, this difference was not visible before P14 (Newmaster et al, 2020). Different trajectories in receptor expression in the brain during postnatal development could also be present in the *Magel2*-KO model, and could be responsible of the differences we observed in adult mice. Further analyses of the PN7-PN8 pups will be useful to test this hypothesis.

6.6 CONCLUSIONS AND FUTURE DIRECTIONS

In conclusion, through this extensive mapping of the WT and *Magel2*-KO mouse we provided new important insights on when and how the oxytocinergic system changes. We highlighted a strong sexual dimorphism in

OTR quantities and modification patterns, both in WT and *Magel2*-KO males and females. These differences could be due to a different regulation mechanism of OTR expression in the CNS, and will need further analyses to be understood.

We also demonstrated that an oxytocin treatment at birth can have strong, long-lasting effects not only on the behavioural phenotype of *Magel2*-KO mice, but also on their oxytocin receptor levels. Regarding this, it would be interesting to see if this treatment also has short-term effects on OTR distribution: for this reason, we're currently extending the autoradiographic analysis to PN8 *Magel2*-KO and WT pups.

Understanding how and when the oxytocinergic system modifies its shape in mouse brain will be fundamental to develop new, spatially and temporally targeted therapies to treat neurodevelopmental disorders.

7. EVALUATION OF NEONATAL OXYTOCIN ADMINISTRATION ON HIPPOCAMPAL DEVELOPMENT IN THE MAGEL2 MOUSE MODEL OF AUTISM

7.1 CONTRIBUTIONS

In this work, I collected brain slices coming from adult WT and Magel2-KO male mice, and performed all the autoradiographic analysis. The OTR expression data were correlated with behavioural and functional outcomes of Magel2-KO mice. However,

7.2

Acute neonatal oxytocin impacts hippocampal network development and restores adult social memory deficits in a mouse model of autism.

Alessandra Bertoni¹, Fabienne Schaller¹, Roman Tyzio¹, Stephane Gaillard², Francesca Santini⁴, Marion Xolin¹, Diabé Diabira¹, Radhika Vaidyanathan³, Valery Matarazzo¹, Igor Medina¹, Elizabeth Hammock³, Jinwei Zhang⁵, Bice Chini⁴, Jean-Luc Gaiarsa¹, Françoise Muscatelli¹#

¹ *Institute of Neurobiology of Méditerranée (INMED), Institut National de la Santé et de la Recherche Médicale (INSERM) UMR 1249, Aix-Marseille Université, Marseille, France.*

² *Phenotype-expertise, Marseille, France.*

³ *a, Tallahassee, FL, USA.*

⁴ *Institute of Neuroscience, National Research Council (CNR), Department of Medical Biotechnology and Translational Medicine, Università degli Studi di Milano Milan, and NeuroMI Milan Center for Neuroscience, University of Milano-Bicocca, Italy.*

⁵ *Institute of Biomedical and Clinical Sciences, College of Medicine and Health, University of Exeter, Hatherly Laboratories, Exeter, EX4 4PS, UK.*

#: *corresponding author*

Email: francoise.muscatelli@inserm.fr.

Institut de Neurobiologie de la Méditerranée (INMED) INSERM-Aix Marseille Université

Campus Scientifique de Luminy, 13273 Marseille, France

Keywords: Magel2, Schaaf-Yang Syndrome, Prader-Willi Syndrome, neurodevelopmental disorder, GABA-shift, Excitation/Inhibition balance, Somatostatin, Parvalbumin.

Number of pages: 27

Number of words (introduction, results, discussion, mat. and meth.): 8928 **Number of figures:** 9 figures and 8 supplementary figures **Supplementary data:** Statistical file

bioRxiv 2020.09.21.306217; doi: <https://doi.org/10.1101/2020.09.21.306217>

ABSTRACT

Several studies on rodent models with an Autism Spectrum Disorders-like (ASD) phenotype, notably *Magel2*-deficient mice, have shown a rescue of deficits in adult social behavior after neonatal administration of oxytocin. However, the neurobiological alterations responsible for the social deficits and the mechanism by which oxytocin-administration in infancy has a rescue effect in adulthood remain unclear.

Here we show that *Magel2*-deficient adult mice exhibit a deficit in social memory that is corrected by neonatal oxytocin administration. We studied hippocampal regions known to be associated with social memory engrams involving the OT-system. At critical stages of development, we characterized cellular, physiological and biochemical alterations of these hippocampal regions in *Magel2*-deficient mice, alterations present in several ASD models. Overall we demonstrate a strong impact of oxytocin-administration at key stages of postnatal hippocampal neurodevelopment, shedding light on the role for oxytocin in treating neurodevelopmental disorders characterized by deficits in social memory.

INTRODUCTION

Oxytocin (OT) and its signaling pathway, the OT-system, are disrupted in several animal models of neurodevelopmental disorders characterized with autism-like phenotypes (1, 2). Indeed, knock-out mouse models of *Ot* (3, 4), *oxytocin receptor (Oxtr)* (5-7), or *ADP-ribosyl cyclase (Cd38)* (8, 9) genes show changes in social behavior. In addition, several rodent models of autism spectrum disorders (ASD) endophenotypes due either to the inactivation of genes such as *Fmr1*, *Cntnap2*, *Magel2*, *Oprm1*, or to environmental valproic acid exposure (VPA), exhibit a disruption of the brain OT-system (1). Many of these models have in common at least two constant phenotypes (10). First, pups isolated from the dam and littermates present a decrease in the number of ultrasonic vocalizations (USVs), the earliest behavioral test that can be performed in mice to measure social deficits. A second robust phenotype is a social recognition memory deficit in adulthood.

OT is thought to regulate aspects of social recognition, social novelty and social memory via interactions with OT-receptors (OXTR) in a number of key brain regions (11). With regard to social memory, a critical role has been ascribed to

hippocampal OXTR expression in the anterior dentate gyrus (aDG) hilar and anterior CA2/CA3distal regions (aCA2/CA3d) (12-15). In the aCA2/CA3d region, OXTRs are expressed in glutamatergic pyramidal neurons (which are also CCK positive) and in GABAergic interneurons, which account for over 90% of OXTR positive cells in the hippocampus (16). Notably, both types of neuron are necessary for the formation of stronger synapses that mediate LTP and social memory (12, 13).

Although most studies of OT-dependent social behaviors have been conducted in adulthood, compelling data support key roles for OT in shaping various behaviors and social traits in infancy (17-21). Genetic mutations and stressful early-life social environments can impair social behaviors via changes in the OT-system (22, 23). On the other way, OT-dependent systems may be particularly vulnerable around the neonatal period where OXTR expression is dynamic, with a strong expression in the first 2 weeks postnatal followed by a decreased expression thereafter (24, 25), and involved in critical functions such as the excitatory-to- inhibitory developmental GABA switch (26-28), a delay in which has been implicated as a driver of several rodent ASD models (27, 29). It has also been demonstrated that, in mouse pups, sensory experience influences OT production and OT shapes neuronal circuits by modulating spontaneous and evoked activity in the cortex (25, 30, 31). Thus, the modulation of GABAergic activity throughout life appears to be an important key factor in the function of OT. In addition, OT acts also on glutamatergic neurons (32) and drives dendritic and synaptic refinement in immature hippocampal glutamatergic neurons (33). Collectively, these studies confirm a role for the OT-system in early postnatal development of diverse brain regions involved in sensory processing, the limbic system, and the generation of motor output related to social behaviors. *MAGEL2* is an imprinted gene that is paternally expressed and is involved in Prader-Willi (34) and Schaaf-Yang syndromes (35) (PWS and SYS, respectively). Both of these genetic neurodevelopmental disorders present feeding difficulties and hypotonia in infancy, followed by alterations in social behavior and deficits in cognition that persist over the lifespan (36). *Magel2* knock-out mouse models are pertinent models for both syndromes (36), mimicking a disturbance in early feeding (poor sucking activity

(37)), and alterations to social behavior and learning abilities in adulthood (38, 39). *Magel2* mRNA is highly expressed in the developing hypothalamus until adulthood and *Magel2^{tm1.1Mus}* knock-out neonates display a deficiency of several hypothalamic neuropeptides, particularly OT (37). Daily administration of OT during the first week of life restores normal sucking activity of *Magel2* KO mice and normalizes social behavior and learning abilities beyond treatment into adulthood (38). Comparable effects have also been reported in other genetic rodent models of ASD, such as the VPA-induced rat model (40), the *Cntnap2* and *Fmr1* KO mouse (41, 42), and maternal separation (43). Furthermore, OT-treatment of human infants with PWS significantly improves early feeding and “social skills” in early infancy (44), confirming the translational relevance of this system. However, the developmental alterations responsible for social behavior deficits in these models, and the mechanism by which OT-treatment exerts its long-lasting beneficial effects, remain mysterious. Here, we aimed to clarify the physiological and cellular mechanisms underlying the loss of social memory in *Magel2^{tm1.1Mus}*-deficient mice and those responsible for the long-term rescue effects of OT.

RESULTS

To overcome the phenotypic heterogeneity of the heterozygous *+m/-p Magel2^{tm1.1Mus}* mouse, due to the stochastic expression of the maternal *Magel2* allele when the paternal allele is deleted (45), *Magel2^{tm1.1Mus}* homozygous (-/-) mice were used (“*Magel2* KO” hereafter). In the following experiments WT and *Magel2* KO pups were naïve or treated for four days (Postnatal day P0, P2, P4 and P6) with one subcutaneous administration of physiological saline (“vehicle”) or oxytocin (2 µg, “OT-treatment” or “+OT”) per day.

Deficits in isolation-induced vocalizations in *Magel2* KO pups and social memory in *Magel2* KO adults are differentially rescued by neonatal OT-treatment.

Mice at suckling age elicit USVs, when separated from their dam and littermates. We found a significant reduction of the number of separation-induced USVs in P8 male and female *Magel2* KO compared to wild-type (WT) pups (Figure 1A-B), demonstrating altered social behavior in early infancy. We confirmed that vehicle or OT-

treatment had no effect on vocalization in WT pups and did not significantly increase the number of USVs recorded in mutant animals (Figure 1C). Thus, OT-treatment did not exert immediately measurable effects on neonatal social behaviors in *Magel2* KO pups.

At adulthood, we focused on social behavior using the three-chamber test in order to assess social exploration (sociability), the preference for social novelty (social discrimination) and social memory (short-term social memory) (46) (Figure 2A). *Magel2* KO males showed levels of sociability and social discrimination similar to WT males but exhibited a significant deficit in social memory (Figure 2B, Figure 2-figure supplement 1). As previously reported (47), we observed a failure of the three-chamber test in revealing sociability in the cohort of female mice (Figure 2-figure supplement 2); a result reproduced in second cohort of WT females (data not shown). As a consequence, we restricted all following studies to male mice.

First, the effects of neonatal vehicle and OT-treatment were assessed in WT male pups at adulthood in the three-chamber test. We found that neither treatment had any measurable effect on sociability, social discrimination or social memory: the amount of time spent sniffing in different compartments was similar to that recorded in untreated WT males (Figures 2 B-C). Furthermore, no significant effects of neonatal OT-treatment were detected on adult performance of novel object recognition (Figure 2-Supplement 3A), open field (Figure 2- Supplement 3B) or elevated plus maze tests (Figure 2-Supplement 3C). Thus, neonatal OT-treatment has no significant adverse or beneficial long-lasting effects on widely used assays of social behavior, object recognition, anxiety-like or motor behaviors in WT animals but a reduction in the distance moved in the open-field in females.

Unsurprisingly, *Magel2* KO-vehicle males presented with a social memory deficit similar to untreated *Magel2* KO males (Figure 2D-B). However, this was rescued by neonatal OT-treatment (Figure 2D). Sociability and social discrimination indices were not affected by *Magel2* deletion or OT-treatment (Figure 2-Supplement 1). Thus, the loss of *Magel2* causes a deficit in USV calls in pups and a deficit in social memory in male *Magel2* KO adults. While the USV deficit was not affected by post-natal OT-treatment, the deficit in social memory was rescued by a neonatal OT-treatment. Due to the robust effect observed on

social memory, we focused our subsequent investigations on the hippocampal region, previously shown to be specifically involved in OT-mediated effects on social memory (12, 13).

aDG and aCA2/CA3d regions are activated by the social memory test in WT and *Magel2* KO mice.

Cells in the aCA2/CA3d and aDG regions have been previously shown to express OXTRs and are involved in social memory (12, 13). We therefore asked whether these cells could be activated by the social memory test. WT and *Magel2* KO mice were sacrificed 90 min after the end of three-chamber test (+SI, for Social Interactions) and their brains examined for cFos immunolabeling, a marker of neuronal activity (Figure 3A). We found a significant increase (83%) in the number of cFos+ cells in the *stratum pyramidale* of aCA2/CA3d in tested WT (WT+SI) compared with untested WT (WT-SI) mice; in *Magel2* KO+SI mice we observed a 25% significant increase of cFos+ cells compared with WT+SI. In the aDG, a significant increase of ~60% of cFos+ cells compared with WT-SI was observed in both WT+SI and *Magel2* KO+SI, mainly in the hilus and *stratum granulare*. Thus, the activation of c-Fos is significant in both regions following social memory test in both genotypes (WT+SI and *Magel2* KO+SI mice) with an increase of cFos activated cells observed in the aCA2/CA3d region in *Magel2* KO+SI. Overall, these data confirm a strong activation of neurons in aCA2/CA3d regions in WT and *Magel2* KO mice following social interactions.

Expression profile of *Magel2* and *Oxtr* in the aDG and aCA2/CA3d regions

Magel2 is known to be highly expressed in hypothalamus, while its expression in hippocampal regions is less well characterized. We investigated the developmental expression of *Magel2* and *Oxtr* transcripts in the anterior hippocampus using RNAscope technique at two different time points (P7 and P21), taking in account the dynamic expression of OXTRs. At P7 (Figure 4A), we detected *Oxtr* and *Magel2* mRNAs in the aCA2/CA3d region with *Magel2* more expressed in the deep layer of the *stratum pyramidale*, a fainter expression is also detected all over the layer. At this stage, *Oxtr* transcripts were more concentrated in the CA2 region, compared to *Magel2*. At P21 (Figure 4), the level of *Magel2* transcripts was reduced but still present in the deep layer of

aCA2/CA3d region and *Oxtr* transcripts were also strongly expressed in pyramidal cells. Expression of *Magel2* and *Oxtr* was also detected in few cells of the *stratum oriens* and *stratum radiatum* where co-expression can be observed. In the DG, an expression of *Oxtr* and *Magel2* is detected in the hilus, some cells presenting a co-localization of both transcripts.

In adulthood, based on the *in-situ* hybridization maps of Allen Brain Atlas, we could confirm expression of *Magel2* in the CA3 deep layer of the *stratum pyramidale* (not shown). Then, we consulted the public Allen brain RNAseq data from cortex and hippocampal samples (<http://celltypes.brainmap.org/rnaseq/mouse/cortex-and-hippocampus>) to define the cell types expressing *Magel2* and *Oxtr*. *Oxtr* transcripts are expressed in GABAergic interneurons mainly in SST and also in parvalbumin (PV) and Calbindin expressing interneurons. Expression is also detected in glutamatergic neurons of a CA2-CA3 region co-expressing CCK. *Magel2* is faintly detected in the glutamatergic neurons only. Finally, from RNAseq data extracted from the atlas of cell types from Linnarsson Lab.

(<http://mousebrain.org/genesearch.html>) co-expression of *Oxtr* and *Magel2* is detected in the CA3 excitatory neurons of adult mice and also in several interneuron sub-populations expressing SST or SST and PV such as the axo-axonic long-range projections interneurons and the basket bistratified cells. These sub-populations of interneurons represent a small number of cells that have a wide and diverse spectrum of actions. These data suggest that the lack of *Magel2* can alter the *Oxtr* expressing excitatory neurons in the aCA2/CA3d region and also the SST or PV interneurons.

The quantity of OT-binding sites is increased in the aCA2/CA3d and aDG regions of *Magel2* KO adult mice and normalized in the aDG following an OT-treatment

We then looked at the distribution of OT-binding sites in *Magel2* KO-vehicle or *Magel2* KO+OT compared with WT-vehicle hippocampi by autoradiography (Figure 5). We observed a significant increase of OT-binding sites in the aCA2/CA3 (100%, Figure 5A-B) and aDG (80%, Figure 5C-D) regions but not in the ventral CA1/CA2/CA3 region (Figure 5E-F). In *Magel2*

KO+OT we observed a normalization of the quantity of OT-binding sites in the aDG, but not in the aCA2/CA3 region where OT-binding sites level was decreased but remained elevated compared to WT (Figure 5A-B). The binding study indicate subregions specific modulation of OXTR in the hippocampus. We then asked if this subregion specific effect could be linked to specific changes in neuronal subpopulations in the same regions.

The number of SST+ neurons is increased in the aCA2/CA3d and aDG regions of *Magel2* KO adult mice and normalized following an OT-treatment.

In the anterior adult hippocampus OXTRs are expressed in pyramidal cells and in SST and/or PV interneurons of aCA2/CA3d region and in interneurons of aDG (see above, (12, 16)). In control mice following social memory test, cFos expression was detected in 23 or 30% of SST-immunopositive cells (SST+) and 22 or 28% of PV+ cells in the aCA2/CA3d or aDG regions following the social memory test, respectively (Figure 6-figure supplement 1), suggesting an involvement of those interneurons in social memory. Then we quantified the number of SST+ and PV+ cells in *Magel2* KO versus WT adult hippocampi and observed a significant higher number of SST+ cells in both aCA2/CA3d (1.6 x) and aDG (1.8 x) regions of *Magel2* KO animals (Figure 6 A-F and M-N). PV+ cells are present in the same quantity in both genotypes (Figure 6-figure supplement 2). In contrast, the number of SST+ cells was significantly decreased in both aCA2/CA3d (less 12%) and DG regions (less 17%) in OT-treated *Magel2* KO mice compared with untreated WT mice (Figure 6 G-L and O-P). An increase of SST+ neurons was observed in anterior hippocampus of adult *Magel2* KO and, conversely, OT-treatment of *Magel2* KO pups was associated with a slight decrease of SST+ neurons in adult mutant compared with WT hippocampi. PV+ cells were equally abundant in both genotypes (Figure 6-figure supplement 2). This change in the quantity of SST+ cells might have consequences in the alteration of the excitation/inhibition (E/I) balance.

GABAergic and glutamatergic activities are altered in *Magel2* KO aCA3d pyramidal neurons and neonatal OT-treatment normalizes the GABAergic activity but reduces the glutamatergic activity in WT mice.

Alterations in GABA/glutamate (Excitatory/Inhibitory; E/I) balance is an electrophysiological feature frequently associated with multiple neurodevelopmental disorders. In addition, here, with an alteration of the quantity of OXTRs and of SST+ cells, we expect an alteration of the E/I ratio. Hippocampal brain slices of WT, *Magel2* KO, WT+OT and *Magel2* KO+OT juvenile (P25-P30) male mice were analyzed using whole cell patch clamp to record the activity of aCA3d pyramidal neurons (Figure 7A). Spontaneous activities analysis (Figure 7B) revealed a reduced amplitude of postsynaptic glutamatergic currents (sGlut-PSCs) in *Magel2* KO as compared to WT mice (Figure 7D), while the frequency of sGlut-PSCs was not changed (Figure 7C). The same *Magel2* KO neurons presented a significant increase in GABAergic (sGABA-PSCs) frequency (Figure 7E) while the amplitude of sGABA-PSCs was similar to that of WT (Figure 7F). Patch clamp recordings of the glutamatergic and GABAergic miniature currents (mGlut-PSCs and mGABA-PSCs, respectively) showed a significant reduction in amplitude of mGlut-PSCs, with no change in their frequency, in *Magel2* KO neurons compared to WT (Figure 7-figure supplement 1B-C) but no differences in frequencies and amplitudes of mGABA-PSCs (Figure 7-figure supplement 1D-E).

An abnormal dendritic morphology of the *Magel2* KO CA3 pyramidal neurons could be associated with the alterations of the GABAergic or glutamatergic activities. We defined the morphology of recorded CA3d neurons by adding biocytin in the recording solution and performing NeuroLucida reconstruction followed by a Sholl analysis. No differences were revealed in dendritic morphology between *Magel2* KO and WT CA3 pyramidal neurons in juvenile mice (Figure 7-figure supplement 2).

Altogether, those results show that, in *Magel2* KO pyramidal neurons of aCA3d, there is a significant increase in the GABA/Glutamate ratio with no change in their neuronal morphology. We next investigated the effects of OT-treatment on the GABA/Glutamate balance in WT and *Magel2* KO. Quite unexpectedly, the spontaneous glutamatergic activity was significantly reduced in WT+OT mice compared with WT: frequency was considerably reduced (x 2.7), being even lower than in OT-treated mutants (Figure 7C) and the amplitude was reduced (x1.5), being similar to the one observed in mutant mice (Figure 7D). These findings indicate

that OT-treatment reduced strongly the glutamatergic activity in WT juvenile mice without any apparent impact on the behavioral outcome measured (see above). In *Magel2* KO, OT-treatment in the first week of life decreased significantly the frequency of sGABA-PSCs restoring a frequency similar to WT (Figure 7E). There was no effect of OT-treatment on the amplitude of sGABA-PSCs (Figure 7F). However, on the same pyramidal neurons, such treatment in *Magel2* KO+OT reduces significantly the frequency of sGlut-PSCs (2x) compared with the frequency recorded in WT or in the *Magel2* KO mice (Figure 7C). The amplitude of sGlut-PSCs was not changed in *Magel2* KO+OT compared with *Magel2* KO, being reduced in the untreated or OT-treated mutants compared with WT mice (Figure 7D). These results show that OT administration in the first week of life normalized the frequency of spontaneous GABAergic activity and reduced significantly the frequency of spontaneous glutamatergic activity in *Magel2* KO compared with WT untreated mice. OT-treatment in WT juvenile mice reduced strongly the glutamatergic activity (frequency and amplitude).

The excitatory-to-inhibitory developmental GABA-shift is delayed in *Magel2* KO hippocampal neurons

Because *Oxtr* and *Magel2* are expressed in aCA2/CA3d hippocampus in infancy, and because in *Oxtr* KO mice (28) as in several models (48) of autism the depolarizing to hyperpolarizing (D-to-H) developmental GABA switch is delayed, we investigated the GABA switch timing in *Magel2* KO pups. First, we performed calcium (Ca^{2+}) imaging experiments by measuring the percentage of neurons showing GABA-induced Ca^{2+} responses in developing hippocampal neuronal cultures of *Magel2* KO embryos collected at E18.5 (DIV0 for days in vitro 0) (Figure 8A-B). At DIV4, we found a significant two-fold higher proportion of *Magel2* KO neurons increasing Ca^{2+} upon GABA stimulation compared with WT. At DIV8 and DIV11, the percentage of responsive neurons was markedly decreased and similar in both genotypes. We checked that the amplitude of Ca^{2+} responses were similar in both genotypes (Figure 8-figure supplement 1A). Noticeably, comparing the KCl-induced Ca^{2+} responses between WT and *Magel2* KO, we found no increase and even a significant reduction at DIV2, DIV4 and DIV8 in

Magel2 KO cultures (Figure 8-figure supplement 1B), suggesting that the voltage-operated calcium channels were not responsible for the significant higher proportion of *Magel2* KO neurons increasing Ca^{2+} upon GABA stimulation. All together, these results showed a developmental delay in GABA-induced Ca^{2+} responses in cultures of *Magel2* KO embryonic hippocampal neurons and suggest a developmental GABA-shift delay in *Magel2* KO hippocampal neurons.

To further examine whether the action of GABA was altered in *Magel2* KO hippocampal neurons, cell-attached recordings of single GABA_A channels/receptors were performed in acute brain slices in order to measure the Driving Force of GABA_A (DF_{GABA}). DF_{GABA} translates the differences in the actions of GABAergic synapses via GABA_A-receptors revealing a hyperpolarizing or depolarizing response of GABA, associated with mature or immature neurons, respectively. Thus, we measured the DF_{GABA} in aCA3 pyramidal cells (PCs) at postnatal days 1 (P1), 7 (P7) and 15 (P15), on acute brain slices obtained from male mice (Figure 8C). At P1, both *Magel2* KO and WT mice did not show significant differences in the DF_{GABA} but a tendency to an increase of DF_{GABA} in *Magel2* KO compared with WT. Significant difference in the DF_{GABA} was observed at P7 with a 1.8 fold increase of the DF_{GABA} value in mutant neurons, whereas a similar DF_{GABA} was obtained at P15. Since *Magel2* and *Oxtr* are expressed in interneurons (Ins), in which a GABA shift has been also described (49), we also measured the DF_{GABA} in INs and observed similar values in CA3 interneurons of mutant and WT mice (Figure 8-figure supplement 1C). Noticeably, at P7, the resting membrane potential (Figure 8-figure supplement 1D), the conductance (Figure 8-figure supplement 1F) and the capacitance (Figure 8-figure supplement 1E) did not differ statistically between WT and *Magel2* pyramidal neurons. Altogether these data suggest a transient higher GABA depolarizing activity at P7 in CA3 pyramidal neurons of *Magel2* KO pups and consequently a delay in GABA-shift.

Then, at P7, we assessed the effect of the *in vivo* OT-treatment in *Magel2*-KO and WT animals compared with WT untreated pups (Figure 8D). Both *Magel2* KO+OT and WT+OT mice showed a significant decrease in the DF_{GABA} values compared with WT-vehicle, suggesting a reduction in GABA depolarizing activity following an OT administration in infancy.

Post-translational changes in cation-chloride co-transporter KCC2 in *Magel2* KO hippocampus

We then asked if the altered DF_{GABA} values could be due to alteration in the expression of the neuronal transporters of Cl^- in *Magel2* KO. The neuronal level of $[Cl^-]_i$ and Cl^- dependent depolarizing or hyperpolarizing strength of GABA are determined by complex mechanism involving primarily Cl^- extrusion by potassium/chloride cotransporter type 2 (KCC2) whose expression increases progressively during neuronal maturation (Rivera et al., 1999; Stein et al., 2004). In developing WT hippocampal neurons, the emerging activity of KCC2 contributes to progressive lowering of $[Cl^-]_i$ that at P7 shifts GABA action from depolarizing to hyperpolarizing. As consequence, the activation of $GABA_A$ R produces neuronal Cl^- influx.

The quantitative western blot analysis of the total KCC2 protein expression in hippocampi of P7 mice did not reveal statistically significant difference of the amount of KCC2 between WT and *Magel2* KO animals (Figure 9 A-B). The ion-transport activity of KCC2 and its stability at the cellular plasma membrane also strongly depend on posttranslational modifications of multiple phosphorylation sites (50). We therefore applied in a next step phospho-site-specific antibodies, as they were previously shown to quantitatively monitor changes in KCC2 phosphorylation (51-53). Currently, a limited number of such phospho-specific antibody is available. They are directed against the well-known KCC2's phospho-sites Ser⁹⁴⁰ (54) and Thr¹⁰⁰⁷ (52, 53). Western blot analysis revealed that the *Magel2* KO hippocampi (as compared to WT) were characterized by significantly decreased amount of the phosphorylated form of Ser⁹⁴⁰ (P-Ser⁹⁴⁰). The amount of phosphorylated Thr¹⁰⁰⁷ (P-Thr¹⁰⁰⁷) was not statistically different, but albeit higher in *Magel2* KO mice (Figure 9A- B). Thus, in *Magel2* KO mice there was significant decrease of P-Ser⁹⁴⁰ (inactivation of function lee (54)) and no change of P-Thr¹⁰⁰⁷ whose progressive developmental de-phosphorylation is associated with increase of KCC2 activity Friedel (52). At P7, the decreased P-Ser⁹⁴⁰/P-Thr¹⁰⁰⁷ ratio in *Magel2* KO mice may thus result in predominance of

KCC2 internalization over surface expression. As a consequence of the decreased amount of surface expressed molecules, the Cl^- extrusion ability of KCC2 is decreased, causing an increase of $[Cl^-]_i$ and could induce a depolarizing shift of GABA described above (Figure 8C).

DISCUSSION

Here we show that *Magel2* KO mice display two specific and constant phenotypes that are stereotypical of other models characterized by a deficit in OT-system: isolation-induced vocalizations in infancy and social memory at adulthood (10). OT administration in the first week of life rescued the latter but not the former. To understand how neonatal OT-treatment drives such long-term effect in *Magel2* KO mice, we studied the hippocampal regions that contains social memory engrams, which also involve the OT-system, and unraveled several and successive temporal changes in the aDG and aCA2/CA3d hippocampal regions that might contribute to the social memory deficit in *Magel2* KO mice. We showed that *Magel2* deficiency alters the GABAergic developmental sequence probably resulting from post-translational biochemical modifications of KCC2, modifies the activity of pyramidal neurons and presents a higher number of SST-positive interneurons and an increase in the quantity of OT-binding sites at adulthood. Interestingly nearly all those changes are rescued by administration of OT in the first days after birth.

The effect of neonatal OT administration on *Magel2* KO mice

With regard to social behavior, the consequences of postnatal administration of OT in *Magel2* KO mice are consistent with those described previously (38). We have shown a rescue of all social deficits described in adult *Magel2* KO mice without an effect on USVs (here and (38)). The "USV test" measures early communication behavior in rodent pups with an ASD-like phenotype and in particular in those with a deficit in the OT-system; however, the role of OT-system in USV calls remains unknown. We cannot explain yet why the OT-administration in the first week of life does not improve the number of USVs in *Magel2* KO pups (P8).

One surprising finding of the current study is the relatively mild behavioral phenotype of the homozygous mutant, which we expected to be

more profoundly affected than heterozygous animals, previously reported to exhibit a social deficit (38). This difference may reflect differences in behavioral assays used in the two studies (3-chamber test versus open field) or the fact that heterozygous mice grew up with WT littermates, whereas homozygous *-/-* mutants constitute a homogeneous population. Indeed, it has been shown that transgenic mice and their WT littermates can modify each other's behavior (55). The behavior of the mother can also be modified in the presence of one or two genotypes in the same litter and thus impact the behavior of her offspring differently. The modulation of the severity of the social behavior deficits based on the genotype of the *Magel2* KO pups and their environmental context open a number of interesting translational opportunities that will need to be deeply investigated.

Converging evidence suggests that the neurobiological alterations described here may be related to a deficiency in the OT-system of *Magel2* KO mice. Noticeably, Ates et al. (56) showed, *ex vivo*, that lack of *Magel2* expression is associated with significant suppression of the overall activity of oxytocin neurons, suggesting that dysregulation of the OT-system goes beyond oxytocin expression. Furthermore, given the role of *MAGEL2* in ubiquitination, actin regulation and endosomal sorting processes (57), the absence of *Magel2* expression could induce a wide range of post-translational modifications of various molecular and cellular processes in OT and OXTR expressing neurons. Considering The observed long-lasting OT effects could result from a strong impact of OT administration in key developmental hippocampal processes (as discussed below) and can also be achieved by epigenetic modifications that impact gene expression such as the *Oxtr* expression, as observed in prairie voles following a maternal OT administration (58). Transcriptomic and proteomic studies at different developmental ages would help to understand the life-long effect of an early OT- treatment in mutant and WT mice.

Hippocampal alterations in *Magel2* KO in relation with the OT-system: causes and consequences

In vitro, OXTR activation can increase KCC2 phosphorylation (on Ser⁹⁴⁰) via a PKC -dependent pathway (28), allowing translocation of KCC2 to the cell membrane and post-translational modifications that collectively enhance KCC2

mediated Cl⁻ transport (54, 59), mechanisms which may also be relevant to control of the GABAergic developmental sequence *in vivo* (60). We therefore hypothesized that the low level of mature OT and/or the lack of *Magel2* in OXTR- positive neurons in *Magel2* KO neonates could induce a deficit in KCC2 Ser⁹⁴⁰ phosphorylation which, in turn, could induce a delay in GABA shift. Our findings are consistent with that hypothesis: we confirm that the GABAergic developmental sequence is transiently delayed in *Magel2* KO mice during the first week of life, with GABA_A-mediated responses more depolarizing in *Magel2* KO than WT pyramidal neurons at P7. We furthermore show that this electrophysiological deficit corresponds well with decreased functional KCC2 at the cell membrane, caused by a deficit of Ser⁹⁴⁰ phosphorylation.

Although a delay in the developmental GABA-shift in *Magel2* KO pyramidal neurons were no longer detectable at P15, there are compelling reasons to suspect that transient disruption of GABAergic maturation in the immediate postnatal period could be enough to permanently alter neural circuit dynamics. Indeed, P7 is a critical milestone in the development of GABAergic neurons in the mouse neocortex and hippocampus, characterized by major changes in network dynamics (e.g. end of *in vitro* giant-depolarizing-potentials (61) and *in vivo* early sharp waves (62)), intrinsic membrane properties (e.g. input resistance) and synaptic connectivity (63). Altogether those data suggest that the absence of *Magel2* delays neuronal maturation during this critically vulnerable period of brain development, resulting in a distinct adult phenotype. Whether the delay of the GABA-shift alone is sufficient to derail neurotypical developmental trajectory remains a key question for future study: notably, similar or longer GABA-shift delays have been observed in several models of autism (64, 65) and in *Oxtr* KO mouse models (28). Recently, Kang et al. (66) showed in *Disc1* KO mouse model, that elevated depolarizing GABA signaling is a precursor for the later E/I imbalance (in favor of inhibition) and social impairment. Similarly, we showed that, in a KCC2 mutant mouse, the GABA shift delay is responsible for the E/I alteration (60).

Importantly, OT-treatment has a relative hyperpolarizing effect at P7 in *Magel2* KO and WT pups compared with WT-vehicle animals that might modify the maturation of the circuitry.

The E/I ratio and social behavior

Reductions in synaptic signal-to-noise in cortical and hippocampal pyramidal neurons, driven by a change in the ratio of dendritic excitatory and inhibitory synapses, are widely thought to contribute to reduced efficiency of signal processing in ASD, a mechanism known as the E/I ratio hypothesis (67). We confirm E/I imbalance characterized by increased GABAergic activity and lower glutamatergic activity in CA3 neurons in *Magel2* KO mice, consistent with observations made in other ASD models (68-71). Furthermore, we report that perinatal OT administration restored normal GABAergic activity in *Magel2* KO mice without improving glutamatergic transmission. Unexpectedly, perinatal OT treatment has a significant impact on the WT neurons inducing a strong reduction of glutamatergic activity without affecting GABAergic activity. This is a significant observation, because it shows that, although the ASD-like behavior *Magel2* KO animals correlated with a change in E/I ratio, E/I imbalance in OT treated WT animals was not sufficient to drive detectable changes in social behavior or cognitive performance. We therefore conclude that E/I imbalance characterized by isolated decreased spontaneous glutamatergic transmission is unlikely to underlie the ASD traits investigated here, and suggest that an upper threshold of GABAergic or glutamatergic activity, but not the E/I ratio *per se*, may be important for normal development.

Role of oxytocin receptors and somatostatin neurons.

In adult *Magel2* KO mice we observed increased OT-binding in the DG and CA2/CA3d regions of the anterior hippocampus compared to WT mice. OT administration in *Magel2* KO neonates normalized hippocampal OT binding sites in adulthood, suggesting that the increased expression of OXTR observed in *Magel2* KO hippocampus may be a consequence of the reduced OT production reported in these animals (37). This observation supports the idea that life-long OXTR expression is to some extent determined by early life OT binding, described as a “hormonal imprinting” effect (58, 72).

Since hippocampal OXTRs are mainly expressed in PV and SST interneurons, we quantified those populations and found a significant increase (1.6x to 1.8x) in the number of aDG and aCA2/CA3d SST+ neurons in mutant mice, the number of PV+ interneurons was not modified. OT-treatment

normalized the number of SST-expressing neurons in *Magel2* KO pups, revealing a causal link between the administration of OT in infancy and the quantity of SST+ neurons. This result may reflect actual changes in the number of SST+ neurons, or alternatively changes in SST expression and hence more reliable detection of SST- synthesizing neurons. Interestingly, OT modulates the activity of the SST+ neurons, increasing the excitability of SST interneurons (31) but no studies report an effect of OT on SST production.

SST interneurons have recently been shown to play a role in the modulation of social behavior (73, 74) and a reduction in the number of PV or SST interneurons has been reported to be associated with social deficits or ASD. Noticeably, a link between altered social memory and an increase in SST cell number has been recently reported in LPS-treated female neonates (75). It is tempting to speculate that OXTR-transmission regulates the activity of SST hippocampal interneurons and the production/release of mature SST and impacts social memory. Further work is needed to fully characterize the role of OXTRs on SST interneurons in relation with social memory.

Conclusions

Short-term OT-treatment in infancy reduced behavioral traits associated with ASD in adulthood and permanently rescued functional and cellular hippocampal alterations that were identified in *Magel2* KO mice. However, we do not know whether the deficient OT-system observed in *Magel2* KO mice (37, 38) is the only cause of these alterations since the lack of *Magel2* expression may disrupt neuronal development and circuit formation via signaling pathways independent of OT. Another open question is whether developmental alterations in the *Magel2* KO are a consequence of dysfunction in a single sequential pathway, or whether they reflect parallel interconnected circuits in the developing hippocampus. Finally, and surprisingly, postnatal OT-treatment plays a role in many key processes, suggesting a pleiotropic action of oxytocin stimulating the maturation of hippocampal circuitry involved in social memory and possibly other behavioral deficits. A significant impact of such treatment was also observed in WT animals without any effect on social behavioral as tested. Overall, we have shown that OT-treatment in infancy has a significant impact and rescues permanent specific hippocampal alterations in

Magel2 KO mice at different developmental ages, many of these hippocampal alterations have been described in several models of neurodevelopmental disorders with ASD (see discussion). In addition, OT deficit has often been described in rodent models of ASD (see introduction). Taken together, our findings reinforce the idea that OT-treatment in early life may represent a viable therapeutic strategy for patients with SYS or PWS and possibly other neurodevelopmental disorders.

MATERIALS AND METHODS

Animals

To perform functional studies, we chose to work with the *Magel2* *tm1.1Mus* homozygous (-/-) mice, here named *Magel2* KO, in order to have a greater homogeneity in the values, allowing a better analysis of the effects of the mutation.

Magel2 *tm1.1Mus*_{+/+} (WT) and *Magel2* *tm1.1Mus*_{-/-} (*Magel2* KO) mice were maintained on a C57BL/6J genetic background and stabulated in standard conditions, with *ad-libitum* access to food and water. Mice were handled and cared for in accordance with the Guide for the Care and Use of Laboratory Animals (N.R.C., 1996) and the European Communities Council Directive of September 22th 2010 (2010/63/EU, 74). Experimental protocols were approved by the institutional Ethical Committee guidelines for animal research with the accreditation no. B13-055-19 from the French Ministry of Agriculture. We maintain grouped-house mice (3-5 mice/cage). All efforts were made to minimize the number of animals used. *Magel2*-deficient mice were generated as previously described (37). Due to the parental imprinting of *Magel2* (paternally expressed only), to obtain heterozygote mice (+m/-p), males carrying the mutation on the maternal allele (-m/+p) were crossed with wild-type C57BL/6J females.

To obtain homozygote mice, *Magel2* KO homozygote males and females were crossed. Importantly, we checked that *Magel2* KO mothers had a similar maternal behavior as WT mothers. All mice were genotyped by PCR starting from DNA extracted from tail snips (around 3 mm), using the following couples of primers: M12KO F (5'-CCCTGGGTTGACTGACTCAT-3') and M12KO R (5'-TCTTCTTCTGGTGGCTTTG-3') to discriminate the mutant allele from the WT, 71456 F (5'-CACTCGATCACGTATGGCTCCATCA-

3') and 71457 R (5'-GATGGCAGGCACTGACTTACATGCTG-3') to discriminate the heterozygous from the homozygous mice.

Oxytocin Treatment

WT pups and *Magel2* KO pups were removed from their mother, placed on a heating pad, given a subcutaneous (s.c.) injection and quickly returned to the mother. The solutions injected were isotonic saline (10 µl) for the control mice and 2 µg of OT (Phoenix Pharmaceuticals Inc., cat #051-01) diluted in isotonic saline (10 µl) for the treated mice. The treatment was performed during the first week of life every other day (P0, P2, P4, P6).

Behavior

All the behavioral tests were performed by Phenotype Expertise, Inc. (France). For all tests, animals were first acclimated to the behavioral room for 30 minutes.

Ultrasonic vocalization (USVs). Early social communication was tested by analyzing isolation-induced ultrasonic vocalizations (USVs) in P8 pups of both sexes. Briefly, after 30 min of habituation to the testing room, P8 pups were isolated from the mother and gently transferred to a new cage on a heating pad (37°C). After 5 min of separation, each pup was transferred in an isolation box located inside an anechoic box (54 x 57 x 41 cm; Coubourn instruments, PA, USA). USVs were recorded for 300 s by an ultrasonic microphone (Avisoft UltraSoundGate condenser microphone capsule CM16/CMPA, Avisoft bioacoustic, Germany) sensitive to frequencies of 10-250 kHz. Recordings were done using Avisoft recorder software (version 4.2) with a sampling rate of 250 kHz in 16-bit format. Data were analyzed for the total number of calls using Avisoft SASLab software.

Elevated-Plus Maze. The EPM is used to assess anxiety state of animals. The device consists of a labyrinth of 4 arms 5 cm wide located 80 cm above the ground. Two opposite arms are open (without wall) while the other two arms are closed by side walls. The light intensity was adjusted to 20 Lux on the open arms. Mice were initially placed on the central platform and left free to explore the cross-shaped labyrinth for 5 minutes. Maze was cleaned and wiped with H₂O and with 70% ethanol between each mouse. Animal movement was video-tracked using Ethovision software 11.5 (Noldus). Time spent in open and closed arms, the number of entries

in open arms, as well as the distance covered, are directly measured by the software.

Open-field. Open-field test was performed in a 40 x 40 cm square arena with an indirect illumination of 60 lux. Mouse movement was video-tracked using Ethovision software 11.5 (Noldus) for 10 minutes. Total distance traveled and time in center (exclusion of a 5 cm border arena) are directly measured by the software. Grooming (time and events) and rearing were manually counted in live using manual functions of the software, by an experimented behaviorist. The open-field arena was cleaned and wiped with H₂O and with 70% ethanol between each mouse.

New object recognition. The arena used for the novel object recognition test was the same used for the open-field test. The arena was cleaned and wiped with 70% ethanol between each mouse. Two identical objects (50 ml orange corning tube) were placed in the opposite corners of the arena, 10 cm from the side walls. The tested mouse was placed at the opposite side of the arena and allowed to explore the arena for 10 min. After 1h, one object was randomly replaced with another novel object, which was of similar size but differ in the shape and color with the previous object (white and blue lego bricks). Then, the same mouse was placed in the arena and allowed to explore the two objects (a new and an "old" familiar object) for 10 min. The movement of the mice was video-tracked with Ethovision 11.5 software. Time of exploration of both objects (nose located in a 2 cm area around object) was automatically measured by the software.

Three-chamber social preference test. The test was performed as described previously (46). The three-chamber apparatus consisted of a Plexiglas box (50x25 cm) with removable floor and partitions dividing the box into three chambers with 5-cm openings between chambers. The task was carried out in four trials. The three-chambers apparatus was cleaned and wiped with 70% ethanol between each trial and each mouse.

In the first trial (habituation), a test mouse was placed in the center of the three-chamber unit, where two empty wire cages were placed in the left and right chambers to habituate the test mouse to arena. The mouse was allowed to freely explore each chamber. The mouse was video-tracked for 5 min using Ethovision software. At the end of the trial, the animal was gently directed to the central chamber with doors closed. In the second trial

(social exploration), a 8-weeks old C57BL/6J mouse (S1) was placed randomly in one of the two wire cages to avoid a place preference. The second wire cage remained empty (E). Then, doors between chambers were opened and the test mouse was allowed to freely explore the arena for 10 min. At the end of the trial, animal was gently directed to the central chamber with doors closed. A second 8-weeks old C57BL/6J mouse (S2) was placed in the second wire cage for the third trial (social discrimination). Thus, the tested mouse had the choice between a familiar mouse (S1) and a new stranger mouse (S2) for 10 min. At the end of the trial, the mouse was returned to home-cage for 30 min. For the fourth trial (short-term social memory), S2 was replaced by a new stranger mouse (S3), the familiar mouse (S1) staying the same. Then tested mouse was allowed to freely explore the arena for 10 min. Time spent in each chamber and time of contact with each wire cage (with a mouse or empty) were calculated using Ethovision software. The measure of the real social contact is represented by the time spent in nose-to-nose interactions with the unfamiliar or familiar mouse. This test was performed using grouped-house mice of 4 months old.

Primary hippocampal cultures

Embryonic day 18 dissociated hippocampal neurons were obtained from wild-type and *Mage12* KO timed pregnant mice as previously described (76) with slightly modifications here described. Briefly, the hippocampi of E18 embryos were dissociated by an enzymatic treatment (0.25% trypsin for 18 min at 37°C) followed by mechanic dissociation with a fire-smoothed Pasteur pipette or p1000µl/p200µl tips. For calcium imaging experiments, 200 000 cell/well (in MW 6 wells) were plated on round 26 mm glass coverslips pre-coated with poly-L-lysine containing Neurobasal medium (Life Technologies) augmented with B27 supplement (2% v/v; Life Technologies), L-glutamine (2mM), penicillin/streptomycin (100U/ml) and 25µM Glutamate. This media was replaced with glutamate-free media after 5 hours. Neurons were then maintained at 37°C in humidified atmosphere (95% air and 5% CO₂), and half of the medium was refreshed twice a week.

Calcium imaging recordings

Calcium imaging experiments were carried out as previously described (28). Briefly, hippocampal neurons were loaded with the membrane-

permeable fluorescent Ca^{2+} indicator Fura-2/AM (1 μM ; SigmaAldrich) for 40 min at 37°C , 5% CO_2 . The cells were then placed into the recording chamber of an inverted microscope (Axiovert 100, Zeiss), washed with the extracellular recording solution, KRH buffer, and imaged through a 40x objective (Zeiss). Fura-2/AM was excited at 380 nm and at 340 nm through a Polychrom V, (TILL Photonics GmbH) controlled by the TillVisION software 4.01. Emitted light was acquired at 505nm at 1Hz, and images collected with a CCD Imago-QE camera (TILL Photonics GmbH). The fluorescence ratio F340/380 ($\Delta\text{F340/380}$) was used to express Ca^{2+} concentrations in regions of interest (ROI) corresponding to neuronal cell bodies. 100 μM GABA was administered in the recording solution and temporal changes in $\Delta\text{F340/380}$ were followed. Increases in $\Delta\text{F340/380}$ higher than 0.04 units were considered reliable Ca^{2+} responses. After wash with KRH buffer and recover, KCl (50mM) was administered to identify viable neurons. Responses with a $\Delta\text{F340/380}$ smaller than 0.1 units were excluded from the analyses. From DIV8 on, 1 μM TTX (Tocris, cat #1069) was added to this extracellular recording solution.

Hippocampal slice preparation and electrophysiological recordings

Brains were removed and immersed into ice-cold ($2-4^\circ\text{C}$) artificial cerebrospinal fluid (ACSF) with the following composition (in mM): 126 NaCl, 3.5 KCl, 2 CaCl_2 , 1.3 MgCl_2 , 1.2 NaH_2PO_4 , 25 NaHCO_3 and 11 glucose, pH 7.4 equilibrated with 95% O_2 and 5% CO_2 . Hippocampal slices (400 μm thick) were cut with a vibrating microtome (Leica VT 1000s, Germany) in ice cold oxygenated choline-replaced ACSF and were allowed to recover at least 90 min in ACSF at room (25°C) temperature. Slices were then transferred to a submerged recording chamber perfused with oxygenated (95% O_2 and 5% CO_2) ACSF (3 ml/min) at 34°C .

Whole-cell patch clamp recordings were performed from P20-P25 CA3 pyramidal neurons in voltage-clamp mode using an Axopatch 200B (Axon Instrument, USA). To record the spontaneous and miniature synaptic activity, the glass recording electrodes (4-7 $\text{M}\Omega$) were filled with a solution containing (in mM): 100 KGluconate, 13 KCl, 10 HEPES, 1.1 EGTA, 0.1 CaCl_2 , 4 MgATP and 0.3 NaGTP. The pH of the

intracellular solution was adjusted to 7.2 and the osmolality to 280 mOsmol l^{-1} . The access resistance ranged between 15 to 30 $\text{M}\Omega$. With this solution, the GABA_A receptor-mediated postsynaptic current (GABAA-PSCs) reversed at -70mV. GABA-PSCs and glutamate mediated synaptic current (Glut-PSCs) were recorded at a holding potential of -45mV. At this potential GABA-PSC are outwards and Glut-PSCs are inwards. Spontaneous synaptic activity was recorded in control ACSF and miniature synaptic activity was recorded in ACSF supplemented with tetrodotoxin (TTX, 1 μM). Spontaneous and miniature GABA-PSCs and Glut-PSCs were recorded with Axoscope software version 8.1 (Axon Instruments) and analyzed offline with Mini Analysis Program version 6.0 (Synaptosoft).

Single GABA_A channel recordings were performed at P1, P7 and P15 visually identified hippocampal CA3 pyramidal cells in cell-attached configuration using Axopatch-200A amplifier and pCLAMP acquisition software (Axon Instruments, Union City, CA). Data were low-pass filtered at 2 kHz and acquired at 10 kHz. The glass recording electrodes (4-7 $\text{M}\Omega$) were filled with a solution containing (in mM) for recordings of single GABA_A channels: NaCl 120, KCl 5, TEA-Cl 20, 4-aminopyridine 5, CaCl_2 0.1, MgCl_2 10, glucose 10, Hepes-NaOH 10. The pH of pipette solutions was adjusted to 7.2 and the osmolality to 280 mOsmol l^{-1} . Analysis of currents through single channels and current-voltage relationships were performed using Clampfit 9.2 (Axon Instruments) as described by (77).

Morphological analysis

During electrophysiological recordings, biocytin (0.5%, Sigma, USA) was added to the pipette solution for post hoc reconstruction. Images were acquired using a Leica SP5 X confocal microscope, with a 40x objective and 0.5 μm z-step. Neurons were reconstructed three-dimensionally using NeuroLucida software version 10 (MBF Bioscience) from 3D stack images. The digital reconstructions were analyzed with the software L-Measure to measure the number of primary branches and the total number of ramifications of each neuron (78). Comparisons between groups were done directly in L-Measure.

Immunohistochemistry and quantification

WT and mutant mice were deeply anaesthetized with intraperitoneal injection of the ketamine/xylazine mixture and transcardially perfused with 0.9% NaCl saline followed by Antigenfix (Diapath, cat #P0014). Brains were post-fixed in Antigenfix overnight at 4°C and included in agar 4%. 50 µm-thick coronal sections were sliced using a vibratome (Zeiss) and stored in PBS at 4°C. Floating slices (of the hippocampal region corresponding to slices 68 to 78 on Allen Brain Atlas) were incubated for 1 hour with blocking solution containing 0.1% (v/v) Triton X-100, 10% (v/v) normal goat serum (NGS) in PBS, at room temperature. Sections were then incubated with primary antibodies diluted in incubation solution (0.1% (v/v) Triton X-100, 3% (v/v) NGS, in PBS), overnight at 4°C. After 3 x 10 min washes in PBS, brain sections were incubated with secondary antibodies diluted in the incubation solution, for 2 hours at RT. Sections were washed 3 x 10 min in PBS and mounted in Fluoromount-G (EMS, cat #17984-25). Primary antibodies used were: rabbit polyclonal anti-cFos (1:5000, Santa Cruz Biotech, cat #ab190289), goat polyclonal anti-Sst (D20) (1:500, Santa Cruz Biotech, cat #sc-7819), mouse monoclonal anti-Sst (H-11) (1:500, Santa Cruz Biotech, cat #sc-74556), goat polyclonal anti-PV (1:6000, SWANT, cat #PVG213). Fluorochrome-conjugated secondary antibodies used were: goat anti-rabbit Alexa Fluor 647 (1:500, Invitrogen, cat # A32733), goat anti-rabbit Alexa Fluor 488 (1:500, Invitrogen, cat #A-31565), goat anti-mouse Alexa Fluor 488 (1:500, Invitrogen, cat #A21121), donkey anti-goat Alexa Fluor 488 (1:500, Invitrogen, cat # A32814). For c-Fos, PV and SST quantification, images were acquired using a fluorescence microscope (Zeiss Axioplan 2 microscope with an Apotome module), and z stacks of 8 µm were performed for each section. Counting were performed on the right and left hippocampus for 5-7 sections (cFos) or 7-9 sections (PV, SST) per animal in the hippocampal regions indicated on the figures and corresponding to slices 68 to 78 on Allen Brain Atlas.

OT binding assay

Adult WT and mutant mice were sacrificed and non-perfused mouse brain were frozen in -25°C isopentane and stored at -80°C until cut. 14 µm thick brain slices were cut using a cryostat (Frigocut-2700, Reichert-Jung) and collected on

chromallume-coated slides and stored at -80°C until use. Slides were pre-incubated for 5 minutes in a solution of 0.2% paraformaldehyde in phosphate-buffered saline (pH 7.4), and rinsed twice in 50 mM Tris HCl + 0.1% BSA buffer. Slides were then put in a humid chamber and covered with 400 µL of incubation medium (50 mM Tris HCl, 0.025% bacitracin, 5 mM MgCl₂, 0.1% BSA) containing the radiolabeled I [125] OVTA (Perkin Elmer), at a concentration of 10 pM. After a 2h incubation under gentle agitation, the incubation medium is removed and slides are rinsed twice in ice-cold incubation medium and a third time in ice-cold distilled water. Each slide is then dried in a stream of cold air, and placed in a X-ray cassette in contact with a KODAK film for 3 days.

ROIs were chosen and analyzed through ImageJ, using Paxinos' Mouse Brain Atlas as a reference to find the brain areas of interest. To remove background noise caused by nonspecific binding, each slide was compared with its contiguous one, which had been incubated in presence of an excess of "cold" oxytocin (2 µM). Net grey intensity was quantified and then converted to nCi/mg tissue equivalent using a calibration curve. For each region, a minimum of 4 slices per brain were included in the analysis. Data plotted on graphs are the differences between the total and the nonspecific binding. Right and left hemispheres were kept separate.

Chromogenic In situ Hybridization

Fresh-frozen brains from WT mice at post-natal days (P)7, P21, and P28 were sectioned in a cryostat in the coronal plane at 20µm thickness and mounted on Superfrost Plus slides and stored at -80°C. RNA detection was performed on tissue sections using RNAscope 2.5HD Duplex Assay (Cat #322430, Advanced Cell Diagnostics (ACD), Hayward, CA). The two probes used are synthetic oligonucleotide probes complementary to the nucleotide sequence 1198 – 2221 of Oxt (NM_001081147.1) (Oxt-E4-C2, ACD Cat #411101-C2) and 3229 – 4220

of Magel2 (NM_013779.2) (Magel2-01, ACD Cat #535901). Briefly, slides were fixed in 4% paraformaldehyde in PBS (pH 9.5) on ice for 2 hours and dehydrated in increasing concentrations of alcohol, then stored in 100% ethanol overnight at -20°C. The slides were air dried for 10 minutes, then pretreated in target retrieval solution (ref. 322001, ACD) for 5 minutes while boiling, after

which, slides were rinsed 2 times in water followed by 100% ethanol and then air dried. A hydrophobic barrier pen (ImmEdge) was used to create a barrier around selected sections. Selected sections were then incubated with protease plus (ref. 322331, ACD) for 15 minutes in a HybEZ oven (ACD) at 40°C, followed by water washes. The sections were then hybridized with the probe mixture at 40°C for 2 hr per slide. Unbound hybridization probes were removed by washing 2 times in wash buffer. After hybridization, sections were subjected to signal amplification using the HD 2.5 detection Kit following the kit protocol. Hybridization signal was detected using a mixture of fast-RED solutions A and B (60:1) for Oxt-E4-C2 and a mixture of Fast-GREEN solutions A and B (50:1) for Magel2-01. The slides were then counterstained with Gill's hematoxylin and air-dried in a 60°C oven for 15 min. Slides were cooled and cover-slipped with Vectamount TM (Vector Laboratories, Inc. Burlingame, CA). Slides were imaged at 4x and 20x on a bright field microscope (Keyence BZ-X710, Keyence Corp., Osaka, Japan). Hippocampal sections were investigated for colocalization of Oxt (red) with Magel2 (blue-green) transcripts.

Western Blot

P7 mice were sacrificed and hippocampi were dissected and rapidly frozen in liquid nitrogen and stored at -80°C until protein extraction. Hippocampi were lysed in lysis buffer (50 mM Tris/HCl, pH 7.5, 1 mM EGTA, 1 mM EDTA, 50 mM sodium fluoride, 5 mM sodium pyrophosphate, 1 mM sodium orthovanadate, 1% (w/v) Triton-100, 0.27 M sucrose, 0.1% (v/v) 2-mercaptoethanol, and protease inhibitors (complete protease inhibitor cocktail tablets, Roche, 1 tablet per 50 mL)) and protein concentrations were determined following centrifugation of the lysate at 16,000 x g at 4 °C for 20 minutes using the Bradford method with bovine serum albumin as the standard. Tissue lysates (15 µg) in SDS sample buffer (1X NuPAGE LDS sample buffer (Invitrogen), containing 1% (v/v) 2-mercaptoethanol) were subjected to electrophoresis on polyacrylamide gels and transferred to nitrocellulose membranes. The membranes were incubated for 30 min with TBS-Tween buffer (TTBS, Tris/HCl, pH 7.5, 0.15 M NaCl and 0.2% (v/v) Tween-20) containing 5% (w/v) skim milk. The membranes were then immunoblotted in 5% (w/v) skim milk in TTBS with the indicated primary antibodies overnight at

4°C. The blots were then washed six times with TTBS and incubated for 1 hour at room temperature with secondary HRP-conjugated antibodies diluted 5000-fold in 5% (w/v) skim milk in TTBS. After repeating the washing steps, the signal was detected with the enhanced chemiluminescence reagent. Immunoblots were developed using ChemiDoc™ Imaging Systems (Bio-Rad). Primary antibodies used were: anti-KCC2 phospho-Ser940 (Thermo Fisher Scientific, cat #PA5-95678), anti-KCC2 phospho-Thr1007 (Thermo Fisher Scientific, cat #PA5-95677), anti-Pan-KCC2, residues 932-1043 of human KCC2 (NeuroMab, cat #73-013), anti(neuronal)-β-Tubulin III (Sigma-Aldrich, cat #T8578). Horseradish peroxidase-coupled (HRP) secondary antibodies used for immunoblotting were from Pierce. Figures were generated using Photoshop and Illustrator (Adobe). The relative intensities of immunoblot bands were determined by densitometry with ImageJ software.

Statistical Analysis

Statistical analyses were performed using GraphPad Prism (GraphPad Software, Prism 7.0 software, Inc, La Jolla, CA, USA). All statistical tests were two-tailed and the level of significance was set at P<0.05. Appropriate tests were conducted depending on the experiment; tests are indicated in the figure legends or detailed in supplementary statistical file. Values are indicated as Q2 (Q1, Q3), where Q2 is the median, Q1 is the first quartile and Q3 is the third quartile when non-parametric tests were performed and scatter dot plots report Q2 (Q1,Q3) or as mean ± SEM when parametric tests were performed usually in histograms. N refers to the number of animals or primary culture preparations, while n refers to the number of brain sections or hippocampi or cells recorded.

Mann-Whitney (MW) non-parametric test or t-test (parametric test) were performed to compare two matched or unmatched groups. ANOVA or Kruskal-Wallis tests were performed when the different groups have been experienced in the same experimental design only; if this was not the case, MW or t-test were used. One-way ANOVA followed by Bonferroni or Dunnett's or Tukey's post-hoc tests were used to compare three or more independent groups. Two-way ANOVA followed by Bonferroni post-hoc test was performed to compare the effect of two factors on unmatched groups. *: p< 0.05; **: p <0.01; ***: p<0.001;

****: $p < 0.0001$. All the statistical analyses (corresponding to each figure) are reported in a specific file.

Acknowledgements

The authors thank the Foundation for Prader-Willi Research (FPWR) grants, Agence Nationale pour la Recherche (ANR-14-CE13-0025-01), Thyssen Foundation (Grant 10.16.2.018MN), Prader-Willi France and Fondation Jérôme LeJeune for their financial support.

The authors thank Pr. Simon McCullan for comments and careful reading of the manuscript. Dr. A. Baude for her technical advices, Dr F. Michel for his help in microscopy and the use of image softwares,

Financial disclosures

Fabienne Schaller and Françoise Muscatelli are co-inventors on a patent to use oxytocin in the treatment of infant feeding disorder, e.g. Prader-Willi Syndrome (No. WO/2011/147889; US/2014/US9125862B2). The other authors have indicated they have no potential conflicts of interest to disclose.

REFERENCES

1. Wagner S, Harony-Nicolas H. Oxytocin and Animal Models for Autism Spectrum Disorder. *Current topics in behavioral neurosciences*. 2018;35:213-37.
2. Muscatelli F, Desarmenien MG, Matarazzo V, Grinevich V. Oxytocin Signaling in the Early Life of Mammals: Link to Neurodevelopmental Disorders Associated with ASD. *Current topics in behavioral neurosciences*. 2018;35:239-68.
3. Winslow JT, Hearn EF, Ferguson J, Young LJ, Matzuk MM, Insel TR. Infant vocalization, adult aggression, and fear behavior of an oxytocin null mutant mouse. *Horm Behav*. 2000;37(2):145-55.
4. Ferguson JN, Aldag JM, Insel TR, Young LJ. Oxytocin in the medial amygdala is essential for social recognition in the mouse. *J Neurosci*. 2001;21(20):8278-85.
5. Takayanagi Y, Yoshida M, Bielsky IF, Ross HE, Kawamata M, Onaka T, et al. Pervasive social deficits, but normal parturition, in oxytocin receptor-deficient mice. *Proc Natl Acad Sci U S A*. 2005;102(44):16096-101.
6. Sala M, Braida D, Lentini D, Busnelli M, Bulgheroni E, Capurro V, et al. Pharmacologic rescue of impaired cognitive flexibility, social deficits, increased aggression, and seizure susceptibility in oxytocin receptor null mice: a neurobehavioral model of autism. *Biol Psychiatry*. 2011;69(9):875-82.
7. Sala M, Braida D, Donzelli A, Martucci R, Busnelli M, Bulgheroni E, et al. Mice heterozygous for the oxytocin receptor gene (*Oxtr*(+/-)) show impaired social behaviour but not increased aggression or cognitive inflexibility: evidence of a selective haploinsufficiency gene effect. *J Neuroendocrinol*. 2013;25(2):107-18.
8. Jin D, Liu HX, Hirai H, Torashima T, Nagai T, Lopatina O, et al. CD38 is critical for social behaviour by regulating oxytocin secretion. *Nature*. 2007;446(7131):41-5.
9. Liu HX, Lopatina O, Higashida C, Tsuji T, Kato I, Takasawa S, et al. Locomotor activity, ultrasonic vocalization and oxytocin levels in infant CD38 knockout mice. *Neurosci Lett*. 2008;448(1):67-70.
10. Caldwell HK, Aulino EA, Freeman AR, Miller TV, Witchev SK. Oxytocin and behavior: Lessons from knockout mice. *Developmental neurobiology*. 2017;77(2):190-201.
11. Johnson ZV, Walum H, Xiao Y, Riefkohl PC, Young LJ. Oxytocin receptors modulate a social salience neural network in male prairie voles. *Horm Behav*. 2017;87:16-24.
12. Raam T, McAvoy KM, Besnard A, Veenema AH, Sahay A. Hippocampal oxytocin receptors are necessary for discrimination of social stimuli. *Nature communications*. 2017;8(1):2001.
13. Lin YT, Hsieh TY, Tsai TC, Chen CC, Huang CC, Hsu KS. Conditional Deletion of Hippocampal CA2/CA3a Oxytocin Receptors Impairs the Persistence of Long-Term Social Recognition Memory in Mice. *J Neurosci*. 2018;38(5):1218-31.
14. Okuyama T. Social memory engram in the hippocampus. *Neurosci Res*. 2018;129:17-23.
15. Cilz NI, Cymerblit-Sabba A, Young WS. Oxytocin and Vasopressin in the Rodent Hippocampus. *Genes Brain Behav*. 2018:e12535.

16. Young WS, Song J. Characterization of Oxytocin Receptor Expression Within Various Neuronal Populations of the Mouse Dorsal Hippocampus. *Frontiers in molecular neuroscience*. 2020;13:40.
17. Bosch OJ, Neumann ID. Brain vasopressin is an important regulator of maternal behavior independent of dams' trait anxiety. *Proc Natl Acad Sci U S A*. 2008;105(44):17139-44.
18. Eaton JL, Roache L, Nguyen KN, Cushing BS, Troyer E, Papademetriou E, et al. Organizational effects of oxytocin on serotonin innervation. *Dev Psychobiol*. 2012;54(1):92-7.
19. Miller TV, Caldwell HK. Oxytocin during Development: Possible Organizational Effects on Behavior. *Frontiers in endocrinology*. 2015;6:76.
20. Lefevre A, Sirigu A. The two fold role of oxytocin in social developmental disorders: A cause and a remedy? *Neurosci Biobehav Rev*. 2016;63:168-76.
21. Muscatelli F, Desarmenien MG, Matarazzo V, Grinevich V. Oxytocin Signaling in the Early Life of Mammals: Link to Neurodevelopmental Disorders Associated with ASD. *Current topics in behavioral neurosciences*. 2017.
22. Veenema AH. Toward understanding how early-life social experiences alter oxytocin- and vasopressin-regulated social behaviors. *Horm Behav*. 2012;61(3):304-12.
23. Perkeybile AM, Carter CS, Wroblewski KL, Puglia MH, Kenkel WM, Lillard TS, et al. Early nurture epigenetically tunes the oxytocin receptor. *Psychoneuroendocrinology*. 2019;99:128-36.
24. Hammock EA. Developmental perspectives on oxytocin and vasopressin. *Neuropsychopharmacology : official publication of the American College of Neuropsychopharmacology*. 2015;40(1):24-42.
25. Mitre M, Marlin BJ, Schiavo JK, Morina E, Norden SE, Hackett TA, et al. A Distributed Network for Social Cognition Enriched for Oxytocin Receptors. *J Neurosci*. 2016;36(8):2517-35.
26. Tyzio R, Cossart R, Khalilov I, Minlebaev M, Hubner CA, Represa A, et al. Maternal oxytocin triggers a transient inhibitory switch in GABA signaling in the fetal brain during delivery. *Science*. 2006;314(5806):1788-92.
27. Tyzio R, Nardou R, Ferrari DC, Tsintsadze T, Shahrokhi A, Eftekhari S, et al. Oxytocin-mediated GABA inhibition during delivery attenuates autism pathogenesis in rodent offspring. *Science*. 2014;343(6171):675-9.
28. Leonzino M, Busnelli M, Antonucci F, Verderio C, Mazzanti M, Chini B. The Timing of the Excitatory-to-Inhibitory GABA Switch Is Regulated by the Oxytocin Receptor via KCC2. *Cell reports*. 2016;15(1):96-103.
29. Banerjee A, Rikhye RV, Breton-Provencher V, Tang X, Li C, Li K, et al. Jointly reduced inhibition and excitation underlies circuit-wide changes in cortical processing in Rett syndrome. *Proc Natl Acad Sci U S A*. 2016.
30. Zheng JJ, Li SJ, Zhang XD, Miao WY, Zhang D, Yao H, et al. Oxytocin mediates early experience dependent cross-modal plasticity in the sensory cortices. *Nat Neurosci*. 2014;17(3):391-9.
31. Maldonado P, Nuno-Perez, A., Kirchner, J., Hammock, E., Gjorgjieva, J. and Lohmann, C. . Oxytocin shapes spontaneous activity patterns in the developing visual cortex by activating somatostatin interneurons. *bioRxiv*. 2020.
32. Tirko NN, Eyring KW, Carcea I, Mitre M, Chao MV, Froemke RC, et al. Oxytocin Transforms Firing Mode of CA2 Hippocampal Neurons. *Neuron*. 2018;100(3):593-608 e3.
33. Ripamonti S, Ambrozkiewicz MC, Guzzi F, Gravati M, Biella G, Bormuth I, et al. Transient oxytocin signaling primes the development and function of excitatory hippocampal neurons. *eLife*. 2017;6.
34. Boccaccio I, Glatt-Deeley H, Watrin F, Roeckel N, Lalande M, Muscatelli F. The human MAGEL2 gene and its mouse homologue are paternally expressed and mapped to the Prader-Willi region. *Hum Mol Genet*. 1999;8(13):2497-505.

35. Schaaf CP, Gonzalez-Garay ML, Xia F, Potocki L, Gripp KW, Zhang B, et al. Truncating mutations of MAGEL2 cause Prader-Willi phenotypes and autism. *Nat Genet.* 2013.
36. Fountain MD, Schaaf CP. Prader-Willi Syndrome and Schaaf-Yang Syndrome: Neurodevelopmental Diseases Intersecting at the MAGEL2 Gene. *Diseases.* 2016;4(1).
37. Schaller F, Watrin F, Sturny R, Massacrier A, Szepetowski P, Muscatelli F. A single postnatal injection of oxytocin rescues the lethal feeding behaviour in mouse newborns deficient for the imprinted *Magel2* gene. *Hum Mol Genet.* 2010;19(24):4895-905.
38. Meziane H, Schaller F, Bauer S, Villard C, Matarazzo V, Riet F, et al. An Early Postnatal Oxytocin Treatment Prevents Social and Learning Deficits in Adult Mice Deficient for *Magel2*, a Gene Involved in Prader-Willi Syndrome and Autism. *Biol Psychiatry.* 2015;78(2):85-94.
39. Fountain MD, Aten E, Cho MT, Juusola J, Walkiewicz MA, Ray JW, et al. The phenotypic spectrum of Schaaf-Yang syndrome: 18 new affected individuals from 14 families. *Genet Med.* 2017;19(1):45-52.
40. Dai YC, Zhang HF, Schon M, Bockers TM, Han SP, Han JS, et al. Neonatal Oxytocin Treatment Ameliorates Autistic-Like Behaviors and Oxytocin Deficiency in Valproic Acid-Induced Rat Model of Autism. *Frontiers in cellular neuroscience.* 2018;12:355.
41. Penagarikano O, Lazaro MT, Lu XH, Gordon A, Dong H, Lam HA, et al. Exogenous and evoked oxytocin restores social behavior in the *Cntnap2* mouse model of autism. *Science translational medicine.* 2015;7(271):271ra8.
42. Francis SM, Sagar A, Levin-Decanini T, Liu W, Carter CS, Jacob S. Oxytocin and vasopressin systems in genetic syndromes and neurodevelopmental disorders. *Brain Res.* 2014.
43. Mansouri M, Pouretamad H, Roghani M, Wegener G, Ardalan M. Autistic-Like Behaviours and Associated Brain Structural Plasticity are Modulated by Oxytocin in Maternally Separated Rats. *Behav Brain Res.* 2020:112756.
44. Tauber M, Boulanouar K, Diene G, Cabal-Berthoumieu S, Ehlinger V, Fichaux-Bourin P, et al. The Use of Oxytocin to Improve Feeding and Social Skills in Infants With Prader-Willi Syndrome. *Pediatrics.* 2017.
45. Matarazzo V, Muscatelli F. Natural breaking of the maternal silence at the mouse and human imprinted Prader-Willi locus: A whisper with functional consequences. *Rare diseases.* 2013;1:e27228.
46. Zhang JB, Chen L, Lv ZM, Niu XY, Shao CC, Zhang C, et al. Oxytocin is implicated in social memory deficits induced by early sensory deprivation in mice. *Molecular brain.* 2016;9(1):98.
47. Karlsson SA, Haziri K, Hansson E, Kettunen P, Westberg L. Effects of sex and gonadectomy on social investigation and social recognition in mice. *BMC neuroscience.* 2015;16:83.
48. Ben-Ari Y. Is birth a critical period in the pathogenesis of autism spectrum disorders? *Nat Rev Neurosci.* 2015;16(8):498-505.
49. Tyzio R, Minlebaev M, Rheims S, Ivanov A, Jorquera I, Holmes GL, et al. Postnatal changes in somatic gamma-aminobutyric acid signalling in the rat hippocampus. *Eur J Neurosci.* 2008;27(10):2515-28.
50. Zhang J, Cordshagen A, Medina I, Nothwang HG, Wisniewski JR, Winklhofer M, et al. Staurosporine and NEM mainly impair WNK-SPAK/OSR1 mediated phosphorylation of KCC2 and NKCC1. *PLoS One.* 2020;15(5):e0232967.
51. Kahle KT, Merner ND, Friedel P, Silayeva L, Liang B, Khanna A, et al. Genetically encoded impairment of neuronal KCC2 cotransporter function in human idiopathic generalized epilepsy. *EMBO Rep.* 2014;15(7):766-74.
52. Friedel P, Kahle KT, Zhang J, Hertz N, Pisella LI, Buhler E, et al. WNK1-regulated inhibitory phosphorylation of the KCC2 cotransporter maintains the depolarizing action of GABA in immature neurons. *Sci Signal.* 2015;8(383):ra65.

53. de Los Heros P, Alessi DR, Gourlay R, Campbell DG, Deak M, Macartney TJ, et al. The WNK-regulated SPAK/OSR1 kinases directly phosphorylate and inhibit the K⁺-Cl⁻ cotransporters. *Biochem J.* 2014;458(3):559-73.
54. Lee HH, Deeb TZ, Walker JA, Davies PA, Moss SJ. NMDA receptor activity downregulates KCC2 resulting in depolarizing GABA_A receptor-mediated currents. *Nat Neurosci.* 2011;14(6):736-43.
55. Kalbassi S, Bachmann SO, Cross E, Robertson VH, Baudouin SJ. Male and Female Mice Lacking Neuroligin-3 Modify the Behavior of Their Wild-Type Littermates. *eNeuro.* 2017;4(4).
56. Ates T, Oncul M, Dilsiz P, Topcu IC, Civas CC, Alp MI, et al. Inactivation of Magel2 suppresses oxytocin neurons through synaptic excitation-inhibition imbalance. *Neurobiol Dis.* 2019;121:58-64.
57. Tacer KF, Potts PR. Cellular and disease functions of the Prader-Willi Syndrome gene MAGEL2. *Biochem J.* 2017;474(13):2177-90.
58. Kenkel WM, Perkeybile AM, Yee JR, Pournajafi-Nazarloo H, Lillard TS, Ferguson EF, et al. Behavioral and epigenetic consequences of oxytocin treatment at birth. *Sci Adv.* 2019;5(5):eaav2244.
59. Kahle KT, Deeb TZ, Puskarjov M, Silayeva L, Liang B, Kaila K, et al. Modulation of neuronal activity by phosphorylation of the K-Cl cotransporter KCC2. *Trends Neurosci.* 2013;36(12):726-37.
60. Pisella LI, Gaiarsa JL, Diabira D, Zhang J, Khalilov I, Duan J, et al. Impaired regulation of KCC2 phosphorylation leads to neuronal network dysfunction and neurodevelopmental pathology. *Sci Signal.* 2019;12(603).
61. Ben-Ari Y, Spitzer NC. Nature and nurture in brain development. *Trends Neurosci.* 2004;27(7):361.
62. Leinekugel X, Khazipov R, Cannon R, Hirase H, Ben-Ari Y, Buzsaki G. Correlated bursts of activity in the neonatal hippocampus in vivo. *Science.* 2002;296(5575):2049-52.
63. Shi Y, Grieco SF, Holmes TC, Xu X. Development of Local Circuit Connections to Hilar Mossy Cells in the Mouse Dentate Gyrus. *eNeuro.* 2019;6(2).
64. He Q, Nomura T, Xu J, Contractor A. The Developmental Switch in GABA Polarity Is Delayed in Fragile X Mice. *Journal of Neuroscience.* 2014;34(2):446-50.
65. Ben-Ari Y. The GABA excitatory/inhibitory developmental sequence: a personal journey. *Neuroscience.* 2014;279:187-219.
66. Kang E, Song J, Lin Y, Park J, Lee JH, Hussani Q, et al. Interplay between a Mental Disorder Risk Gene and Developmental Polarity Switch of GABA Action Leads to Excitation-Inhibition Imbalance. *Cell reports.* 2019;28(6):1419-28 e3.
67. Sohal VS, Rubenstein JLR. Excitation-inhibition balance as a framework for investigating mechanisms in neuropsychiatric disorders. *Mol Psychiatry.* 2019;24(9):1248-57.
68. Harrington AJ, Raissi A, Rajkovich K, Berto S, Kumar J, Molinaro G, et al. MEF2C regulates cortical inhibitory and excitatory synapses and behaviors relevant to neurodevelopmental disorders. *eLife.* 2016;5.
69. Tabuchi K, Blundell J, Etherton MR, Hammer RE, Liu X, Powell CM, et al. A neuroligin-3 mutation implicated in autism increases inhibitory synaptic transmission in mice. *Science.* 2007;318(5847):71-6.
70. Unichenko P, Yang JW, Kirischuk S, Kolbaev S, Kilb W, Hammer M, et al. Autism Related Neuroligin-4 Knockout Impairs Intracortical Processing but not Sensory Inputs in Mouse Barrel Cortex. *Cerebral cortex.* 2017:1-14.
71. Wood L, Shepherd GM. Synaptic circuit abnormalities of motor-frontal layer 2/3 pyramidal neurons in a mutant mouse model of Rett syndrome. *Neurobiol Dis.* 2010;38(2):281-7.
72. Carter CS. Developmental consequences of oxytocin. *Physiol Behav.* 2003;79(3):383-97.

73. Perez SM, Boley A, Lodge DJ. Region specific knockdown of Parvalbumin or Somatostatin produces neuronal and behavioral deficits consistent with those observed in schizophrenia. *Translational psychiatry*. 2019;9(1):264.
74. Scheggia D, Manago F, Maltese F, Bruni S, Nigro M, Dautan D, et al. Somatostatin interneurons in the prefrontal cortex control affective state discrimination in mice. *Nat Neurosci*. 2020;23(1):47-60.
75. Smith C, Kingsbury, M., Dziabis, J., Hanamsagar, R., Malacon, K. Tran, J., Norris, A., Gulino, M. and Bilbo, S. Neonatal immune challenge induces female-specific changes in social behavior and somatostatin cell number, independent of microglial inflammatory signaling *bioRxiv*. 2020.
76. Kaech S, Banker G. Culturing hippocampal neurons. *Nature protocols*. 2006;1(5):2406-15.
77. Tyzio R, Ivanov A, Bernard C, Holmes GL, Ben-Ari Y, Khazipov R. Membrane potential of CA3 hippocampal pyramidal cells during postnatal development. *J Neurophysiol*. 2003;90(5):2964-72.
78. Scorcioni R, Polavaram S, Ascoli GA. L-Measure: a web-accessible tool for the analysis, comparison and search of digital reconstructions of neuronal morphologies. *Nature protocols*. 2008;3(5):866-76.

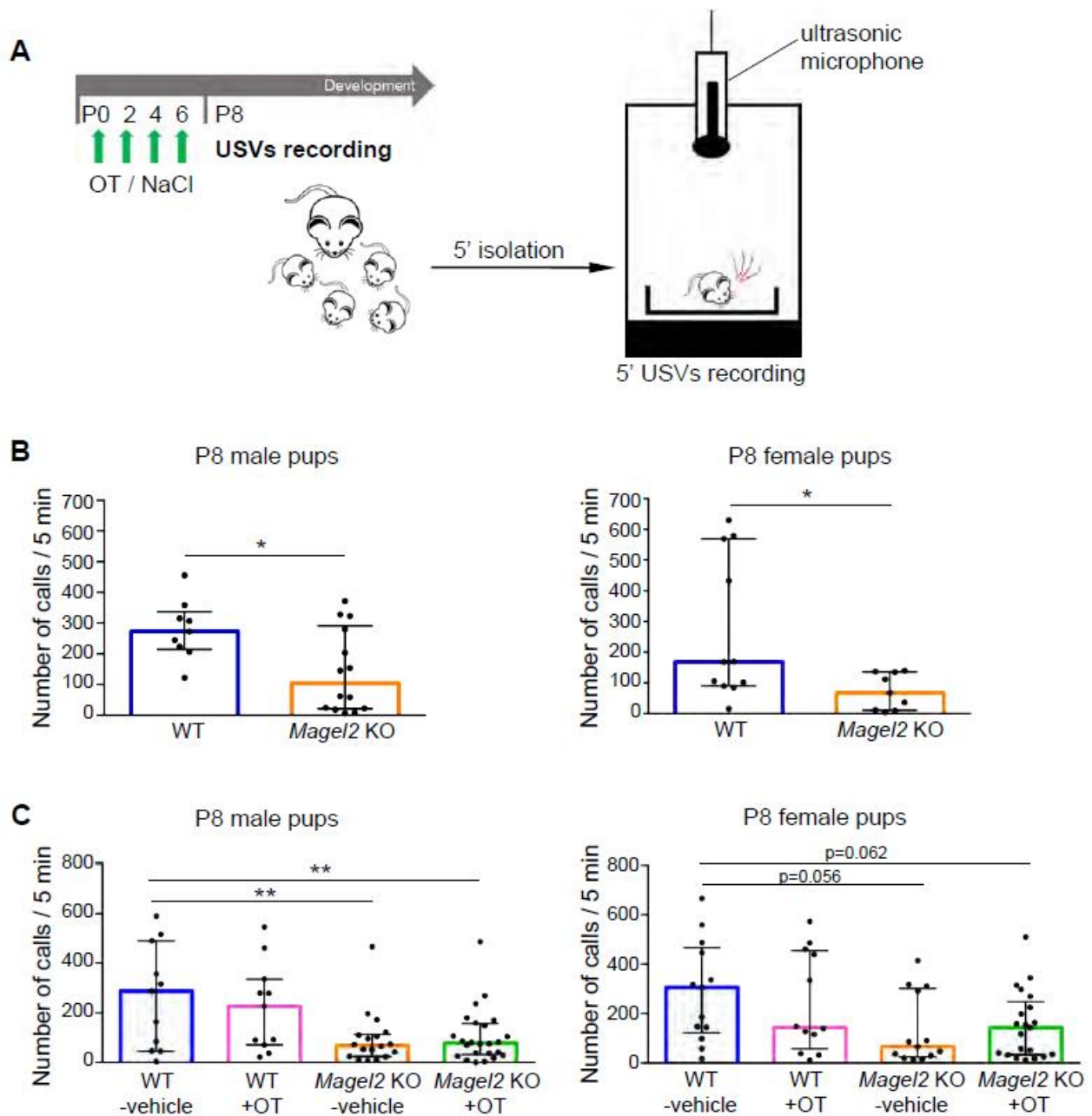
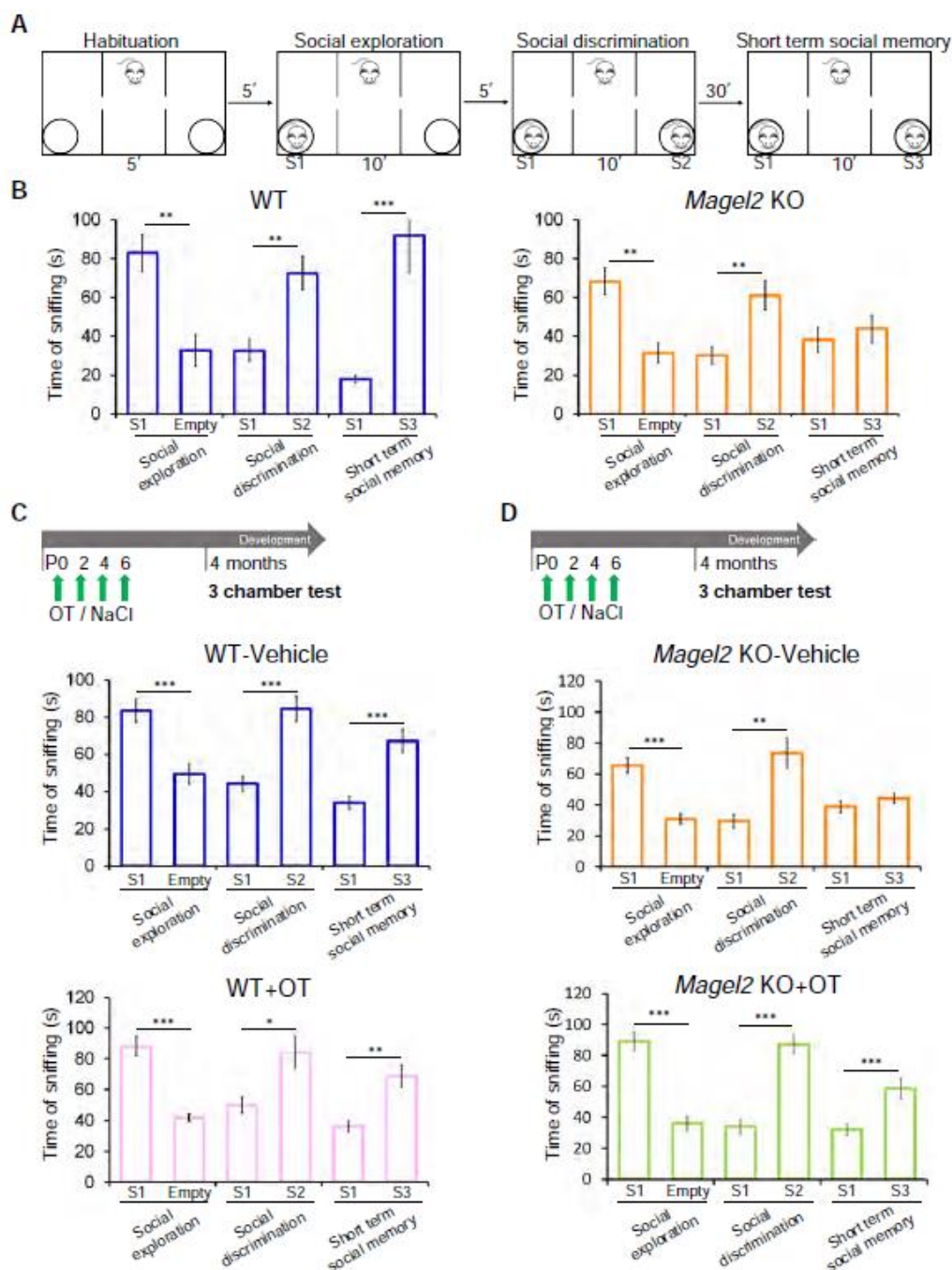


Figure 1: Ultrasonic vocalization calls (USVs) in male and female *Magel2* KO pups (P8) versus WT pups and having been OT-treated or vehicle-treated in neonates. (A) Paradigm of the USVs recordings. Number of total calls, measured during 5 min isolation after pup separation, is indicated in the histograms (B-D). (B) Comparison of the number of calls recorded in male ($N=14$) and female ($N=9$) *Magel2* KO and WT pups (males $N=9$; females $N=11$). (C) Effect of the OT-treatment in WT (males $N=11$; females $N=12$; in pink) and in *Magel2* KO pups (males $N=24$; females $N=21$; in green) versus vehicle-treated WT (males $N=11$; females $N=13$; in blue) and vehicle-treated *Magel2* KO (males $N=18$; females $N=13$; in orange). Histograms indicate the median (Q_2) and quartiles (Q_1, Q_3) with scattered plots that show individual data points. (B) Mann-Whitney test, (C) One-way ANOVA + Dunnett's post hoc test. * $P < 0.05$, ** $P < 0.01$. Statistical analysis is reported in Supplemental Table 1.



behavior in three-chamber test of male *Magel2* KO adult versus WT adults and having been OT-treated or vehicle-treated in neonates. Paradigm of the three-chamber test. Sniffing time between mice is measured in each test. (B) WT males ($N=9$) show normal behavior in all the steps of the test; *Magel2* KO males ($N=9$) show a significant impairment in short term social memory. (C) WT mice were treated in the first week of life with vehicle or OT and then tested at four months. WT mice treated with vehicle ($N=18$) or treated with OT ($N=10$) have similar profiles with significant differences in each step of the test. (D) *Magel2* KO mice were treated in the first week of life with vehicle or OT and then tested at four months. *Magel2* KO-vehicle ($N=19$) mice show a significant difference in the social exploration and social discrimination, but, in short term social memory, they do not show a higher sniffing time with the novel mouse. OT-treated *Magel2* KO ($N=19$) mice present significant differences in each step of the step. Data represented in histograms report the interaction time (time of sniffing in seconds) as mean \pm SEM. Mann-WhitneyTest. * $P<0.05$, ** $P<0.01$, *** $P<0.001$. Statistical analysis is reported in Supplemental Table 2.

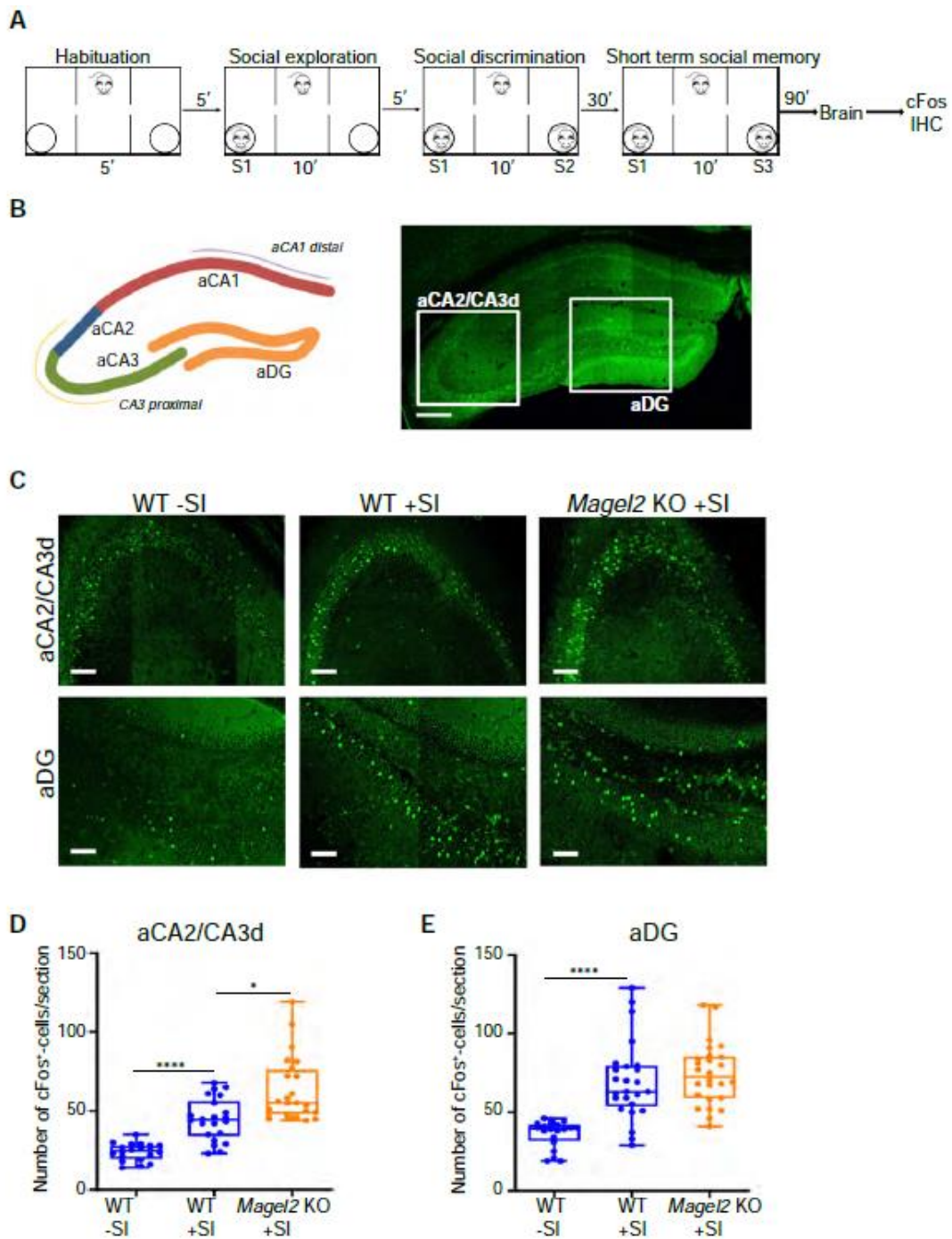


Figure 3: cFos activity in aCA2/CA3d and aDG regions of Magel2 KO and WT male mice following the social memory task in the three-chamber test. (A) Paradigm of the three-chamber test (+SI) followed 90 min later by dissection of the brains and immunohistochemistry experiments. Control mice (-SI) were not tested in the three-chamber test. (B-C) cFos-immunolabeling on coronal brain sections in the aCA2/CA3d and aDG regions as indicated in (B) of WT-SI, WT+SI and Magel2 KO+SI mice (C). (D-E) Quantification of cFos+ cells/section in WT-SI ($n=18$, $N=3$), WT+SI ($n=24$, $N=4$) and Magel2 KO+SI ($n=24$, $N=4$) in the aCA2/CA3d region (D) and in the aDG region (E). N : number of animals, n : number of sections/hippocampus. Scale bar: 500 μ m (B); 100 μ m (C). Data represented in box and whisker-plots report the number of cFos + cells by sections (6 sections/ hippocampus) with the median (Q_2) and quartiles (Q_1 , Q_3) for the genotype and treatment. One-way ANOVA + Dunnett's post hoc test, **** $P < 0.001$. Statistical analysis is reported in Supplemental Table 3.

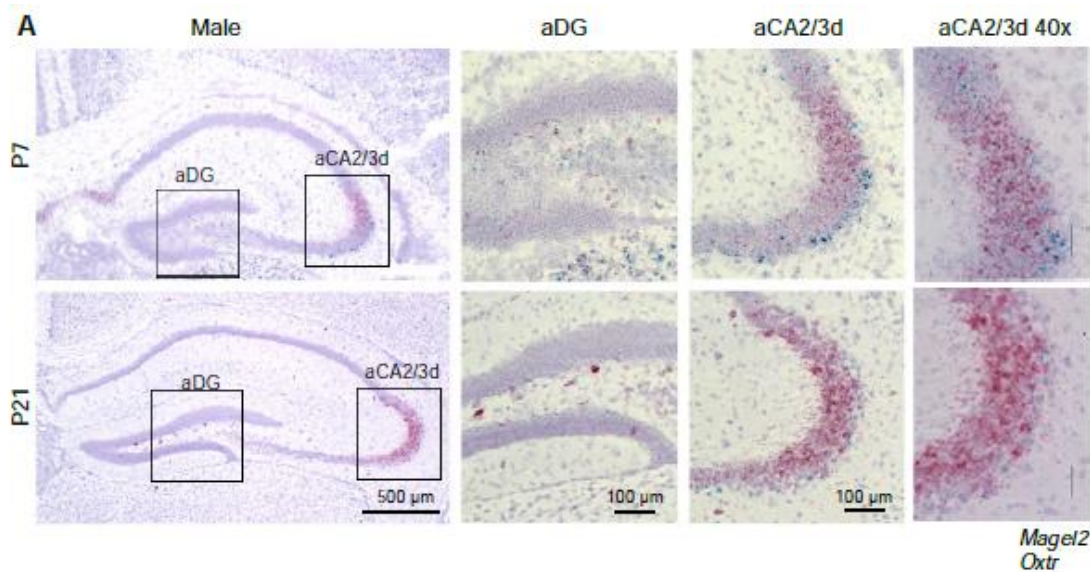
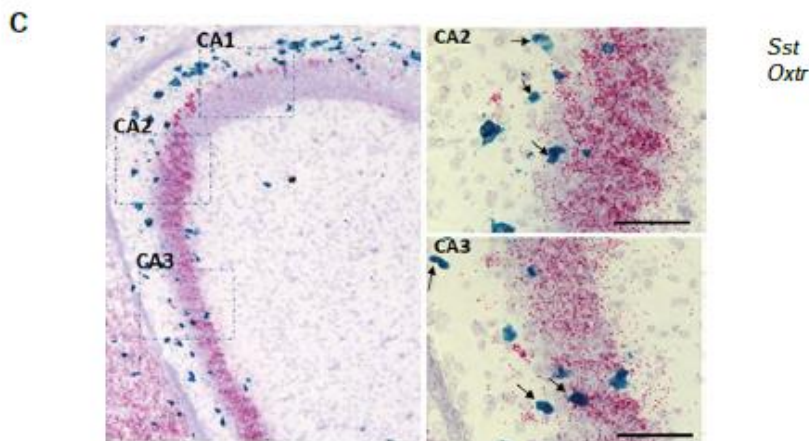
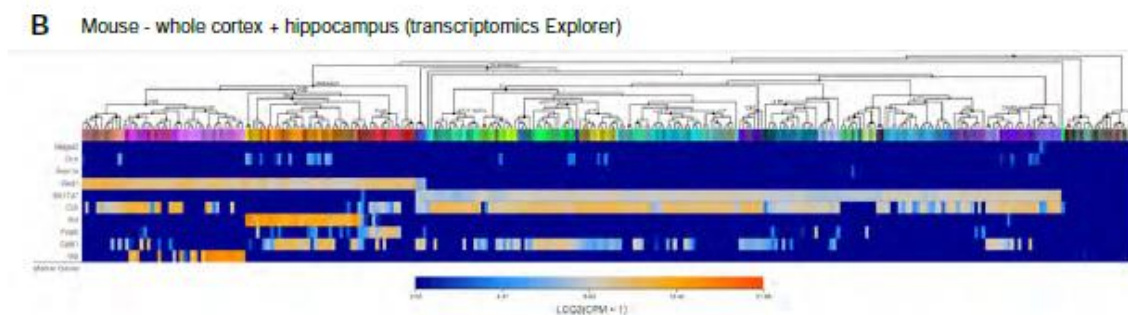


Figure 4:



Expression of *Magel2* and *Oxytocin receptor (Oxt)* transcripts in hippocampus of wild-type male mice at P7 and P21. (A) Representative image obtained by RNAscope technology showing the respective localization of *Magel2* (blue) and *Oxt* (pink) transcripts in dentate gyrus (DG) and aCA2/CA3d region of hippocampus. (B) Heatmap of mouse cortex and hippocampus transcriptomic data in Allen Cell types Database (2015 - Allen Institute) indicating the expression of *Magel2*, *Oxt*, *Avpr1a*, *Gad1*, *Slc17A7*, *Cck*, *Sst*, *Pvalb*, *Calb1* and *Vip* transcripts. *Magel2* and *Oxt* are expressed in glutamatergic (*Slc17A7*⁺) neurons of the CA3 region. *Oxt* transcripts are also present in GABAergic (*Gad1*⁺) interneurons expressing *Sst*, *Pvalb*, *Calb1*. (C) Representative image obtained by RNAscope technique showing the respective localization of *Sst* (blue) and *Oxt* (pink) transcripts in the aCA2/CA3 region from hippocampal slices of WT male pups at P10. Arrows indicate colocalization of both transcripts in the same cell. Scale bar: 100μm.

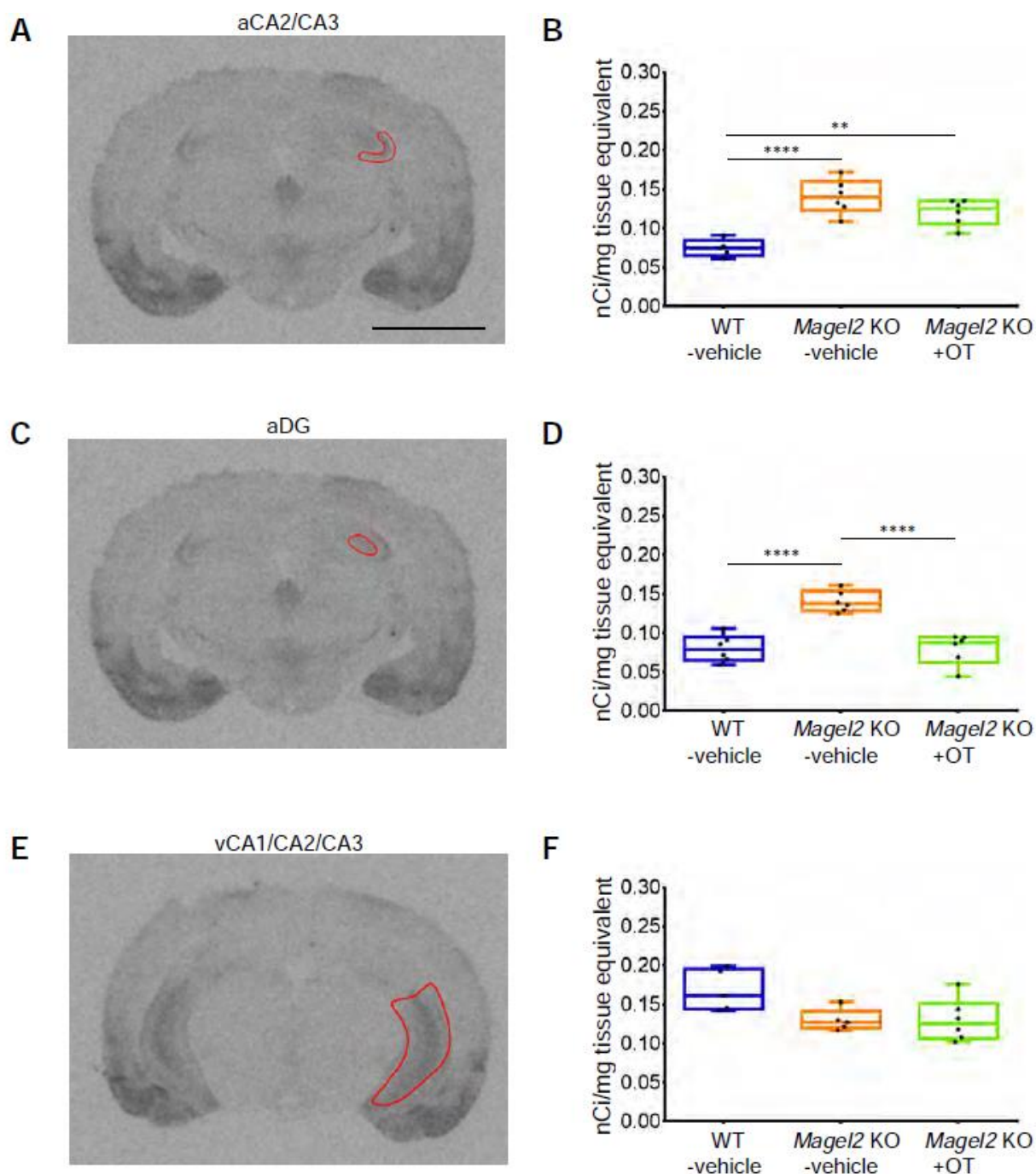


Figure 5: Quantification of OT binding sites by brain autoradiography in *Magel2* KO male mice treated with OT or vehicle versus WT-vehicle male mice. (A-C-E) Representative sections of autoradiographic labeling of OT binding sites displayed in grayscale, showing the regions of interest (ROI) selected for analysis: (A) anterior CA2/CA3 (aCA2/CA3), (C) dentate gyrus (aDG) and (E) ventral CA1/CA2/CA3 (vCA1/CA2/CA3) regions of hippocampus. (B-D-F) Quantification of OT binding sites expressed as nCi/mg of tissue equivalent in (B) anterior CA2/CA3, (D) dentate gyrus and (F) ventral CA1/CA2/CA3 regions of hippocampus. Histograms report median (Q2) and quartiles (Q1, Q3). OT binding sites in nCi/mg of tissue equivalent. 3 (N) mice and 6 (n) hippocampi have been analyzed for each group. Data represented in box and whisker-plots report the quantity of radiolabeling by hippocampus, with scattered plots that show individual data points. One-way ANOVA + Bonferroni post hoc test, ** $P < 0.01$, **** $P < 0.0001$. Scale Bar: 3 mm. Statistical analysis is reported in Table 5.

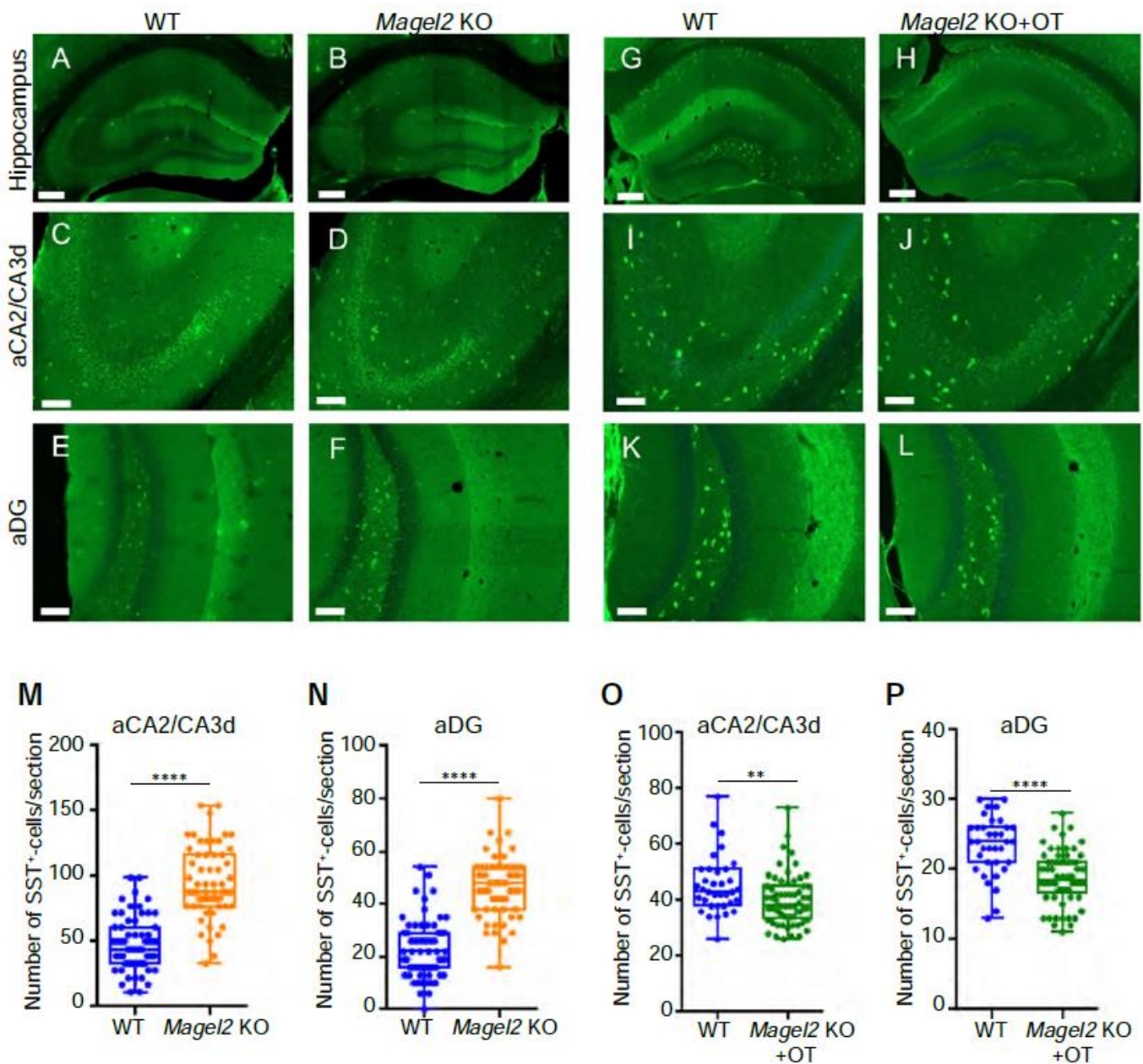


Figure 6: Quantification of somatostatin (SST) immunopositive cells in the anterior hippocampus region of Magel2 KO adult mice having or not been treated by OT in the first week of life and compared with WT mice. (A-L) Immunolabeling on coronal hippocampal sections at adulthood in WT (A,C,E) and Magel2 KO (B,D,F), and in WT (G,I,K) and Magel2 KO+OT (H,J,L) with a magnification in the aCA2/CA3d region (C,D,I,J) and in the DG region (E,F,K,L) in which the SST⁺ cells are counted. (M-P) Number of SST⁺ cells by section in both aCA2/CA3d (M,O) and aDG (N,P) and comparing WT (N=4, n= 48) with Magel2 KO (N=4, n=48) animals (M,N) or WT (N=3, n=36) with Magel2 OT+ (N=5, n=56) (O,P) mice. N: number of animals, n: number of sections/hippocampus. Data represented in whisker-plots report the number of SST⁺ cells by section with Q2(Q1, Q3), with scattered plots showing individual data points. Mann-Whitney Test **P<0.01, ***P<0.001. Scale bar (A-H): 500 μ m; (C-L): 100 μ m. Statistical analysis is reported in Table 6.

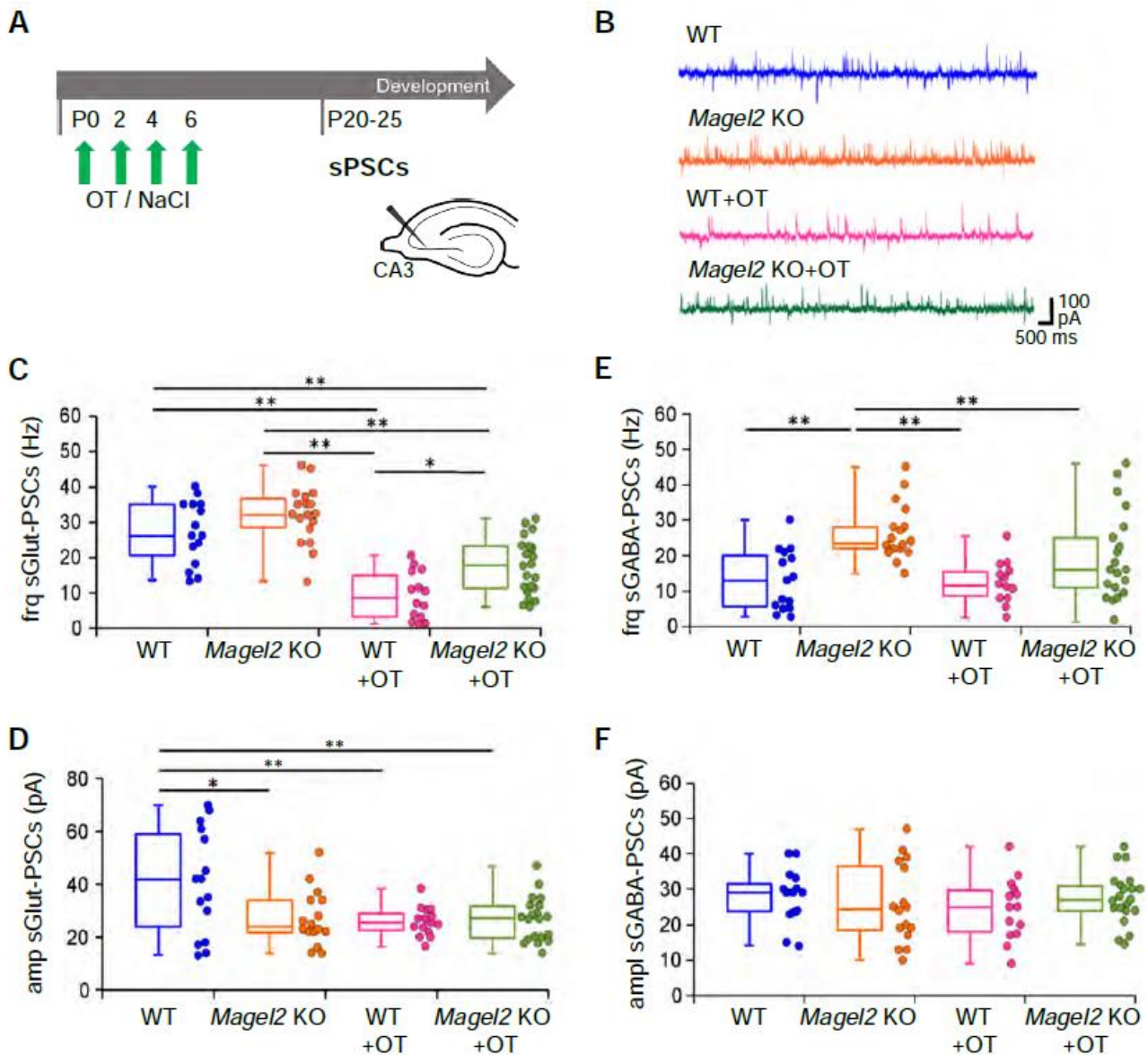


Figure 7: Spontaneous Glutamatergic and GABAergic synaptic activity of CA3 pyramidal neurons in the anterior hippocampus region of Magel2 KO mice versus WT juvenile mice and having been OT-treated or vehicle-treated in neonates. (A) Paradigm of the test. WT or Magel2 KO mice have been or not injected with OT in the first week of life then neurons are recorded in brain slices at P25. (B) Examples of whole cell recordings performed at a holding potential of -45 mV for each genotype or treatment. The glutamatergic synaptic currents are inwards and the GABAergic synaptic currents are outwards (C-D) Values in the different genotypes and treatment of the Glut-sPSCs frequency (C) and amplitude (D). (E-F) Values in the different genotypes and treatment of the GABA-sPSCs frequency (E) and amplitude (F). Magel2 KO ($N=7$, $n=16$), WT ($N=7$, $n=15$), Magel2 KO+OT, ($N=5$, $n=21$) and WT+OT ($N=4$, $n=15$) have been analyzed, with N : number of mice and n : number of recorded cells. Data represented in whisker-plots report the different values of recorded cells with mean \pm SEM, with scattered plots showing individual data points. One-way ANOVA + Tuckey post hoc test. $*P<0.05$, $**P<0.01$. Statistical analysis is reported in Supplemental Table 7.

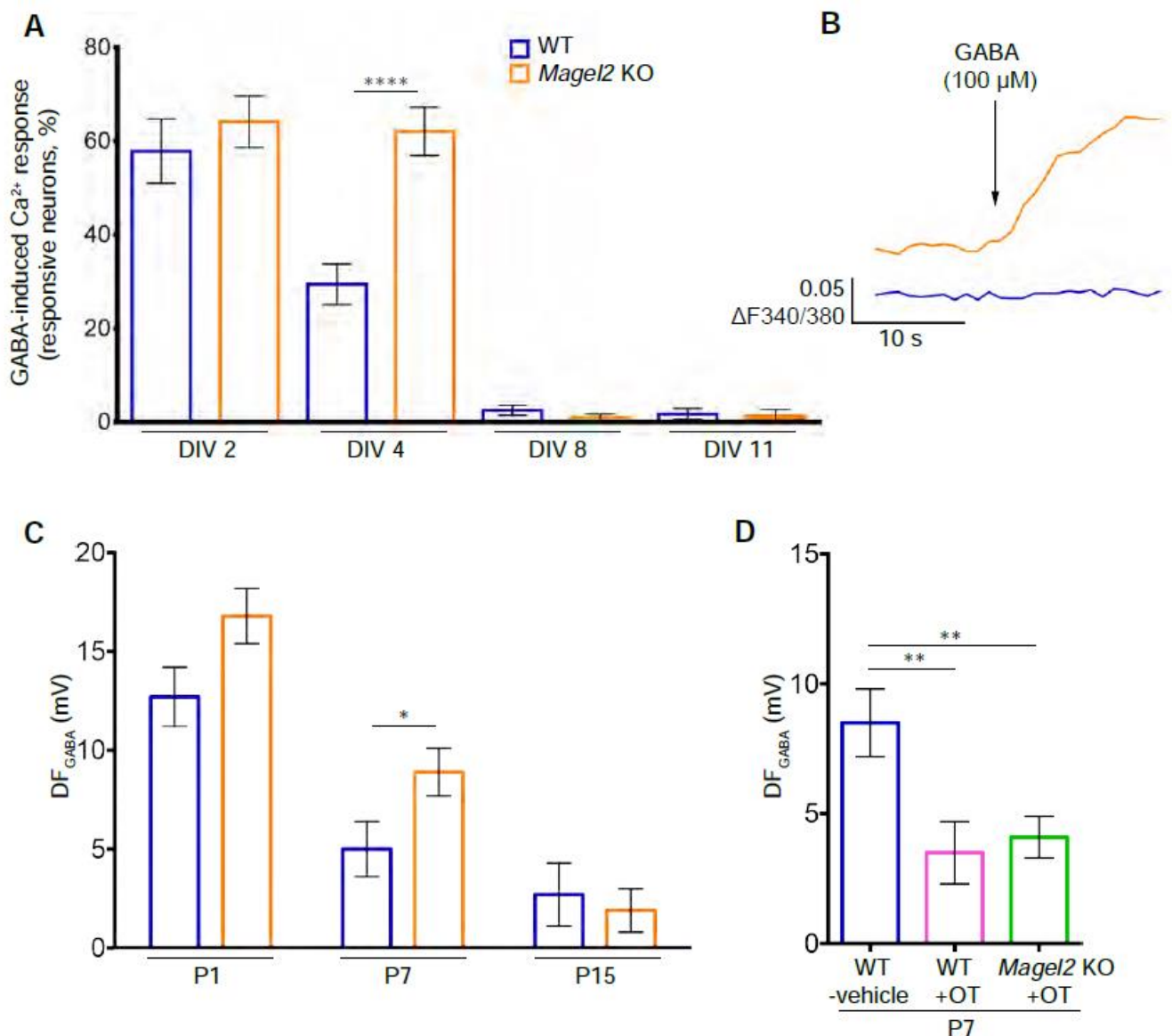


Figure 8. The excitatory-to-inhibitory developmental GABA-shift in *Magel2* KO versus WT hippocampi and the effect on an OT-treatment. (A-B) GABA-induced Ca^{2+} responses in *Magel2* KO developing hippocampal neuronal cultures versus WT. (A) Percentage of WT and *Magel2* KO E18 hippocampal neurons showing GABA-induced Ca^{2+} responses at selected in vitro days (DIV). (B) Representative traces of $[Ca^{2+}]_i$ variations ($\Delta F_{340/380}$) in DIV4 WT and *Magel2* KO neurons upon 100 μ M GABA administration. Data are presented in histograms with mean \pm SEM; unpaired *t* test with Welch's correction: **** $P < 0.0001$. (C-D) Average values of the driving force for GABA (DF_{GABA}) of aCA3 pyramidal neurons in *Magel2* KO versus WT mice (C) and, following an OT-treatment, with WT+OT and *Magel2* KO+OT compared with WT (D). (C) To reveal a delay of the GABA shift between *Magel2* KO versus WT mice, measures were performed at P1, P7 and P15 using cell-attached recordings of single GABA_A channels. Data are presented in histograms with mean \pm SEM; unpaired *t* test with Welch's correction: * $P < 0.05$. (D) To assess the effect of an OT-treatment on the GABA-shift delay, measures were performed at P7. N: number of mice and n: number of recorded cells. One-way ANOVA + Dunnett's post hoc test: ** $P < 0.01$. Statistical analysis is reported in Supplemental Table 8.

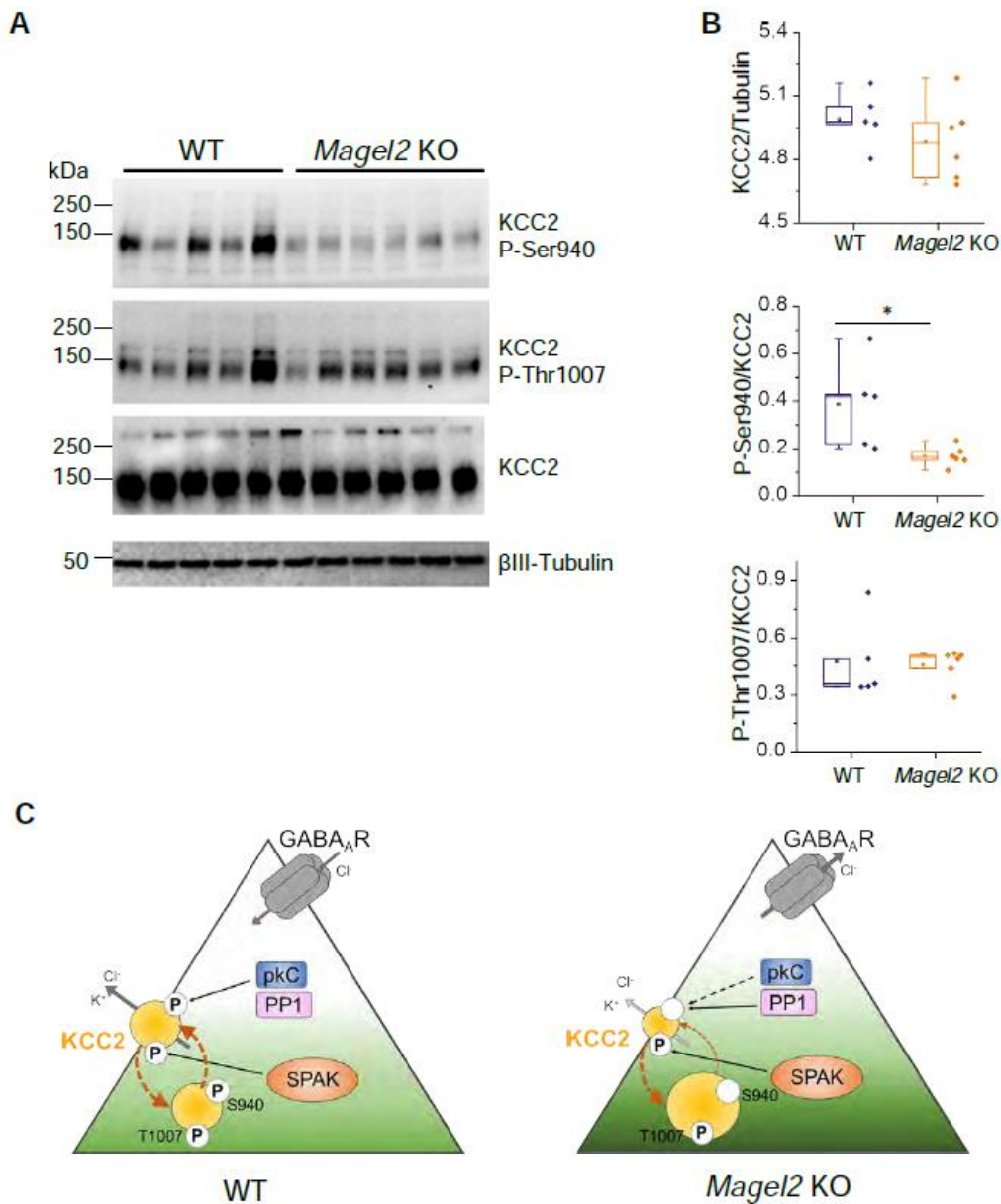


Figure 9. Abundance and phosphorylation state of KCC2 in WT and *Magel2* KO pups (P7). (A) Immunoblot analysis of WT (N=5) and *Magel2* KO (N=6) hippocampi of P7 mice with pan-KCC2 antibody or phosphorylation site-specific antibodies recognizing P-Ser940 or P-Thr1007 of KCC2. An antibody recognizing neuron-specific β 3 tubulin was used to normalize the quantity of proteins. Numbers on the left indicate molecular weight. (B) Boxplots report band intensities from (A) as $Q2(Q1, Q3)$, with scattered plot showing individual data points. Mann-Whitney test, $*P < 0.05$. (C) A model of KCC2-dependent control of neuronal Cl⁻ in *Magel2* KO pups. At this stage of neuronal development, the surface expression of KCC2, that determines its ion-transport activity, depends on the ratio of reciprocal phosphorylation of its Ser940 and Thr1007 residues. The Ser940 phosphorylation increases KCC2's cell surface stability, whereas the Thr1007 phosphorylation exerts opposite to Ser940 effect and favors internalization (shown with brown arrows). Compared to WT, the CA3 neurons in hippocampi from *Magel2* KO mice are characterized by depolarizing action of GABA (e.g. activation of GABA generates Cl⁻ efflux) that reflects higher [Cl⁻]_i. In *Magel2* KO hippocampi the amount of KCC2's Ser940 phosphorylation is significantly lower as compared to WT hippocampi whereas the amount of phosphorylated Thr1007 remains unchanged. Respectively, the decreased P-Ser940/P-Thr1007 ratio results in predominance of KCC2 internalization over surface expression. As consequence of the decreased amount of surface expressed molecules, the Cl⁻ extrusion ability of KCC2 is

decreased that causes increase of [Cl⁻]_i and depolarizing shift of GABA. The model includes also important components that are known to control the level of Ser940 and Thr1007 phosphorylation. The Ser940 is directly phosphorylated by kinase C (pkC) and dephosphorylated under pathology conditions by protein phosphatase type 1 (PP1). The Thr1007 is directly phosphorylated by SPAK. It remains to be elucidated whether in Magel2 KO mice the decreased level of Ser940 results from reduction of pkC activity or enhancement of PP1 action. Statistical analysis is reported in Supplemental Table 9.

8. GENERAL DISCUSSION AND CONCLUSIONS

My PhD project has been completely focused on the detection, the detailed mapping and the functional investigation of the oxytocin receptor in the mouse brain. In particular, my aim was to selectively target the homodimeric component of this receptor population, in order to see in which brain areas are they usually distributed, and how many they are compared to monomeric OTRs.

The importance of dimeric GPCRs in the development of new therapies resides in their peculiar signaling, trafficking and desensitization properties, that actually make them a pharmacological entity on their own. Knowing where they are expressed and to which degree would allow us to “tailor” the therapeutic approach only in selected brain areas, in order to avoid any possible adverse, non-wanted secondary effect mediated by monomeric receptors.

To gain a better insight of the localization of dimeric OTRs in the CNS, I started to develop a technique that would allow dimers detection, and in parallel I employed a universally accepted technique to map the receptor in all its forms in mouse brain. Moreover, I worked to find new tools to characterize the homodimeric OTR population also from a functional point of view.

New insights into OTR homodimers functionality

First, I completed the pharmacological characterization of a series of bivalent ligands specifically designed by our research group to target OTR homodimers. Two of them (dOTK₂-C8 and dOTK₂-C10) were already known to behave as superagonists towards the homodimeric portion of OTRs: they can activate a Gq-mediated pathway at a concentration 1000 lower than that required for their monomeric counterpart (Busnelli et al, 2016).

The data obtained from this work allowed us not only to have a more detailed view of their functionality, but also to collect novel information about the signaling properties of OTR homodimers. We established that compared to the monomeric dOTK, all the bivalent ligands we developed are functional selective for the OTR, because differently from endogenous OT they could only activate Gq, Gi2 and Gi3-mediated signaling pathways. More interestingly, the fact that all the obtained dose-response curves were monophasic made us hypothesize that OTR homodimers might not be able to couple to Gi2 and Gi3, while a fraction of them is actually coupled to Gq. From previous studies, we already knew that this fraction corresponded to approximately the 30% of the total OTR receptors present in the cell (Busnelli, Mauri et al. 2013); however, its signaling properties were still unknown. We also observed a peculiar β -arrestin recruiting profile of the bivalents, intermediate between that of oxytocin and that of the dOTK monomer. In particular, we hypothesized that the efficiency gain over dOTK (which is especially visible for dOTK₂-C8 and dOTK₂-C10) might be due to the fact that OTR homodimers have a facilitated interaction with β -arrestin, and therefore might be internalized more than monomers.

In the context of my PhD project, these information will be as useful as those obtained through the mapping techniques I used to localize OTRs. In fact, while the Nanoruler system and the autoradiography studies will provide a detailed map of OTR monomers and homodimers in the brain, further studies conducted through these bivalent ligands will allow a “functional isolation” of the homodimeric population, and in some cases even a pharmacological dissection of its signaling mechanisms. Both these aspects are fundamental for translational studies in neurodevelopmental disorders, and both must be taken into account in the design of new therapeutic molecules.

Strengths and limitations of the Nanoruler system

Other than the functional features of dimeric OTRs, understanding where this population is expressed in the brain, and on which areas it works to mediate its effects, is equally fundamental for the development of safer and more targeted therapies.

OTR dimers are already known to be present in endogenous tissues; however, their peculiar pharmacological properties, together with their exact localization in the brain, are still widely unknown. The main reason for this is because all the techniques currently used to study receptor oligomers in native tissues require antibodies, and therefore they are not suitable to be applied on OTRs. Because of their resolution these techniques can only prove molecular proximity, but not actual dimerization.

For most of my PhD project I worked with Prof. Tommaso Bellini’s group (Complex Fluids and Molecular biophysics Laboratory, University of Milan) to develop a DNA-based, antibody-free approach to map OTR homodimeric structures in the rodent brain. We started to develop a DNA “Nanoruler” technology which is based on an OT analog tagged with two complementary DNA hairpins, Pan and Dis. These two hairpins have been designed in order to open and hybridize only if two conditions occur at the same time: they must be closer than 6 nm, and a third oligonucleotidic sequence, called Trigger, must be present in solution. The newly formed Pan-Dis-Trigger would function as a “primer” for a Hybridization Chain Reaction step, that is needed to amplify the signal; the implementation of fluorescent probes called H1 and H2 would make the DNA product resulting from this amplification step visible as a light spot in confocal microscopy. Although quite similar in concept to Proximity Ligation Assay, our system would allow a much higher resolution, because our DNA hairpins would be linked to a single 1 kDa molecule, and not to a 100 kDa antibody. Therefore, the steric hindrance between Pan and Dis would be much lower, and they could interact only if they were at a real distance of 6 nm. On the contrary, using bulky molecules as antibodies could bring the two DNA strands in close proximity even when the real distance between two receptors is wider than 16 nm (the actual resolution for PLA is calculated around 200 nm), generating a false positive result. Moreover, once optimized our technique would require less steps than PLA, granting a lower risk of aspecific signal generation.

The Nanoruler system has been conceived in response to an increasing need of high resolution, high sensitivity detection techniques. In this context, the more interesting results are obtained through techniques that employ fluorescence microscopy. However, often the photostability of the fluorophores used, together with the high

background noise of the fluorescent signal, make these techniques not suitable to detect small quantities of target molecules; this is especially true for studies *in vivo*, but it applies to *in vitro* systems too. Many attempts have been made to overcome these issues: most of them aim to reduce the background noise through the use of gold nanoparticles (AuNPs), that have excellent fluorescence quenching abilities (Swierczewska et al, 2011), or modify FRET protocols in order to obtain a sub-nanometer resolution (Son et al, 2020). An interesting biosensor developed by Wang and colleagues allows to detect down to 10 fM of DNA using two probes linked to a PolyA strand anchored to a gold surface (Wang et al, 2019). Even if the technique they developed has a slightly different aim compared to the Nanoruler, taking advantage of the PolyA strand, that has a defined nucleotidic length and is strongly anchored to the gold electrode, could allow us to test the effective resolution of our system. In fact, we still don't know what happens if Pan and Dis are more than 6 nm apart, because with our *in vitro* tests the distance between the hairpins couldn't be controlled. In this sense it could also be useful to exploit the so-called DNA "Origami" structures, that have already been successfully used to measure distances between molecular structures (Bian et al, 2019).

Through this set of experiments we've had the chance to better understand both strengths and limitations of our set of sequences. PAGE gels allowed us to confirm that, at least *in vitro*, our system is highly specific; instability of the H2 probe was corrected, and a cellular staining protocol is under preparation.

A point that still needs to be addressed is the complexity of the binding kinetics of DNA-tagged ligands.

The superagonism of the two dialyzed DNA-tagged compounds in experiments carried on with the addition of NaCl could be due to a positive cooperativity phenomenon, mediated by the presence of the DNA itself. Our current hypothesis is that some unexpected interaction between our DNA strands, mediated by their charges or by their steric hindrance, might produce an increase in the binding abilities of two OT analogues inside dimeric OTRs. We could observe a similar phenomenon in the binding curves of two of the bivalent ligands we previously characterized, where the docking of the first pharmacophore of the bivalent molecule would constrain the second one in a very reduced volume, increasing *de facto* its local concentration and drastically reducing the entropy cost for the binding of the second pharmacophore (Busnelli et al, 2016).

If confirmed, this peculiar behaviour could represent an advantage for the next set of experiments, because it would allow us to work a very low concentrations and avoid any aspecific result given by binding to other receptors (i.e., V1aR). However, more experiments will be needed to understand why NaCl addition to the binding buffer causes such a dramatic modification of the binding curve.

New insights into sexually dimorphic features of the oxytocinergic system

In parallel with the development of the Nanoruler system, I also conducted an extensive autoradiographic mapping of the murine brain, in physiologic and pathologic environments. As we only have a rough idea of the results the Nanoruler technique will provide, data obtained with autoradiographic studies will be fundamental to critically evaluate those obtained with the new approach, in terms of sensitivity and resolution. Interestingly, this analysis revealed a marked sexual dimorphism in how the oxytocinergic system is distributed

and in how it reacts to OT treatments. Concerning OTR levels, WT females showed to have two times more OTR than males in almost every analyzed area. More interestingly, the absence of a functional *Magel2* in KO animals had opposite effects on males and females, resulting in a “flattening” of the differences in OTR levels observed in WT animals. This opposite effect is clearly visible also in OT-treated mice: while in males OT is often able to restore physiologic OTR quantities, in females the treatment couldn't modify in any way receptor levels. This raises many interesting questions about which might be the regulation mechanisms that works so differently in males and females. It is also important to notice that all the latest studies over neurodevelopmental disorders are conducted almost exclusively on male animals. However, our results point out the importance of including females in these works, because results obtained from observations made in males only might not be applicable to both sexes.

The autoradiographic quantification of OTR in the hippocampus and dentate gyrus of male mice has also already provided interesting information about the correlation between OTR variations in the brain and the long-term behavioural outcomes of a neonatal, subchronic OT treatment at birth. Although the molecular mechanisms through which the absence of *Magel2* affects OTR distribution in the CNS, these results alone provide useful information for the development of safer and targeted therapies.

Conclusions and future directions

This work has already provided many new important information about the dynamics of OTR distribution in mouse brain, and has paved the way for the development of new, high-resolution tools for the detection of OTR monomeric and dimeric population in native tissues. The next steps will include the finalization of the Nanoruler system project, that now requires to test the whole system in cell cultures and brain slices. Once ready to be applied on brain slices, the results provided by this innovative technique will be compared with the extensive autoradiographic analysis we have already performed on mouse brain slices, to see how the monomeric and dimeric population behave in different physiologic and pathologic situations. We also plan to implement the Nanoruler protocol with fluorescent ligands staining, in order to distinguish monomers from dimers even in confocal microscopy. Lastly, to gain a better insight into the mechanism through which the OT treatment at birth is able to produce long term effects on behavioural phenotypes, we are in the process of including PN7 mice pups in our autoradiographic panel.

9. BIBLIOGRAPHY (GENERAL)

Aaron J. Towers et al (2018), Epigenetic dysregulation of Oxt in Tet1-deficient mice has implications for neuropsychiatric disorders, *JCI Insight*. 2018;3(23):e120592.

AbdAlla S, Lothar H, el Missiry A, Langer A, Sergeev P, el Faramawy Y, Quitterer U. Angiotensin II AT2 receptor oligomers mediate G-protein dysfunction in an animal model of Alzheimer disease. *J Biol Chem*. 2009 Mar 6;284(10):6554-65. doi: 10.1074/jbc.M807746200. Epub 2008 Dec 11. PMID: 19074441.

Adan RA, Cox JJ, van Kats JP, Burbach JP. Thyroid hormone regulates the oxytocin gene. *J Biol Chem*. 1992 Feb 25;267(6):3771-7. PMID: 1371278.

Adan RA, Cox JJ, Beischlag TV, Burbach JP. A composite hormone response element mediates the transactivation of the rat oxytocin gene by different classes of nuclear hormone receptors. *Mol Endocrinol*. 1993 Jan;7(1):47-57. doi: 10.1210/mend.7.1.8383287. PMID: 8383287.

Albizu L, Cottet M, KralikovaMet al (2010), Time-resolved FRET between GPCR ligands reveals oligomers in native tissues. *Nat Chem Biol* 6(8):587–594.

Alonso-Gonzalez A, Rodriguez-Fontenla C, Carracedo A. De novo Mutations (DNMs) in Autism Spectrum Disorder (ASD): Pathway and Network Analysis. *Front Genet*. 2018 Sep 21;9:406. doi: 10.3389/fgene.2018.00406. PMID: 30298087; PMCID: PMC6160549.

Ang YS, Yung LY. Rational design of hybridization chain reaction monomers for robust signal amplification. *Chem Commun (Camb)*. 2016 Mar 18;52(22):4219-22. doi: 10.1039/c5cc08907g. PMID: 26912178.

Antoni FA, Chadio SE (1989), Essential role of magnesium in oxytocin-receptor affinity and ligand specificity. *Biochem J* 257:611-614.

Ates T, Oncul M, Dilsiz P, Topcu IC, Civas CC, Alp MI, Aklan I, Ates Oz E, Yavuz Y, Yilmaz B, Sayar Atasoy N, Atasoy D. Inactivation of Magel2 suppresses oxytocin neurons through synaptic excitation-inhibition imbalance. *Neurobiol Dis*. 2019 Jan;121:58-64. doi: 10.1016/j.nbd.2018.09.017. Epub 2018 Sep 19. PMID: 30240706.

Axelsson JF, Leeuwen FW. Differential localization of estrogen receptors in various vasopressin synthesizing nuclei of the rat brain. *J Neuroendocrinol*. 1990 Apr 1;2(2):209-16. doi: 10.1111/j.1365-2826.1990.tb00852.x. PMID: 19210385.

Baio J, Wiggins L, Christensen DL, Maenner MJ, Daniels J, Warren Z, Kurzius-Spencer M, Zahorodny W, Robinson Rosenberg C, White T, Durkin MS, Imm P, Nikolaou L, Yeargin-Allsopp M, Lee LC, Harrington R, Lopez M, Fitzgerald RT, Hewitt A, Pettygrove S, Constantino JN, Vehorn A, Shenouda J, Hall-Lande J, Van Naarden Braun K, Dowling NF. Prevalence of Autism Spectrum Disorder Among Children Aged 8 Years - Autism and Developmental Disabilities Monitoring Network, 11 Sites, United States, 2014. *MMWR Surveill Summ*. 2018 Apr 27;67(6):1-23. doi: 10.15585/mmwr.ss6706a1. Erratum in: *MMWR Morb Mortal Wkly Rep*. 2018 May 18;67(19):564. Erratum in: *MMWR Morb Mortal Wkly Rep*. 2018 Nov 16;67(45):1280. Corrected and republished in: *MMWR Morb Mortal Wkly Rep*. 2018 Nov 16;67(45):1279. PMID: 29701730; PMCID: PMC5919599.

Bandy TJ, Brewer A, Burns JR, Marth G, Nguyen T, Stulz E. DNA as supramolecular scaffold for functional molecules: progress in DNA nanotechnology. *Chem Soc Rev*. 2011 Jan;40(1):138-48. doi: 10.1039/b820255a. Epub 2010 Aug 9. PMID: 20694258.

- Barberis C, Mouillac B, Durroux T. Structural bases of vasopressin/oxytocin receptor function. *J Endocrinol.* 1998 Feb;156(2):223-9. doi: 10.1677/joe.0.1560223. PMID: 9518866.
- Bennett JA, Germani T, Haqq AM, Zwaigenbaum L. Autism spectrum disorder in Prader-Willi syndrome: A systematic review. *Am J Med Genet A.* 2015 Dec;167A(12):2936-44. doi: 10.1002/ajmg.a.37286. Epub 2015 Aug 29. PMID: 26331980.
- Bian X, Zhang Z, Xiong Q, De Camilli P, Lin C. A programmable DNA-origami platform for studying lipid transfer between bilayers. *Nat Chem Biol.* 2019 Aug;15(8):830-837. doi: 10.1038/s41589-019-0325-3. Epub 2019 Jul 18. PMID: 31320758; PMCID: PMC6650167.
- Bischof JM, Van Der Ploeg LH, Colmers WF, Wevrick R. Magel2-null mice are hyper-responsive to setmelanotide, a melanocortin 4 receptor agonist. *Br J Pharmacol.* 2016 Sep;173(17):2614-21. doi: 10.1111/bph.13540. Epub 2016 Jul 27. PMID: 27339818; PMCID: PMC4978157.
- Black M, Schuler M, Nair P. Prenatal drug exposure: neurodevelopmental outcome and parenting environment. *J Pediatr Psychol.* 1993 Oct;18(5):605-20. doi: 10.1093/jpepsy/18.5.605. PMID: 7507525; PMCID: PMC3139096.
- Blume A, Bosch OJ, Miklos S, Torner L, Wales L, Waldherr M, Neumann ID. Oxytocin reduces anxiety via ERK1/2 activation: local effect within the rat hypothalamic paraventricular nucleus. *Eur J Neurosci.* 2008 Apr;27(8):1947-56. doi: 10.1111/j.1460-9568.2008.06184.x. PMID: 18412615.
- Blundell J, Tabuchi K, Bolliger MF, Blaiss CA, Brose N, Liu X, Südhof TC, Powell CM. Increased anxiety-like behavior in mice lacking the inhibitory synapse cell adhesion molecule neuroligin 2. *Genes Brain Behav.* 2009 Feb;8(1):114-26. doi: 10.1111/j.1601-183X.2008.00455.x. Epub 2008 Nov 11. PMID: 19016888; PMCID: PMC2648807.
- Bosch OJ, Young LJ. Oxytocin and Social Relationships: From Attachment to Bond Disruption. *Curr Top Behav Neurosci.* 2018;35:97-117. doi: 10.1007/7854_2017_10. PMID: 28812266; PMCID: PMC5815947.
- Boog G. Obstetrical complications and subsequent schizophrenia in adolescent and young adult offsprings: is there a relationship? *Eur J Obstet Gynecol Reprod Biol.* 2004 Jun 15;114(2):130-6. doi: 10.1016/j.ejogrb.2003.09.041. PMID: 15140504.
- Borroto-Escuela DO, Romero-Fernandez W, Garriga P, Ciruela F, Narvaez M, Tarakanov AO, Palkovits M, Agnati LF, Fuxe K (2013), G protein-coupled receptor heterodimerization in the brain. *Methods Enzymol* 521:281-294.
- Braunschweig D, Ashwood P, Krakowiak P, Hertz-Picciotto I, Hansen R, Croen LA, Pessah IN, Van de Water J. Autism: maternally derived antibodies specific for fetal brain proteins. *Neurotoxicology.* 2008 Mar;29(2):226-31. doi: 10.1016/j.neuro.2007.10.010. Epub 2007 Nov 6. PMID: 18078998; PMCID: PMC2305723.
- Brownstein, M. J., Russell, J. T., & Gainer, H. (1980). Synthesis, transport, and release of posterior pituitary hormones. *Science.* 207, 373–378 <https://doi.org/10.1126/science.6153132>
- Buijs RM. Intra- and extrahypothalamic vasopressin and oxytocin pathways in the rat. Pathways to the limbic system, medulla oblongata and spinal cord. *Cell Tissue Res.* 1978 Sep 26;192(3):423-35. doi: 10.1007/BF00212323. PMID: 699026.

Buijs RM, De Vries GJ, Van Leeuwen FW, Swaab DF. Vasopressin and oxytocin: distribution and putative functions in the brain. *Prog Brain Res.* 1983;60:115-22. doi: 10.1016/S0079-6123(08)64379-4. PMID: 6665132.

Bundy, D. C. (2001). Autoradiography. *Current Protocols in Protein Science.* 10 (11), 1-6 <https://doi.org/10.1002/0471140864.ps1011s10>

Busnelli M, Chini B. Molecular Basis of Oxytocin Receptor Signalling in the Brain: What We Know and What We Need to Know. *Curr Top Behav Neurosci.* 2018;35:3-29. doi: 10.1007/7854_2017_6. PMID: 28812263.

Busnelli M, Mauri M, Parenti M et al (2013), Analysis of GPCR dimerization using acceptor photobleaching resonance energy transfer techniques. *Methods Enzymol* 521:311–327.

Busnelli M, Sauliere A, Manning M et al (2012), Functional selective oxytocin-derived agonists discriminate between individual G protein family subtypes. *J Biol Chem* 287(6):3617–3629.

Busnelli M, Kleinau G, Muttenthaler M, Stoev S, Manning M, Bibic L, Howell LA, McCormick PJ, Di Lascio S, Braida D, Sala M, Rovati GE, Bellini T, Chini B. Design and Characterization of Superpotent Bivalent Ligands Targeting Oxytocin Receptor Dimers via a Channel-Like Structure. *J Med Chem.* 2016 Aug 11;59(15):7152-66. doi: 10.1021/acs.jmedchem.6b00564. Epub 2016 Jul 28. PMID: 27420737.

Calebiro D, Rieken F, Wagner J, Sungkaworn T, Zabel U, Borzi A, Cocucci E, Zürn A, Lohse MJ. Single-molecule analysis of fluorescently labeled G-protein-coupled receptors reveals complexes with distinct dynamics and organization. *Proc Natl Acad Sci U S A.* 2013 Jan 8;110(2):743-8. doi: 10.1073/pnas.1205798110. Epub 2012 Dec 24. PMID: 23267088; PMCID: PMC3545784.

Cardoso AR, Lopes-Marques M, Silva RM, Serrano C, Amorim A, Prata MJ, Azevedo L. Essential genetic findings in neurodevelopmental disorders. *Hum Genomics.* 2019 Jul 9;13(1):31. doi: 10.1186/s40246-019-0216-4. PMID: 31288856; PMCID: PMC6617629.

Casanova EL, Gerstner Z, Sharp JL, Casanova MF, Feltus FA. Widespread Genotype-Phenotype Correlations in Intellectual Disability. *Front Psychiatry.* 2018 Oct 29;9:535. doi: 10.3389/fpsy.2018.00535. PMID: 30420816; PMCID: PMC6217001.

Cassidy SB, Schwartz S, Miller JL, Driscoll DJ. Prader-Willi syndrome. *Genet Med.* 2012 Jan;14(1):10-26. doi: 10.1038/gim.0b013e31822bead0. Epub 2011 Sep 26. PMID: 22237428.

Champagne FA, Curley JP, Swaney WT, Hasen NS, Keverne EB. (2009). Paternal influence on female behavior: the role of Peg3 in exploration, olfaction, and neuroendocrine regulation of maternal behavior of female mice. *Behav Neurosci* 123:469-80

Chahrour M, Jung SY, Shaw C, Zhou X, Wong ST, Qin J, Zoghbi HY. MeCP2, a key contributor to neurological disease, activates and represses transcription. *Science.* 2008 May 30;320(5880):1224-9. doi: 10.1126/science.1153252. PMID: 18511691; PMCID: PMC2443785.

Charman T, Young GS, Brian J, Carter A, Carver LJ, Chawarska K, Curtin S, Dobkins K, Elsabbagh M, Georgiades S, Hertz-Picciotto I, Hutman T, Iverson JM, Jones EJ, Landa R, Macari S, Messinger DS, Nelson CA, Ozonoff S, Saulnier C, Stone WL, Tager-Flusberg H, Webb SJ, Yirmiya N, Zwaigenbaum L. Non-ASD outcomes at 36 months in siblings at familial risk for autism spectrum disorder (ASD): A baby siblings research consortium (BSRC) study. *Autism Res.* 2017 Jan;10(1):169-178. doi: 10.1002/aur.1669. Epub 2016 Jul 15. PMID: 27417857; PMCID: PMC5993543.

Chaviaras S, Mak P, Ralph D et al (2010), Assessing the antidepressant-like effects of carbetocin, an oxytocin agonist, using a modification of the forced swimming test. *Psychopharmacology (Berl)* 210(1):35–43.

Chini B, Mouillac B, Ala Y, Balestre MN, Cotte N, Trumpp-Kallmeyer S, Hoflack J, Elands J, Hibert M, Manning M, et al (1995), Molecular basis for agonist selectivity in the vasopressin/oxytocin receptor family. *Adv Exp Med Biol* 395:321-328.

Chini B, Mouillac B, Balestre MN, Trumpp-Kallmeyer S, Hoflack J, Hibert M, Andriolo M, Pupier S, Jard S, Barberis C. Two aromatic residues regulate the response of the human oxytocin receptor to the partial agonist arginine vasopressin. *FEBS Lett.* 1996 Nov 18;397(2-3):201-6. doi: 10.1016/s0014-5793(96)01135-0. PMID: 8955347.

Christensen DL, Braun KVN, Baio J, Bilder D, Charles J, Constantino JN, Daniels J, Durkin MS, Fitzgerald RT, Kurzius-Spencer M, Lee LC, Pettygrove S, Robinson C, Schulz E, Wells C, Wingate MS, Zahorodny W, Yeargin-Allsopp M. Prevalence and Characteristics of Autism Spectrum Disorder Among Children Aged 8 Years - Autism and Developmental Disabilities Monitoring Network, 11 Sites, United States, 2012. *MMWR Surveill Summ.* 2018 Nov 16;65(13):1-23. doi: 10.15585/mmwr.ss6513a1. PMID: 30439868; PMCID: PMC6237390.

Chruścicka B, Wallace Fitzsimons SE, Borroto-Escuela DO, Druelle C, Stamou P, Nally K, Dinan TG, Cryan JF, Fuxe K, Schellekens H. Attenuation of Oxytocin and Serotonin 2A Receptor Signaling through Novel Heteroreceptor Formation. *ACS Chem Neurosci.* 2019 Jul 17;10(7):3225-3240. doi: 10.1021/acchemneuro.8b00665. Epub 2019 May 8. PMID: 31038917.

Chung SK, McCabe JT, Pfaff DW. Estrogen influences on oxytocin mRNA expression in preoptic and anterior hypothalamic regions studied by in situ hybridization. *J Comp Neurol.* 1991 May 8;307(2):281-95. doi: 10.1002/cne.903070209. PMID: 1856326.

Collingridge GL, Isaac JT, Wang YT. Receptor trafficking and synaptic plasticity. *Nat Rev Neurosci.* 2004 Dec;5(12):952-62. doi: 10.1038/nrn1556. PMID: 15550950.

Conti F, Sertic S, Reversi A et al (2009), Intracellular trafficking of the human oxytocin receptor: evidence of receptor recycling via a Rab4/Rab5 “short cycle”. *Am J Physiol Endocrinol Metab* 296(3):E532–E542.

Corradini I, Focchi E, Rasile M, Morini R, Desiato G, Tomasoni R, Lizier M, Ghirardini E, Fesce R, Morone D, Barajon I, Antonucci F, Pozzi D, Matteoli M. Maternal Immune Activation Delays Excitatory-to-Inhibitory Gamma-Aminobutyric Acid Switch in Offspring. *Biol Psychiatry.* 2018 Apr 15;83(8):680-691. doi: 10.1016/j.biopsych.2017.09.030. Epub 2017 Nov 14. PMID: 29146047.

Cottet M, Albizu L, Perkovska S et al (2010), Past, present and future of vasopressin and oxytocin receptor oligomers, prototypical GPCR models to study dimerization processes. *Curr Opin Pharmacol* 10(1):59–66.

Cottet M, Faklaris O, Maurel D, Scholler P, Doumazane E, Trinquet E, Pin JP, Durroux T (2012), BRET and Time-resolved FRET strategy to study GPCR oligomerization: from cell lines toward native tissues. *Front Endocrinol (Lausanne)* 3:92.

Coulton, G. R. & de Belleruche, J. (1992). *In Situ Hybridization: Medical Applications*. Springer, Dordrecht. <https://doi.org/10.1007/978-94-011-2984-8>

Coyle JT, Price DL, DeLong MR. Alzheimer's disease: a disorder of cortical cholinergic innervation. *Science.* 1983 Mar 11;219(4589):1184-90. doi: 10.1126/science.6338589. PMID: 6338589.

- Crawley JN. Translational animal models of autism and neurodevelopmental disorders. *Dialogues Clin Neurosci*. 2012 Sep;14(3):293-305. PMID: 23226954; PMCID: PMC3513683.
- Crutcher E, Pal R, Naini F, Zhang P, Laugsch M, Kim J, Bajic A, Schaaf CP. mTOR and autophagy pathways are dysregulated in murine and human models of Schaaf-Yang syndrome. *Sci Rep*. 2019 Nov 4;9(1):15935. doi: 10.1038/s41598-019-52287-2. PMID: 31685878; PMCID: PMC6828689.
- Curatolo P, Arpino C, Stazi MA, Medda E. Risk factors for the co-occurrence of partial epilepsy, cerebral palsy and mental retardation. *Dev Med Child Neurol*. 1995 Sep;37(9):776-82. doi: 10.1111/j.1469-8749.1995.tb12061.x. PMID: 7589860.
- De la Mora MP, Pe´rez-Carrera D, Crespo-Ram´irez M, Tarakanov A, Fuxe K, Borroto-Escuela DO (2016), Signaling in dopamine D2 receptor-oxytocin receptor heterocomplexes and its relevance for the anxiolytic effects of dopamine and oxytocin interactions in the amygdala of the rat. *Biochim Biophys Acta* 1862(11):2075–2085.
- Devost D, Zingg HH (2003), Identification of dimeric and oligomeric complexes of the human oxytocin receptor by co-immunoprecipitation and bioluminescence resonance energy transfer. *J Mol Endocrinol* 31(3):461–471
- Dhamne SC, Silverman JL, Super CE, Lammers SHT, Hameed MQ, Modi ME, Copping NA, Pride MC, Smith DG, Rotenberg A, Crawley JN, Sahin M. Replicable in vivo physiological and behavioral phenotypes of the Shank3B null mutant mouse model of autism. *Mol Autism*. 2017 Jun 15;8:26. doi: 10.1186/s13229-017-0142-z. PMID: 28638591; PMCID: PMC5472997.
- Dai, Y. C., H. F. Zhang, et al. (2018). Neonatal Oxytocin Treatment Ameliorates Autistic-Like Behaviors and Oxytocin Deficiency in Valproic Acid-Induced Rat Model of Autism. *Front Cell Neurosci* 12: 355.
- de Vrij FM, Levena J, van der Linde HC, Koekkoek SK, De Zeeuw CI, Nelson DL, Oostra BA, Willemsen R. Rescue of behavioral phenotype and neuronal protrusion morphology in Fmr1 KO mice. *Neurobiol Dis*. 2008 Jul;31(1):127-32. doi: 10.1016/j.nbd.2008.04.002. Epub 2008 Apr 25. PMID: 18571098; PMCID: PMC2481236.
- Devos J, Weselake SV, Wevrick R. Magel2, a Prader-Willi syndrome candidate gene, modulates the activities of circadian rhythm proteins in cultured cells. *J Circadian Rhythms*. 2011 Dec 30;9(1):12. doi: 10.1186/1740-3391-9-12. PMID: 22208286; PMCID: PMC3278377.
- Dichter GS, Felder JN, Green SR, Rittenberg AM, Sasson NJ, Bodfish JW. Reward circuitry function in autism spectrum disorders. *Soc Cogn Affect Neurosci*. 2012 Feb;7(2):160-72. doi: 10.1093/scan/nsq095. Epub 2010 Dec 8. PMID: 21148176; PMCID: PMC3277365.
- Diezmann F, Seitz O. DNA-guided display of proteins and protein ligands for the interrogation of biology. *Chem Soc Rev*. 2011 Dec;40(12):5789-801. doi: 10.1039/c1cs15054e. Epub 2011 May 17. PMID: 21589953.
- Dombret C, Nguyen T, Schakman O, Michaud JL, Hardin-Pouzet H, et al. (2012). Loss of Maged1 results in obesity, deficits of social interactions, impaired sexual behavior and severe alteration of mature oxytocin production in the hypothalamus. *Human molecular genetics* 21:4703-17
- Dumais KM, Veenema AH. Vasopressin and oxytocin receptor systems in the brain: Sex differences and sex-specific regulation of social behavior. *Front Neuroendocrinol*. 2016 Jan;40:1-23. doi: 10.1016/j.yfrne.2015.04.003. Epub 2015 May 4. PMID: 25951955; PMCID: PMC4633405.

- Dykens EM, Lee E, Roof E. Prader-Willi syndrome and autism spectrum disorders: an evolving story. *J Neurodev Disord*. 2011 Sep;3(3):225-37. doi: 10.1007/s11689-011-9092-5. Epub 2011 Aug 20. PMID: 21858456; PMCID: PMC3261277.
- Ebert A, Brüne M. Oxytocin and Social Cognition. *Curr Top Behav Neurosci*. 2018;35:375-388. doi: 10.1007/7854_2017_21. PMID: 29019100.
- Ebert A, Edel MA, Gilbert P, Brüne M. Endogenous oxytocin is associated with the experience of compassion and recalled upbringing in Borderline Personality Disorder. *Depress Anxiety*. 2018 Jan;35(1):50-57. doi: 10.1002/da.22683. Epub 2017 Sep 7. PMID: 28881460.
- Edlow AG. Maternal obesity and neurodevelopmental and psychiatric disorders in offspring. *Prenat Diagn*. 2017 Jan;37(1):95-110. doi: 10.1002/pd.4932. Epub 2016 Nov 7. PMID: 27684946; PMCID: PMC5572633.
- Edmiston E, Jones KL, Vu T, Ashwood P, Van de Water J. Identification of the antigenic epitopes of maternal autoantibodies in autism spectrum disorders. *Brain Behav Immun*. 2018 Mar;69:399-407. doi: 10.1016/j.bbi.2017.12.014. Epub 2017 Dec 28. PMID: 29289663; PMCID: PMC5857423.
- Eftekhari S, Shahrokhi A, Tsintsadze V et al (2014), Response to comment on “oxytocin-mediated GABA inhibition during delivery attenuates autism pathogenesis in rodent offspring”. *Science* 346(6206):176.
- Elagoz Yuksel M, Yuceturk B, Karatas OF, Ozen M, Dogangun B. The altered promoter methylation of oxytocin receptor gene in autism. *J Neurogenet*. 2016 Sep-Dec;30(3-4):280-284. doi: 10.1080/01677063.2016.1202951. Epub 2016 Aug 5. PMID: 27309964.
- Fanelli F, Barbier P, Zanchetta D, de Benedetti PG, Chini B. Activation mechanism of human oxytocin receptor: a combined study of experimental and computer-simulated mutagenesis. *Mol Pharmacol*. 1999 Jul;56(1):214-25. doi: 10.1124/mol.56.1.214. PMID: 10385703.
- Fatemi SH, Reutiman TJ, Folsom TD, Thuras PD. GABA(A) receptor downregulation in brains of subjects with autism. *J Autism Dev Disord*. 2009 Feb;39(2):223-30. doi: 10.1007/s10803-008-0646-7. Epub 2008 Sep 23. PMID: 18821008; PMCID: PMC2697059.
- Fatemi SH, Reutiman TJ, Folsom TD, Rustan OG, Rooney RJ, Thuras PD. Downregulation of GABAA receptor protein subunits $\alpha 6$, $\beta 2$, δ , ϵ , $\gamma 2$, θ , and $\rho 2$ in superior frontal cortex of subjects with autism. *J Autism Dev Disord*. 2014 Aug;44(8):1833-45. doi: 10.1007/s10803-014-2078-x. PMID: 24668190.
- Favre N, Fanelli F, Missotten M, Nichols A, Wilson J, di Tiani M, Rommel C, Scheer A (2005), The DRY motif as a molecular switch of the human oxytocin receptor. *Biochemistry* 44:9990-10008.
- Feliciano, P. *Cntnap2*^{-/-} autism model. *Nat Genet* 43, 1053 (2011). <https://doi.org/10.1038/ng.1002>
- Ferguson KM. Structure-based view of epidermal growth factor receptor regulation. *Annu Rev Biophys*. 2008;37:353-73. doi: 10.1146/annurev.biophys.37.032807.125829. PMID: 18573086; PMCID: PMC2745238.
- Ferguson JN, Young LJ, Hearn EF, Matzuk MM, Insel TR, Winslow JT. (2000). Social amnesia in mice lacking the oxytocin gene. *Nat Genet* 25:284-8
- Ferrè S, Casado V, Devi LA, Filizola M, Jockers R, Lohse MJ, Milligan G, Pin JP, Guitart X (2014), G protein-coupled receptor oligomerization revisited: functional and pharmacological perspectives. *Pharmacol Rev* 66:413-434.

- Fombonne E. Epidemiology of pervasive developmental disorders. *Pediatr Res*. 2009 Jun;65(6):591-8. doi: 10.1203/PDR.0b013e31819e7203. PMID: 19218885.
- Fombonne E. Editorial: The rising prevalence of autism. *J Child Psychol Psychiatry*. 2018 Jul;59(7):717-720. doi: 10.1111/jcpp.12941. PMID: 29924395.
- Fountain MD, Schaaf CP. Prader-Willi Syndrome and Schaaf-Yang Syndrome: Neurodevelopmental Diseases Intersecting at the MAGEL2 Gene. *Diseases*. 2016 Jan 13;4(1):2. doi: 10.3390/diseases4010002. PMID: 28933382; PMCID: PMC5456300.
- Fountain MD, Tao H, Chen CA, Yin J, Schaaf CP. Magel2 knockout mice manifest altered social phenotypes and a deficit in preference for social novelty. *Genes Brain Behav*. 2017 Jul;16(6):592-600. doi: 10.1111/gbb.12378. Epub 2017 Apr 4. PMID: 28296079; PMCID: PMC5495607.
- Freeman SM, Inoue K, Smith AL, Goodman MM, Young LJ. The neuroanatomical distribution of oxytocin receptor binding and mRNA in the male rhesus macaque (*Macaca mulatta*). *Psychoneuroendocrinology*. 2014 Jul;45:128-41. doi: 10.1016/j.psyneuen.2014.03.023. Epub 2014 Apr 12. PMID: 24845184; PMCID: PMC4043226.
- Freeman SM, Young LJ (2016), Comparative Perspectives on Oxytocin and Vasopressin Receptor Research in Rodents and Primates: Translational Implications. *J Neuroendocrinol* 28(4).
- Fujiwara, T., M. Sanada, et al. (2016). Unusual social behavior in HPC-1/syntaxin1A knockout mice is caused by disruption of the oxytocinergic neural system. *J Neurochem* 138(1): 117-123.
- Gaugler T, Klei L, Sanders SJ, Bodea CA, Goldberg AP, Lee AB, et al. Most genetic risk for autism resides with common variation. *Nat Genet*. 2014;46(8):881–885. doi: 10.1038/ng.3039.
- Gekas C, Dieterlen-Lièvre F, Orkin SH, Mikkola HK. The placenta is a niche for hematopoietic stem cells. *Dev Cell*. 2005 Mar;8(3):365-75. doi: 10.1016/j.devcel.2004.12.016. PMID: 15737932.
- Gerasimenko M, Cherepanov SM, Furuhashi K, et al. Nicotinamide riboside supplementation corrects deficits in oxytocin, sociability and anxiety of CD157 mutants in a mouse model of autism spectrum disorder. *Sci Rep*. 2020;10(1):10035. Published 2020 Jun 22. doi:10.1038/s41598-019-57236-7
- Gigliucci, V., M. Leonzino, et al. (2014). Region specific up-regulation of oxytocin receptors in the opioid oprm1 (-/-) mouse model of autism. *Front Pediatr* 2: 91.
- Gilissen C, Hehir-Kwa JY, Thung DT, van de Vorst M, van Bon BW, Willemsen MH, Kwint M, Janssen IM, Hoischen A, Schenck A, Leach R, Klein R, Tearle R, Bo T, Pfundt R, Yntema HG, de Vries BB, Kleefstra T, Brunner HG, Vissers LE, Veltman JA. Genome sequencing identifies major causes of severe intellectual disability. *Nature*. 2014 Jul 17;511(7509):344-7. doi: 10.1038/nature13394. Epub 2014 Jun 4. PMID: 24896178.
- Gilman SR, Iossifov I, Levy D, Ronemus M, Wigler M, Vitkup D. Rare de novo variants associated with autism implicate a large functional network of genes involved in formation and function of synapses. *Neuron*. 2011 Jun 9;70(5):898-907. doi: 10.1016/j.neuron.2011.05.021. PMID: 21658583; PMCID: PMC3607702.
- Gimpl G (2016), Interaction of G protein coupled receptors and cholesterol. *Chem Phys Lipids* 199:61-73.
- Gimpl G, Fahrenholz F. The oxytocin receptor system: structure, function, and regulation. *Physiol Rev*. 2001 Apr;81(2):629-83. doi: 10.1152/physrev.2001.81.2.629. PMID: 11274341.

- Gimpl G, Klein U, Reilander H et al (1995), Expression of the human oxytocin receptor in baculovirus-infected insect cells: high-affinity binding is induced by a cholesterol-cyclodextrin complex. *Biochemistry* 34(42):13794–13801
- Glendining KA, Jasoni CL. Maternal High Fat Diet-Induced Obesity Modifies Histone Binding and Expression of Oxtr in Offspring Hippocampus in a Sex-Specific Manner. *Int J Mol Sci.* 2019 Jan 15;20(2):329. doi: 10.3390/ijms20020329. PMID: 30650536; PMCID: PMC6359595.
- Gomes I, Sierra S, Devi LA. Detection of Receptor Heteromerization Using In Situ Proximity Ligation Assay. *Curr Protoc Pharmacol.* 2016 Dec 13;75:2.16.1-2.16.31. doi: 10.1002/cpph.15. PMID: 27960030; PMCID: PMC5758307.
- Gong L, Gao F, Li J et al (2015), Oxytocin-induced membrane hyperpolarization in pain-sensitive dorsal root ganglia neurons mediated by Ca(2+)/nNOS/NO/KATP pathway. *Neuroscience* 289:417–428.
- Gottschalk MG, Domschke K. Oxytocin and Anxiety Disorders. *Curr Top Behav Neurosci.* 2018;35:467-498. doi: 10.1007/7854_2017_25. PMID: 28812274.
- Greengard P. The neurobiology of slow synaptic transmission. *Science.* 2001 Nov 2;294(5544):1024-30. doi: 10.1126/science.294.5544.1024. PMID: 11691979.
- Gregory SG, Connelly JJ, Towers AJ, Johnson J, Biscocho D, Markunas CA, Lintas C, Abramson RK, Wright HH, Ellis P, Langford CF, Worley G, Delong GR, Murphy SK, Cuccaro ML, Persico A, Pericak-Vance MA. Genomic and epigenetic evidence for oxytocin receptor deficiency in autism. *BMC Med.* 2009 Oct 22;7:62. doi: 10.1186/1741-7015-7-62. PMID: 19845972; PMCID: PMC2774338.
- Grinevich V, Desarménien MG, Chini B, Tauber M, Muscatelli F. Ontogenesis of oxytocin pathways in the mammalian brain: late maturation and psychosocial disorders. *Front Neuroanat.* 2015 Jan 20;8:164. doi: 10.3389/fnana.2014.00164. PMID: 25767437; PMCID: PMC4341354.
- Grinevich V, Knobloch-Bollmann HS, Eliava M, Busnelli M, Chini B. Assembling the Puzzle: Pathways of Oxytocin Signaling in the Brain. *Biol Psychiatry.* 2016 Feb 1;79(3):155-64. doi: 10.1016/j.biopsych.2015.04.013. Epub 2015 Apr 25. PMID: 26001309.
- Grotegut CA, Mao L, Pierce SL et al (2016), Enhanced uterine contractility and stillbirth in mice lacking G protein-coupled receptor kinase 6 (GRK6): implications for oxytocin receptor desensitization. *Mol Endocrinol* 30(4):455–468.
- Guastella AJ, Hickie IB. Oxytocin Treatment, Circuitry, and Autism: A Critical Review of the Literature Placing Oxytocin Into the Autism Context. *Biol Psychiatry.* 2016 Feb 1;79(3):234-42. doi: 10.1016/j.biopsych.2015.06.028. Epub 2015 Jul 2. PMID: 26257243.
- Gurevich VV, Gurevich EV. Molecular Mechanisms of GPCR Signaling: A Structural Perspective. *Int J Mol Sci.* 2017 Nov 24;18(12):2519. doi: 10.3390/ijms18122519. PMID: 29186792; PMCID: PMC5751122.
- Gurumurthy CB, Lloyd KCK. Generating mouse models for biomedical research: technological advances. *Dis Model Mech.* 2019 Jan 8;12(1):dmm029462. doi: 10.1242/dmm.029462. PMID: 30626588; PMCID: PMC6361157.
- Hagerman RJ, Berry-Kravis E, Kaufmann WE, Ono MY, Tartaglia N, Lachiewicz A, Kronk R, Delahunty C, Hessel D, Visootsak J, Picker J, Gane L, Tranfaglia M. Advances in the treatment of fragile X syndrome. *Pediatrics.* 2009 Jan;123(1):378-90. doi: 10.1542/peds.2008-0317. PMID: 19117905; PMCID: PMC2888470.

- Hammock EA. Developmental perspectives on oxytocin and vasopressin. *Neuropsychopharmacology*. 2015 Jan;40(1):24-42. doi: 10.1038/npp.2014.120. Epub 2014 May 27. PMID: 24863032; PMCID: PMC4262889.
- Hammock EA, Levitt P. Oxytocin receptor ligand binding in embryonic tissue and postnatal brain development of the C57BL/6J mouse. *Front Behav Neurosci*. 2013 Dec 11;7:195. doi: 10.3389/fnbeh.2013.00195. PMID: 24376405; PMCID: PMC3858721.
- Han Y, Moreira IS, Urizar E, Weinstein H, Javitch JA. Allosteric communication between protomers of dopamine class A GPCR dimers modulates activation. *Nat Chem Biol*. 2009 Sep;5(9):688-95. doi: 10.1038/nchembio.199. Epub 2009 Aug 2. PMID: 19648932; PMCID: PMC2817978.
- Hanamsagar R, Bilbo SD. Sex differences in neurodevelopmental and neurodegenerative disorders: Focus on microglial function and neuroinflammation during development. *J Steroid Biochem Mol Biol*. 2016 Jun;160:127-33. doi: 10.1016/j.jsbmb.2015.09.039. Epub 2015 Oct 23. PMID: 26435451; PMCID: PMC4829467.
- Harony-Nicolas, H., M. Kay, et al. (2017). Oxytocin improves behavioral and electrophysiological deficits in a novel Shank3-deficient rat. *Elife* 6.
- Hasbi A, Devost D, Laporte SA et al (2004), Real-time detection of interactions between the human oxytocin receptor and G protein-coupled receptor kinase-2. *Mol Endocrinol* 18(5):1277–1286.
- Hayashi R, Kasahara Y, Hidema S, Fukumitsu S, Nakagawa K, Nishimori K. Oxytocin Ameliorates Impaired Behaviors of High Fat Diet-Induced Obese Mice. *Front Endocrinol (Lausanne)*. 2020;11:379. Published 2020 Jul 3. doi:10.3389/fendo.2020.00379
- Heinecke K, Seher A, Schmitz W, Mueller TD, Sebald W, Nickel J. Receptor oligomerization and beyond: a case study in bone morphogenetic proteins. *BMC Biol*. 2009 Sep 7;7:59. doi: 10.1186/1741-7007-7-59. PMID: 19735544; PMCID: PMC2749821.
- Heise C, Preuss JM, Schroeder JC, Battaglia CR, Kolibius J, Schmid R, Kreutz MR, Kas MJH, Burbach JPH, Boeckers TM. Heterogeneity of Cell Surface Glutamate and GABA Receptor Expression in Shank and CNTN4 Autism Mouse Models. *Front Mol Neurosci*. 2018 Jun 19;11:212. doi: 10.3389/fnmol.2018.00212. PMID: 29970989; PMCID: PMC6018460.
- Higashida H, Lopatina O, Yoshihara T, Pichugina YA, Soumarokov AA, Munesue T, Minabe Y, Kikuchi M, Ono Y, Korshunova N, Salmina AB. Oxytocin signal and social behaviour: comparison among adult and infant oxytocin, oxytocin receptor and CD38 gene knockout mice. *J Neuroendocrinol*. 2010 May;22(5):373-9. doi: 10.1111/j.1365-2826.2010.01976.x. Epub 2010 Jan 5. PMID: 20141571.
- Higashida H, Yokoyama S, Munesue T, Kikuchi M, Minabe Y, Lopatina O. 2011. CD38 gene knockout juvenile mice: a model of oxytocin signal defects in autism. *Biol Pharm Bull* 34:1369-72
- Hiller C, Kuhhorn J, Gmeiner P (2013), Class A G-protein-coupled receptor (GPCR) dimers and bivalent ligands. *J Med Chem* 56:6542-6559.
- Hines RM, Wu L, Hines DJ, Steenland H, Mansour S, Dahlhaus R, Singaraja RR, Cao X, Sammler E, Hormuzdi SG, Zhuo M, El-Husseini A. Synaptic imbalance, stereotypies, and impaired social interactions in mice with altered neuroligin 2 expression. *J Neurosci*. 2008 Jun 11;28(24):6055-67. doi: 10.1523/JNEUROSCI.0032-08.2008. PMID: 18550748; PMCID: PMC6670530.

- Hisahara S, Shimohama S. Dopamine receptors and Parkinson's disease. *Int J Med Chem*. 2011;2011:403039. doi: 10.1155/2011/403039. Epub 2011 Jun 13. PMID: 25954517; PMCID: PMC4411877
- Hoare S, Copland JA, Strakova Z et al (1999), The proximal portion of the COOH terminus of the oxytocin receptor is required for coupling to g(q), but not g(i). Independent mechanisms for elevating intracellular calcium concentrations from intracellular stores. *J Biol Chem* 274 (40):28682–28689
- Hoon M, Bauer G, Fritschy JM, Moser T, Falkenburger BH, Varoqueaux F. Neuroigin 2 controls the maturation of GABAergic synapses and information processing in the retina. *J Neurosci*. 2009 Jun 24;29(25):8039-50. doi: 10.1523/JNEUROSCI.0534-09.2009. PMID: 19553444; PMCID: PMC6666037.
- Horie, K., K. Inoue, et al. (2018). Oxytocin receptor knockout prairie voles generated by CRISPR/Cas9 editing show reduced preference for social novelty and exaggerated repetitive behaviors. *Horm Behav*.
- Hörnberg H, Pérez-Garci E, Schreiner D, et al. Rescue of oxytocin response and social behaviour in a mouse model of autism. *Nature*. 2020;584(7820):252-256. doi:10.1038/s41586-020-2563-7
- Huang H, Michetti C, Busnelli M, Managò F, Sannino S, Scheggia D, Giancardo L, Sona D, Murino V, Chini B, Scattoni ML, Papaleo F. Chronic and acute intranasal oxytocin produce divergent social effects in mice. *Neuropsychopharmacology*. 2014 Apr;39(5):1102-14. doi: 10.1038/npp.2013.310. Epub 2013 Nov 4. PMID: 24190025; PMCID: PMC3957104.
- Hughes HK, Mills Ko E, Rose D, Ashwood P. Immune Dysfunction and Autoimmunity as Pathological Mechanisms in Autism Spectrum Disorders. *Front Cell Neurosci*. 2018 Nov 13;12:405. doi: 10.3389/fncel.2018.00405. PMID: 30483058; PMCID: PMC6242891.
- Innamorati, G., Le Gouill, C., Balamotis, M., & Birnbaumer, M. (2001). The long and the short cycle. Alternative intracellular routes for trafficking of G-protein-coupled receptors. *Journal of Biological Chemistry*. 276 (16), 13096-13103 <https://doi.org/10.1074/jbc.M009780200>
- Insel, T. R. (1990). Regional Changes in Brain Oxytocin Receptors Post-Partum: Time-Course and Relationship to Maternal Behaviour. *Journal of Neuroendocrinology*. 2 (4), 539-545 <https://doi.org/10.1111/j.1365-2826.1990.tb00445.x>
- Israel, J.-M., Poulain, D. A., & Oliet, S. H. R. (2008). Oxytocin-Induced Postinhibitory Rebound Firing Facilitates Bursting Activity in Oxytocin Neurons. *Journal of Neuroscience*. 28 (2), 385-394 <https://doi.org/10.1523/jneurosci.5198-07.2008>
- Ivell, R., & Richter, D. (1984). Structure and comparison of the oxytocin and vasopressin genes from rat. *Proceedings of the National Academy of Sciences of the United States of America*. 81 (7 I), 2006-2010 <https://doi.org/10.1073/pnas.81.7.2006>
- Jamain S, Quach H, Betancur C, Råstam M, Colineaux C, Gillberg IC, Soderstrom H, Giros B, Leboyer M, Gillberg C, Bourgeron T; Paris Autism Research International Sibpair Study. Mutations of the X-linked genes encoding neuroligins NLGN3 and NLGN4 are associated with autism. *Nat Genet*. 2003 May;34(1):27-9. doi: 10.1038/ng1136. PMID: 12669065; PMCID: PMC1925054. Jin D, Liu HX, Hirai H, Torashima T, Nagai T, et al. (2007). CD38 is critical for social behaviour by regulating oxytocin secretion. *Nature* 446:41-5
- Jensen, E. (2014). Technical review: In situ hybridization. *Anatomical Record*. 297 (8), 1349-1353 <https://doi.org/10.1002/ar.22944>

- Jin D, Liu HX, Hirai H, Torashima T, Nagai T, Lopatina O, Shnayder NA, Yamada K, Noda M, Seike T, Fujita K, Takasawa S, Yokoyama S, Koizumi K, Shiraishi Y, Tanaka S, Hashii M, Yoshihara T, Higashida K, Islam MS, Yamada N, Hayashi K, Noguchi N, Kato I, Okamoto H, Matsushima A, Salmina A, Munesue T, Shimizu N, Mochida S, Asano M, Higashida H. CD38 is critical for social behaviour by regulating oxytocin secretion. *Nature*. 2007 Mar 1;446(7131):41-5. doi: 10.1038/nature05526. Epub 2007 Feb 7. PMID: 17287729.
- Jaramillo TC, Speed HE, Xuan Z, Reimers JM, Escamilla CO, Weaver TP, Liu S, Filonova I, Powell CM. Novel Shank3 mutant exhibits behaviors with face validity for autism and altered striatal and hippocampal function. *Autism Res*. 2017 Jan;10(1):42-65. doi: 10.1002/aur.1664. Epub 2016 Aug 5. PMID: 27492494; PMCID: PMC5274551.
- Jesso S, Morlog D, Ross S, Pell MD, Pasternak SH, Mitchell DG, Kertesz A, Finger EC. The effects of oxytocin on social cognition and behaviour in frontotemporal dementia. *Brain*. 2011 Sep;134(Pt 9):2493-501. doi: 10.1093/brain/awr171. Epub 2011 Aug 22. PMID: 21859765.
- Jordan BA, Devi LA (1999), G-protein-coupled receptor heterodimerization modulates receptor function. *Nature* 399:697-700.
- Jurek B, Neumann ID. The Oxytocin Receptor: From Intracellular Signaling to Behavior. *Physiol Rev*. 2018 Jul 1;98(3):1805-1908. doi: 10.1152/physrev.00031.2017. PMID: 29897293.
- Jurek B, Slattery DA, Maloumby R, Hillerer K, Koszinowski S, Neumann ID, van den Burg EH. Differential contribution of hypothalamic MAPK activity to anxiety-like behaviour in virgin and lactating rats. *PLoS One*. 2012;7(5):e37060. doi: 10.1371/journal.pone.0037060. Epub 2012 May 17. PMID: 22615888; PMCID: PMC3355176.
- Karimi P, Kamali E, Mousavi SM, Karahmadi M. Environmental factors influencing the risk of autism. *J Res Med Sci*. 2017 Feb 16;22:27. doi: 10.4103/1735-1995.200272. PMID: 28413424; PMCID: PMC5377970.
- Karpenko, I. A., Kreder, R., Valencia, C., Villa, P., Mendre, C., Mouillac, B., ... Klymchenko, A. S. (2014). Red fluorescent turn-on ligands for imaging and quantifying G protein-coupled receptors in living cells. *ChemBioChem*. 15 (3), 359-363 <https://doi.org/10.1002/cbic.201300738>
- Kasai RS, Ito SV, Awane RM, Fujiwara TK, Kusumi A. The Class-A GPCR Dopamine D2 Receptor Forms Transient Dimers Stabilized by Agonists: Detection by Single-Molecule Tracking. *Cell Biochem Biophys*. 2018 Jun;76(1-2):29-37. doi: 10.1007/s12013-017-0829-y. Epub 2017 Nov 7. PMID: 29116599; PMCID: PMC5913388.
- Kataoka S, Takuma K, Hara Y, Maeda Y, Ago Y, Matsuda T. Autism-like behaviours with transient histone hyperacetylation in mice treated prenatally with valproic acid. *Int J Neuropsychopharmacol*. 2013 Feb;16(1):91-103. doi: 10.1017/S1461145711001714. Epub 2011 Nov 18. PMID: 22093185.
- Katritch V, Cherezov V, Stevens RC. Structure-function of the G protein-coupled receptor superfamily. *Annu Rev Pharmacol Toxicol*. 2013;53:531-56. doi: 10.1146/annurev-pharmtox-032112-135923. Epub 2012 Nov 8. PMID: 23140243; PMCID: PMC3540149.
- Kerppola TK (2008), Bimolecular fluorescence complementation (BiFC) analysis as a probe of protein interactions in living cells. *Annu Rev Biophys* 37:465-487.
- Kim SH, MacIntyre DA, Hanyaloglu AC et al (2016), The oxytocin receptor antagonist, atosiban, activates pro-inflammatory pathways in human amnion via G(alpha) signalling. *Mol Cell Endocrinol* 420:11-23.

- Kim J, Stirling KJ, Cooper ME, Ascoli M, Momany AM, McDonald EL, Ryckman KK, Rhea L, Schaa KL, Cosentino V, Gadow E, Saleme C, Shi M, Hallman M, Plunkett J, Teramo KA, Muglia LJ, Feenstra B, Geller F, Boyd HA, Melbye M, Marazita ML, Dagle JM, Murray JC (2013), Sequence variants in oxytocin pathway genes and preterm birth: a candidate gene association study. *BMC Med Genet* 14:77.
- King LB. Specialized Networks for Social Cognition: A Defining Role for the Oxytocin Receptor. *J Neurosci*. 2016 Aug 10;36(32):8283-5. doi: 10.1523/JNEUROSCI.1446-16.2016. PMID: 27511002; PMCID: PMC6601865.
- Klein BY, Tamir H, Hirschberg DL, Glickstein SB, Welch MG. Oxytocin modulates mTORC1 pathway in the gut. *Biochem Biophys Res Commun*. 2013 Mar 15;432(3):466-71. doi: 10.1016/j.bbrc.2013.01.121. Epub 2013 Feb 11. PMID: 23410756; PMCID: PMC3619035.
- Knobloch HS, Charlet A, Hoffmann LC, Eliava M, Khrulev S, Cetin AH, Osten P, Schwarz MK, Seeburg PH, Stoop R, Grinevich V. Evoked axonal oxytocin release in the central amygdala attenuates fear response. *Neuron*. 2012 Feb 9;73(3):553-66. doi: 10.1016/j.neuron.2011.11.030. PMID: 22325206.
- Knuesel, I., Chicha, L., Britschgi, M. et al. Maternal immune activation and abnormal brain development across CNS disorders. *Nat Rev Neurol* 10, 643–660 (2014). <https://doi.org/10.1038/nrneurol.2014.187>
- Koenig K, Klin A, Schultz R. Deficits in social attribution ability in Prader-Willi syndrome. *J Autism Dev Disord*. 2004 Oct;34(5):573-82. doi: 10.1007/s10803-004-2551-z. PMID: 15628610.
- Krishnan A, Schiöth HB. The role of G protein-coupled receptors in the early evolution of neurotransmission and the nervous system. *J Exp Biol*. 2015 Feb 15;218(Pt 4):562-71. doi: 10.1242/jeb.110312. PMID: 25696819.
- Krishnan K, Lau BY, Ewall G, Huang ZJ, Shea SD. MECP2 regulates cortical plasticity underlying a learned behaviour in adult female mice. *Nat Commun*. 2017 Jan 18;8:14077. doi: 10.1038/ncomms14077. PMID: 28098153; PMCID: PMC5253927.
- Kwok J, Hall HA, Murray AL, Auyeung B. The association between analgesic drug use in pregnancy and neurodevelopmental disorders: protocol for an umbrella review. *Syst Rev*. 2020 Sep 2;9(1):202. doi: 10.1186/s13643-020-01465-9. PMID: 32878642; PMCID: PMC7469356.
- Laffray S, Bouali-Benazzouz R, Papon MA, Favereaux A, Jiang Y, Holm T, Spriet C, Desbarats P, Fossat P, Le Feuvre Y, Decossas M, Héliot L, Langel U, Nagy F, Landry M. Impairment of GABAB receptor dimer by endogenous 14-3-3 ζ in chronic pain conditions. *EMBO J*. 2012 Aug 1;31(15):3239-51. doi: 10.1038/emboj.2012.161. Epub 2012 Jun 12. PMID: 22692127; PMCID: PMC3411072.
- Lagerström MC, Schiöth HB. Structural diversity of G protein-coupled receptors and significance for drug discovery. *Nat Rev Drug Discov*. 2008 Apr;7(4):339-57. doi: 10.1038/nrd2518. Erratum in: *Nat Rev Drug Discov*. 2008 Jun;7(6):542. PMID: 18382464.
- Lawson SK, Gray AC, Woehrle NS. Effects of oxytocin on serotonin 1B agonist-induced autism-like behavior in mice. *Behav Brain Res*. 2016;314:52-64. doi:10.1016/j.bbr.2016.07.027
- Lebois EP, Thorn C, Edgerton JR, Popiolek M, Xi S. Muscarinic receptor subtype distribution in the central nervous system and relevance to aging and Alzheimer's disease. *Neuropharmacology*. 2018 Jul 1;136(Pt C):362-373. doi: 10.1016/j.neuropharm.2017.11.018. Epub 2017 Nov 11. PMID: 29138080.

- Lee HJ, Macbeth AH, Pagani JH, Young WS, 3rd (2009), Oxytocin: the great facilitator of life. *Prog Neurobiol* 88:127-151.
- Lee SP, So CH, Rashid AJ, Varghese G, Cheng R, Lança AJ, O'Dowd BF, George SR. Dopamine D1 and D2 receptor Co-activation generates a novel phospholipase C-mediated calcium signal. *J Biol Chem*. 2004 Aug 20;279(34):35671-8. doi: 10.1074/jbc.M401923200. Epub 2004 May 24. PMID: 15159403.
- Lee, J. H., J. Y. Zhang, et al. (2018). Impaired social behaviors and minimized oxytocin signaling of the adult mice deficient in the N-methyl-d-aspartate receptor GluN3A subunit. *Exp Neurol* 305: 1-12.
- Lefkowitz RJ, Shenoy SK. Transduction of receptor signals by beta-arrestins. *Science*. 2005 Apr 22;308(5721):512-7. doi: 10.1126/science.1109237. PMID: 15845844.
- Leng, G., & Ludwig, M. (2008). Neurotransmitters and peptides: Whispered secrets and public announcements. *Journal of Physiology*. 586, 5625–5632 <https://doi.org/10.1113/jphysiol.2008.159103>
- Leonzino M, Busnelli M, Antonucci F, Verderio C, Mazzanti M, Chini B. The Timing of the Excitatory-to-Inhibitory GABA Switch Is Regulated by the Oxytocin Receptor via KCC2. *Cell Rep*. 2016 Apr 5;15(1):96-103. doi: 10.1016/j.celrep.2016.03.013. Epub 2016 Mar 24. PMID: 27052180; PMCID: PMC4826440.
- Levy D, Ronemus M, Yamrom B, Lee YH, Leotta A, Kendall J, Marks S, Lakshmi B, Pai D, Ye K, Buja A, Krieger A, Yoon S, Troge J, Rodgers L, Iossifov I, Wigler M. Rare de novo and transmitted copy-number variation in autistic spectrum disorders. *Neuron*. 2011 Jun 9;70(5):886-97. doi: 10.1016/j.neuron.2011.05.015. PMID: 21658582.
- Liu W, Pappas GD, Carter CS. (2005). Oxytocin receptors in brain cortical regions are reduced in haploinsufficient (+/-) reeler mice. *Neurol Res* 27:339-45
- Liu X, Kawashima M, Miyagawa T, Otowa T, Latt KZ, Thiri M, Nishida H, Sugiyama T, Tsurusaki Y, Matsumoto N, Mabuchi A, Tokunaga K, Sasaki T (2015), Novel rare variations of the oxytocin receptor (OXTR) gene in autism spectrum disorder individuals. *Hum Genome Var* 2:15024.
- Loat CS, Curran S, Lewis CM, Duvall J, Geschwind D, Bolton P, Craig IW. Methyl-CpG-binding protein 2 polymorphisms and vulnerability to autism. *Genes Brain Behav*. 2008 Oct;7(7):754-60. doi: 10.1111/j.1601-183X.2008.00414.x. PMID: 19125863; PMCID: PMC3645848.
- Lohse MJ. Dimerization in GPCR mobility and signaling. *Curr Opin Pharmacol*. 2010 Feb;10(1):53-8. doi: 10.1016/j.coph.2009.10.007. Epub 2009 Nov 10. PMID: 19910252.
- Lohse, M. J., & Hoffmann, C. (2014). Arrestin interactions with G protein-coupled receptors. *Handbook of Experimental Pharmacology*. 219, 15-56 https://doi.org/10.1007/978-3-642-41199-1_2
- Lohse MJ, Nuber S, Hoffmann C. Fluorescence/bioluminescence resonance energy transfer techniques to study G-protein-coupled receptor activation and signaling. *Pharmacol Rev*. 2012 Apr;64(2):299-336. doi: 10.1124/pr.110.004309. Epub 2012 Mar 8. PMID: 22407612.
- Lu Q, Lai J, Du Y, Huang T, Prukpitikul P, Xu Y, Hu S. Sexual dimorphism of oxytocin and vasopressin in social cognition and behavior. *Psychol Res Behav Manag*. 2019 May 17;12:337-349. doi: 10.2147/PRBM.S192951. PMID: 31191055; PMCID: PMC6529726.
- Lukas, M., Bredewold, R., Neumann, I. D., & Veenema, A. H. (2010). Maternal separation interferes with developmental changes in brain vasopressin and oxytocin receptor binding in male rats. *Neuropharmacology*. 58 (1), 78-87 <https://doi.org/10.1016/j.neuropharm.2009.06.020>

- Lutz, W. H., Londowski, J. M., & Kumar, R. (1990). The synthesis and biological activity of four novel fluorescent vasopressin analogs. *Journal of Biological Chemistry*. 265 (8), 4657-4663
- Ma WJ, Hashii M, Munesue T, Hayashi K, Yagi K, Yamagishi M, Higashida H, Yokoyama S (2013), Non-synonymous single-nucleotide variations of the human oxytocin receptor gene and autism spectrum disorders: a case-control study in a Japanese population and functional analysis. *Mol Autism* 4:22.
- Maejima Y, Sedbazar U, Suyama S, Kohno D, Onaka T, Takano E, Yoshida N, Koike M, Uchiyama Y, Fujiwara K, Yashiro T, Horvath TL, Dietrich MO, Tanaka S, Dezaki K, Oh-I S, Hashimoto K, Shimizu H, Nakata M, Mori M, Yada T. Nesfatin-1-regulated oxytocinergic signaling in the paraventricular nucleus causes anorexia through a leptin-independent melanocortin pathway. *Cell Metab*. 2009 Nov;10(5):355-65. doi: 10.1016/j.cmet.2009.09.002. PMID: 19883614.
- Maillard J, Park S, Croizier S, Vanacker C, Cook JH, Prevot V, Tauber M, Bouret SG. Loss of *Magel2* impairs the development of hypothalamic Anorexigenic circuits. *Hum Mol Genet*. 2016 Aug 1;25(15):3208-3215. doi: 10.1093/hmg/ddw169. Epub 2016 Jun 10. PMID: 27288456; PMCID: PMC5179922.
- Mak P, Broussard C, Vacy K et al (2012), Modulation of anxiety behavior in the elevated plus maze using peptidic oxytocin and vasopressin receptor ligands in the rat. *J Psychopharmacol* 26 (4):532-542.
- Marco EM, Macrì S, Laviola G. Critical age windows for neurodevelopmental psychiatric disorders: evidence from animal models. *Neurotox Res*. 2011 Feb;19(2):286-307. doi: 10.1007/s12640-010-9205-z. Epub 2010 Jul 7. PMID: 20607469.
- Marder E. Neuromodulation of neuronal circuits: back to the future. *Neuron*. 2012 Oct 4;76(1):1-11. doi: 10.1016/j.neuron.2012.09.010. PMID: 23040802; PMCID: PMC3482119.
- Marlin BJ, Mitre M, D'amour JA, Chao MV, Froemke RC. Oxytocin enables maternal behaviour by balancing cortical inhibition. *Nature*. 2015 Apr 23;520(7548):499-504. doi: 10.1038/nature14402. Epub 2015 Apr 15. PMID: 25874674; PMCID: PMC4409554.
- Mastinu A, Premoli M, Maccarinelli G, Grilli M, Memo M, Bonini SA. Melanocortin 4 receptor stimulation improves social deficits in mice through oxytocin pathway. *Neuropharmacology*. 2018 May 1;133:366-374. doi: 10.1016/j.neuropharm.2018.02.007. Epub 2018 Feb 15. PMID: 29454840.
- Matson JL, Rieske RD, Williams LW. The relationship between autism spectrum disorders and attention-deficit/hyperactivity disorder: an overview. *Res Dev Disabil*. 2013 Sep;34(9):2475-84. doi: 10.1016/j.ridd.2013.05.021. Epub 2013 Jun 7. PMID: 23751293.
- Matthys A, Haegeman G, Van Craenenbroeck K, Vanhoenacker P. Role of the 5-HT7 receptor in the central nervous system: from current status to future perspectives. *Mol Neurobiol*. 2011 Jun;43(3):228-53. doi: 10.1007/s12035-011-8175-3. Epub 2011 Mar 22. PMID: 21424680.
- May T, Adesina I, McGillivray J, Rinehart NJ. Sex differences in neurodevelopmental disorders. *Curr Opin Neurol*. 2019 Aug;32(4):622-626. doi: 10.1097/WCO.0000000000000714. PMID: 31135460.
- May T, Sciberras E, Brignell A, Williams K. Autism spectrum disorder: updated prevalence and comparison of two birth cohorts in a nationally representative Australian sample. *BMJ Open*. 2017 May 9;7(5):e015549. doi: 10.1136/bmjopen-2016-015549. PMID: 28490562; PMCID: PMC5623420.
- McAllister CJ, Whittington JE. A short clinical overview of Prader-Willi syndrome. *Clin Obes*. 2011 Aug;1(4-6):184-8. doi: 10.1111/j.1758-8111.2011.00022.x. Epub 2011 Sep 29. PMID: 25585908.

- McDuffie A, Thurman AJ, Hagerman RJ, Abbeduto L. Symptoms of Autism in Males with Fragile X Syndrome: A Comparison to Nonsyndromic ASD Using Current ADI-R Scores. *J Autism Dev Disord*. 2015 Jul;45(7):1925-37. doi: 10.1007/s10803-013-2013-6. PMID: 24414079; PMCID: PMC4096070.
- McGrath, J. C., Arribas, S., & Daly, C. J. (1996). Fluorescent ligands for the study of receptors. *Trends in Pharmacological Sciences*. 17 (11), 393-399 [https://doi.org/10.1016/S0165-6147\(96\)40004-9](https://doi.org/10.1016/S0165-6147(96)40004-9)
- McPartland JC. Considerations in biomarker development for neurodevelopmental disorders. *Curr Opin Neurol*. 2016 Apr;29(2):118-22. doi: 10.1097/WCO.0000000000000300. PMID: 26844621; PMCID: PMC4798424.
- Melis MR, Succu S, Iannucci U et al (1997), Oxytocin increases nitric oxide production in the paraventricular nucleus of the hypothalamus of male rats: correlation with penile erection and yawning. *Regul Pept* 69(2):105–111
- Mens, W. B. J., Witter, A., & Van Wimersma Greidanus, T. B. (1983). Penetration of neurohypophyseal hormones from plasma into cerebrospinal fluid (CSF): Half-times of disappearance of these neuropeptides from CSF. *Brain Research*. 262 (1), 143-149. [https://doi.org/10.1016/0006-8993\(83\)90478-X](https://doi.org/10.1016/0006-8993(83)90478-X)
- Mercer RE, Michaelson SD, Chee MJ, Atallah TA, Wevrick R, Colmers WF. Magel2 is required for leptin-mediated depolarization of POMC neurons in the hypothalamic arcuate nucleus in mice. *PLoS Genet*. 2013;9(1):e1003207. doi: 10.1371/journal.pgen.1003207. Epub 2013 Jan 17. PMID: 23341784; PMCID: PMC3547795.
- Messinger DS, Young GS, Webb SJ, Ozonoff S, Bryson SE, Carter A, Carver L, Charman T, Chawarska K, Curtin S, Dobkins K, Hertz-Picciotto I, Hutman T, Iverson JM, Landa R, Nelson CA, Stone WL, Tager-Flusberg H, Zwaigenbaum L. Early sex differences are not autism-specific: A Baby Siblings Research Consortium (BSRC) study. *Mol Autism*. 2015 Jun 4;6:32. doi: 10.1186/s13229-015-0027-y. PMID: 26045943; PMCID: PMC4455973.
- Meziane, H., F. Schaller, et al. (2015). An Early Postnatal Oxytocin Treatment Prevents Social and Learning Deficits in Adult Mice Deficient for Magel2, a Gene Involved in Prader-Willi Syndrome and Autism. *Biol Psychiatry* 78(2): 85-94.
- Michalon A, Sidorov M, Ballard TM, Ozmen L, Spooren W, Wettstein JG, Jaeschke G, Bear MF, Lindemann L. Chronic pharmacological mGlu5 inhibition corrects fragile X in adult mice. *Neuron*. 2012 Apr 12;74(1):49-56. doi: 10.1016/j.neuron.2012.03.009. PMID: 22500629.
- Milligan G, Bouvier M (2005), Methods to monitor the quaternary structure of G protein coupled receptors. *FEBS J* 272:2914-2925.
- Milligan G, Ward RJ, Marsango S. GPCR homo-oligomerization. *Curr Opin Cell Biol*. 2019 Apr;57:40-47. doi: 10.1016/j.ceb.2018.10.007. Epub 2018 Nov 16. PMID: 30453145; PMCID: PMC7083226.
- Minakova, E., J. Lang, et al. (2019). Melanotan-II reverses autistic features in a maternal immune activation mouse model of autism. *PLoS One* 14(1): e0210389.
- Mineur YS, Huynh LX, Crusio WE. Social behavior deficits in the Fmr1 mutant mouse. *Behav Brain Res*. 2006 Mar 15;168(1):172-5. doi: 10.1016/j.bbr.2005.11.004. Epub 2005 Dec 15. PMID: 16343653.

- Mitre M, Marlin BJ, Schiavo JK, Morina E, Norden SE, Hackett TA, Aoki CJ, Chao MV, Froemke RC. A Distributed Network for Social Cognition Enriched for Oxytocin Receptors. *J Neurosci*. 2016 Feb 24;36(8):2517-35. doi: 10.1523/JNEUROSCI.2409-15.2016. PMID: 26911697; PMCID: PMC4764667.
- Mizutani S, Safwat MA, Goto K, Tsujimoto M, Nakazato H, Itakura A, Mizuno M, Kurauchi O, Kikkawa F, Tomoda Y. Initiating and responsible enzyme of arginine vasopressin degradation in human placenta and pregnancy serum. *Regul Pept*. 1995 Nov 10;59(3):371-8. doi: 10.1016/0167-0115(95)00108-n. PMID: 8577942.
- Modi ME, Inoue K, Barrett CE, Kittelberger KA, Smith DG, Landgraf R, Young LJ. Melanocortin Receptor Agonists Facilitate Oxytocin-Dependent Partner Preference Formation in the Prairie Vole. *Neuropsychopharmacology*. 2015 Jul;40(8):1856-65. doi: 10.1038/npp.2015.35. Epub 2015 Feb 5. PMID: 25652247; PMCID: PMC4839509.
- Mohr, E., Schmitz, E., & Richter, D. (1988). A single rat genomic DNA fragment encodes both the oxytocin and vasopressin genes separated by 11 kilobases and oriented in opposite transcriptional directions. *Biochimie*. 70 (5), 649-654 [https://doi.org/10.1016/0300-9084\(88\)90249-0](https://doi.org/10.1016/0300-9084(88)90249-0)
- Moldrich RX, Leanage G, She D, Dolan-Evans E, Nelson M, Reza N, Reutens DC. Inhibition of histone deacetylase in utero causes sociability deficits in postnatal mice. *Behav Brain Res*. 2013 Nov 15;257:253-64. doi: 10.1016/j.bbr.2013.09.049. Epub 2013 Oct 5. PMID: 24103642.
- Moretti P, Bouwknecht JA, Teague R, Paylor R, Zoghbi HY. Abnormalities of social interactions and home-cage behavior in a mouse model of Rett syndrome. *Hum Mol Genet*. 2005 Jan 15;14(2):205-20. doi: 10.1093/hmg/ddi016. Epub 2004 Nov 17. PMID: 15548546.
- Mouillac, B., Manning, M., & Durroux, T. (2008). Fluorescent Agonists and Antagonists for Vasopressin/Oxytocin G Protein-Coupled Receptors: Usefulness in Ligand Screening Assays and Receptor Studies. *Mini-Reviews in Medicinal Chemistry*. 8 (10), 996-1005 <https://doi.org/10.2174/138955708785740607>
- Moy, S. S., B. L. Teng, et al. 2019. Prosocial effects of an oxytocin metabolite, but not synthetic oxytocin receptor agonists, in a mouse model of autism. *Neuropharmacology* 144: 301-311.
- Muscattelli, F., D. N. Abrous, et al. (2000). Disruption of the mouse Necdin gene results in hypothalamic and behavioral alterations reminiscent of the human Prader-Willi syndrome. *Hum Mol Genet* 9(20): 3101-3110.
- Nagarajan RP, Hogart AR, Gwye Y, Martin MR, LaSalle JM. Reduced MeCP2 expression is frequent in autism frontal cortex and correlates with aberrant MECP2 promoter methylation. *Epigenetics*. 2006 Oct-Dec;1(4):e1-11. doi: 10.4161/epi.1.4.3514. PMID: 17486179; PMCID: PMC1866172.
- Nakamura H, Itakura A, Okamura M, Ito M, Iwase A, Nakanishi Y, Okada M, Nagasaka T, Mizutani S. Oxytocin stimulates the translocation of oxytocinase of human vascular endothelial cells via activation of oxytocin receptors. *Endocrinology*. 2000 Dec;141(12):4481-5. doi: 10.1210/endo.141.12.7832. PMID: 11108258.
- Negishi Y, Ieda D, Hori I, Nozaki Y, Yamagata T, Komaki H, Tohyama J, Nagasaki K, Tada H, Saitoh S. Schaaf-Yang syndrome shows a Prader-Willi syndrome-like phenotype during infancy. *Orphanet J Rare Dis*. 2019 Dec 2;14(1):277. doi: 10.1186/s13023-019-1249-4. PMID: 31791363; PMCID: PMC6888944.
- Newmaster KT, Nolan ZT, Chon U, Vanselow DJ, Weit AR, Tabbaa M, Hidema S, Nishimori K, Hammock EAD, Kim Y. Quantitative cellular-resolution map of the oxytocin receptor in postnatally developing mouse

brains. *Nat Commun.* 2020 Apr 20;11(1):1885. doi: 10.1038/s41467-020-15659-1. PMID: 32313029; PMCID: PMC7171089.

Neumann ID. Brain oxytocin: a key regulator of emotional and social behaviours in both females and males. *J Neuroendocrinol.* 2008 Jun;20(6):858-65. doi: 10.1111/j.1365-2826.2008.01726.x. PMID: 18601710.

Nicholas AP, Hancock MB. Evidence for substance P, serotonin and oxytocin input to medullary catecholamine neurons with diencephalic projections. *Brain Res Bull.* 1989 Feb;22(2):213-23. doi: 10.1016/0361-9230(89)90046-4. PMID: 2468399.

Niemeyer CM. Semisynthetic DNA-protein conjugates for biosensing and nanofabrication. *Angew Chem Int Ed Engl.* 2010 Feb 8;49(7):1200-16. doi: 10.1002/anie.200904930. PMID: 20091721.

Niemeyer CM, Sano T, Smith CL, Cantor CR. Oligonucleotide-directed self-assembly of proteins: semisynthetic DNA--streptavidin hybrid molecules as connectors for the generation of macroscopic arrays and the construction of supramolecular bioconjugates. *Nucleic Acids Res.* 1994 Dec 25;22(25):5530-9. doi: 10.1093/nar/22.25.5530. PMID: 7530841; PMCID: PMC310113.

Niswender CM, Conn PJ. Metabotropic glutamate receptors: physiology, pharmacology, and disease. *Annu Rev Pharmacol Toxicol.* 2010;50:295-322. doi: 10.1146/annurev.pharmtox.011008.145533. PMID: 20055706; PMCID: PMC2904507.

Niu M, Han Y, Dy ABC, Du J, Jin H, Qin J, Zhang J, Li Q, Hagerman RJ. Autism Symptoms in Fragile X Syndrome. *J Child Neurol.* 2017 Sep;32(10):903-909. doi: 10.1177/0883073817712875. Epub 2017 Jun 15. PMID: 28617074.

Nusbaum MP, Blitz DM. Neuropeptide modulation of microcircuits. *Curr Opin Neurobiol.* 2012 Aug;22(4):592-601. doi: 10.1016/j.conb.2012.01.003. Epub 2012 Feb 1. PMID: 22305485; PMCID: PMC3346881.

Oakley RH, Laporte SA, Holt JA et al (2001), Molecular determinants underlying the formation of stable intracellular G protein-coupled receptor-beta-arrestin complexes after receptor endocytosis*. *J Biol Chem* 276(22):19452–19460.

Oncul M, Dilsiz P, Ates Oz E, Ates T, Aklan I, Celik E, Sayar Atasoy N, Atasoy D. Impaired melanocortin pathway function in Prader-Willi Syndrome gene-Magel2 deficient mice. *Hum Mol Genet.* 2018 Sep 15;27(18):3129-3136. doi: 10.1093/hmg/ddy216. PMID: 29878108.

Ostrowski, Nancy L. (1998). Oxytocin receptor mRNA expression in rat brain: Implications for behavioral integration and reproductive success. *Psychoneuroendocrinology.* 23 (8), 989-1004 [https://doi.org/10.1016/S0306-4530\(98\)00070-5](https://doi.org/10.1016/S0306-4530(98)00070-5)

Owen SF, Tuncdemir SN, Bader PL, Tirko NN, Fishell G, Tsien RW. Oxytocin enhances hippocampal spike transmission by modulating fast-spiking interneurons. *Nature.* 2013 Aug 22;500(7463):458-62. doi: 10.1038/nature12330. Epub 2013 Aug 4. PMID: 23913275; PMCID: PMC5283693.

Parenti I, Rabaneda LG, Schoen H, Novarino G. Neurodevelopmental Disorders: From Genetics to Functional Pathways. *Trends Neurosci.* 2020 Aug;43(8):608-621. doi: 10.1016/j.tins.2020.05.004. Epub 2020 Jun 5. PMID: 32507511.

- Passoni, I., Leonzino, M., Gigliucci, V., Chini, B., & Busnelli, M. (2016). Carbetocin is a Functional Selective Gq Agonist That Does Not Promote Oxytocin Receptor Recycling After Inducing β -Arrestin-Independent Internalisation. *Journal of Neuroendocrinology*. 28 (4) <https://doi.org/10.1111/jne.12363>
- Patterson PH. Immune involvement in schizophrenia and autism: etiology, pathology and animal models. *Behav Brain Res*. 2009 Dec 7;204(2):313-21. doi: 10.1016/j.bbr.2008.12.016. Epub 2008 Dec 24. PMID: 19136031.
- Pearlmutter AF, Soloff MS (1979), Characterization of the metal ion requirement for oxytocin-receptor interaction in rat mammary gland membranes. *J Biol Chem* 254:3899-3906.
- Peça J, Feliciano C, Ting JT, Wang W, Wells MF, Venkatraman TN, Lascola CD, Fu Z, Feng G. Shank3 mutant mice display autistic-like behaviours and striatal dysfunction. *Nature*. 2011 Apr 28;472(7344):437-42. doi: 10.1038/nature09965. Epub 2011 Mar 20. PMID: 21423165; PMCID: PMC3090611.
- Peñagarikano O, Abrahams BS, Herman EI, et al. Absence of CNTNAP2 leads to epilepsy, neuronal migration abnormalities, and core autism-related deficits. *Cell*. 2011;147(1):235-246. doi:10.1016/j.cell.2011.08.040
- Peñagarikano O, Lázaro MT, Lu XH, Gordon A, Dong H, Lam HA, Peles E, Maidment NT, Murphy NP, Yang XW, Golshani P, Geschwind DH. Exogenous and evoked oxytocin restores social behavior in the Cntnap2 mouse model of autism. *Sci Transl Med*. 2015 Jan 21;7(271):271ra8. doi: 10.1126/scitranslmed.3010257. PMID: 25609168; PMCID: PMC4498455.
- Percy AK. Rett syndrome: exploring the autism link. *Arch Neurol*. 2011 Aug;68(8):985-9. doi: 10.1001/archneurol.2011.149. PMID: 21825235; PMCID: PMC3674963.
- Poliak S, Gollan L, Martinez R, Custer A, Einheber S, Salzer JL, Trimmer JS, Shrager P, Peles E. Caspr2, a new member of the neurexin superfamily, is localized at the juxtaparanodes of myelinated axons and associates with K⁺ channels. *Neuron*. 1999 Dec;24(4):1037-47. doi: 10.1016/s0896-6273(00)81049-1. PMID: 10624965.
- Poliak S, Salomon D, Elhanany H, Sabanay H, Kiernan B, Pevny L, Stewart CL, Xu X, Chiu SY, Shrager P, Furley AJ, Peles E. Juxtaparanodal clustering of Shaker-like K⁺ channels in myelinated axons depends on Caspr2 and TAG-1. *J Cell Biol*. 2003 Sep 15;162(6):1149-60. doi: 10.1083/jcb.200305018. Epub 2003 Sep 8. PMID: 12963709; PMCID: PMC2172860.
- Portoghese PS, Larson DL, Sayre LM, Yim CB, Ronsisvalle G, Tam SW, Takemori AE (1986), Opioid agonist and antagonist bivalent ligands. The relationship between spacer length and selectivity at multiple opioid receptors. *J Med Chem* 29:1855-1861.
- Postina R, Kojro E, Fahrenholz F (1998), Identification of neurohypophysial hormone receptor domains involved in ligand binding and G protein coupling. *Adv Exp Med Biol* 449:371-385.
- Preikšaitienė E, Ambrozaitytė L, Maldžienė Ž, Morkūnienė A, Cimbalistienė L, Rančelis T, Utkus A, Kučinskis V. Identification of genetic causes of congenital neurodevelopmental disorders using genome wide molecular technologies. *Acta Med Litu*. 2016;23(2):73-85. doi: 10.6001/actamedica.v23i2.3324. PMID: 28356794; PMCID: PMC5088740.
- Qian A, Wang W, Sanborn BM (1998), Evidence for the involvement of several intracellular domains in the coupling of oxytocin receptor to G α (q/11). *Cell Signal* 10(2):101–105.

- Rapoport JL, Giedd JN, Gogtay N. Neurodevelopmental model of schizophrenia: update 2012. *Mol Psychiatry*. 2012 Dec;17(12):1228-38. doi: 10.1038/mp.2012.23. Epub 2012 Apr 10. PMID: 22488257; PMCID: PMC3504171.
- Reversi A, Rimoldi V, Brambillasca S et al (2005), Effects of cholesterol manipulation on the signaling of the human oxytocin receptor. *Am J Physiol Regul Integr Comp Physiol* 291(4): R861–R869.
- Richard S, Zingg HH. The human oxytocin gene promoter is regulated by estrogens. *J Biol Chem*. 1990 Apr 15;265(11):6098-103. PMID: 2108152.
- Richard, S. & Zingg, H. H. (1991) The human oxytocin gene promoter is regulated by oestrogens. *Journal of Biological Chemistry* 266, 21428–21433.
- Rilling JK, Young LJ. The biology of mammalian parenting and its effect on offspring social development. *Science*. 2014 Aug 15;345(6198):771-6. doi: 10.1126/science.1252723. Epub 2014 Aug 14. PMID: 25124431; PMCID: PMC4306567.
- Rimoldi, V., Reversi, A., Taverna, E., Rosa, P., Francolini, M., Cassoni, P., ... Chini, B. (2003). Oxytocin receptor elicits different EGFR/MAPK activation patterns depending on its localization in caveolin-1 enriched domains. *Oncogene*. 22 (38), 6054-6060 <https://doi.org/10.1038/sj.onc.1206612>
- Rivera C, Voipio J, Payne JA et al (1999), The K⁺/Cl⁻ co-transporter KCC2 renders GABA hyperpolarizing during neuronal maturation. *Nature* 397(6716):251–255.
- Robin NH, Shprintzen RJ. Defining the clinical spectrum of deletion 22q11.2. *J Pediatr*. 2005 Jul;147(1):90-6. doi: 10.1016/j.jpeds.2005.03.007. PMID: 16027702.
- Romero-Fernandez W, Borroto-Escuela DO, Agnati LF et al (2013), Evidence for the existence of dopamine D2-oxytocin receptor heteromers in the ventral and dorsal striatum with facilitatory receptor-receptor interactions. *Mol Psychiatry* 18(8):849–850.
- Ronald A, Simonoff E, Kuntsi J, Asherson P, Plomin R. Evidence for overlapping genetic influences on autistic and ADHD behaviours in a community twin sample. *J Child Psychol Psychiatry*. 2008 May;49(5):535-42. doi: 10.1111/j.1469-7610.2007.01857.x. Epub 2008 Jan 21. PMID: 18221348.
- Rosenbaum, D. M., Rasmussen, S. G. F., & Kobilka, B. K. (2009). The structure and function of G-protein-coupled receptors. *Nature*. 459, 356–363 <https://doi.org/10.1038/nature08144>
- Rosenberg RE, Law JK, Yenokyan G, McGready J, Kaufmann WE, Law PA. Characteristics and concordance of autism spectrum disorders among 277 twin pairs. *Arch Pediatr Adolesc Med*. 2009 Oct;163(10):907-14. doi: 10.1001/archpediatrics.2009.98. PMID: 19805709.
- Sabatier, N. (2006). α -melanocyte-stimulating hormone and oxytocin: A peptide signalling cascade in the hypothalamus. *Journal of Neuroendocrinology*. 459, 356–363. <https://doi.org/10.1111/j.1365-2826.2006.01464.x>
- Sabatier N, Caquineau C, Dayanithi G, Bull P, Douglas AJ, Guan XM, Jiang M, Van der Ploeg L, Leng G. Alpha-melanocyte-stimulating hormone stimulates oxytocin release from the dendrites of hypothalamic neurons while inhibiting oxytocin release from their terminals in the neurohypophysis. *J Neurosci*. 2003 Nov 12;23(32):10351-8. doi: 10.1523/JNEUROSCI.23-32-10351.2003. PMID: 14614094; PMCID: PMC6741015.

Sala, M., D. Braidà, et al. (2011). Pharmacologic rescue of impaired cognitive flexibility, social deficits, increased aggression, and seizure susceptibility in oxytocin receptor null mice: a neurobehavioral model of autism. *Biol Psychiatry* 69(9): 875-882.

Sala, M., D. Braidà, et al. (2013). Mice heterozygous for the oxytocin receptor gene (*Oxtr*(+/-)) show impaired social behaviour but not increased aggression or cognitive inflexibility: evidence of a selective haploinsufficiency gene effect. *J Neuroendocrinol* 25(2): 107-118.7

Salahpour A, Espinoza S, Masri B, Lam V, Barak LS, Gainetdinov RR. BRET biosensors to study GPCR biology, pharmacology, and signal transduction. *Front Endocrinol (Lausanne)*. 2012 Aug 29;3:105. doi: 10.3389/fendo.2012.00105. PMID: 22952466; PMCID: PMC3430160.

Samaco RC, McGraw CM, Ward CS, Sun Y, Neul JL, Zoghbi HY. Female *Mecp2*(+/-) mice display robust behavioral deficits on two different genetic backgrounds providing a framework for pre-clinical studies. *Hum Mol Genet*. 2013 Jan 1;22(1):96-109. doi: 10.1093/hmg/ddt406. Epub 2012 Oct 1. PMID: 23026749; PMCID: PMC3522402.

Samaco RC, Nagarajan RP, Braunschweig D, LaSalle JM. Multiple pathways regulate MeCP2 expression in normal brain development and exhibit defects in autism-spectrum disorders. *Hum Mol Genet*. 2004 Mar 15;13(6):629-39. doi: 10.1093/hmg/ddh063. Epub 2004 Jan 20. PMID: 14734626.

Sanborn BM, Dodge K, Monga M et al (1998), Molecular mechanisms regulating the effects of oxytocin on myometrial intracellular calcium. *Adv Exp Med Biol* 449:277–286.

Sanders SJ, Ercan-Sencicek AG, Hus V, Luo R, Murtha MT, Moreno-De-Luca D, Chu SH, Moreau MP, Gupta AR, Thomson SA, Mason CE, Bilguvar K, Celestino-Soper PB, Choi M, Crawford EL, Davis L, Wright NR, Dhodapkar RM, DiCola M, DiLullo NM, Fernandez TV, Fielding-Singh V, Fishman DO, Frahm S, Garagaloyan R, Goh GS, Kammela S, Klei L, Lowe JK, Lund SC, McGrew AD, Meyer KA, Moffat WJ, Murdoch JD, O'Roak BJ, Ober GT, Pottenger RS, Raubeson MJ, Song Y, Wang Q, Yaspan BL, Yu TW, Yurkiewicz IR, Beaudet AL, Cantor RM, Curland M, Grice DE, Günel M, Lifton RP, Mane SM, Martin DM, Shaw CA, Sheldon M, Tischfield JA, Walsh CA, Morrow EM, Ledbetter DH, Fombonne E, Lord C, Martin CL, Brooks AI, Sutcliffe JS, Cook EH Jr, Geschwind D, Roeder K, Devlin B, State MW. Multiple recurrent de novo CNVs, including duplications of the 7q11.23 Williams syndrome region, are strongly associated with autism. *Neuron*. 2011 Jun 9;70(5):863-85. doi: 10.1016/j.neuron.2011.05.002. PMID: 21658581; PMCID: PMC3939065.

Sano T, Smith CL, Cantor CR. Immuno-PCR: very sensitive antigen detection by means of specific antibody-DNA conjugates. *Science*. 1992 Oct 2;258(5079):120-2. doi: 10.1126/science.1439758. PMID: 1439758.

Satoh Y, Endo S, Nakata T, Kobayashi Y, Yamada K, Ikeda T, Takeuchi A, Hiramoto T, Watanabe Y, Kazama T. ERK2 contributes to the control of social behaviors in mice. *J Neurosci*. 2011 Aug 17;31(33):11953-67. doi: 10.1523/JNEUROSCI.2349-11.2011. PMID: 21849556; PMCID: PMC6623182.

Savaskan E, Ehrhardt R, Schulz A, Walter M, Schächinger H. Post-learning intranasal oxytocin modulates human memory for facial identity. *Psychoneuroendocrinology*. 2008 Apr;33(3):368-74. doi: 10.1016/j.psyneuen.2007.12.004. Epub 2008 Jan 24. PMID: 18221838.

Schaaf CP, Gonzalez-Garay ML, Xia F, Potocki L, Gripp KW, Zhang B, Peters BA, McElwain MA, Drmanac R, Beaudet AL, Caskey CT, Yang Y. Truncating mutations of *MAGEL2* cause Prader-Willi phenotypes and autism. *Nat Genet*. 2013 Nov;45(11):1405-8. doi: 10.1038/ng.2776. Epub 2013 Sep 29. PMID: 24076603; PMCID: PMC3819162.

- Schaller, F., F. Watrin, et al. (2010). A single postnatal injection of oxytocin rescues the lethal feeding behaviour in mouse newborns deficient for the imprinted *Magel2* gene. *Hum Mol Genet* 19(24): 4895-4905.
- Schoepp DD. Unveiling the functions of presynaptic metabotropic glutamate receptors in the central nervous system. *J Pharmacol Exp Ther.* 2001 Oct;299(1):12-20. PMID: 11561058.
- Scott-Van Zeeland AA, Dapretto M, Ghahremani DG, Poldrack RA, Bookheimer SY. Reward processing in autism. *Autism Res.* 2010 Apr;3(2):53-67. doi: 10.1002/aur.122. PMID: 20437601; PMCID: PMC3076289.
- Semple E, Shalabi F, Hill JW. Oxytocin Neurons Enable Melanocortin Regulation of Male Sexual Function in Mice. *Mol Neurobiol.* 2019 Sep;56(9):6310-6323. doi: 10.1007/s12035-019-1514-5. Epub 2019 Feb 12. PMID: 30756300; PMCID: PMC6684847.
- Sgritta M, Dooling SW, Buffington SA, et al. Mechanisms Underlying Microbial-Mediated Changes in Social Behavior in Mouse Models of Autism Spectrum Disorder. *Neuron.* 2019;101(2):246-259.e6. doi:10.1016/j.neuron.2018.11.018
- Sharma K, LeBlanc R, Haque M, Nishimori K, Reid MM, Teruyama R. Sexually dimorphic oxytocin receptor-expressing neurons in the preoptic area of the mouse brain. *PLoS One.* 2019 Jul 11;14(7):e0219784. doi: 10.1371/journal.pone.0219784. PMID: 31295328; PMCID: PMC6622548.
- Sharna S.S. et al (2020), Altered Caecal Neuroimmune Interactions in the Neuroligin-3R451C Mouse Model of Autism. *Front Cell Neurosci.* 9;14:85.
- Shi L, Fatemi SH, Sidwell RW, Patterson PH. Maternal influenza infection causes marked behavioral and pharmacological changes in the offspring. *J Neurosci.* 2003 Jan 1;23(1):297-302. doi: 10.1523/JNEUROSCI.23-01-00297.2003. PMID: 12514227; PMCID: PMC6742135.
- Shi L, Smith SE, Malkova N, Tse D, Su Y, Patterson PH. Activation of the maternal immune system alters cerebellar development in the offspring. *Brain Behav Immun.* 2009 Jan;23(1):116-23. doi: 10.1016/j.bbi.2008.07.012. Epub 2008 Aug 9. PMID: 18755264; PMCID: PMC2614890.
- Silverman JL, Yang M, Turner SM, Katz AM, Bell DB, et al. (2010). Low stress reactivity and neuroendocrine factors in the BTBR T+tf/J mouse model of autism. *Neuroscience* 171:1197-20.
- Skuse DH, Lori A, Cubells JF, Lee I, Conneely KN, Puura K, Lehtimaki T, Binder EB, Young LJ (2014), Common polymorphism in the oxytocin receptor gene (*OXTR*) is associated with human social recognition skills. *Proc Natl Acad Sci USA* 111:1987-1992.
- Smith MP, Ayad VJ, Mundell SJ et al (2006), Internalization and desensitization of the oxytocin receptor is inhibited by Dynamin and clathrin mutants in human embryonic kidney 293 cells. *Mol Endocrinol* 20(2):379-388.
- Sofroniew MV. Projections from vasopressin, oxytocin, and neurophysin neurons to neural targets in the rat and human. *J Histochem Cytochem.* 1980 May;28(5):475-8. doi: 10.1177/28.5.7381192. PMID: 7381192.
- Sofroniew MV. Vasopressin and oxytocin in the mammalian brain and spinal cord. *Trends in Neurosciences.* 6,1983,Pages 467-472, [https://doi.org/10.1016/0166-2236\(83\)90221-7](https://doi.org/10.1016/0166-2236(83)90221-7).
- Solek CM, Farooqi N, Verly M, Lim TK, Ruthazer ES. Maternal immune activation in neurodevelopmental disorders. *Dev Dyn.* 2018;247(4):588-619. doi:10.1002/dvdy.24612

- Soloff MS, Alexandrova M, Fernstrom MJ (1979), Oxytocin receptors: triggers for parturition and lactation? *Science* 204:1313-1315.
- Song T et al (2019), Altered Behaviors and Impaired Synaptic Function in a Novel Rat Model With a Complete Shank3 Deletion. *Front. Cell. Neurosci.* 13:111.
- Soorya L, Kolevzon A, Zweifach J, Lim T, Dobry Y, Schwartz L, Frank Y, Wang AT, Cai G, Parkhomenko E, Halpern D, Grodberg D, Angarita B, Willner JP, Yang A, Canitano R, Chaplin W, Betancur C, Buxbaum JD. Prospective investigation of autism and genotype-phenotype correlations in 22q13 deletion syndrome and SHANK3 deficiency. *Mol Autism.* 2013 Jun 11;4(1):18. doi: 10.1186/2040-2392-4-18. PMID: 23758760; PMCID: PMC3707861.
- Spencer CM, Graham DF, Yuva-Paylor LA, Nelson DL, Paylor R. Social behavior in Fmr1 knockout mice carrying a human FMR1 transgene. *Behav Neurosci.* 2008 Jun;122(3):710-5. doi: 10.1037/0735-7044.122.3.710. PMID: 18513141.
- Sridharan, R., Zuber, J., Connelly, S. M., Mathew, E., & Dumont, M. E. (2014). Fluorescent approaches for understanding interactions of ligands with G protein coupled receptors. *Biochimica et Biophysica Acta - Biomembranes.* 18 (38), 15–33 <https://doi.org/10.1016/j.bbamem.2013.09.005>
- Srivastava, A., Gupta, B., Gupta, C., & Shukla, A. K. (2015). Emerging Functional Divergence of β -Arrestin Isoforms in GPCR Function. *Trends in Endocrinology and Metabolism.* 26, 628-642 <https://doi.org/10.1016/j.tem.2015.09.001>
- Stearns NA, Schaevitz LR, Bowling H, Nag N, Berger UV, Berger-Sweeney J. Behavioral and anatomical abnormalities in Mecp2 mutant mice: a model for Rett syndrome. *Neuroscience.* 2007 May 25;146(3):907-21. doi: 10.1016/j.neuroscience.2007.02.009. Epub 2007 Mar 23. PMID: 17383101.
- Stefanik P, Olexova L, Krskova L. (2015). Increased sociability and gene expression of oxytocin and its receptor in the brains of rats affected prenatally by valproic acid. *Pharmacol Biochem Behav* 131C:42-50
- Sun J, Nan G (2016), The mitogen-activated protein kinase (MAPK) signaling pathway as a discovery target in stroke. *J Mol Neurosci* 59(1):90–98.
- Tacer KF, Potts PR. Cellular and disease functions of the Prader-Willi Syndrome gene MAGEL2. *Biochem J.* 2017 Jun 16;474(13):2177-2190. doi: 10.1042/BCJ20160616. PMID: 28626083; PMCID: PMC5594744.
- Takayanagi, Y., M. Yoshida, et al. (2005). Pervasive social deficits, but normal parturition, in oxytocin receptor-deficient mice. *Proc Natl Acad Sci U S A* 102(44): 16096-16101.
- Tanaka M, Sato A, Kasai S, Hagino Y, Kotajima-Murakami H, Kashii H, Takamatsu Y, Nishito Y, Inagaki M, Mizuguchi M, Hall FS, Uhl GR, Murphy D, Sora I, Ikeda K. Brain hyperserotonemia causes autism-relevant social deficits in mice. *Mol Autism.* 2018 Nov 26;9:60. doi: 10.1186/s13229-018-0243-3. PMID: 30498565; PMCID: PMC6258166.
- Tauber M, Boulanouar K, Diene G, Çabal-Berthoumieu S, Ehlinger V, Fichaux-Bourin P, Molinas C, Faye S, Valette M, Pourrinet J, Cessans C, Viaux-Sauvelon S, Bascoul C, Guedeney A, Delhanty P, Geenen V, Martens H, Muscatelli F, Cohen D, Consoli A, Payoux P, Arnaud C, Salles JP. The Use of Oxytocin to Improve Feeding and Social Skills in Infants With Prader-Willi Syndrome. *Pediatrics.* 2017 Feb;139(2):e20162976. doi: 10.1542/peds.2016-2976. PMID: 28100688.

- Teng, B. L., V. D. Nikolova, et al. (2016). Reversal of social deficits by subchronic oxytocin in two autism mouse models. *Neuropharmacology* 105: 61-71.
- Tennese AA, Wevrick R. Impaired hypothalamic regulation of endocrine function and delayed counterregulatory response to hypoglycemia in *Magel2*-null mice. *Endocrinology*. 2011 Mar;152(3):967-78. doi: 10.1210/en.2010-0709. Epub 2011 Jan 19. PMID: 21248145; PMCID: PMC3198964.
- Terrillon, S., Cheng, L. L., Stoev, S., Mouillac, B., Barberis, C., Manning, M., & Durroux, T. (2002). Synthesis and characterization of fluorescent antagonists and agonists for human oxytocin and vasopressin V1a receptors. *Journal of Medicinal Chemistry*. 45 (12), 2579-2588 <https://doi.org/10.1021/jm010526+>
- Terrillon S, Durroux T, Mouillac B et al (2003), Oxytocin and vasopressin V1a and V2 receptors form constitutive homo- and heterodimers during biosynthesis. *Mol Endocrinol* 17 (4):677–691.
- Terrillon S, Bouvier M (2004), Roles of G-protein-coupled receptor dimerization. *EMBO Rep* 5:30-34.
- Tick B, Bolton P, Happé F, Rutter M, Rijdsdijk F. Heritability of autism spectrum disorders: a meta-analysis of twin studies. *J Child Psychol Psychiatry*. 2016 May;57(5):585-95. doi: 10.1111/jcpp.12499. Epub 2015 Dec 27. PMID: 26709141; PMCID: PMC4996332.
- Tomizawa K, Iga N, Lu YF, Moriwaki A, Matsushita M, Li ST, Miyamoto O, Itano T, Matsui H. Oxytocin improves long-lasting spatial memory during motherhood through MAP kinase cascade. *Nat Neurosci*. 2003 Apr;6(4):384-90. doi: 10.1038/nn1023. PMID: 12598900.
- Tsuji C, Fujisaku T, Tsuji T. Oxytocin ameliorates maternal separation-induced ultrasonic vocalisation calls in mouse pups prenatally exposed to valproic acid. *J Neuroendocrinol*. 2020;32(4):e12850. doi:10.1111/jne.12850
- Tsujimoto M, Mizutani S, Adachi H, Kimura M, Nakazato H, Tomoda Y. Identification of human placental leucine aminopeptidase as oxytocinase. *Arch Biochem Biophys*. 1992 Feb 1;292(2):388-92. doi: 10.1016/0003-9861(92)90007-j. PMID: 1731608.
- Tyzio R, Nardou R, Ferrari DC et al (2014), Oxytocin-mediated GABA inhibition during delivery attenuates autism pathogenesis in rodent offspring. *Science* 343(6171):675–679.
- Uhl-Bronner S, Waltisperger E, Martínez-Lorenzana G, Condes Lara M, Freund-Mercier MJ. Sexually dimorphic expression of oxytocin binding sites in forebrain and spinal cord of the rat. *Neuroscience*. 2005;135(1):147-54.
- Vaidyanathan R, Hammock EA. Oxytocin receptor dynamics in the brain across development and species. *Dev Neurobiol*. 2017 Feb;77(2):143-157. doi: 10.1002/dneu.22403. Epub 2016 Jun 6. PMID: 27273834.
- Valant C, Robert Lane J, Sexton PM, Christopoulos A (2012), The best of both worlds? Bitopic orthosteric/allosteric ligands of G protein-coupled receptors. *Annu Rev Pharmacol Toxicol* 52:153-178.
- Valeeva G, Valiullina F, Khazipov R (2013), Excitatory actions of GABA in the intact neonatal rodent hippocampus in vitro. *Front Cell Neurosci* 7:20.
- Villar VA, Cuevas S, Zheng X et al (2016), Localization and signaling of GPCRs in lipid rafts. *Methods Cell Biol* 132:3–23.

- Voineagu I, Wang X, Johnston P, Lowe JK, Tian Y, Horvath S, Mill J, Cantor RM, Blencowe BJ, Geschwind DH. Transcriptomic analysis of autistic brain reveals convergent molecular pathology. *Nature*. 2011 May 25;474(7351):380-4. doi: 10.1038/nature10110. PMID: 21614001; PMCID: PMC3607626.
- Wagner S, Harony-Nicolas H. Oxytocin and Animal Models for Autism Spectrum Disorder. *Curr Top Behav Neurosci*. 2018;35:213-237. doi: 10.1007/7854_2017_15. PMID: 28864977.
- Waltenspühl Y, Schöppe J, Ehrenmann J, Kummer L, Plückthun A. Crystal structure of the human oxytocin receptor. *Sci Adv*. 2020 Jul 15;6(29):eabb5419. doi: 10.1126/sciadv.abb5419. PMID: 32832646; PMCID: PMC7439316.
- Wang C, He Y, Xu P, Yang Y, Saito K, Xia Y, Yan X, Hinton A Jr, Yan C, Ding H, Yu L, Shu G, Gupta R, Wu Q, Tong Q, Lagor WR, Flores ER, Xu Y. TAp63 contributes to sexual dimorphism in POMC neuron functions and energy homeostasis. *Nat Commun*. 2018 Apr 18;9(1):1544. doi: 10.1038/s41467-018-03796-7. PMID: 29670083; PMCID: PMC5906443.
- Wang X, McCoy PA, Rodriguiz RM, Pan Y, Je HS, Roberts AC, Kim CJ, Berrios J, Colvin JS, Bousquet-Moore D, Lorenzo I, Wu G, Weinberg RJ, Ehlers MD, Philpot BD, Beaudet AL, Wetsel WC, Jiang YH. Synaptic dysfunction and abnormal behaviors in mice lacking major isoforms of Shank3. *Hum Mol Genet*. 2011 Aug 1;20(15):3093-108. doi: 10.1093/hmg/ddr212. Epub 2011 May 10. PMID: 21558424; PMCID: PMC3131048.
- Wang, Y., S. Zhao, et al. (2018). Oxytocin improves animal behaviors and ameliorates oxidative stress and inflammation in autistic mice. *Biomed Pharmacother* 107: 262-269.
- Wathes DC, Borwick SC, Timmons PM, Leung ST, Thornton S. Oxytocin receptor expression in human term and preterm gestational tissues prior to and following the onset of labour. *J Endocrinol*. 1999 Apr;161(1):143-51. doi: 10.1677/joe.0.1610143. PMID: 10194538.
- Whitaker-Azmitia, P. M. (2005). Behavioral and cellular consequences of increasing serotonergic activity during brain development: a role in autism? *Int J Dev Neurosci* 23(1): 75-83.
- Whittington J, Holland A. A review of psychiatric conceptions of mental and behavioural disorders in Prader-Willi syndrome. *Neurosci Biobehav Rev*. 2018 Dec;95:396-405. doi: 10.1016/j.neubiorev.2018.10.006. Epub 2018 Oct 28. PMID: 30392879.
- Wilfert AB, Sulovari A, Turner TN, Coe BP, Eichler EE. Recurrent de novo mutations in neurodevelopmental disorders: properties and clinical implications. *Genome Med*. 2017 Nov 27;9(1):101. doi: 10.1186/s13073-017-0498-x. PMID: 29179772; PMCID: PMC5704398.
- Wills S, Cabanlit M, Bennett J, Ashwood P, Amaral D, Van de Water J. Autoantibodies in autism spectrum disorders (ASD). *Ann N Y Acad Sci*. 2007 Jun;1107:79-91. doi: 10.1196/annals.1381.009. PMID: 17804535.
- Winslow JT, Insel TR. The social deficits of the oxytocin knockout mouse. *Neuropeptides*. 2002 Apr-Jun;36(2-3):221-9. doi: 10.1054/npep.2002.0909. PMID: 12359512.
- Wright C, Shin JH, Rajpurohit A, Deep-Soboslay A, Collado-Torres L, Brandon NJ, Hyde TM, Kleinman JE, Jaffe AE, Cross AJ, Weinberger DR. Altered expression of histamine signaling genes in autism spectrum disorder. *Transl Psychiatry*. 2017 May 9;7(5):e1126. doi: 10.1038/tp.2017.87. PMID: 28485729; PMCID: PMC5534955.

Wrzal PK, Devost D, Petrin D et al (2012), Allosteric interactions between the oxytocin receptor and the beta2-adrenergic receptor in the modulation of ERK1/2 activation are mediated by heterodimerization. *Cell Signal* 24(1):342–350.

Yamahara N, Nomura S, Suzuki T, Itakura A, Ito M, Okamoto T, Tsujimoto M, Nakazato H, Mizutani S. Placental leucine aminopeptidase/oxytocinase in maternal serum and placenta during normal pregnancy. *Life Sci.* 2000 Mar 3;66(15):1401-10. doi: 10.1016/s0024-3205(00)00451-3. PMID: 11210715.

Yan H, Park SH, Finkelstein G, Reif JH, LaBean TH. DNA-templated self-assembly of protein arrays and highly conductive nanowires. *Science.* 2003 Sep 26;301(5641):1882-4. doi: 10.1126/science.1089389. PMID: 14512621.

Yang M, Bozdagi O, Scattoni ML, Wöhr M, Roulet FI, Katz AM, Abrams DN, Kalikhman D, Simon H, Woldeyohannes L, Zhang JY, Harris MJ, Saxena R, Silverman JL, Buxbaum JD, Crawley JN. Reduced excitatory neurotransmission and mild autism-relevant phenotypes in adolescent Shank3 null mutant mice. *J Neurosci.* 2012 May 9;32(19):6525-41. doi: 10.1523/JNEUROSCI.6107-11.2012. PMID: 22573675; PMCID: PMC3362928.

Ylisaukko-oja T, Rehnström K, Auranen M, Vanhala R, Alen R, Kempas E, Ellonen P, Turunen JA, Makkonen I, Riikonen R, Nieminen-von Wendt T, von Wendt L, Peltonen L, Järvelä I. Analysis of four neuroligin genes as candidates for autism. *Eur J Hum Genet.* 2005 Dec;13(12):1285-92. doi: 10.1038/sj.ejhg.5201474. PMID: 16077734.

Yoshimura R, Kimura T, Watanabe D, Kiyama H. Differential expression of oxytocin receptor mRNA in the developing rat brain. *Neurosci Res.* 1996 Feb;24(3):291-304. doi: 10.1016/0168-0102(95)01003-3. PMID: 8815448.

Zadeh JN, Steenberg CD, Bois JS, Wolfe BR, Pierce MB, Khan AR, Dirks RM, Pierce NA. NUPACK: Analysis and design of nucleic acid systems. *J Comput Chem.* 2011 Jan 15;32(1):170-3. doi: 10.1002/jcc.21596. PMID: 20645303.

Zocher M, Fung JJ, Kobilka BK, Muller DJ (2012), Ligand-specific interactions modulate kinetic, energetic, and mechanical properties of the human beta2 adrenergic receptor. *Structure* 20:1391-1402.

10. RESUME

10.1 RESUME (FRENCH)

Dans le système nerveux central, l'ocytocine (OT) et son récepteur (OTR) sont considérés comme des régulateurs clés des comportements sociaux et non sociaux. L'ocytocine s'avère donc être une molécule thérapeutique prometteuse des troubles neurodéveloppementaux ; cependant, afin de définir son véritable potentiel en thérapie, nous devons comprendre le fonctionnement du système ocytocinergique dans le système nerveux central. En particulier, nous n'avons pas encore une vision claire et globale ni des zones du cerveau impliquées dans l'activité pharmacologique de l'administration d'ocytocine, ni des voies de signalisation qui régulent ses effets thérapeutiques. Par conséquent, la compréhension de la localisation et des propriétés de signalisation de l'OTR dans le cerveau est une étape cruciale pour développer de nouvelles approches thérapeutiques efficaces et sûres.

Le récepteur à l'ocytocine (OTR) est un récepteur couplé à la protéine G qui est capable de former des complexes homo- ou hétérodimériques ayant des propriétés pharmacologiques distinctes. Cependant, l'identification de ces complexes dans des environnements endogènes est problématique : les techniques actuellement utilisées pour les étudier dans les tissus natifs ne peuvent prouver que la proximité moléculaire entre deux protomères, mais pas leur dimérisation réelle. En ce qui concerne l'OTR, aucun anticorps fiable n'est disponible, et ses faibles niveaux d'expression dans le SNC ; localisation et la quantification précises de véritables complexes OTR homodimériques sont difficiles à réaliser.

J'ai travaillé dans différentes directions pour trouver de nouveaux outils permettant d'étudier le récepteur de l'ocytocine dans les tissus endogènes, sous des formes monomères ou homodimères. Les objectifs étaient les suivants :

1) La caractérisation pharmacologique d'une série de ligands bivalents qui ont été précédemment conçus dans notre laboratoire afin de cibler spécifiquement les homodimères OTR. Nous avons montré un "agonisme sélectif fonctionnel" des composés homobivalents "dOTK2-Cn", qui sont des outils pertinents pour étudier les propriétés de signalisation des homodimères OTR.

2) Le développement d'une nouvelle approche pour cartographier la présence et la distribution des structures dimériques OTR dans le cerveau de la souris. Cette nouvelle approche, la technologie des "nanoroulettes" d'ADN (collaboration avec le groupe du professeur Tommaso Bellini, Université de Milan) que nous avons conçu fonctionne sur les cultures cellulaires et nous prévoyons de l'appliquer à des tranches de cerveau de souris.

3) La comparaison de cette nouvelle approche avec une méthodologie plus commune et universellement acceptée (autoradiographie des récepteurs) afin d'étudier les éventuels changements de distribution des OTR spécifiques à une région (sous leurs formes monomères ou dimères/oligomères) dans un modèle de souris génétiquement modifiée (Magel2-KO) du syndrome de Prader-Willi, une maladie génétique

neurodéveloppemental (Collaboration Dr. F.Muscatelli, Marseille, France). J'ai révélé des effets importants sur l'expression des OTRs chez les souris *Magel2*-KO en comparaison aux souris sauvages. J'ai également montré que, chez les souris mâles, un traitement néonatal par injection d'OT, qui est efficace pour soulager les symptômes autistiques, est capable de modifier les niveaux des OTRs dans plusieurs des régions analysées, telles que l'hippocampe et l'amygdale.

4) L'évaluation d'un dimorphisme sexuel dans les distributions des OTRs chez les souris sauvage et *Magel2*-KO. En comparant les mâles et les femelles de chaque groupe, grâce à ma cartographie autoradiographique des OTRs, j'ai effectivement trouvé une modulation des OTRs en fonction du sexe dans toutes les régions cérébrales incluses dans l'analyse, ce qui suggère que chez les mâles et les femelles il y a une régulation différente du système ocytocinergique en réponse aux modifications environnementales et génétiques.

10.2 RESUME (ENGLISH)

In the central nervous system, oxytocin (OT) and its receptor (OTR) are considered key regulators of social and non-social behaviours. Oxytocin is thus proving to be a promising therapeutic molecule in the field of neurodevelopmental disorders; however, in order to define its true translational potential we still need to gather detailed information about the functioning of the oxytocinergic system in the CNS. In many cases we still do not have a comprehensive view of which are the brain areas involved in the pharmacological activity of oxytocin administration, and a precise knowledge of which are the signaling pathways that regulate its therapeutic effects is also missing. Therefore, understanding the localization and the signaling properties of the OTR in the brain is a crucial step to develop new, effective and safe therapeutic approaches.

The OTR is a G protein coupled receptor, which is able to form homo or heterodimeric complexes with distinct pharmacological properties. However, targeting GPCRs complexes in endogenous environments is often problematic: the techniques currently used to study them in native tissues can only prove molecular proximity between two protomers, not their actual dimerization.

For these reasons, in my project I worked in different directions to find new tools to study the oxytocin receptor in endogenous tissues, in its monomeric or homodimeric forms. The aims included:

- 1) The pharmacological characterization of a series of bivalent ligands previously designed in our laboratory in order to specifically target OTR homodimers. Through this work we provided novel information about the “functional selective agonism” of these homobivalent compounds, highlighting their potential to become a unique tool to investigate the signaling properties of OTR homodimers.
- 2) The development of a new approach to map the presence and distribution of OTR dimers in the mouse brain. This new approach, called DNA “Nanoruler” technique that we have designed in collaboration with Prof. Tommaso Bellini’s group (University of Milan), has already been proved to work *in vitro*; we now plan to apply it on cellular cultures and on mouse brain slices.
- 3) The comparison of such new approach with a more common and universally accepted methodology (receptor autoradiography) in order to investigate possible region-specific changes of OTR distributions (in their monomeric or dimeric/oligomeric forms) in a mouse model of Prader-Willi Syndrome, the *Magel2*-KO mouse (collaboration with Dr. F. Muscatelli, Marseille, France). By comparing WT and KO animals, I found significant genotype-induced effects on OTR expression in *Magel2*-KO mice. Moreover, I showed that in male mice a neonatal OT treatment, which is known to be able to rescue some of the autistic traits of this model, is also able to modify OTR levels in several analyzed regions, such as the hippocampus and the amygdala.
- 4) The evaluation of any possible sexual dimorphism in OTR distributions between WT and *Magel2*-KO animals, in order to highlight any possible sexual dimorphism in receptor fluctuations in wild type and *Magel2*-KO mice. By comparing males and females of each group, through my autoradiographic mapping of the OTR I found a sex-dependent modulation of the OTR in all the brain areas included in the analysis. These differences

suggest that in males and females there is a different regulation of the oxytocinergic system in response to environmental and genetic modifications.